The University of Nottingham
UNITED KINGDOM · CHINA · MALAYSIA

PYROLYSIS OF NAPIER GRASS TO BIO-OIL AND CATALYTIC UPGRADING TO HIGH GRADE BIO-FUEL

ISAH YAKUB MOHAMMED, BEng, MSc.

Thesis submitted to the University of Nottingham for the degree of Doctor of Philosophy

December 2016

ABSTRACT

Biomass is one of the renewable energy resources that has carbon in its building blocks that can be processed into liquid fuel. Napier grass biomass is a herbaceous lignocellulosic material with potentials of high biomass yield. Utilization of Napier grass for bio-oil production via pyrolysis is very limited. Bio-oil generally has poor physicochemical properties such as low pH value, high water content, poor chemical and thermal stabilities which makes it unsuitable for direct use as fuel and therefore requires further processing. Upgrading of bio-oil to liquid fuel is still at early stage of research. Several studies are being carried out to upgrade bio-oil to transportation fuel. However, issues regarding reaction mechanisms and catalyst deactivation amongst others remain a challenge.

This thesis gives insights and understanding of conversion of Napier grass biomass to liquid biofuel. The material was assessed as received and characterized using standard techniques. Pyrolysis was conducted in a fixed bed reactor and effect of pyrolysis temperature, nitrogen flow rate and heating rate on product distribution and characteristics were investigated collectively and pyrolysis products characterized. Effects of different aqueous pre-treatments on the pyrolysis product distribution and characteristics was evaluated. Subsequently, in-situ catalytic and non-catalytic, and ex-situ catalytic upgrading of bio-oil derived from Napier grass using Zeolite based catalysts (microporous and mesoporous) were investigated. Upgraded bio-oil was further fractionated in a micro-laboratory distillation apparatus.

The experimental results showed that high bio-oil yield up to 51 wt% can be obtained from intermediate pyrolysis of Napier grass at 600 ^{o}C, 50 ^{o}C/min and 5 L/min nitrogen flow in a fixed bed reactor. The bio-oil collected was a two-phase liquid, organic (16

wt%) and aqueous (35 wt%) phase. The organic phase consists mainly of various benzene derivatives and hydrocarbons while the aqueous phase was predominantly water, acids, ketones, aldehydes and some phenolics and other water-soluble organics. Non-condensable gas (29 wt%) was made-up of methane, hydrogen, carbon monoxide and carbon dioxide with high hydrogen/carbon monoxide ratio. Bio-char (20 wt%) was a porous carbonaceous material, rich in mineral elements. Aqueous pre-treatment of Napier grass with deionized water at severity factor of 0.9 reduced ash content by 64 wt% and produced bio-oil with 71 % reduction in acid and ketones. Performance of mesoporous zeolites during both in-situ and ex-situ upgrading outweighed that of microporous zeolite, producing less solid and highly deoxygenated organic bio-oil rich in alkanes and monoaromatic hydrocarbons. The Upgraded bio-oil produced 38 wt% light fraction, 48 wt% middle distillate and 7.0wt% bottom product. This study demonstrated that bio-oil derived from Napier grass can be transformed to that high-grade bio-oil via catalytic upgrading over hierarchical mesoporous zeolite.

LIST OF PUBLICATIONS

Journal Articles

1. **Isah Yakub Mohammed**, Yousif Abdalla Abakr, Suzana Yusup, Peter Adeniyi Alaba and Feroz Kabir Kazi. "Upgrading of Bio-oil Derived from Napier Grass Using Microporous and Hierarchical Mesoporous Zeolites" ***Under revision, Journal of Cleaner Production***
2. **Isah Yakub Mohammed**, Yousif Abdalla Abakr, Suzana Yusup and Feroz Kabir Kazi **(2017)**. "Valorization of Napier Grass via Intermediate Pyrolysis: Optimization Using Response Surface Methodology and Pyrolysis Products Characterization" ***Journal of Cleaner Production*** 142, 1848-1866
3. **Isah Yakub Mohammed**, Yousif Abdalla Abakr, Mukhtar Musa, Suzana Yusup, Ajit Singh and Feroz Kabir Kazi. **(2016)** "Valorization of Bambara groundnut shell via intermediate pyrolysis: Products distribution and characterization" ***Journal of Cleaner Production*** 139, 717-728
4. **Isah Yakub Mohammed**, Chun Hsion Lim, Feroz Kabir Kazi, Suzana Yusup, Hon Loong Lam, Yousif Abdalla Abakr **(2016)** "Co-pyrolysis of Rice Husk with Underutilized Biomass Species: A Sustainable Route for Production of Precursors for Fuels and Valuable Chemicals" ***Waste and Biomass Valorization***. *DOI:* 10.1007/s12649-016-9599-9
5. **Isah Yakub Mohammed**, Yousif Abdalla Abakr, Feroz Kabir Kazi, Suzana Yusup, **(2016)** "Effects of Pretreatments of Napier Grass with Deionized Water, Sulfuric Acid and Sodium Hydroxide on Pyrolysis Oil Characteristics" ***Waste and Biomass Valorization*** DOI: 10.1007/s12649-016-9594-1

6. Chun Hsion Lim, **Isah Yakub Mohammed**, Yousif Abdalla Abakr, Feroz Kabir Kazi, Suzana Yusup, Hon Loong Lam **(2016)** "Novel input-output prediction approach for biomass pyrolysis" ***Journal of Cleaner Production*** DOI: 10.1016/j.jclepro.2016.04.141
7. **Isah Yakub Mohammed**, Feroz Kabir Kazi, Suzana Yusup, Peter Adeniyi Alaba, Yahaya Muhammad Sani Yousif Abdalla Abakr **(2016)** "Catalytic Intermediate Pyrolysis of Napier Grass in a Fixed Bed Reactor with ZSM-5, HZSM-5 and Zinc-Exchanged Zeolite-A as the Catalyst" ***Energies*** 9 (4), 246. DOI: 10.3390/en9040246
8. **Isah Yakub Mohammed**, Yousif Abdalla Abakr, Feroz Kabir, Suzana Yusup **(2015)** "Effect of Aqueous Pretreatment on Pyrolysis Characteristics of Napier Grass" ***Journal of Engineering Science & Technology*** 10(11), 1487 – 1496
9. **Isah Yakub Mohammed**, Yousif A. Abakr, Feroz K. Kazi, Suzana Yusup, Ibraheem Alshareef, and Soh A. Chin **(2015)** " Comprehensive characterization of Napier grass as a feedstock for thermochemical conversion" ***Energies*** 8(5): 3403-3417. DOI: 10.3390/en8053403
10. **Isah Yakub Mohammed**, Yousif Abdalla Abakr, Feroz Kabir Kazi, Suzan Yusuf, Ibraheem Alshareef and Soh Aik Chin **(2015)** "Pyrolysis of Napier Grass in a Fixed Bed Reactor: Effect of Operating Conditions on Product Yields and Characteristics" ***BioResources*** 10(4), 6457-6478.
11. **Isah Yakub Mohammed**, Feroz Kabir Kazi, Yousif Abdalla Abakr, Suzana Yusuf, and Md Abdur Razzaque **(2015)**. "Novel Method for the Determination of Water Content and Higher Heating Value of Pyrolysis Oil" ***BioResources*** 10(2), 2681-2690.

12. Chun Hsion Lim, **Isah Yakub Mohammed**, Yousif Abdalla Abakr, Feroz Kabir Kazi, Suzana Yusup, Hon Loong Lam **(2015) "**Element Characteristic Tolerance for Semi-batch Fixed Bed Biomass Pyrolysis" ***Chemical Engineering Transactions*** 45, 1285-1290
13. Peter Alaba, Yahaya Muhammad Sani, **Isah Yakub Mohammed**, Wan Mohd Ashri Wan Daud **(2015)** "Insight into catalyst deactivation mechanism and suppression techniques in thermocatalytic deoxygenation of bio-oil over zeolites" ***Reviews in Chemical Engineering*** 32, 71-91.

Conference Proceedings

1. **Isah Yakub Mohammed**, Y A Abakr, F K Kazi, S Yusuf, I Alshareef and Soh Aik Chin **(2015)** "Catalytic Pyrolysis of Napier Grass in a Fixed Bed Reactor" ***28th Symposium of Malaysian Chemical Engineers, Palm Garden Hotel, IOI Resort Putrajaya 21-22 October***, 683-691
2. **Isah Yakub Mohammed,** Abdalla, A. Y., Feroz, K. K., Suzana, Y., Ibraheem, A., & Chin, S. A. **(2015)** "Pyrolysis of Oil Palm Residues in a Fixed Bed Tubular Reactor" ***Proceedings of The 7th Asia-Pacific Power and Energy Engineering Conference (APPEEC 2015) April 12-14, Beijing, China,*** 3(04), 185.
3. **Isah Yakub Mohammed,** Kabir, F., Yusuf, S., Alshareef, I., Soh, A.C. **(2014)** "Higher Heating Values (HHV) Prediction Model from Biomass Proximate Analysis Data" ***Proceedings of ICCE2014: International Conference & Exhibition on Clean Energy, October 20-22, Quebec, Canada,*** 292-300

Communications/ Posters

1. **Isah Yakub Mohammed**, Abdalla, A. Y., Feroz, K. K., Suzana, Y., Ibraheem, A., & Chin, S. A. **(2015)** "Upgrading of Bio-oil to Fuel and Chemicals" ***Poster Presentation at CFF-UNMC Doctoral Training Partnership (DTP) Week 2015***
2. **Isah Yakub Mohammed**, F. K. Kabir, S. Yusuf, I. Alshareef **(2014)** "Pyrolysis of Napier Grass" ***Poster Presentation at University of Nottingham Postgraduate Week 2014***
3. **Isah Yakub Mohammed**, F K Kabir, S Yusuf, I Alshareef **(2014)** "Pyrolysis of Napier Grass to Bio-Oil and Subsequent Upgrading to Cooking and Heating Grade Fuel" ***CFF-UNMC Doctoral Training Partnership (DTP) Book of Abstracts***

ACKNOWLEDGEMENT

All praises to the Almighty God for the gift of life, health, strength, wisdom, protection and guidance throughout this program.

I use this opportunity to thank my supervisors, Dr Yousif Abdalla Abakr, Dr Feroz Kabir Kazi and Dr Suzana Yusup for their guidance and support from the beginning to the end of this research work. I wish to acknowledge the effort of laboratory supervisors for their assistance and cooperation throughout the laboratory works. My sincere appreciations go to the Crops for the Future (CFF) and the University of Nottingham for the sponsorship to carry out this research.

I wish to register my due regards to my parents, Alhaji Isah Haruna (DCP Rtd) and Hajiya Aishatu Isah Haruna for their love, care, support and prayers since birth to date. May the Almighty God reward them. Special thanks to all my brothers and sisters for their encouragements and prayers.

Sincere appreciations go to my wife, Aisha Musa Ejiko, my children, Al.amin Mohammed Myhib and Kareema Mohammed Myhib for their understanding, encouragement and endurance throughout this program. I love you all. I also want to thank my father and mother in-law for their support and prayers.

To all my friends, I thank you for your encouragements and prayers.

TABLE OF CONTENTS

List of Figures

List of Tables

NOMENCLATURE

AAK	Acids, aldehydes and ketones
AAS	Atomic absorption spectrometer
AC	Ash content
ACL	Acid leachate
ACTNGS	Acid treated Napier grass stem
AK	Acids and ketones
ALL	Alkaline leachate
ALTNGS	Alkaline treated Napier grass stem
ARHC	Aromatic hydrocarbon
ASTM	American Society for Testing and Materials
BD	Benzene derivative
BET	Brunauer Emmet Teller
BSI	British Standards Institution
C	Carbon (wt %)
c	Cellulose
CFF	Crops For the Future
DFET	Diesel final evaporation temperature
DOD	Degree of deoxygenation
DTG	Derivative thermogravimetric
DTG	Derivative of thermogravimetric
e	Extractives
EDX	Energy dispersive x-ray
EN	European Standard
EOS	Esters and other organic compounds
FC	Fixed carbon
FTIR	Fourier transformed infrared
GC-MS	Gas chromatograph mass spectrometer
GC-TCD	Gas chromatography-thermal conductivity detector
H	Hydrogen (wt %)
h	Hemicellulose
HC	Hydrocarbon
HHV	Higher heating value (MJ/kg)
KFET	Kerosene final evaporation temperature
l	Lignin
L/S	Liquid-solid ratio (wt/wt)
MARHC	Methoxyaromatic hydrocarbon
MEST	Methyl ester
MPHOL	Methoxyphenol

N	Nitrogen (wt %)
N/Gas	Non-condensable
NCP	Non-catalytic pyrolysis
NGS	Napier Grass Stem
NIST	National Institute of Standards and Technology
NS	Nitrogenous and sulphur containing compounds
O	Oxygen (wt %)
OVAC	Other value added chemicals
PAH	Polyaromatic hydrocarbon
PHOL	Phenol
PMSFET	Premium motor spirit final evaporation temperature
R_{50}	Recalcitrance index of bio-char
RH	Rice husk
RNGS	Raw Napier grass stem
Ro	Severity factor
rpm	Revolution per minute
S	Sulphur (wt %)
SAR	Silica alumina ratio
SEM	Scanning electron microscope
SGW	Sago waste
TGA	Thermogravimetric analyser
TPD	Temperature programmed desorption
VAC	Value added chemicals
VM	Volatile matter
WL	Water leachate
WTNGS	Water treated Napier grass stem
XRD	X-ray diffraction
$Y_{bio\text{-}char}$	Bio-char yield (wt %)
$Y_{bio\text{-}oil}$	Bio-oil yield (wt %)
YE	Energy yield (%)
YM	Mass yield (wt %)
$Y_{Noncondensable}$	Non-condensable yield (wt %)

CHAPTER ONE

1. INTRODUCTION

1.1 General Introduction

Emission of greenhouse gases (GHG) from the use of fossil fuel continues to generate serious concerns due to its negative impacts on the climate change. Only recently, the United Nations conference on climate change held in Paris November 2015 with the participants from over 180 countries set a target to limit the global temperature rise to below 2 °C (COP21, 2015). To achieve this, a drastic reduction in energy contribution from fossil fuel and development of more alternative and sustainable energy sources is needed in order to maintain energy security (Mohammed et al., 2016a). Solar, wind, geothermal, ocean wave, mini-hydro and biomass are renewable energy sources with promising options of mitigating emission of GHGs in addition to maintaining energy security (Park et al., 2014; Ming et al., 2014). According to the renewables global status report (RGSR, 2015), these energy sources constitutes about 19% of the global total energy consumption with higher contribution from biomass (Figure1.1)

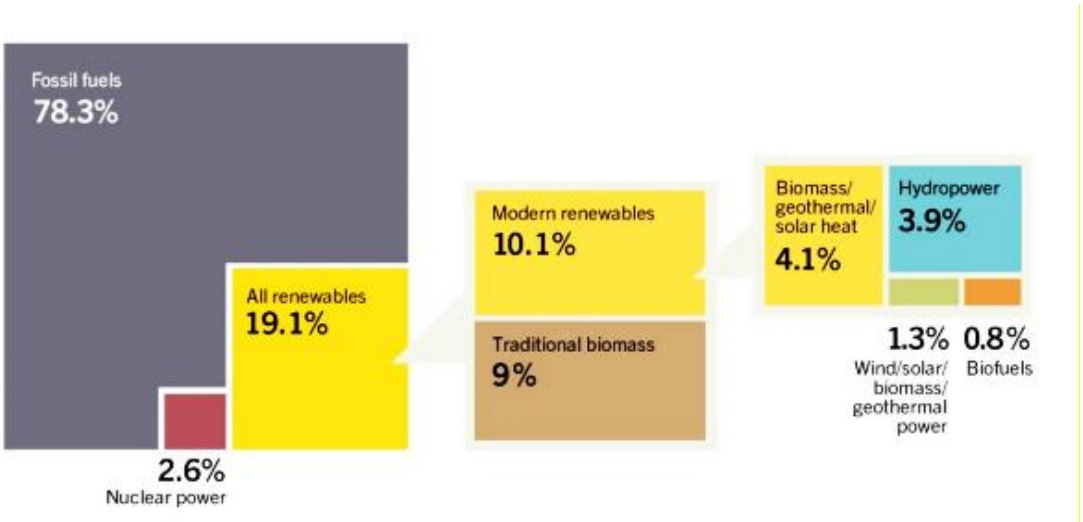

Figure 1.1: Renewable energy share of global final energy consumption (RGSR, 2015)

Furthermore, among the renewable energy sources, biomass is the only source that has carbon in its building blocks which can be processed into liquid fuel (Anex et al., 2010; Swanson et al., 2010; Amutio et al., 2013; Mohammed et al., 2016b). Examples of biomass resources are wood, grasses, crop residues, oil seeds, non-fossil industrial wastes, municipal solid waste, animal wastes, aquatic plants and algae (Duku et al., 2011; Ghayal and Pandya, 2013; Said et al., 2013; Shaaban and Petinrin, 2014). These materials are further grouped based on the origin as terrestrial and aquatic as summarized in Table 1.1. The terrestrial biomasses are all kinds of resource of biological origin on the land which encompasses all the materials used for the processing of first, second generation biofuels and biodegradable municipal solid waste. On the other hand, biomaterials from water bodies such as algae, microalgae, microbacterium, macro algae (large seaweeds) make up the aquatic biomass and are currently being considered as suitable raw material for the development third generation biofuel (Tumuluru et al., 2011; Srirangan et al., 2012).

Table 1.1: summary of biomass classification

Classification		Materials
Terrestrial	First generation	Sugar cane, corn, barley, maize, cassava, sweet potato, sweet sorghum, amaranth
	Second generation	Forestry byproducts, Agricultural and wood industry residues, miscanthus, switch grass, common reed, reed, canary grass, giant reed, cynara cardu, Indian shrub, SRW-willow, SRC-popula, eucalyptus Biodegradable municipal solid wastes
Aquatic		Microalgae, Microbacterium, macroalgae (large seaweeds)

1.2 Biomass Energy Application

Biomass is the oldest source of energy in the world. Application of Biomass in modern energy systems is gaining interest in recent time as a result of the need to reduce the GHG and recent development in the improvement of conversion technologies (Mizsey and Racz, 2010). Biomass is used in different forms either directly or indirectly, depending on the sector and the conversion process as shown in the Figure 1.2.

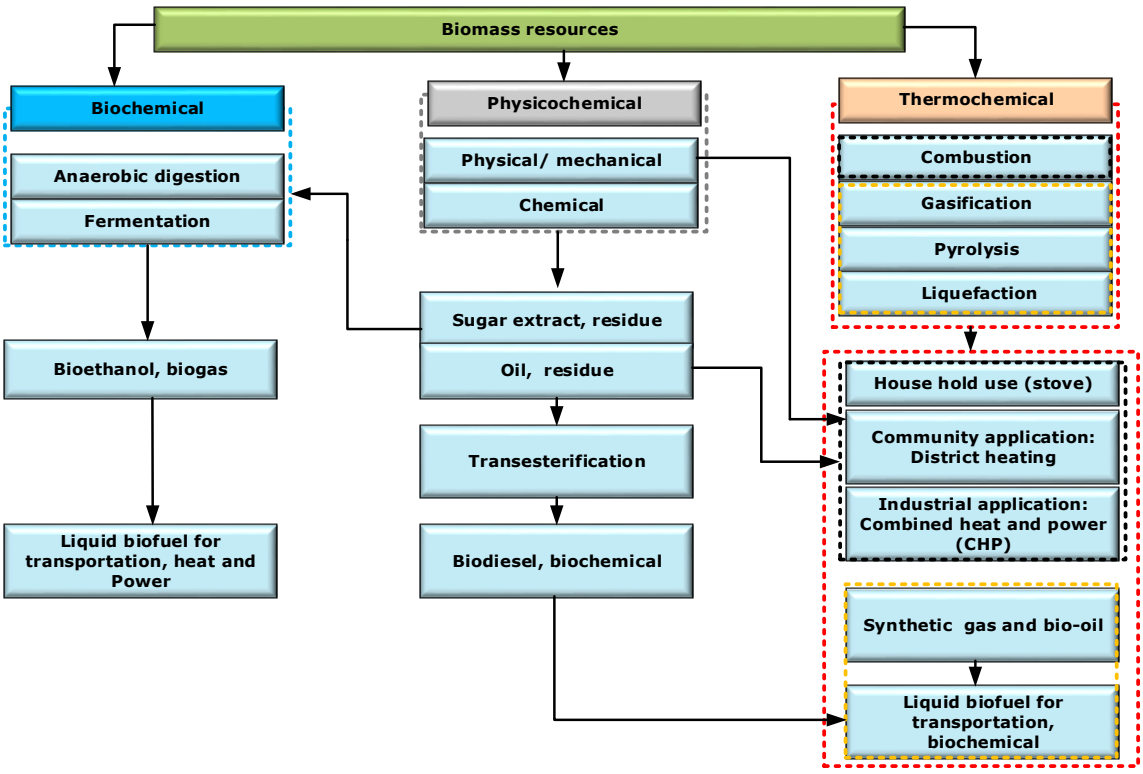

Figure 1.2: Biomass and current applications

1.2.1 Direct biomass application for bioenergy

Direct application of biomass for heating via thermochemical conversion (combustion) remains the oldest and the most well established technology (Mizsey and Racz, 2010). This technique is applied from small scale, medium scale to large scale. The small scale application is the traditional use of biomass as a source of heat for domestic purposes while the medium scale application are mostly for community or district heating (Kshirsagar and Kalamkar, 2014). Studies have shown that biomass is currently being used either directly or combined with other solid fuels for power generation in industrial scales. Biomass combustion with solid fuel such coal is referred to as co-firing. The proportion biomass in co-firing with coal can varies from few weight-percent up to 40wt%. Currently, between 3 to 5wt% biomass is being co-fired with coal on pulverized coal boilers for power generation with capacities in the range of 50 to 700MW (American Coal Council, 2014; Ndibe et al., 2015). Co-firing remains very attractive alternative for electricity production from biomass as it can be applied to a large extent, on the existing power generation infrastructure. This brings about relatively low investment costs due to incorporation of a portion of biomass in the fuel. This approach is used as one of the GHG emission reduction strategies since biomass has lower sulphur and nitrogen contents compared to most coals. However, the chemical composition of biomass differs from that of coal especially the presence of alkaline and alkaline earth metals in the biomass pose some operational challenges such as corrosion, fouling and slagging of the process equipment which may have additional cost implications Biopower Factsheet, 2000; Hayter and Tanner, 2004; American Coal Council, 2014; Ndibe et al., 2015; Johnston and Van Kooten, 2015). Furthermore, higher heating value of biomass is the range of 12-20MJ/kg relative to

that of coal which is between 27 and 33MJ/kg, hence the need for pre-processing (densification) prior to co-firing, which is an additional cost.

1.2.2 Indirect biomass application for first generation biofuel

Processing biomass into liquid biofuels such as bioethanol and biodiesel has been carried out in the past and are commonly referred to as first generation biofuels. They represent the largest biofuels currently being consumed in the transportation industry in Brazil and United states. In 2014, the total global production of biodiesel and bioethanol was 31 and 91 Billion litres with contribution from other countries such as Germany, Canada, Argentina, China, Indonesia and Thailand (RGSR, 2015). Bioethanol is produced mostly from corn and sugarcane through physicochemical process where the grain is modified or juice extraction takes place, and subsequent conversion through biochemical process (fermentation). Biodiesel is obtained via transesterification of vegetable oil. The oil extraction from the oil seeds is carried out through mechanical press or chemical solvent extraction (Duku et al., 2011; Srirangan et al., 2012; Ghobadian, 2012). However, these raw materials are food items and raises ethical concern of food to fuel from public. Compared to fossil gasoline, bioethanol has poor physicochemical properties such as high vapour pressure, miscibility with water, corrosive and lower energy density and therefore makes it unsuitable for use as substitute to fossil petrol but being used in blend with gasoline to improve the overall fuel properties due to its high octane number and high heat of vaporization. The production process of bioethanol is labour intensive which translate to high running cost. Even though, this will depend on government policy as currently the production is economically viable due tax waver and grant (Hellsmark and Jacobsson, 2009; Balat, 2011; Srirangan et al., 2012). For biodiesel, technical

challenges are high alcohol-vegetable oil ratio requirement, reaction temperature, extremely low water content reactants and low fatty acid content. The presence of water and high fatty acid generally lead to catalyst degradation which in turn results in soap formation and lower conversion (Gerhard 2010; Demirbas, 2011; Jakeria et al., 2014). Although, the property of biodiesel is similar to that of fossil diesel and thus can be blended or fully used since diesel engine cars are being developed. From the economic stand point, the major obstacle facing biodiesel production is high cost of the raw material which constitutes about 70% of production cost. As such, large scale production is currently not economically feasible (Carraretto et al., 2004; Yan et al., 2014).

1.2.3 Indirect biomass application for second generation biofuel

Biodiesel from non-edible vegetable oil

Non-edible oil from seeds are known as second generation feedstock for the production of second generation biofuel. Vegetable oil from neem, jatropha, rubber and karanja seeds are the most commonly used due to additional benefits derive from the source plants such as medicines, dyes, ornamentals, feeds, soil enrichment, afforestation (Takase et al., 2015). The oil extraction from the seed follows similar technique used for the first generation feedstock and subsequent transesterification to produce biodiesel. However, these seeds are characterized by low oil yield (25-40 wt%) (Takase et al., 2015; Kumar et al., 2015). This low oil yield coupled with other productive resources such as land, water, labour for the plant growth and the high processing costs rendered it unattractive for large scale development (Stephenson 2008; Kumar et al., 2015). Second generation biodiesel production is focused mainly on the utilization of oil seed without much consideration to the available biomass from

the source plant. Application of parts of the source plant and residue after oil extraction as sources of energy in the production process will reduce solid waste generation and lower the total investment costs.

Bioethanol from lignocellulosic biomass

Lignocellulosic biomass such as such as forest residues, agro-wastes, energy grasses, aquatic plants, algae constitute part of the second generation biomass. These materials have reduced the initial public fear (food for energy) associated with first generation biofuels in addition to having low levels of sulphur, nitrogen, and inorganic minerals (ash) which makes them relatively environmentally friendly (Mohammed et al., 2015a). Processing of lignocellulosic materials into bioethanol through biochemical process has been reported. The process is catalysed by enzymes or microorganisms which breaks down the structural component of lignocellulosic material (hemicellulose and cellulose) into their respective monomeric units and subsequent fermentation into ethanol. This process is characterized by high selectivity and product yield in addition to low energy requirement. However, slow process kinetics, high upstream processing (pre-treatment) and enzyme costs, generation of large volume of by-products (unconverted lignin and solid wastes) are the limiting factors (Srirangan et al., 2012; Cherubini, 2010; Balat, 2011; Bridgwater, 2012; Baeyens et al., 2015; Sawatdeenarunat et al., 2015). Although, these coproducts, particularly the lignin can be upgraded into biofuel or valuable chemicals through other catalytic processes to reduce the production costs.

Biofuel precursor from lignocellulosic biomass

Lignocellulosic biomass materials are also being converted into various biofuel or precursors through hydrothermal liquefaction, gasification and pyrolysis

(thermochemical conversion). In hydrothermal liquefaction, biomass is processed into liquid product known as biocrude oil without prior drying of the feedstock. This technique can be used for most of the lignocellulosic biomass but recent researches have focused on its application for production biocrude oil from algae, the third generation biomass feedstock. Typical process conditions are temperature and pressure between 280 and 370 °C and 10 and 25 MPa respectively. The biocrude oil has relatively high heating value but highly viscos and constitutes heteroatoms such as oxygen, nitrogen and therefore rendered its direct application as biofuel. The need for high pressure at relatively high temperatures in transporting slurry feedstock in the hydrothermal system remains a technological challenge for large scale process due to limited industrial scale experience (Toor et al., 2010; Elliott et al., 2015).

Gasification is the thermal decomposition of biomass under controlled or uncontrolled oxygen to produce combustible gas as the major product. In gasification pathways, biomass is disintegrated into its fundamental building blocks, carbon II oxide (CO) and hydrogen (H_2) called synthetic gas which can be used for heat and electricity generation. The gas product can also be further processed into liquid biofuel through catalytic conversion (Bridgwater, 2012; Chadwick et al., 2014; Heidenreich and Foscolo, 2015; Mirmoshtaghi et al., 2016). However, most gasification reactors require very small particle size feedstock which is both capital and energy intensive. Production of tar, particulate matter, sulphur oxides (SOx), nitrogen oxides (NOx) and ammonia are commonly encountered in the product gas stream. These contaminant must be reduced to barest minimum for the syngas application in combustion engines and downstream processing into liquid fuel. Although a number of gas cleaning techniques such as filtration and catalytic conversion (cracking and catalytic reforming) of tar have

been reported. However, the most efficient and popular one is yet to be developed for large scale application (Asadullah, 2014; Mirmoshtaghi et al., 2016).

Pyrolysis is similar to the gasification but the thermal decomposition of biomass is done in total absence of oxygen to produce solid, liquid and gas products. This process has high improved efficiency, environmental suitability and flexibility as virtually any biomass type can be handled to generate different products (Bridgwater, 2012; Chadwick et al., 2014; Heidenreich and Foscolo, 2015). Pyrolysis process remains more attractive as it comprises fewer steps compared to gasification pathways, and it does not disintegrate the biomass to its fundamental building blocks and then reconstruct to liquid fuel. In addition, high liquid yield (known as bio-oil) which is of most interest can be obtained through pyrolysis process under a careful control of process parameters such as inert gas flowrate, pyrolysis temperature, heating rate, vapour residence time, reactor type, and the temperature regime between the reaction and cooling zone (Bridgwater, 2012; Eom et al., 2012). However, production of bio-oil from biomass via pyrolysis requires energy at different stages. Energy is consumed during biomass collection, bio-oil production stage (size reduction, feeding, pyrolysis and cooling) and bio-oil transportation. Study has shown that about 82% of the total energy requirement for a bio-oil production process is consumed at the production stage mainly during size reduction and pyrolysis (high temperature is needed to decompose the biomass) (Ning et al., 2013). Though, the challenge of high energy requirement may be compensated through efficient utilization of other pyrolysis products (bio-char and non-condensable gas). Furthermore, climate change mitigation is an unresolved issue between the cons and pros of biofuels utilization. Production of biofuel can be said to reduce GHGs only when it produce residuals that

render the use of fossil fuels unnecessary. Consequently, production of second generation biofuels should be carefully synchronized to encourage more agricultural food production and the use of marginal lands for cultivation of energy crops in order to develop a sustainable bioenergy system (Caputo, 2014).

1.3 Problem Statement

Production of bio-oil from herbaceous energy grasses such as miscanthus, switchgrass through pyrolysis have been reported in the literature. However, these plants require some level of nutrients and water during cultivation (Richter et al. 2008; Cadoux et al., 2012; Imam and Capareda, 2012; Serapiglia et al., 2015; Rena et al., 2016; Shemfe et al., 2016). The use of fertilizer, water and other productive resources for the cultivation of such crops for bioenergy production instead of food crops is a cause for great concern and potential food scarcity.

Napier grass is a herbaceous energy crop with higher biomass yield and can be cultivated without any nutrient requirement (Samson et al., 2005; Flores et al., 2012). Studies on the utilization of Napier grass for bio-oil production via pyrolysis have not been carried out extensively. Only few studies have been reported recently in the literature where the effect of a specific pyrolysis process parameter was investigated using a classical approach. In order to fully explore the potential of the Napier grass for bio-oil production, there is a need to evaluate the combined effects of the most important process parameters on the pyrolysis products distribution using statistical experimental design approach, which is one of the goals of this research.

Generally, bio-oil from lignocellulosic biomass through pyrolysis has poor properties such as thermal instability, corrosiveness and high water and oxygen contents. These

characteristics make it unsuitable as direct substitute to fossil fuel and therefore require further processing. Upgrading of bio-oil to liquid biofuels and chemicals is at the early stage of development. Literature reviews have shown that bio-oil can be upgraded into fuel via zeolite cracking and hydrodeoxygenation. However, issues regarding reaction mechanisms, kinetics and catalyst deactivation needed further understanding.

To further evaluate the bioenergy potentials of Napier grass, catalytic upgrading of bio-oil derived from Napier grass is necessary. Currently, no such studies have been reported in the literature. Upgrading of bio-oil into high-grade liquid fuel has great importance for Malaysian rural applications. Therefore, focus has been given to the upgrading of bio-oil derived from Napier grass via pyrolysis into high-grade fuel.

1.4 Research Scope and Limitations

In this research, a locally grown Napier grass biomass is to be assessed physicochemically and used as a feedstock for bio-oil production through pyrolysis process in a fixed-bed reactor. Evaluation of pyrolysis products distribution is limited to mass and energy balances. Catalytic upgrading of bio-oil is limited to batch wise zeolite cracking in a newly designed laboratory scale upgrading rig. The upgraded oil is to be further fractionated into light, middle and heavy distillates using a laboratory scale distillation apparatus. Physicochemical and chemical composition of all products is to be evaluated using analytical instruments.

1.5 Aim and Objectives

The aim of this research is to carry out pyrolysis of Napier grass biomass to bio-oil and subsequent upgrading to high-grade fuel. The detail objectives are as follows:

- To assess the physicochemical characteristics of Napier grass biomass for thermochemical conversion
- To evaluate pyrolysis products distribution from Napier grass as potential energy resources
- To investigate effects of aqueous pre-treatments of Napier grass on bio-oil quality.
- To carry out in-situ and ex-situ catalytic upgrading of bio-oil derived from Napier grass to high-grade fuel.

1.6 Thesis Overview

This thesis is structured as follows:

- **Chapter One: General Introduction**

  This chapter provides a background of different sources of biofuels and benefits of using lignocellulosic materials for the development of new biofuels. It highlights the importance of pyrolysis process for bio-oil production, outlines the current challenges in the bio-oil upgrading and the need for further understanding towards production good quality biofuel.

- **Chapter Two: Literature Review**

  Chapter two summarizes literature review on biomass pyrolysis to bio-oil. It discusses progress on valorisation of Napier grass. It also provides reviews on catalytic bio-oil upgrading, types of catalysts used and current challenges. It further discusses ways of improving the current bio-oil upgrading process.

- **Chapter Three: Materials and Experimental Methodology**

  Chapter three provides detail information on Napier grass biomass and chemical reagents used in this study. It gives details of pyrolysis method and reactor system

used in this study. It explains the analytical procedures adopted for the characterization of materials and products. It provides an overview of techniques for the catalyst characterization before and after upgrading and the modification procedures adopted. It also details out the distillation technique used for fractionation of the upgraded bio-oil.

- **Chapter Four: Pyrolysis of Napier grass and products Characterization**

  This chapter discusses results of the characterization of Napier grass biomass. It provides detail information on the results of pyrolysis product distribution and their characteristics. It discusses the quality of bio-oil obtained from the feedstock, analyses the energy consumption at each stage in the bio-oil production and highlights possible area of application of each of the pyrolysis products.

- **Chapter Five: Improving Bio-oil Quality *via* Biomass Pre-treatment**

  Chapter five discusses different biomass pre-treatment as it affects pyrolysis and pyrolysis products. It gives experimental results of different aqueous pre-treatments of Napier grass and their impacts on bio-oil yield and chemical composition. It suggests the pre-treatment method suitable for the production of bio-oil from Napier grass and application for residual generated in the pre-treatment process.

- **Chapter Six: In-situ Upgrading of Bio-oil Derived from Napier Grass**

  This chapter deals with both in-situ catalytic and non-catalytic upgrading of bio-oil. In the former, it examines impact of zeolite based catalysts on the pyrolysis product distribution and characteristics. It discusses how catalyst/biomass ratio affected the product distribution and the quality of the resulting bio-oil. In the later, it evaluates experimental results of the synergism between Napier grass and other biomass species and the impact on yield and quality of product bio-oil.

- **Chapter Seven: Catalytic Upgrading of Bio-oil Derived from Napier Grass**

  This seven deals *ex-situ* upgrading of bio-oil. It examines impact of different zeolite-based catalysts on upgraded product distribution and characteristics. It discusses how other operating parameters affected the product distribution and the quality of the resulting upgraded bio-oil. It also evaluates experimental results of micro-lab fractionation of the upgraded bio-oil in to light, middle and heavy distillates.

- **Chapter Eight: General Conclusion and Recommendation for Future Studies**

  Chapter eight gives general concluding remarks of the overall thesis. It highlighted challenges encountered and proposes future studies.

CHAPTER TWO

2. LITERATURE REVIEW

2.1 Introduction

This chapter consists of three parts. The first part, section 2.2 provides an overview of composition of lignocellulosic materials, biomass pyrolysis process, pyrolysis reaction mechanisms. Section 2.3 gives an overview of Napier grass as a potential raw material for bioenergy production. It also presents a critical literature review on valorisation of Napier grass via pyrolysis, products distribution and characterization. Finally, section 2.4 dwells on review of different catalytic process of upgrading of bio-oil. It further discusses ways of improving the current bio-oil upgrading through zeolite cracking.

2.2 Composition of Lignocellulosic Biomass

Lignocellulosic materials exhibit different characteristics in terms of structural or compositional, chemical or elemental constituents. They consist of various complex organic materials and some amount of inorganic contents with different solid and fluid associated with one another (Vassilev et al., 2010; Vassilev et al., 2012). The organic phase of biomass consists of solid crystalline and amorphous matters (cellulose, hemicellulose, lignin and extractives). While the inorganic part is made up of minerals from phosphates, carbonates, silicates, chlorides, sulphates, oxyhydroxides, nitrates silicates, phosphates, hydroxides and various glasses, silicates. The fluid phase constitutes liquid, moisture and gas associated with both organic and inorganic matter (Vassilev et al., 2010; Vassilev et al., 2012). Cellulose, hemicellulose and lignin represent the major components of lignocellulosic biomass with percentage composition in the range of 85 to 95% while the remaining account for the organic extractives, inorganic materials and others. The proportion and composition of cellulose, hemicellulose and lignin varies depending on the plant species. For example, woody materials have more lignin and less cellulose and hemicellulose while reverse

is the case in herbaceous crops (Xu et al., 2013a & b). Cellulose is a linear homogeneous structural polysaccharide having D-glucose units with general formula $(C_6H_{10}O_5)_n$ with 1, 4-β-glycosidic bond and glucose dimer called cellobiose joined together with hemicelluloses and lignin (Haafiz et al., 2013; Brinchi et al., 2013; Collard and Blin, 2014). Each monomeric entity of cellulose is made up of triple hydroxyl group with tendencies of forming hydrogen bond (Maya and Sabu, 2008). Hemicellulose is a nonlinear heterogeneous polysaccharide consisting of different monomeric unit of sugars like L-arabinose, D-galactose, D-mannose, D-xylose, D-glucose unit and sugar acids which are inter-linked, linked to microfibrils of cellulose and has a chemical formula $(C_5H_{10}O_5)n$ (Burhenne et al., 2013; Collard and Blin, 2014). Lignin is made up of three different hydroxycinnamyl alcohol monomers such as p-coumaryl, coniferyl and sinapyl alcohols coupled haphazardly through ether linkage or carbon-carbon bond to form p-hydroxyphenyl (H), guaiacyl (G) and syringyl (S) type of lignin respectively. The chemical formula for H, G and S types are $(C_9H_{10}O_2)n$, $(C_{10}H_{12}O_3)n$ and $(C_{11}H_{14}O_4)n$ respectively. Lignin serves as cementing unit that binds the cellulose micro-fibrils together thereby providing mechanical strength (Heitner et al., 2010; Burhenne et al., 2013; Collard and Blin, 2014). A schematic representation of a lignocellulosic biomass is shown below (Figure 2.1).

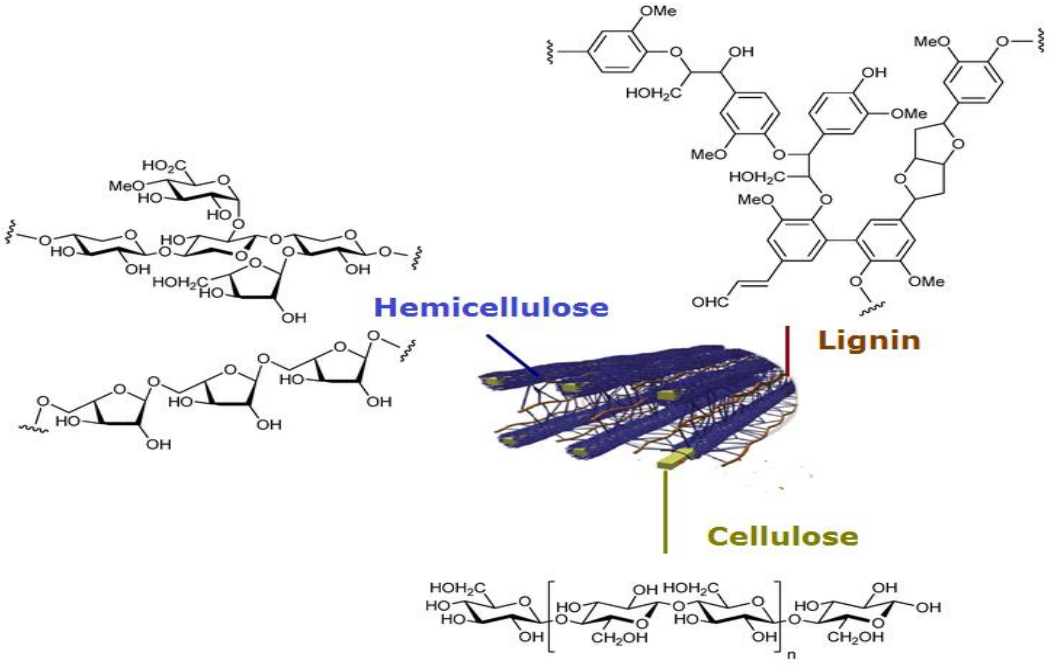

Figure 2.1: Model representation of cellulose, hemicelluloses and lignin in lignocellulosic biomass (adopted from Doherty et al., 2011)

2.3 Biomass Pyrolysis Reaction Mechanism

Pyrolysis is a thermochemical process in which materials are converted into solid (bio-char), liquid (bio-oil), and gaseous products (non-condensable) under an inert environment (Bridgwater, 2012; Eom et al., 2012). Generally, there are different types of pyrolysis namely; slow, intermediate and fast pyrolysis. Slow pyrolysis is also referred to as carbonization. It is carried out at a temperature up to 400 °C, for 60 min to days, with a typical product distribution of about 35% bio-char, 30% bio-oil, and 35% non-condensable gas. Fast pyrolysis can produce up to 80% bio-oil, 12% bio-char, and 13% non-condensable gas at temperature around 500 °C, with high heating rates, a short vapour residence time of about 1 s, and rapid cooling of volatiles (Bridgwater, 2012). For intermediate pyrolysis, the operating conditions are 500–650 °C and the

vapour residence time is approximately 10 to 30 s. About 40%–60% of the total product yield is usually bio-oil, 15%–25% bio-char and 20%–30% non-condensable gas. In addition, unlike fast pyrolysis, intermediate pyrolysis produce bio-oil with less reactive tar which can be used directly as a fuel in engines and boilers, and dry char suitable for both agricultural and energy applications (Kebelmann et al., 2013; Mahmood et al., 2013; Tripathi et al., 2016). Pyrolysis reactor represents the core unit of the entire pyrolysis process. It plays a very important role in the product distribution and accounts for about 10%–15% of the total capital cost (Bridgwater, 2012). A range of reactor designs are available, which include bubbling fluidized-bed, circulating fluidized-bed, fixed-bed, auger, ablative, and rotating cone. These reactors have been studied extensively to improve the efficiency of pyrolysis processes and the quality of bio-oil production. However, each reactor type has specific characteristics, pros and cons. In general, a good reactor design should exhibit high heating and heat transfer rates and should have an excellent temperature control capability (Bridgwater, 2012; Mohammed et al., 2016a). Pyrolysis of lignocellulosic biomass proceeds through a number chemical reactions which occur simultaneously. The mechanisms of the reactions are believed to originate from the decomposition of hemicellulose, cellulose and lignin of the biomass with each component displaying separate mechanism and reaction rate (Kan et al., 2016; Anca-Couce, 2016). This makes the process so complex to be represented by a single reaction model. To gain insight on the nature and type of reaction pathways occurring during pyrolysis of lignocellulosic materials, most researchers have focused on the classical investigation of the individual components as the foundation of the likely reaction mechanisms.

2.3.1 Pyrolysis mechanism of hemicellulose

Pyrolysis of hemicelluloses are rarely carried out and most studies employed the investigation of xylan, a major component of hemicellulose to represent hemicellulose (Collard and Blin, 2014; Kan et al., 2016; Anca-Couce, 2016). Decomposition of xylan consist of several pathways (Figure 2.2). At temperature between 150 and 240^{o}C, dehydration reaction is observed, resulting in water formation. Under this condition, fragmentation of methoxy, carboxylic and acetyl functional groups take place which lead to the corresponding formation of methanol, formic acid and acetic acid. Carbon IV oxides is also released during this period due to the decarboxylation reaction (Shen et al., 2010a; Collard and Blin, 2014). As temperature progresses beyond 240^{o}C up to 320^{o}C, pyrolysis proceeds via fast depolymerization which involve cleavage of the glyosidic bond between the monomeric units, leading to the formation of anhydrosugar (levoglucosan) and formation of unstable carbonyls and carboxylics which further undergo fragmentation and dehydration to produce water, carbon II and carbon IV oxides. Between 380 and 800^{o}C, the remaining solid (char) undergo transformation such as aromatization and demethylation which result in the formation of methane, hydrogen and carbon II oxide (Patwardhan et al., 2011; Collard and Blin, 2014).

2.3.2 Pyrolysis mechanism of cellulose

Cellulose pyrolysis reaction pathway has been widely reported in the literature, making it the most investigated component of the lignocellulosic biomass (Van de Velden et al., 2010; Collard and Blin, 2014; Kan et al., 2016; Anca-Couce, 2016). Pyrolysis of cellulose has been reported to be similar to that of hemicellulose. However, production of less char and more sugars are observed compared to the pyrolysis of hemicellulose

which is greatly influenced by the nature of mineral elements, stability of monomeric units and level of amorphous component (Anca-Couce, 2016).

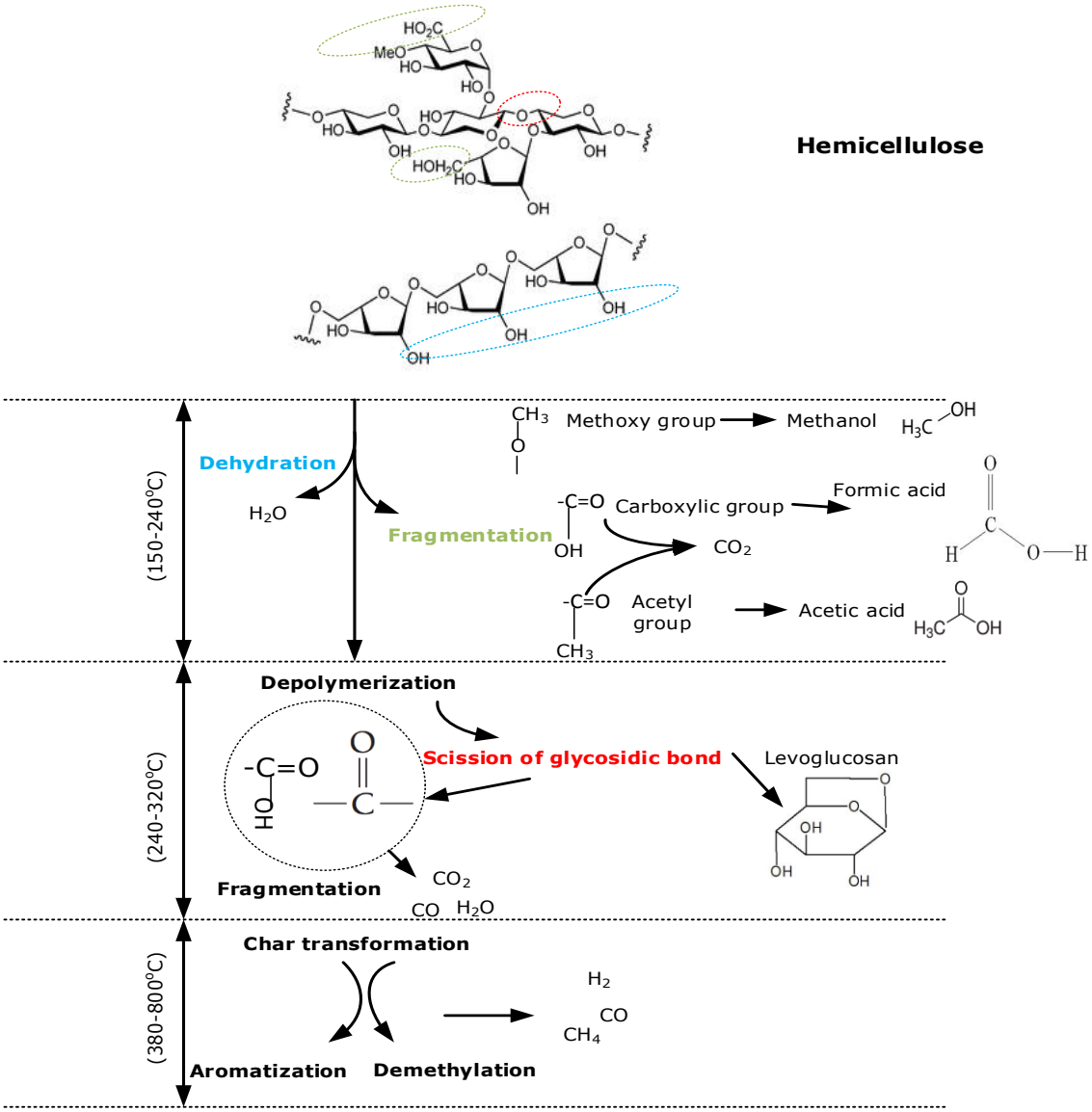

Figure 2.2: Schematic representation of pyrolysis pathway of hemicellulose (Collard and Blin, 2014; Anca-Couce, 2016)

Decomposition of cellulose progresses via dehydration, depolymerization, fragmentation and charring (Figure 2.3). Intermediate product known as anhydocellulose or active cellulose is produced at temperature between 150 and 300°C through dehydration or depolymerization reactions (Van de Velden et al., 2010; Collard and Blin, 2014). As the temperature progressed from 300°C to 390°C, fast depolymerization with several reactions occurring simultaneously. This result in high liquid yield (anhydro-oligosaccharides and anhydro-saccharides). Unstable carbonyls and carboxylics are also produced which further undergo fragmentation and dehydration to produce water, carbon II and carbon IV oxides (Shen and Gu, 2009; Wang et al., 2011; Collard and Blin, 2014). At temperature between 380 and 800°C, similar reaction pathways recorded in hemicellulose pyrolysis under this temperature range are observed (Patwardhan et al., 2011; Collard and Blin, 2014; Anca-Couce, 2016).

2.3.3 Pyrolysis mechanism of lignin

Thermal decomposition of lignin occurs over a wide-range of temperature as presented in Figure 2.4 due to its high thermal stability. At temperature between 180 and 245°C, a number reactions take place. Dehydration via the O-H groups and fragmentation of linkages between the monomeric units triggered the formation of water, formaldehydes, phenolics and the release carbon II and carbon IV oxides (Shen et al., 2010b; Mu et al. 2013; Collard and Blin, 2014). As the temperature increased above 300°C, carbon-carbon scission occurred resulting in the release of methane, aldehydes, acids and alkyl-phenols. Temperature between 360 and 400°C lead to disruption of aromatic rings which eventually produce phenols (Candelier et al., 2011; Huang et al., 2012; Mu et al., 2013; Collard and Blin, 2014). Disruption of methoxy group is said to

have also occurred at 400°C which result in methanol formation. Beyond 430°C, evolution of methane is observed. Aromatization of char via demethylation reaction release the non-condensables at temperature above 450°C. Further increase in temperature to 500°C and above produces hydrogen through redisposition of benzene rings (Collard and Blin, 2014).

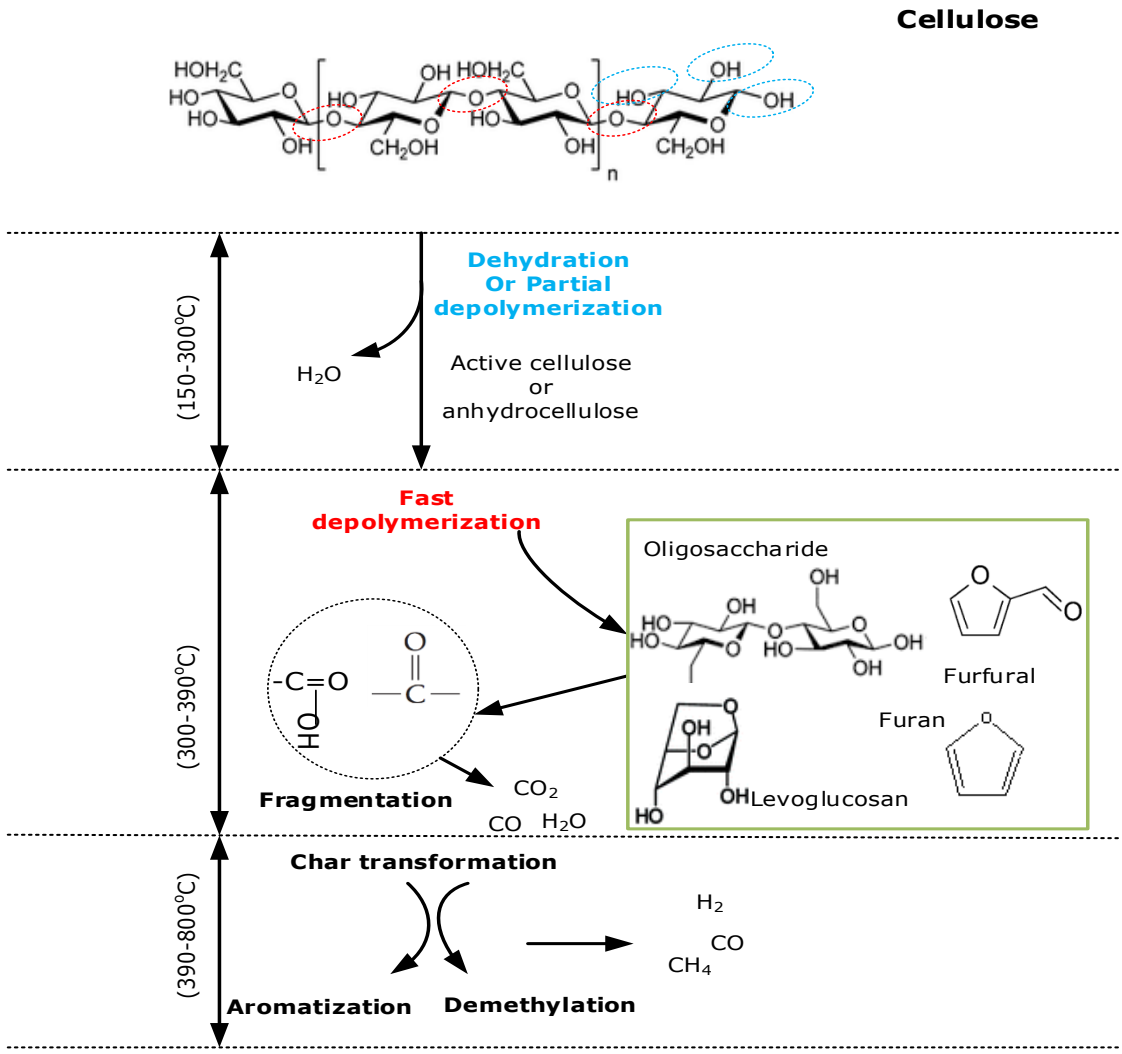

Figure 2.3: **Schematic representation of pyrolysis pathway of cellulose** Collard and Blin, 2014; Anca-Couce, 2016)

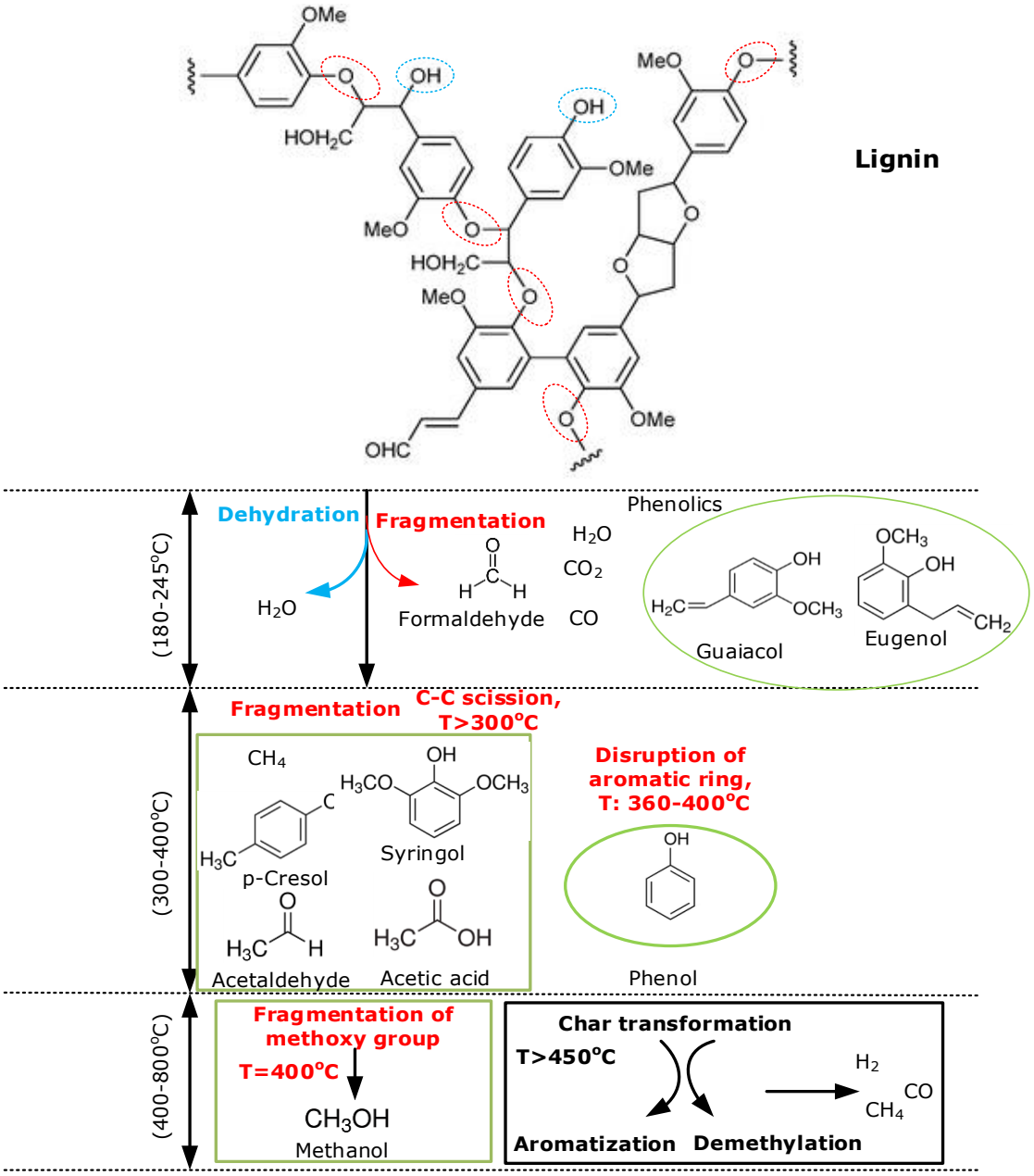

Figure 2.4: Schematic representation of pyrolysis pathway of lignin Collard and Blin, 2014; Anca-Couce, 2016)

Literature have shown that there is existence of interaction between the different components of the biomass during pyrolysis. Studies by Hosoya et al. (2007) on Cellulose-hemicellulose and cellulose-lignin interactions in wood pyrolysis at gasification temperature showed that there is substantial interaction between cellulose and lignin during pyrolysis. They observed that during cellulose-lignin pyrolysis, lignin enhanced the formation of low molecular weight products from cellulose and inhibited char formation while cellulose on the other hand deters formation of secondary char from lignin but promoted the yield of lignin-derived phenolics. They reported that no strong interaction between cellulose and hemicellulose during pyrolysis. Wang et al. (2011) reported that interaction between hemicellulose and lignin during pyrolysis favours production lignin-derived phenolics but inhibits formation of hydrocarbons. Contrary to the findings by Hosoya et al. (2007), they reported that there is strong interaction between hemicellulose-cellulose which promotes the formation of furans but inhibits production of levoglucosan. They also stated that the presence of cellulose favoured the yield of hemicellulose-derived acetic acid and furfural. In addition, mineral elements naturally present in the biomass also have significant impact on the reaction mechanisms (Kan et al., 2016; Anca-Couce, 2016). Consequently, simple addition of reaction mechanism of each component of the lignocellulosic biomass may not totally represent the actual mechanism of the lignocellulosic biomass pyrolysis. Additional challenges facing most of the pyrolysis reaction mechanisms reported in the literature are lack of inclusion of extractive decomposition and char formation steps, which are critical in biomass pyrolysis (Kan et al., 2016; Anca-Couce, 2016).

2.4 Kinetic Modelling of Biomass Pyrolysis

Many biomass decomposition kinetic models have been reported in the literature with different materials having dissimilar kinetic parameters such as frequency factor and activation energy. These variations could be mainly attributed to the diversity in the chemical make-up (cellulose, hemicellulose and lignin; volatile matter, ash and composition) of each material, operating condition used (particle size, heating rate, temperature, inert gas flow rate and reactor type) and reaction mechanism adopted. Studies by Chan et al. (1985) proposed pyrolysis mechanism for a lignocellulosic material according to the equation (2.1). The process consists of primary decomposition of biomass into gas, liquid and char and subsequent reaction of primary tar into secondary tar. Similar pyrolysis scheme has been proposed by many researchers such as Font et al. (1990); Di Blasi (2001); (2002) and (2008).

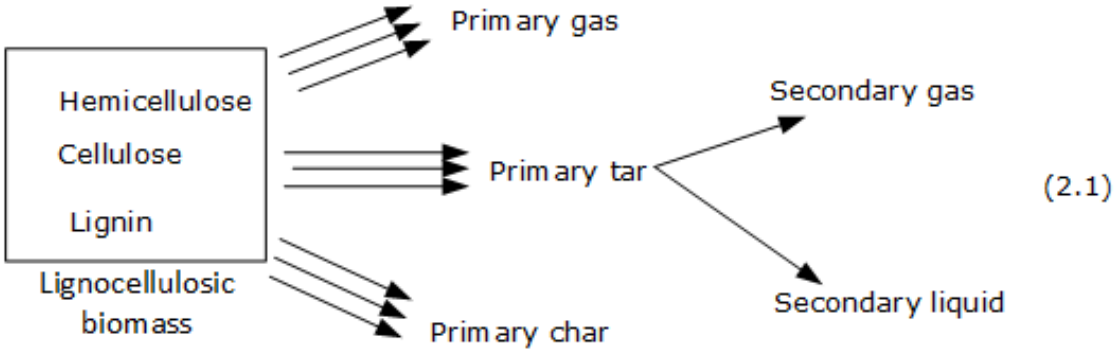

(2.1)

Recent studies have shown that kinetic analysis of a pyrolysis process can be examined by single step global model (SSGM) to evaluate the kinetic triplets such as pre-exponential factor, activation energy, and mechanism model. The SSGM is the simplest kinetics model which assumes that the decomposition rate of the pyrolysis process depends on an arbitrary reaction order according to reaction scheme represented in

equation (2.2). Generally, the rate of reaction for heterogeneous material in a thermogravimetric process is given by equation (2.3).

$$Biomass \xrightarrow{k} Volatile + char \tag{2.2}$$

$$\frac{d\alpha}{dT} = k(T)f(\alpha) \tag{2.3}$$

k(T) is the temperature dependent constant of the reaction; *f*(α) is the reaction mechanism model for an ideal reaction. T is the absolute temperature in Kelvin and α is the conversion, which is given by:

$$\alpha = \frac{m_0 - m_t}{m_0 - m_f} \tag{2.4}$$

m_0 is the initial sample mass; m_t is the sample mass at a specific time; m_f is the post-pyrolysis sample mass. By applying the Arrhenius law, the term k(T) in equation (2.3) becomes:

$$k(T) = Aexp\left(-\frac{E}{RT}\right) \tag{2.5}$$

where R is the ideal gas constant, which is 8.314 J mol^{-1} K^{-1}; A is the apparent pre-exponential factor in min^{-1} and E is the activation energy in J mol^{-1}. By applying linear non-isothermal condition with heating rate (β= dT/dt) and combining with equation (2.3), equation (2.5) turned to:

$$\frac{d\alpha}{dT} = \frac{A}{\beta} exp\left(-\frac{E}{RT}\right) f(\alpha) \tag{2.6}$$

Several model-free methods have applied equation (2.6) to estimate the kinetic parameters using multiple β for the thermogravimetric experiments. For a one-step decomposition process, model-free techniques like Ozawa-Flynn-Wall (OFW), Starink, Friedman and Kissinger–Akahira–Sunose (KAS) are used to evaluates E at various α without assumption of any specific reaction model (Vyazovkin et al. 2011). Based on the ICTAC Kinetics Committee recommendations published in Vyazovkin et al. (2011), an accurate estimation of E_α could be achieved from a modified Kissinger–Akahira–Sunose (MKAS) method formulated using Starink equation (Starink, 2003) as expressed in equation (2.7).

$$ln\frac{\beta_i}{T_{\alpha,i}^{1.92}} = Const - 1.0008\left(\frac{E_\alpha}{RT_\alpha}\right) \tag{2.7}$$

T_α and E_α are the temperature and apparent activation energy at a specific α, respectively. The value of E_α is evaluated from the slope of the linear graph of $ln\frac{\beta_i}{T_{\alpha,i}^{1.92}}$ versus 1/ T_α.

To evaluate reaction kinetic model *f*(α), some mathematical models that describes the solid-state reaction kinetics are employed as summarised in Table 2.1.

Table 2.1: Mathematical expression of an ideal reaction model in solid-state SSGM (Vyazovkin et al. 2011)

Models	Description	*f(α)*
Reaction order	First-order (L1)	$1 - \alpha$
	Second-order (L2)	$(1 - \alpha)^2$
	Third-order (L3)	$(1 - \alpha)^3$
Diffusion	1-D diffusion (D1)	$1/2\alpha$
	2-D diffusion (D2)	$[-\ln(1 - \alpha)]^{-1}$
	3-D diffusion-Jander (D3)	$[3/2(1 - \alpha)^{2/3}]/[1-(1 - \alpha)^{1/3}]$
	Ginstling-Brounshtein (D4)	$[3/2(1 - \alpha)^{1/3}]/[1-(1 - \alpha)^{1/3}]$
Nucleation	Avrami-Erofeyev (A1)	$2(1 - \alpha)[-\ln(1 - \alpha)]^{1/2}$
	Avrami-Erofeyev (A2)	$3(1 - \alpha)[-\ln(1 - \alpha)]^{1/3}$
	Avrami-Erofeyev (A3)	$1.5(1 - \alpha)[-\ln(1 - \alpha)]^{1/3}$
	Avrami-Erofeyev (A4)	$4(1 - \alpha)[-\ln(1 - \alpha)]^{3/4}$
Geometrical contraction	Contracting area (R2)	$2(1 - \alpha)^{1/2}$
	Contracting volume (R3)	$3(1 - \alpha)^{1/3}$
Power law	2/3-Power law (P2/3)	$(2/3)\alpha^{-1/2}$
	2-Power law (P2)	$2\alpha^{1/2}$
	3-Power law (P3)	$3\alpha^{1/3}$
	4-Power law (P4)	$4\alpha^{1/4}$

2.5 Pyrolysis of Napier Grass

Napier grass (*Pennisetum purpureum*) also known as elephant grass, Uganda grass. It is an underutilized herbaceous plant which can be cultivated up to four times in a year with a ratio of energy output to the energy input of around 25:1 and high biomass yield between 25 and 35 oven dry tons per hectare annually, which corresponds to 100 barrels of oil energy equivalent per hectare (Samson et al., 2005; Flores et al., 2012). Comparing with other energy grasses such as Miscanthus, switchgrass, these materials have only between 10 and 20 oven dry tons biomass yield per hectare per annum and require some nutrient input during cultivation (Richter et al., 2008; Cadoux et al., 2012; Imam and Capareda, 2012; Serapiglia et al., 2015; Ren et al., 2016;

Shemfe et al., 2016). Flores et al. (2012) have reported that Napier grass can be grown without any nutrient or fertilizer input. They evaluated the performance of two Napier grass species with and without application of nitrogen fertilizer under the Cerrado climatic condition (semi-humid tropical climate). Their findings revealed that the biomass yield was between 30 to 42 oven dry tons per hectare and showed no response to nitrogen fertilization. Recent study on environmental and economic benefit analysis of Napier grass has been reported by Tsai and Tsai (2016). Their result shows that Napier grass can mitigate CO_2 emissions to the order of 5 million Gg per annum. The energy equivalent was found to be 11 million barrels per 100 000 hectare annually which equals to 110 barrels of oil energy equivalent per hectare. This value strongly agrees with the findings reported by Samson et al. (2005); Flores et al. (2012). Cultivation of Napier grass follows conventional farming practices. It outcompetes weeds and therefore, requires lower establishment costs. This makes it one of the best potential energy crops for the development of efficient and economic bioenergy systems (Samson et al., 2005; Flores et al., 2012).

Recently, investigations have also shown that Napier grass can be incorporated into tree plantations such as oil palm, rubber tree plantations where there exist a large area of unused spaces, estimated at 26.63% of the total space (Zhou et al., 2012; Mohammed et al., 2015a). Field study conducted by Mohammed et al. (2015a) on intercropping of Napier grass with oil palm produced higher biomass yield. They reported that the plant showed more potential for higher dry weights in shaded conditions due to its elongated stem which contained more biomass than the higher leaf biomass produced in unshaded conditions, which also suggests higher efficiency in fixing atmospheric CO_2. This therefore offers another economic benefit.

Studies on chemical, thermal, structural, morphological and tensile characteristics of Napier grass fibre for biomaterial applications have been reported in the literature (Reddy et al., (2009) and (2012); Parasuram et al., 2013; Ridzuan et al., 2015). Some researchers have recently also reported the thermochemical properties of Napier grass with the aid of thermogravimetric analyser. Braga et al. (2014) evaluated thermal and kinetics parameters of the Napier grass biomass and compared the results with that of rice husk. They reported that Napier grass exhibited less ash content and higher proportion of volatile matter. It was also stated that less energy is required to decompose the structural building blocks of the grass relative to that of the rice husk. They concluded that Napier grass is more suitable for production of bio-oil via pyrolysis. However, this conclusion was not verified as bio-oil production was not actually carried out by the authors. Similar analysis was as well conducted by Fontes et al. (2014) but in this case, both thermal and catalytic pyrolysis characteristics of the grass were evaluated. The authors concluded that the catalytic thermogravimetric analysis of the Napier grass produced lower activation energy.

Utilization of Napier grass for the development of biofuels is very limited. Strezov et al. (2008) reported thermochemical conversion of Napier grass to bio-oil, bio-char and non-condensable gas using a pyro-probe type reactor. They investigated effect of heating rate (10 and 50 ^{o}C/min) on the pyrolysis product distribution. In each case, the system was ramped to a maximum temperature of 900 ^{o}C. The authors reported products distribution of 44.7 wt% liquid, 29.3 wt% solid, 26.07 wt% gas and 54.37 wt% liquid, 31 wt% solid, 14.68 wt% gas at 10 and 50 ^{o}C/min respectively under 500 ^{o}C pyrolysis temperature. Bio-oil collected was a two-phase liquid and analysed using gas chromatography-mass spectrometer (GC-MS) without separation into individual

phases. Although, a mixture of methanol and chloroform was used as solvent but there is high tendency of phase separation during the GC-MS analysis and the sample injected may not be the true representation of the whole bio-oil. The result of analysis revealed that the oil was made up of organic acids, phthalate esters, and larger fraction of various benzene chemicals, phenols and pyrans. The authors concluded that high heating rate of 50 ^{o}C/min promoted the formation of smaller acids and benzene fractions in the bio-oil compared to the low heating rate of 10 ^{o}C/min. Composition of the gas was mainly CO_2. Characteristics of the solid product collected was not evaluated.

Lee et al. (2010) reported pyrolysis of Napier grass in an induction-heating reactor. They investigated effect of heating rate between 50 and 200^{o}C/min and biomass particle size within 2mm at pyrolysis temperature of 500^{o}C. Their findings also showed that bio-oil yield increased with heating rate from 50 to 150 ^{o}C/min but declined thereafter. Maximum bio-oil yield of 36wt% was reported at 150 ^{o}C/min with 0.224 mm biomass particle size. The bio-oil yield was lower than those generally obtained from a fast pyrolysis system (50-60 wt %) and was attributed to the low level of heating rate used compared to the fast pyrolysis where up to 1000 ^{o}C/min is normally employed. This conclusion may not be valid as the study was conducted under a constant temperature of 500 ^{o}C which may not be the optimum temperature for complete de-volatilization of various structural components in the biomass. Pyrolysis product distribution is strongly related to the pyrolysis temperature and vapour residence time in the reactor compared to the heating rate (Bridgwater, 2012; Mohammed et al., 2015b). Their findings also reveal that the bio-oil was predominantly acetic acid, phenols, ketones, and nitrogenated hydrocarbons. These chemical species

are polar compounds and are generally present in the aqueous phase of the bio-oil. The major composition of the non-condensed gas reported were furans, olefins and mono-aromatic hydrocarbons (benzene, toluene and xylene). These compounds are expected to be in the condensate and this means that the cooling system used during the study was inefficient and thus, the composition of the bio-oil reported does not represent the whole condensables from the Napier grass.

A study recently conducted by Sousa et al. (2016) on pyrolysis of Napier grass in a fluidized bed reactor with a feed rate between 20 and 35 kg/h, temperature at around 500^{o}C. Maximum oil yield of 28.2 % was recorded. This yield was also far lower relative to a typical bio-oil yield (40-60 %) from a fluidized bed pyrolysis system. The authors attributed it to the accumulation of heavier fractions within the system before the cooling zone. The bio-oil composition reported had principally phenolics, organic acids and traces of levoglucosan and mono-aromatic hydrocarbons. H_2, CO, CO_2, CH_4 and C_2H_6 were the main component detected in the non-condensable gas. However, the yield and composition of the bio-oil collected may have been affected as the authors stated that air was employed as a fluidizing gas instead of an inert gas. Presence of oxygen during pyrolysis has great impact on the kinetics, products distribution and composition. Oxidative pyrolysis process lead to higher composition of CO, CO_2 and H_2O in non-condensable gas and lower yield organic compounds compared to pyrolysis in inert atmosphere (Anca-Couce, 2016). Furthermore, effect of other temperature levels and variations in the fluidizing gas velocity were not also investigated.

Similarly, De Conto et al. (2016) studied pyrolysis of Napier grass in a rotary kiln reactor where the effect of pyrolysis temperature and rotating speed of the reactor were investigated. Information regarding the bio-oil collected by the authors was only

limited to yield. Physicochemical properties and chemical compositions of the bio-oil were not carried out. Furthermore, the authors reported that the non-condensable gas analysed particularly at 600 ^{o}C was made up of high Hydrogen (H2)/Carbon monoxide (CO) ratio which was attributed to the temperature only. However, this may be a combined effect of temperature and vapour residence time in the reactor. From the reactor size and carrier gas flowrate reported by the authors, vapour residence was around 1.425 min (85 sec) which is long enough to result to severe secondary cracking of the pyrolysis vapour at such a high temperature. To date, no study on pyrolysis of Napier grass has been reported in the literature that deals with collective examination of pyrolysis temperature, heating rate, inert gas flowrate on the products distribution and composition. This investigation is needed in order to appropriately evaluate the energy potential of the biomass. Also, there is currently no any classical study on the upgrading of bio-oil derived from Napier grass.

2.6 Pre-treatment of Napier Grass and Subsequent Pyrolysis

Biomass generally is a complex organic material consisting of different degrees of cellulose, hemicellulose, lignin, extractives and minerals. The minerals constitute the ash forming elements which are inorganic in nature. They originate either directly from the fuel or incorporated during fuel handling and cannot be used as energy (Khan et al., 2009). During biomass conversion especially in thermochemical process like pyrolysis, these materials tend to retard conversions, yield and selectivity by promoting side reactions, which lead to the formation of undesired products (Di-Blasi, 2008**;** Jahirul et al., 2012). In addition, they also have high tendencies of causing operational challenges such as fouling, erosion, slagging and corrosion (Lim et al., 2012). Reduction of these inorganic components via a pre-treatment step prior to the

pyrolysis process will go a long way in improving the quality of the oil and life span of the equipment. There are several biomass pre-treatment methods depending on the conversion route and the desired end product. For thermochemical conversion process, hydrothermal, steam explosion, torrefaction and chemical pre-treatments are the most commonly used (Stephanidis et al., 2011; Biswas et al., 2011).

2.6.1 Hydrothermal pre-treatment

Hydrothermal pre-treatment is a non-catalytic aqueous pre-treatment method which involves the use of water as solvent at moderate temperature. Biomass is subjected to cooking under pressure, which enhances extraction of ash up to about 60-75% and sugars (Kim et al., 2009). Process parameters include liquid to solid mass ratio of 15, temperature of 190 ^{o}C, 8-10 minutes residence time, agitation speed of 150 rpm and reactor pressure of 180 psi (Stephanidis et al., 2011; Agbor et al., 2011). Hydrothermal pre-treatment can be regarded as cost effective as solvent cost is relatively very low and requires no post-treatment of effluent. In addition, leachate from this process may contain some amount of sugars from partial solubilisation of hemicellulose, which can be further processed to bioethanol via biochemical process. However, this method can be challenging in large scale operation since it requires large volume of solvent, which will generate corresponding volume of effluent. Proper control of temperature is also needed to avoid formation of degradation products (Agbor et al., 2011).

2.6.2 Steam explosion pre-treatment

Steam explosion of biomass has been carried out by many researchers. This technique was used in the past to extract cellulose for the production of ethanol. It separates hemicellulose, cellulose and lignin component of biomass via mechano-chemical

process, which involves adiabatic expansion of water inside the pore of biomass tissue and auto hydrolysis of the cell components (Biswas et al., 2011). Temperature and pressure between 160-240 ^{o}C and 0.7-4.8 MPa are normally used under few minutes reaction time (Olofsson et al., 2008). Recently, studies by Biswas et al. (2011) on steam explosion of salix wood chips at temperature between 205-228 ^{o}C and 6-12 min reaction time showed about 25 % ash reduction in the biomass. Steam explosion is characterized with release of phenolic compounds from the disruption of lignin, an important component of bio-oil and generation of toxic compound such as organic acids (acetic acid, formic acid and livulinic acid). Acetic acids are released from the acetyl groups in the hemicellulosic fraction while formic acid and livulinic acids are generated from degradation of furfural (Agbor et al., 2011).

2.6.3 Torrefaction

Torrefaction on the other hand, is a mild pyrolysis process usually carried out in an inert environment at a temperature between 200 and 300 ^{o}C for a certain period of time. Pre-treated sample from this approach is easier to handle, thereby making it less energy intensive. This technique is generally employed to improve the characteristics of a solid fuel relative to the original biomass for combustion and gasification applications (Chen et al., 2015).

2.6.4 Chemical pre-treatment

Chemical pre-treatment consists of those methods that use either alkali or mineral acid as solvent to effect changes in original state of biomass in order to improve pyrolysis reactions and product selectivity. Alkali pre-treatment results in disruption of ester and glycosidic side bond which lead to cellulose swelling and fractional decrystalization, incomplete solvation of hemicellulose and structural alteration of

lignin (Menon and Rao, 2012; Yang et al., 2015). The process is mostly conducted with dilute solution of sodium hydroxide (NaOH), $Ca(OH)_2$, ammonium hydroxide (NH_4OH) at temperature between 60-90 ^oC, 1-2 wt% liquid-solid ratio, 10-60 minutes retention time and pressure of about 1-3 MPa (Agbor et al., 2011; Menon and Rao, 2012; Yang et al., 2015). This approach cannot be considered suitable for a pyrolysis process since large portion of lignin is removed, which is an important component of the feedstock in the pyrolysis process. In addition, the cost of pre-treatment appears to be high due to consumption of the alkaline solvent and may requires recovery, thus adding extra cost to the entire process. In acid system, dilute solution of mineral acid such as sulfuric acid (H_2SO_4), hydrochloric acid (HCl), Phosphoric acid (H_3PO_4) is generally employed to eliminate ash and hemicellulose (Tan and Wang, 2009**;** Menon and Rao, 2012). In a typical acid pre-treatment, acid concentration of 0.2-2.5 wt%, temperature between 25 to 100 ^oC and retention time from few minutes to hours under agitation is used (Agbor et al., 2011). Acid pre-treatment releases leachate that is usually highly acidic and requires neutralization. Acid can cause corrosion to equipment and therefore need corrosion resistant materials for construction, which are general expensive (Agbor et al., 2011). Consequently, fundamental studies on pre-treatment of biomass are still needed for significant positive impact on the thermochemical process. The use of acid, alkaline and neutral aqueous pre-treatments of Napier grass, product characterization and their impacts on pyrolysis products distribution has not been reported in the literature, which is one of the objectives of this research.

2.7 Upgrading of Bio-oil

Bio-oil from biomass pyrolysis is a complex mixture consisting predominantly oxygenated organic compounds, phenolics, light hydrocarbons and traces of nitrogen

and sulphur containing compounds depending on the nature of source biomass. The high level of the oxygenated compound in the oil is responsible for its poor physicochemical characteristics such as low pH, low chemical stability, and lower energy content (Hew et al., 2010; Bridgwater, 2012; Mohammed et al., 2015a; Mohammed et al., 2016a). These properties make it unsuitable in most cases for direct application as fuel or refinery-ready feedstock for quality fuel production and other consumer products and therefore require further processing. Several bio-oil upgrading process have been proposed in the literature, which are performed either in-situ or ex-situ.

2.7.1 In-situ upgrading of bio-oil

Upgrading of bio-oil can be carried out in-situ with or without the use of catalyst. The in-situ catalytic upgrading is performed in a vapour phase with the aid of catalyst through a series of chemical reactions such as decarboxylation, dehydration, and decarbonylation where oxygen is removed in the form of CO_2, H_2O and CO prior to condensation of volatiles (Mohammed et al., 2016a). In this approach, the catalyst is mixed with the biomass or arranged in a parked bed after the pyrolysis reactor. Volatiles from the pyrolysing biomass pass through the catalyst bed where the deoxygenation reactions take place. The most commonly used catalysts in this process are zeolite-based materials, particularly ZSM-5, due to their high acidity, shape selective pore structure and high selectivity towards aromatic hydrocarbons. Process parameters governing the yield and quality of bio-oil produced via the in-situ upgrading include pyrolysis temperature, heating rate and catalyst-biomass ratio (CBR) (Jae et al., 2011; Park et al., 2015; Zhang et al., 2015; Gamliel et al., 2015; Yildiz et al., 2015; Liu et al., 2015). This method has been found to promote yield of

pyrolysis oil with improved physical and chemical properties (Mohammed et al., 2016a). Studies are ongoing in this direction particularly in terms of catalysts selectivity towards increasing the production specific value added green chemicals as well as reducing the formation of acids and carbonyl components in the pyrolysis oil (Thangalazhy-Gopakumar et al., 2011; Jae et al., 2011; Vichaphund et al., 2014; Zhang et al., 2015a; Park et al., 2015; Mohammed et al., 2016a). Study by Liu et al. (2015) on the catalytic pyrolysis of duckweed with HZSM-5 revealed that the pyrolysis temperature and CBR affected the distribution of organic component in the product bio-oil. A high temperature was shown to favour the production of total monocyclic aromatic hydrocarbons such as benzene, toluene and xylene (BTX) while polyaromatic hydrocarbons (PAH) such as indenes and naphthalenes decreased with an increase in pyrolysis temperature. This trend was attributed to the exothermic nature of the oligomerization reactions. Similar observations has been reported by Kim et al. (2015) during the in-situ upgrading of pyrolysis vapour from unshiu citrus peel over HZSM-5. Study by Ojha and Vinu (2015) on resource recovery from polystyrene through fast catalytic pyrolysis using a zeolite-based catalyst also followed a similar trend. In terms of CBR, Liu et al. (2015) stated that the increase in CBR promoted formation of BTX, while a downward trend was observed for PAH. This was contrary to the observation made by Ojha and Vinu (2015). They reported that an increase in CBR favoured production of benzene among the mono-aromatics while PAH yield increased with CBR. This difference in the observed trend could be linked to the characteristics of the respective catalysts used during those studies. Catalyst coking, catalyst regeneration and mass and heat transfer limitation are some of the inherent challenges facing this technique (Li et al 2015). Studies on the in-situ catalytic upgrading of bio-oil from Napier grass is very limited. Only recently, Braga et al. (2016) reported catalytic

upgrading of pyrolysis vapour from Napier grass using tungsten trioxide (WO_3) supported on rice husk ash and RHA-MCM-41 as the catalysts in a micro-reactor. The authors reported that phenols, furans, ketones and acetic acid were converted to monoaromatic hydrocarbons over WO_3/RHA at 600 °C and was attributed to the catalytic activity of WO_3. High CBR of 15 (wt/wt) was employed, which may not be practicable technically and economically. Mass balance on the pyrolysis product distribution was not accounted. This information is needed in order to evaluate the actual energy carrier resulting from the process. Therefore, there is need for further investigation so as to establish more detailed information on the yield and characteristic of pyrolysis oil from the in-situ catalytic upgrading of Napier grass pyrolysis vapour.

In-situ non-catalytic upgrading technique is also known as co-pyrolysis. Unlike the other in situ catalytic process where biomass pyrolysis and catalyst bed are in different reactors, which requires more energy, co-pyrolysis is similar to the traditional pyrolysis process, but more than one biomass materials are used as feedstock. This process has been identified as an efficient technique for improving the quantity and quality of the product bio-oil produced in a single reaction step. Successes of this technique have been linked to the synergistic effect of mineral components originally present in the individual biomass, which promote reaction of different biomass components and radicals during the pyrolysis (Abnisa and Daud, 2014). Co-pyrolysis of lignocellulosic biomass with other materials such as coal, waste plastics, tyres, sludge, papers, oils have been reported in the literature (Wu et al., 2016; Chen et al., 2016; Zaafouri et al., 2016). The results of these findings revealed that the product bio-oil had improved

chemical and physicochemical properties. In this process, all the pyrolysis products can be further utilized compared to the bed mixing of catalyst and biomass of the in-situ catalytic process, where bio-char application seem not possible due difficulty in separating the spent catalyst from the resulting bio-char. Studies on co-pyrolysis of NGS with other biomass species has not been reported in the literature, which is part of one of the objectives of this research.

2.7.2 *Ex-situ* catalytic upgrading of bio-oil

Ex-situ catalytic upgrading is any modification carried out on pyrolysis oil from the condensing volatiles with the aid of catalysts. This technique provides more process flexibility as the upgrading step can be manipulated and optimized individually. Several studies are currently being carried with main focus on the catalytic hydroprocessing using transition metal-based catalysts and catalytic cracking with the aid of porous materials (Mortensen et al., 2011; Bertero et al., 2012; Chaiwat et al., 2013; Karimi et al., 2014).

2.7.2.1 Catalytic hydroprocessing of bio-oil

Catalytic hydroprocessing comprises catalytic hydrocracking, hydrodeoxygenation, and hydrotreatment. These processes are usually employed in fossil oil refining for removal of sulphur and other unwanted components from refinery process streams with sulphated CoMo, NiMo, or NiW supported on high surface area carriers such as ɣ-alumina being the most commonly used catalysts (Mortensen et al., 2011; Bridgwater, 2012; Patel and Kumar, 2016). In case of bio-oil, this process modifies bio-oil into biofuel with improved physicochemical properties such low oxygen/carbon (O/C), high hydrogen/carbon (H/C) ratio and high calorific value (Mortensen et al., 2011; Bridgwater, 2012; Chaiwat et al., 2013; Karimi et al., 2014; Ahmadi et al., 2016;

Mortensen et al., 2016; Patel and Kumar, 2016). Oxygen in the bio-oil is removed in form of water through a series of catalytic reactions with hydrogen (Mortensen et al., 2011; Bridgwater, 2012). Hydrodeoxygenation (HDO) is an exothermic process usually conducted at high temperature (250-450^{o}C) and pressure (75 -300bar) (Mortensen et al., 2011). The high pressure is considered as a requirement for high hydrogen solubility in the oil in order to increase the rate of reaction and reduces coking formation in the reactor (Mortensen et al., 2011; Bridgwater, 2012). Two steps non-isothermal hydrotreatment (hydrotreater and hydrocracking) with sulfided ruthenium on carbon as catalyst has been reported to also promote the catalyst life time. The first step is a low temperature stage typically between 180-250^{o}C where high water content was observed in the product. The oil phase of this stage was used in the hydrocracking performed at lower pressure and higher temperature which gives product rich in oil with less moisture content compared to the earlier stage (Mortensen et al., 2011; Bridgwater, 2012). However, significant amount of hydrogen (3–5 wt% relative to bio-oil) is needed to achieved the said fuel quality and thus, making this option expensive for industrial scale application (Widayatno et al., 2016; Resende, 2016). In addition, hydrodeoxygenation is highly an exothermic process and can generate large amount of heat which may be difficult to handle. Catalyst deactivation suppression mechanism and sustainable sources of hydrogen require further understanding.

2.7.2.2 Catalytic cracking of bio-oil

Catalytic cracking of pyrolysis oil over porous materials such as zeolite (HY, mordenite, silica-alumina, silicalite, ZSM-5) is now receiving more attention (Cheng et al., 2014; García et al., 2015; Puertolas et al., 2015; Wang et al., 2016; Cai et al., 2016) . This

process requires no hydrogen and is similar to fluid catalytic cracking used in the fossil oil refinery where zeolite is also employed (Huber and Corma, 2007), hence the technical and economic advantages. ZSM-5 (MFI frame work) is extensively employed in the pyrolysis oil upgrading due to its uniqueness in terms of acidity and selectivity to hydrocarbons (Cheng et al., 2014; García et al., 2015; Puertolas et al., 2015; Wang et al., 2016; Cai et al., 2016). It is a microporous material in nature with a well-defined pore structure which selectively allows diffusion and conversion of molecules (Mante et al., 2014). Application of ZSM-5 for deoxygenation of pyrolysis has been reported in the literature. Studies by Vitolo et al. (2001) on the catalytic cracking of pyrolysis oil produced from wood with ZSM-5 (2g) at temperature between 410 and 450^{o}C in a fixed bed micro-reactor with a feed flow rate of 5.9 ml/h reveal that upgrading reactions such as decarboxylation, decarbonylation, cracking, aromatization, alkylation, isomerisation, cyclisation and oligomerization proceed *via* carbonium ion mechanism which occurred at the acidic sites (Brùnsted acid sites) of the ZSM-5. Coke and tar were also observed as co-products from the catalytic reaction which led to the catalyst poisoning. The upgraded products recorded with fresh ZSM-5 was 11.3 wt% organics, 28.9 wt% aqueous, 47.7 wt% non-condensable and 11 wt% solid. Recently, Saad et al. (2015) reported catalytic cracking of pyrolysis oil derived from rubber wood in a dual reactor using ZSM-5 (3.2 g) at 511 ^{o}C with feed rate of 1.4g/min. They observed the highest organic product yield of 13.36 wt% with 44.93 wt% aqueous phase. Despite the use of dual reactor system, which was meant to reduce coke formation, solid product as high as 29.2 wt% was recorded. They concluded that the low yield of upgraded organic product was due to poor physicochemical properties of the raw pyrolysis oil used.

2.7.3 Catalyst deactivation

Catalyst deactivation during catalytic cracking of bio-oil with ZSM-5 remains a challenge. Oxygen-containing chemical species such as guaiacols, furanic rings and sugars in the pyrolysis oil are perceived to result in coke formation during upgrading due to their instability and deficiency in molar balance (Mahfud et al., 2007; Yan and Le Van Mao, 2010; Duan et al., 2013; Zhang et al., 2014). The coke precursors are said to undergo polymerisation and polycondensation on the catalytic surface, fill up the inner pores of zeolite catalyst and eventually result in the catalyst deactivation (Mortensen et al., 2016; Wei et al., 2016). Researchers have suggested that lignin-derived compounds are more susceptible to char and coke formation during cracking and upgrading of bio-oil derived from lignocellulosic biomass compared to compounds from hemicellulose and cellulose (acid, aldehydes, ketones, ester, and sugars). This was attributed to the complex structure and the bulkiness of the lignin derivatives, which make them too large for the pores of the ZSM-5 catalyst (Zhang et al., 2015b; Wei et al., 2016). Recent studies by Wei et al. (2016) on catalytic cracking of pure phenol and guaiacol as model compounds over ZSM-5 reveal that less catalytic coke was formed with the model compounds compared to the pyrolysis oil. They proposed that there are possible interactions between the derivatives of hemicellulose and cellulose with the lignin-derived compounds during the upgrading reactions. They further investigated cracking of pure pyrolysis oil mixed with 50wt% methanol and phenolic-rich pyrolysis oil fraction mixed with methanol in order to evaluate the ZSM-5 coking condition and hydrocarbon yield. The result shows that the later feedstock produced more hydrocarbon and less coke compared to the former. They concluded that small active molecules are also responsible for the catalyst coking by adhering to the active sites in the pores. Coke deposition on the catalyst during catalytic

valorisation of bio-oil has been identified to be of two categories, catalytic carbon and thermal carbon (Gayubo et al., 2010; Zhang et al., 2011) as shown in Figure 2.1. The catalytic carbon is formed as a result of chemisorption of poisons such as amines and nitrogen-containing heterocyclic compounds, unsaturated and other heavy hydrocarbons on the microstructures of the catalyst due to condensation, hydrogen transfer, and dehydrogenation reactions (Argyle and Bartholomew, 2015). On the other hand, the thermal carbon is the coke formation on the catalysts matrix as a result of high reaction temperature. Both catalytic and thermal carbon can lead to either partial or complete loss of catalytic activity (Zhang et al., 2011; Ibáñez et al., 2014; Argyle and Bartholomew, 2015).

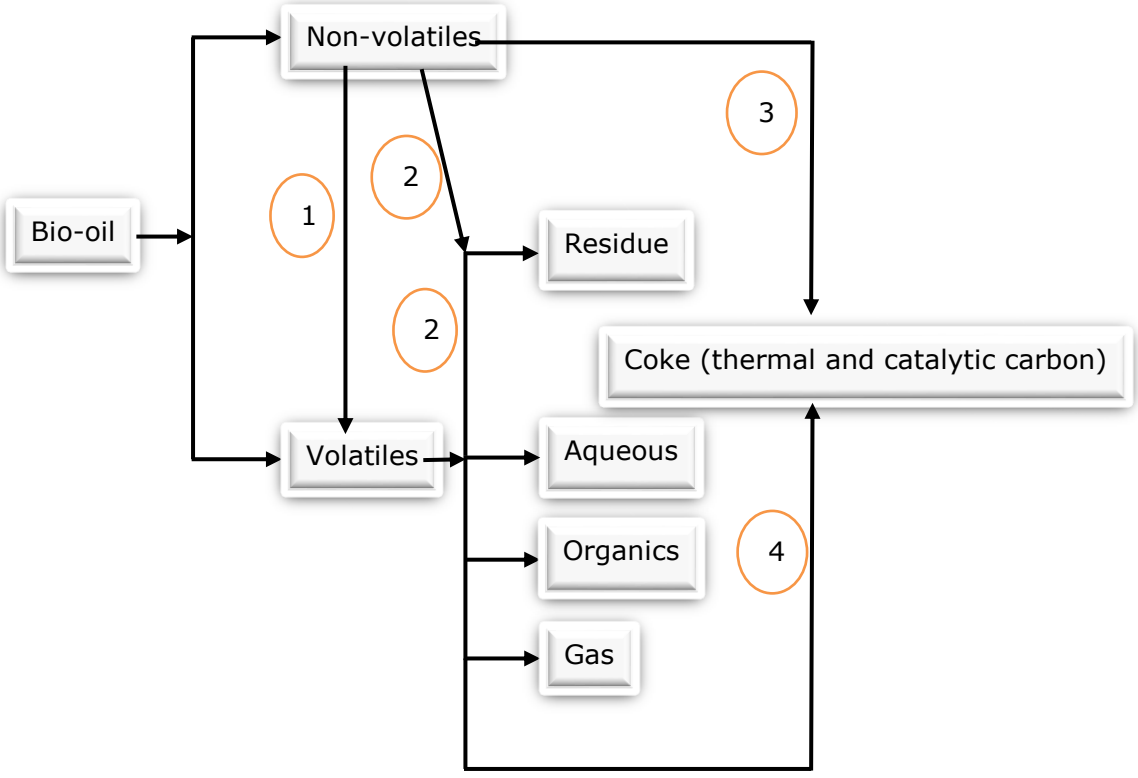

Figure 2.5: Bio-oil deoxygenation scheme showing coke routes adopted from Mortensen et al., (2011). Reactions: (1) cracking; (2) polymerisation; (3) polycondensation (thermal carbon); (4) dehydrogenation, condensation, hydrogen transfer (catalytic carbon)

2.7.4 Zeolite deactivation suppression mechanism

Studies aimed at minimizing catalyst deactivation is as old as the catalytic process development and searching for long-lasting solutions are in progress to ensure industrial process scale-up. Structural modification of zeolite is being given considerable attention in recent time as a solution to coke formation by diffusion limitation (García et al., 2015). Researchers have shown that modification (demetalation) of zeolite in an alkaline medium produced a partial collapse of the zeolite network into more than one level of porosity (micro and mesoprousity) with a network of interconnected cavities and cylindrical channels located in both outer and inner portions of the zeolite crystals (Na et al., 2013; García et al., 2015). The resulting solid from the alkaline treatment tends to exhibit significantly enhanced accessibility of the active site, remarkable hydrothermal stability and longevity of the catalyst as a result of reduction in size of the purely microporous domains and facile diffusion of coke precursors through the mesopore, in addition to retaining the other zeolitic properties of its parent material (Kim et al., 2012; Na et al., 2013; Li et al., 2014a; García et al., 2015). This method is therefore considered as an attractive top-down approach for the development of hierarchical zeolites with superior properties to meet their applications in catalytic cracking processes particularly in the area of upgrading of alternative renewable biofuel (Pérez-Ramírez et al., 2011).

Application of hierarchical mesoporous ZSM-5 in catalytic deoxygenation of pyrolysis vapour have shown significant selectivity and improvement in the quality of pyrolysis oil (Aho et al., 2010; Yu et al., 2012; Lee et al., 2014; Li et al., 2014b; Gamliel et al., 2016). For ex-situ upgrading studies over hierarchical mesoporous ZSM-5, most researchers have focused on the use of synthetic or model bio-oil compounds as a

basis for evaluating the catalyst performance. Botas et al. (2014) reported catalytic deoxygenation of rapeseed oil using hierarchical mesoporous zeolite modified with nickel. The study was conducted in a fixed bed reactor at 550 ^{o}C within reaction time of 180 min under nitrogen atmosphere. The result showed that the upgraded product was free of oxygenated compound. The authors observed reduction in coke formation and was attributed to the improved catalyst pore structure due to enhanced accessibility and mass transport. The catalyst was highly selective to formation of olefins at elevated temperature compared to aromatics. Tian et al. (2016) studied comparative performance of methanol conversion to aromatic over hierarchical mesoporous ZSM-5, microporous ZSM-5 and nonporous ZSM-5. The reaction was conducted in a fixed bed reactor at 550 °C and 1.95 g MeOH g Cat^{-1} h^{-1} weight hourly space velocity (WHSV). Their findings revealed that mesoporous ZSM-5 exhibited superior property (higher conversion capacity and lower deactivation coefficient) over the remaining catalysts. Total conversion of methanol to aromatic was achieved with mesoporous ZSM-5 over 11 hours relative to micro and nanoporous ZSM-5, which lost activity at end of 2 hours and 6 hours respectively. The author ascribed the outstanding performance of mesoporous ZSM-5 to its ordered structure, which permits the full access to acid sites in addition to promoting mass transport that eventually reduced coke formation. Catalytic cracking of canola oil was also carried out by the author over these set of catalysts and similar trend of catalytic activity was observed. 82.7 wt% conversion was achieved with mesoporous ZSM-5 with high selectivity for light olefins (26.9 wt%) while 60.2 and 37.0 wt% conversion was attained with nanoporous and microporous ZSM-5 respectively and the corresponding yield of light olefins was 16.4 and 10.1 wt%.

Recently, Puertolas et al. (2015) reported ex-situ upgrading of pyrolysis oil derived from pine wood to aromatics over hierarchical mesoporous ZSM-5. The study was conducted in a fixed bed reactor at 450 ^{o}C. The upgraded bio-oil over mesoporous ZSM-5 exhibited better physicochemical properties relative to the parent ZSM-5. The catalyst promoted the production of monoaromatic hydrocarbon such as benzene, toluene and xylene (BTX) while decrease in the amount of phenolics, acids, ketones were observed in the upgraded bio-oil. The formation of aromatics was linked to the increased accessible acid sites present at the mesopore walls and external surface. Higher composition of CO in the non-condensable gas with the mesoporous ZSM-5 was observed compared to the parent ZSM-5. The amount of CO in the gas showed a strong linear relationship with the amount of aromatics in the upgraded bio-oil. The authors concluded that mesoporous ZSM-5 favoured decarbonylation reaction compared to the parent ZSM-5, which promoted dehydration reaction. Similarly, deoxygenation of bio-oil derived from wood over metal loaded hierarchical mesoporous ZSM-5 was recently reported by Veses et al. (2016). Catalytic activity of metal loaded hierarchical mesoporous ZSM-5 was compared with that mesoporous ZSM-5. The result showed comparable product distribution. About 57 wt% total liquid, 21 wt% gas and 21 wt% char was recorded with mesoporous ZSM-5 while the metal loaded mesoporous ZSM-5 had 56-60 wt% liquid, 19-22 wt5 gas and 19-22 wt% char. Although, maximum organic phase oil yield relative to the feed bio-oil was achieved (41 wt%) with the metal loaded mesoporous ZSM-5 compared to the mesoporous ZSM-5, which produced about 35 wt%. The corresponding degree of deoxygenation achieved was 42.6% and 35%. However, from the result presented by authors, the upgraded oil produced over mesoporous ZSM-5 had lower phenolics, acid, aldehyde and ketones in addition to higher monoaromatic hydrocarbons and lower polyaromatic hydrocarbons. It can be

seen that upgraded bio-oil over mesoporous ZSM-5 has higher potential to be converted to fuel and valuable chemicals. The presence of less acid and other oxygenate in the oil are general requirement for avoidance of side reactions during storage, prior to further processing to fuels. Monoaromatic are high valuable chemicals and have commercial application in the petrochemical industry while the low amount of polyaromatic hydrocarbons signifies that the oil is less toxic.

Reaction pathways in ex-situ catalytic upgrading towards formation of specific products such as saturated hydrocarbons, olefins, monoaromatic hydrocarbons are still not well established due to the diverse component in the raw pyrolysis oil. Currently, only few classical studies are available in literature particularly with the application of hierarchical mesoporous ZSM-5 in the refinement of the actual pyrolysis oil. In order to develop more realistic ex-situ upgrading process, there is need for further investigations. Furthermore, catalytic upgrading of pyrolysis oil derived from Napier grass over both microporous and hierarchical mesoporous ZSM-5 has not been reported, which is the one of the objectives of this research.

2.8 Conclusion

Valorisation of Napier grass via pyrolysis is currently limited to very few classical studies. Collective evaluation of pyrolysis process parameters on products distribution derived from Napier grass biomass and subsequent assessment of bio-oil, bio-char and non-condensable are needed in order to fully examine the biomass potential for bioenergy production. Certainly, no study currently available on the catalytic upgrading of bio-oil derived from this biomass specie. Therefore, in the following chapters, this study provides comprehensive assessment of pyrolysis of Napier grass biomass, pyrolysis products and parameter optimization for optimal bio-oil production. It

subsequently evaluates impact of pre-treatment of Napier grass on pyrolysis product distribution and characteristics, conversion of bio-oil derived from Napier grass into high-grade bio-oil through in-situ and ex-situ upgrading process using microporous and hierarchical mesoporous ZSM-5.

CHAPTER THREE

3. EXPERIMENTAL METHODOLOGY

3.1 Introduction

This chapter outlines the materials and methods used in this research. It outlines all the analytical techniques and instruments used in material characterization and modifications, production and products evaluation. It also specifies the statistical method and software used for the experimental data analysis and optimization of process parameters.

3.2 Materials

3.2.1 Chemical reagents and biomass

Chemical reagents, Zeolite catalyst used in this study were of analytical grades purchased from various sources, such as Fisher Scientific Sdn. Bhd. Selangor, Malaysia, Sigma-Aldrich Sdn. Bhd. Selangor, Malaysia or Evergreen Engineering and Resources Sdn. Bhd. Selangor, Malaysia. Locally grown Napier grass at the Crops for Future (CFF) research centre field (2°56'07.6"N 101°52'42.8"E) Semenyih, Malaysia, was used as biomass feedstock. Fresh Napier grass stem (NGS) samples (around 3 cm long) were collected and assessed as received as shown in Figure 3.1. This material was dried at 105 °C in an electrical oven to a constant weight in accordance to the British Standard, BS EN 14774-1. Subsequently, the dried samples were shredded in a Retsch® rotor beater mill (SM100, Retsch GmbH, Germany) to particle sizes between 0.2 mm and 2.5 mm and stored in air tight plastic bags for further analysis.

Figure 3.1: Pre-processing of Napier grass. (1) Napier grass on the field (2) chopped Napier grass stem (NGS) in the dryer (3) Rotor beater mill (4) Ground Napier grass biomass

3.3 Methods

3.3.1 Proximate and ultimate analyses of biomass

Proximate and ultimate analyses on dry basis were carried out according to the relevant standard procedures. Volatile matter and ash content were determined following BS EN 15148 and BS EN 14775 respectively**.** Fixed carbon was computed from the remaining bone dry sample mass**.** Major inorganic elements in the ash were determined according to BS EN 15290. About 500mg (0.2 mm) homogenized samples

were placed in a digestion tube (42 x 3OOmm Fovorit, PLT Scientific Sdn. Bhd. Selangor, Malaysia). Hydrogen peroxide (H_2O_2: 30 %, 3.0 mL) (Fisher Scientific Sdn. Bhd. Selangor, Malaysia), nitric acid (HNO_3: 65 %, 8.0 mL) and hydrofluoric acid (HF: 40 %, 1.0 mL) (Fisher Scientific Sdn. Bhd. Selangor, Malaysia) were added and the vessel was closed after a reaction time of 5-10 min to avoid pressure build up. Another tube was treated in the same manner but with no biomass sample (blank). The tubes were arranged with the aid of retort stands in a metallic container filled with silicon oil mounted on a hotplate. The level of silicon oil was adjusted so that it covers the entire section of the tubes containing the samples. The system was gradually heated to 220 ^oC over 60 min and held for another 60 min. The system was then cooled to room temperature and subsequently, boric acid (H_3BO_3: 4 %, 10.0 mL) (Fisher Scientific Sdn. Bhd. Selangor, Malaysia) was added to neutralize the HF. The mixture was reheated rapidly to 180 ^oC and held for 15 min. after cooling to room temperature, the mixture (digest) was transferred to 250 mL plastic bottles. The digestion tubes were carefully rinsed with deionized water (Milli-Q® type 1 ultrapure water) such that the total volume of the digest in the plastic bottles was 200 mL. Standard solution of each analyte was prepared at various concentrations for calibration graph and the corresponding response (absorbance) was determined using atomic absorption spectrometer (AAS) (Analyst 400, Perkin Elmer Sdn Bhd, Selangor, Malaysia). Absorbance of the analytes in blank and digest were also determined and the corresponding concentration calculated using equation 3.1

$$w_i = \frac{(C_{is} - C_{ib}) \times V}{m} \qquad (3.1)$$

Where w_i is the concentration of the element in the sample (mg/kg), C_{is} and C_{ib} are the concentration elements in the diluted digest (mg/L) and blank sample respectively. V is the total volume of the diluted digest (200 mL) and m is the mass of the biomass sample used (0.5 g)

Biomass higher heating value (HHV) was determined using an oxygen bomb calorimeter (Parr 6100, Parr Instruments, Molin, USA). Elemental compositions such as carbon, hydrogen, nitrogen, sulphur and oxygen (CHNSO) were determined using CHNS/O analyser (2400 Series II CHNS/O analyser, Perkin Elmer Sdn Bhd, Selangor, Malaysia). Chemical functional group was evaluated with Fourier transform infrared spectroscopy (Spectrum RXI, PerkinElmer, Selangor, Malaysia). Potassium bromide (KBr) (Fisher Scientific Sdn. Bhd. Selangor, Malaysia) disc (13 mm diameter translucent) was made from a homogenized 2 mg sample in 100 mg KBr using a bench press (Carver 43500, Carver Inc.,USA) by applying 5.5 tones load for 5 min. Spectra were recorded with Spectrum V5.3.1 software within wave number range of 400 to 4000 cm^{-1} at 32 scans and a resolution of 4 cm^{-1}. Structural analysis of the biomass was performed using High-performance liquid chromatography (HPLC-1260 infinity, Agilent Technologies Sdn Bhd, Selangor, Malaysia) according to the Analytical Procedure outlined by National Renewable Laboratory NREL/TP-510-42618. Thermogravimetric analysis was carried out in thermogravimetric simultaneous thermal analyser (TGA) (STA 6000, Perkin Elmer Sdn Bhd, Selangor, Malaysia) in nitrogen atmosphere at 20 mL/min. About 10 mg (particle size of 0.2 mm) of samples were used. Samples were heated from ambient to 100 ^oC at 10 ^oC/min and held for 30 min to allow evaporation of physically absorbed moisture. Thereafter, each sample was heated to 900 ^oC under the same condition.

3.3.2 Pyrolysis and products characterization

Pyrolysis study was conducted either in horizontal or vertical fixed bed pyrolysis system as shown in Figure 3.2 (a) and (b). For samples below 100g, horizontal system was used while samples of a mass of 200 g were tested in a vertical system. The vertical pyrolysis system consists of a fixed bed reactor made of stainless steel (115 cm long, 6 cm inner diameter), a distribution plate of a 1.5mm hole diameter which is placed at 25 cm from the bottom of the tube, two nitrogen preheating sections, a cyclone, oil collector, gas scrubbers and water chiller operating at 3 ^{o}C attached to a coil condenser. Biomass sample (bone dried, 2.5 mm particle size) was placed on a gas distribution plate inside the reactor tube. The setup was heated in a vertical furnace at certain heating rate and under nitrogen atmosphere. The reaction temperature was monitored with a thermocouple (K-type, NTT Heating, Sdn Bhd, Selangor, Malaysia). The reaction time was kept at 60 min after the temperature attained the set-value. Pyrolysis vapour was condensed by passing through a condenser attached to the water chiller and condensate (bio-oil) was collected in a container. Bio-oil, bio-char and non-condensable gas yields were calculated using Equation (3.2), (3.3) and (3.4). The experiment was repeated in triplicates and standard deviations were computed.

$$\text{Yield(wt \%)}_{\text{bio-oil}} = \left[\frac{\text{weight of bio-oil collected}}{\text{weight of biomass feed}}\right] \times 100 \qquad (3.2)$$

$$\text{Yield(wt \%)}_{\text{bio-char}} = \left[\frac{\text{weight of bio-char collected}}{\text{weight of biomass feed}}\right] \times 100 \qquad (3.3)$$

$$\text{Yield(wt \%)}_{\text{N/gas}} = 100 - \left[\text{Yield(wt \%)}_{\text{bio-oil}} + \text{Yield(wt \%)}_{\text{bio-char}}\right] \qquad (3.4)$$

The difference between the two pyrolysis systems are the reactor tube orientation and the absence of cyclone and distribution plate in the horizontal pyrolysis set up. In this case, the sample was placed at the centre of the tube and all other protocols were carried out in similar manner to the vertical arrangement.

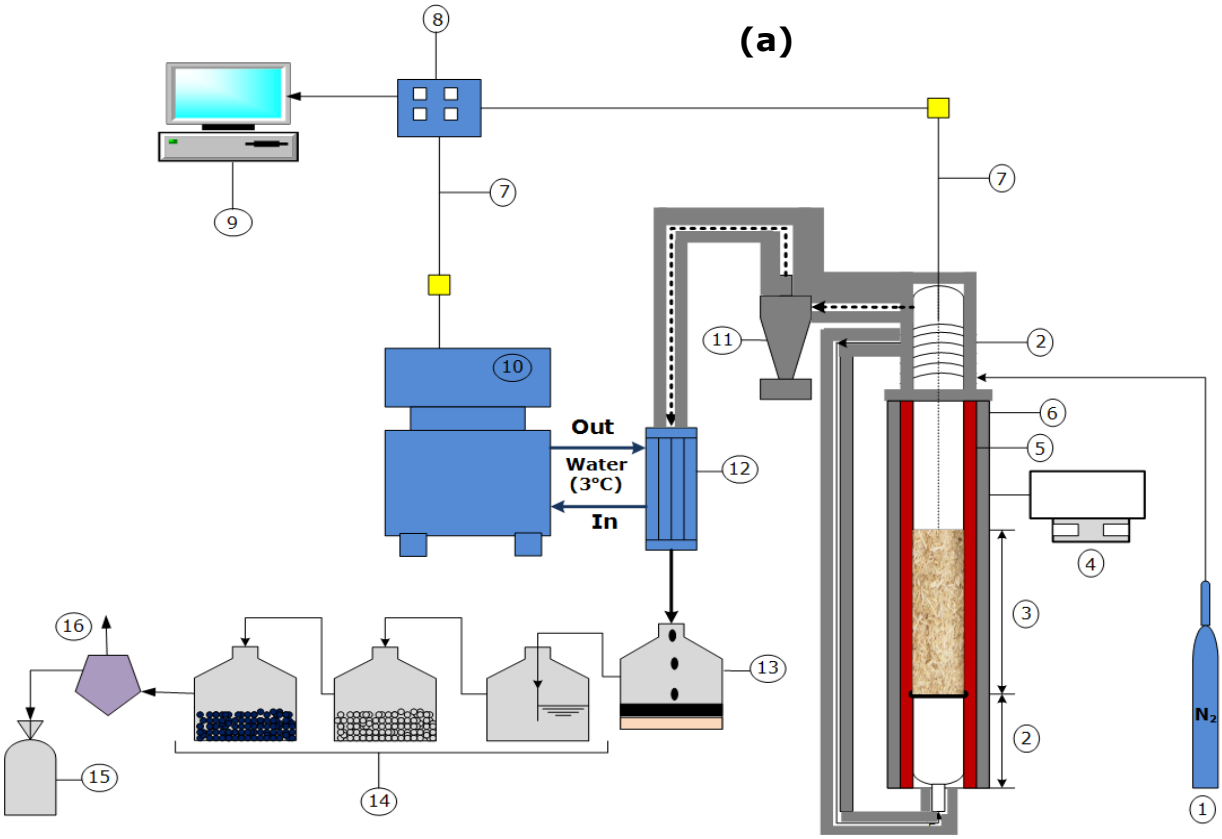

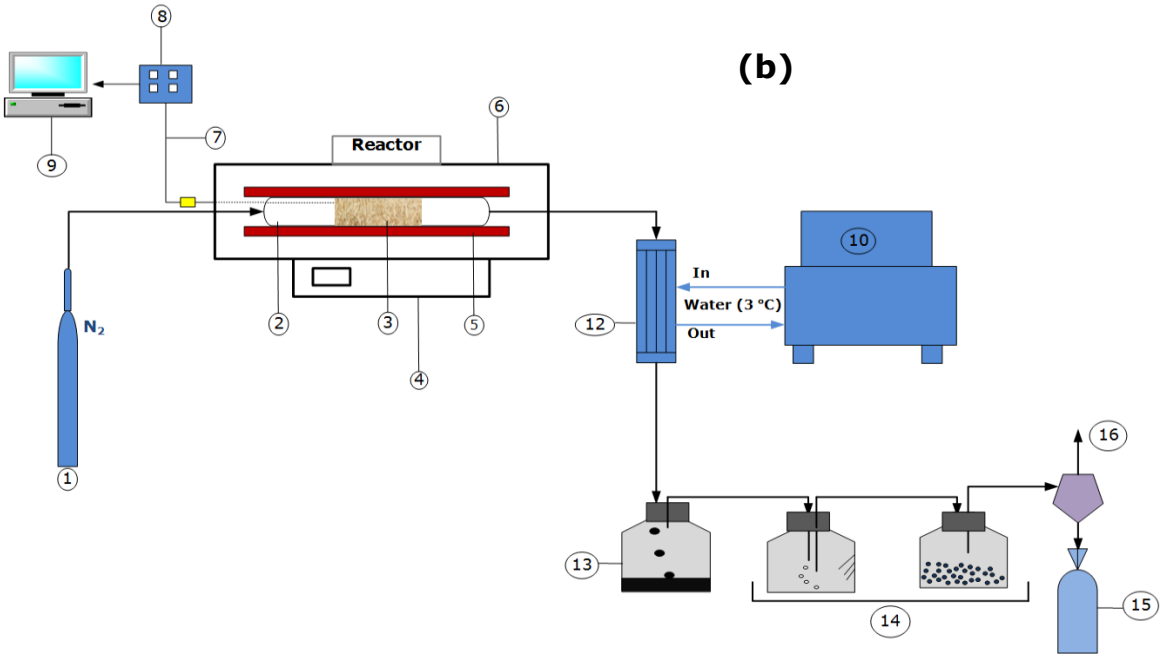

Figure 3.2: Pyrolysis system. (a) Vertical pyrolysis rig; (b) horizontal pyrolysis set-up. (1) Nitrogen cylinder, (2) nitrogen preheating sections, (3) pyrolysis section, (4) furnace controller, (5) heater, (6) insulator, (7) thermocouples, (8) data logger, (9) computer, (10) water chiller, (11) cyclone, (12) condenser, (13) bio-oil collector, (14) gas scrubber, (15) gas sampling bag, (16) gas venting

Characterization of bio-oil, bio-char and non-condensable gas were carried out accordingly using analytical instruments Physicochemical properties of bio-oil such as pH, water content, density and viscosity were analysed with a WalkLAB microcomputer pH meter (TI9000, Trans Instruments, Singapore), Karl Fischer V20 volumetric titrator (Mettler Toledo, Columbus, OH, USA), Anton Paar density meter (DMA 4500 M, Ashland, VA, USA) and Brookfield viscometer (DV-E, Hamilton, NJ, USA) respectively. Solid content of the organic phase was determined as ethanol insoluble. Bio-oil concentration of 1.25 wt% (1 g of bio-oil sample in 80 g of ethanol) was used. The mixture was agitated and then filtered using 0.1µm filter. The filter and retentates was thereafter oven dried at 105°C for 30 min. CHNSO, heating value and FTIR analyses

of bio-oil were carried out using the analytical instruments described in the feedstock characterization. A demountable cell windows (LLC circular KBr cell window pair: 25mm diameter, 4mm thickness; PerkinElmer, Selangor, Malaysia) was used in the FTIR analysis of bio-oil. Approximately 0.1 mL of bio-oil sample was placed on the KBr window and 0.20 mm round Teflon spacer was used in between the windows to allow for path length. Fractionation of the organic phase bio-oil was simulated using TGA in nitrogen atmosphere at 20 mL/min, temperature was increased at a rate of 10 ^{o}C/min from ambient to 500 ^{o}C, to examine the volatile fractions, and the result was compared with simulated distillation of fossil-gasoline, kerosene and diesel. Detail of the chemical composition of the bio-oil was determined using a gas chromatograph-mass spectrometer (GC-MS) (PerkinElmer Clarus® SQ 8, Akron, USA) with a quadruple detector and column (30 m x 0.25 mm x 0.25 µm) (PerkinElmer-Elite™-5ms, Akron, USA). The oven was programmed at an initial temperature of 40 °C, ramp at 5 °C /min to 280 °C and held there for 20 min. The injection temperature, volume, and split ratio were 250 °C, 1 µl, and 50:1 respectively. Helium was used as carrier gas at a flow rate of 1 mL/min. The peaks of the chromatogram were identified by comparing with standard spectra of compounds in the National Institute of Standards and Technology library (NIST, Gaithersburg, USA).

The composition of non-condensable pyrolysis product was monitored offline. The gas sample was collected in a gas sample bag (Tedlar, SKC Inc., USA) and its composition was analysed using a gas chromatography equipped with stainless steel column (Porapak R 80/100) and thermal conductivity detector (TCD). Helium was used as a carrier gas and the GC was programed at 60 ^{o}C, 80 ^{o}C and 200 ^{o}C for oven, injector and TCD temperature respectively. Bio-char proximate and ultimate analyses were

performed following the same analytical procedure adopted for the feedstock characterization above. Scanning electron microscopy-energy dispersive x-ray (SEM-EDX) (SEM, FEI Quanta 400 FE-SEM, Hillsboro, USA) and physisorption analyser (ASAP 2020 Micrometrics, Norcross, USA) were used to evaluate the surface and structural characteristics, and specific surface area (BET) and pore properties of the bio-char respectively. Crystallographic structure in the produced bio-char was examined with X-ray diffraction (XRD) (PANalytical X'pertPro, DSKH Technology Sdn. Bhd. Selangor, Malaysia) between 2Θ angle of 10°–70° at 25 mA, 45 kV, step size of 0.025°and 1.0 s scan rate.

3.3.3 Biomass pre-treatment and pyrolysis

Pre-treatment study was carried out with sodium hydroxide (NaOH) (Sigma-Aldrich Sdn. Bhd. Selangor, Malaysia), sulfuric acid (H_2SO_4) (Sigma-Aldrich Sdn. Bhd. Selangor, Malaysia) and type 1 ultrapure water (Milli-Q® type 1 ultrapure water) as solvents. Known mass of NGS (0.2-2 mm) was used in each experiment with liquid/solid ratio of 5 %w/w under agitation speed of 100 rpm. NaOH and H_2SO_4 processes were conducted at 70 ^oC and 1 hr retention time. For the deionized water, the temperature between 25-38 ^oC was used and the retention time varied from 30 min to 6 hrs. Corresponding pre-treatment severity factor was computed using equation (3.5). Solid residue was separated from leachate using vacuum filtration with the aid of sartolon polyamide filter paper (0.45 µm pore size). The residue was further washed with deionized water until the pH of water wash was around 7. The materials were then dried at 105 ^oC to a constant weight. Samples pre-treated with the pure water, acid and alkaline are herein regarded as WTNGS, ACTNGS and ALTNGS respectively. Mass and energy yields were calculated using equation (3.6) and (3.7).

Pre-treated samples and Leachates were further analysed. Subsequently, biomass pyrolysis was conducted in horizontal pyrolysis system (Figure 3.2b) at 600 ^{o}C, 30 mL/min N_2 and 30 ^{o}C/min heating rate.

$$R_O = t \times \exp\left[\frac{T-100}{14.75}\right] \quad (3.5)$$

$$\text{Yield}_M\,(\%) = \left[\frac{\text{Pretreated weight(g)}}{\text{Initial weight(g)}}\right] \times 100 \quad (3.6)$$

$$\text{Yield}_E\,(\%) = \left[\frac{\text{HHV}_{\text{Pretreated}}\ (\text{MJ/g})}{\text{HHV}_{\text{Initial}}\ (\text{MJ/kg})}\right] \times \text{Yield}_M \quad (3.7)$$

Where t is pre-treatment time (minute), T is pre-treatment temperature (^{o}C). $Yield_M$ and $Yield_E$ are mass and energy yield respectively.

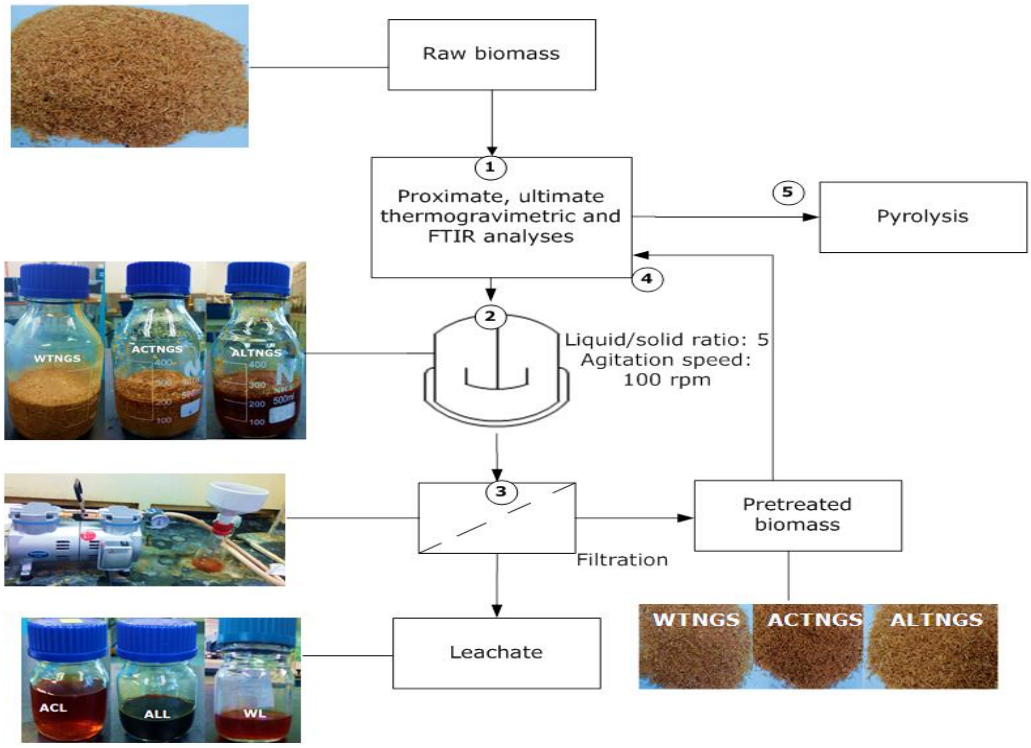

Figure 3.3: Pre-treatment process flow diagram. (RNGS) raw NGS, (WTNGS) water treated NGS, (ACTNGS) acid treated NGS, (ALTNGS) alkaline treated NGS, (WL) water leachate, (ACL) acid leachate and (ALL) alkaline leachate.

3.3.4 In-situ catalytic upgrading of bio-oil

3.3.4.1 Zeolite modification and pyrolysis

Zeolite catalyst was converted to protonic form by calcining at 550 °C in air at 5 °C/min for 5 hours and the resulting solid was designated as ZSM-5. Hierarchical mesoporous ZSM-5 was obtained from desilication of ZSM-5 using NaOH solution. Known amount of ZSM-5 was mixed with different aqueous solution (0.2 and 0.3 M of NaOH) for 2 hrs at 70 °C. The solid was filtered using vacuum filtration with the aid of a polyamide filter and thereafter oven dried at 100 °C. The dried samples were transformed into

H-form with 0.2 M ammonium nitrate (NH_4NO_3) solution at 80 °C for 24 hrs, followed by overnight drying at 100 °C and calcination at 550 °C for 5 hrs. The final alkaline treated solids were designated as 0.2HZSM-5 and 0.3HZSM-5. All the catalysts were characterized according to standard procedures. XRD was used to examine the nature of the crystalline system at 2θ angles between 10° and 60°, 25 mA, 45 kV, step size of 0.025°, and 1.0 s scan rate. SEM was used to evaluate the surface and structural characteristics. Specific surface area and pore properties were determined. Acidity of the catalyst was determined via ammonia-temperature programmed desorption (TPD) using a pulse chemisorption system (ChemiSorb 2720, Micrometrics, Norcross, USA).

In-situ catalytic upgrading was carried out in a vapour phase prior to condensation of volatiles. The catalyst was mixed with the biomass and the mixture was charged into vertical pyrolysis system. Pyrolysis and products collection were carried out according to the detail procedure described in 3.3.2.

3.3.5 In-situ non-catalytic upgrading of bio-oil

In situ non-catalytic upgrading technique is also known as co-pyrolysis. NGS was physically mixed with other biomass species such as rice husk (RH) and sago waste (SGW). Paddy RH and SGW was collected from a rice processing mill Sungai Besar, Selangor, Malaysia and sago flour process plant effluent Pusa Sarawak, Malaysia. The feedstock composition used was varied according to the scenario summarized in Table 3.1. Co-pyrolysis was carried out in a vertical pyrolysis system (Figure 3.2a). Pyrolysis products collection and characterization were carried out according to the detail procedure described in 3.3.2.

Table 3.1: Composition of feedstock

	Case study					
Biomass	**1**	**2**	**3**	**4**	**5**	**6**
NG (wt %)	100	0	0	50	50	30
RH (wt %)	0	100	0	50	0	40
SGW (wt %)	0	0	100	0	50	30

3.3.6 Ex-situ catalytic upgrading of bio-oil and product characterization

Ex-situ catalytic upgrading was performed using liquid bio-oil collected after condensation of pyrolysis vapour. The study was conducted in a self-designed laboratory scale upgrading rig as shown in Figure 3.4. The system consist of a high-pressure reactor (50 mL) made of stainless steel (SS) Swagelok double-ended (FNPT 6.35mm) tube (304L SS/DOT-3E 1800 TC-3EM 124) of length 98.6 mm and 2.4 mm wall thickness, I6D series needle valve (SS-16DKM4-F4, 6.35mm MNPT by 6.35 mm FNPT SS316) attached to a 6.35 mm SS 316 T-piece connected to 6.35 mm fitting from the top of the reactor tube. The remaining end of the T- piece was connected to a reducing adapter (SS-8-RA-4, 12.70mm FNPT by 6.35 mm MNPT, SS316) attached to a rupture disc (SS-RTM8-F4-2, 12.70mm MNPT by 6.35 mm FNPT, SS) joined to a 6.35mm SS extension tube with Skyflex pressure gauge. The bottom of the reactor is closed with 6.35 mm SS ferrule with a thermocouple (K-type, NTT Heating, Sdn Bhd, Selangor, Malaysia) connected to a computer via pico data logger. Before the set-up, known amount of crude bio-oil was mixed with certain amount of catalyst in a closed container and charged into the reactor after the bottom of the reactor is sealed off. The system was purged with nitrogen (99.9% purity, Linde Gases Sdn. Bhd) for about two minutes and the fittings were assembled. The reactor was heated electrically at 50 ^{o}C/min. After the temperature attained the set-value and the required reaction time is reached, the power was switched off and the system was allowed to cool to room

temperature. Subsequently, the valve was opened for gas collection and the reactor tube with remaining was dismantled and weighed. Reactor content was carefully collected in a container. Phase separation was carried out using centrifuge (Eppendorf™ 5430, Fisher Scientific Sdn. Bhd. Selangor, Malaysia) at 6500 rpm for 12 min. Aqueous phase and organic liquid product were separated and weighed. Samples were taking for further analysis. The reactor was thoroughly washed with excess acetone and all its contents were recovered and mixed with remaining content (solid and tar) in the centrifuge tube. Solids in the mixture were separated using vacuum filtration with the aid of sartolon polyamide filter paper (0.45µm pore size) and washed with acetone and oven dried at 60°C overnight. The total liquid, organic, aqueous, solid and gas yield were computed using equations below. The experiment was carried out in triplicates and standard deviations were computed.

$$W_{TLP} = (W_{R2} - W_{R1}) + W_{ACQ} - W_{TSLD} \quad (3.8)$$

$$\text{Yield}(\%)_{TLP} = \left[\frac{W_{TLP}}{W_{RBO}}\right] \times 100 \quad (3.9)$$

$$\text{Yield}(\%)_{ACQ} = \left[\frac{W_{ACQ}}{W_{RBO}}\right] \times 100 \quad (3.10)$$

$$\text{Yield}(\%)_{OLP} = \text{Yield}(\%)_{TLP} - \text{Yield}(\%)_{ACQ} \quad (3.11)$$

$$\text{Yield}(\%)_{SLD} = \left[\frac{(W_{TSLD}) - (W_{IC})}{(W_{RBO})}\right] \times 100 \quad (3.12)$$

$$\text{Yield}(\%)_{GP} = 100 - [\text{Yield}(\%)_{TLP} + \text{Yield}(\%)_{SLD}] \quad (3.13)$$

Where W is weight in gram and the subscript TLP, R_2, R_1, RBO, ACQ, OLP, TSLD, SLD, IC and GP represent total liquid product, reactor and its content, empty reactor, raw bio-oil, aqueous phase, organic liquid product, total solid product, solid yield, initial catalyst weight and gas product respectively.

Characterization of the upgraded liquid product and gas composition were carried out following the analytical procedure for the bio-oil characterization and non-condensable gas analysis as described in section 3.3.2 respectively.

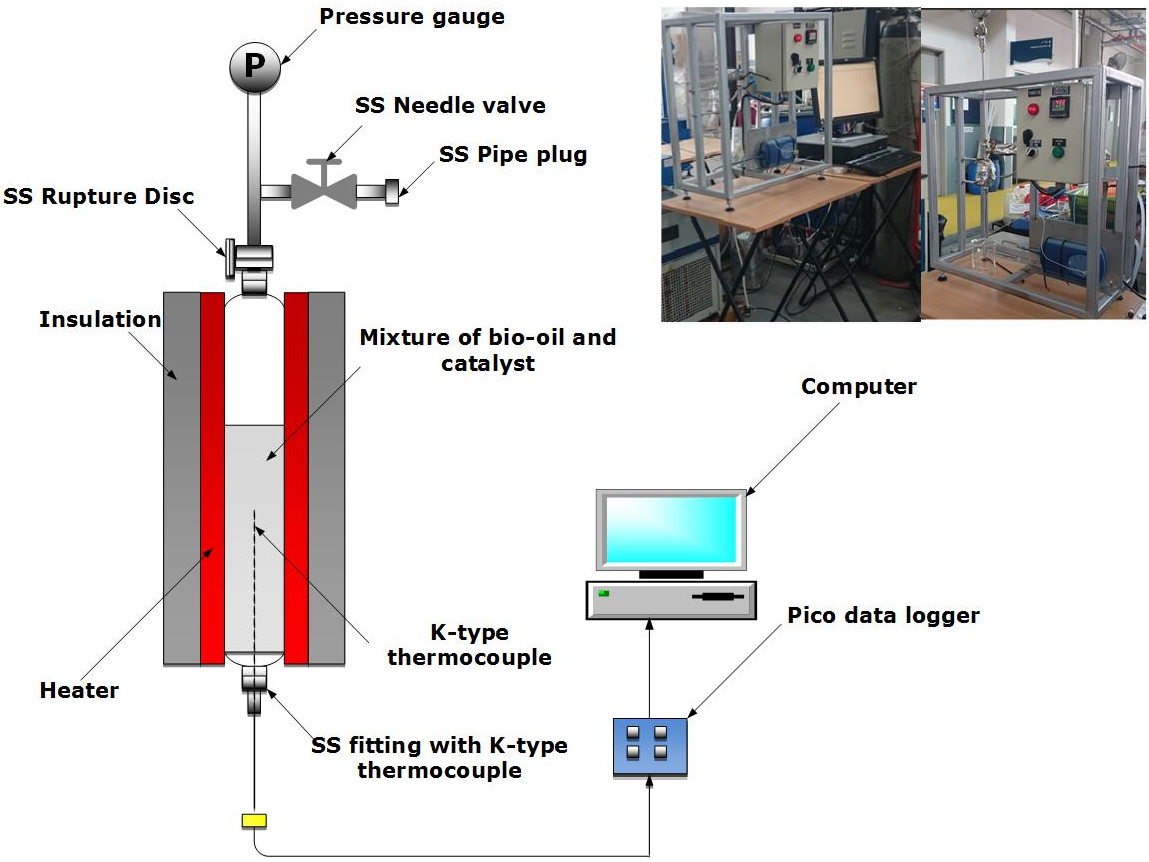

Figure 3.4: Schematic diagram of bio-oil catalytic upgrading system

3.3.7 Fractional distillation of upgraded bio-oil

Known amount of organic product produced from the catalytic upgrading process was transferred into a micro laboratory distillation apparatus (Figure 3.5) (Evergreen Engineering and Resources Sdn. Bhd. Selangor, Malaysia). The organic product was fractionated into three groups; light, medium and heavy distillates with boiling range below 100 °C, 100-200 °C and above 200 °C at atmospheric pressure respectively. The yield of each fraction was calculated using equation 3.14. Physicochemical characteristics (CHNSO, density and HHV) and chemical composition of each fraction were determined following the procedure highlighted in the bio-oil characterization in the section 3.3.2.

$$\text{Yield (\%)}_i = \left[\frac{W_i}{W_{OL}}\right] \times 100 \qquad (3.14)$$

Where W_i and W_{OL} represent the weight of each fraction collected and weight of organic liquid used as feed in the distillation.

Summary of the overall experimental methodology used in this thesis is presented in Figure 3.6 below

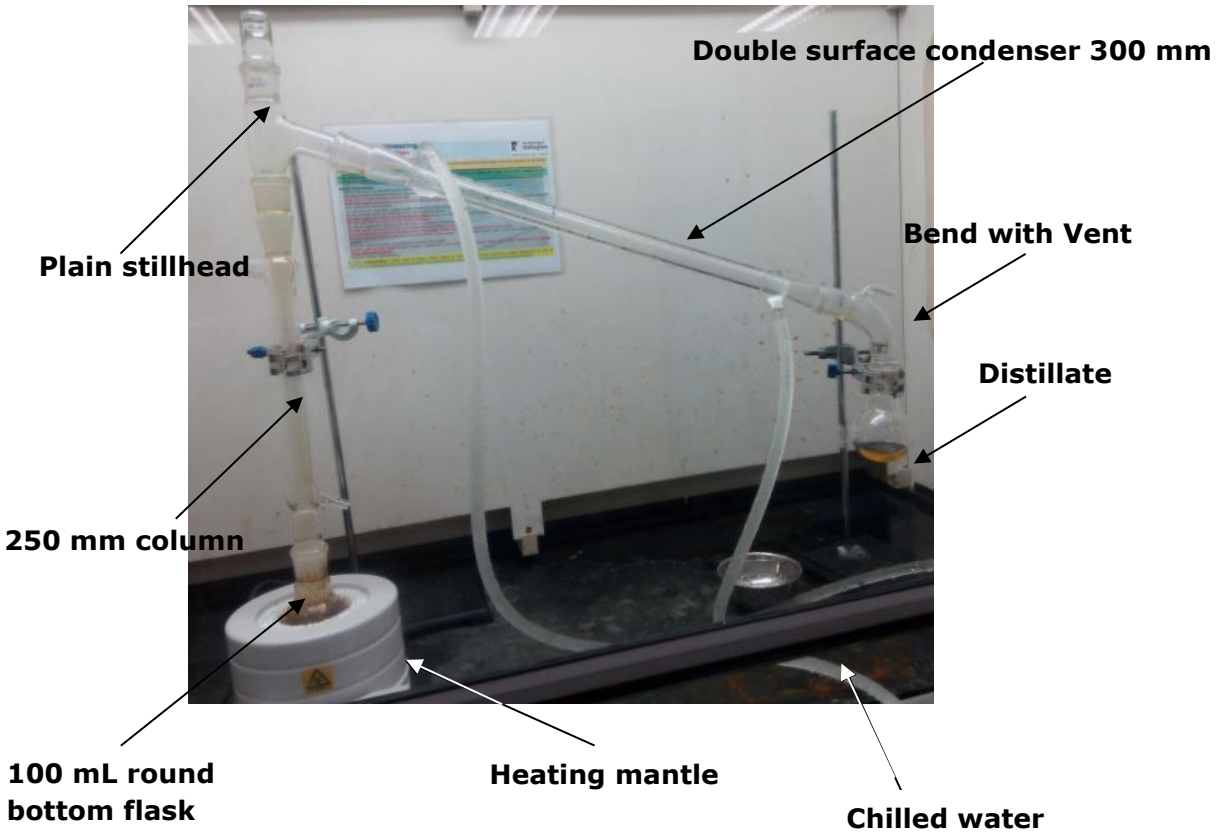

Figure 3.5: Distillation apparatus in a fume hood

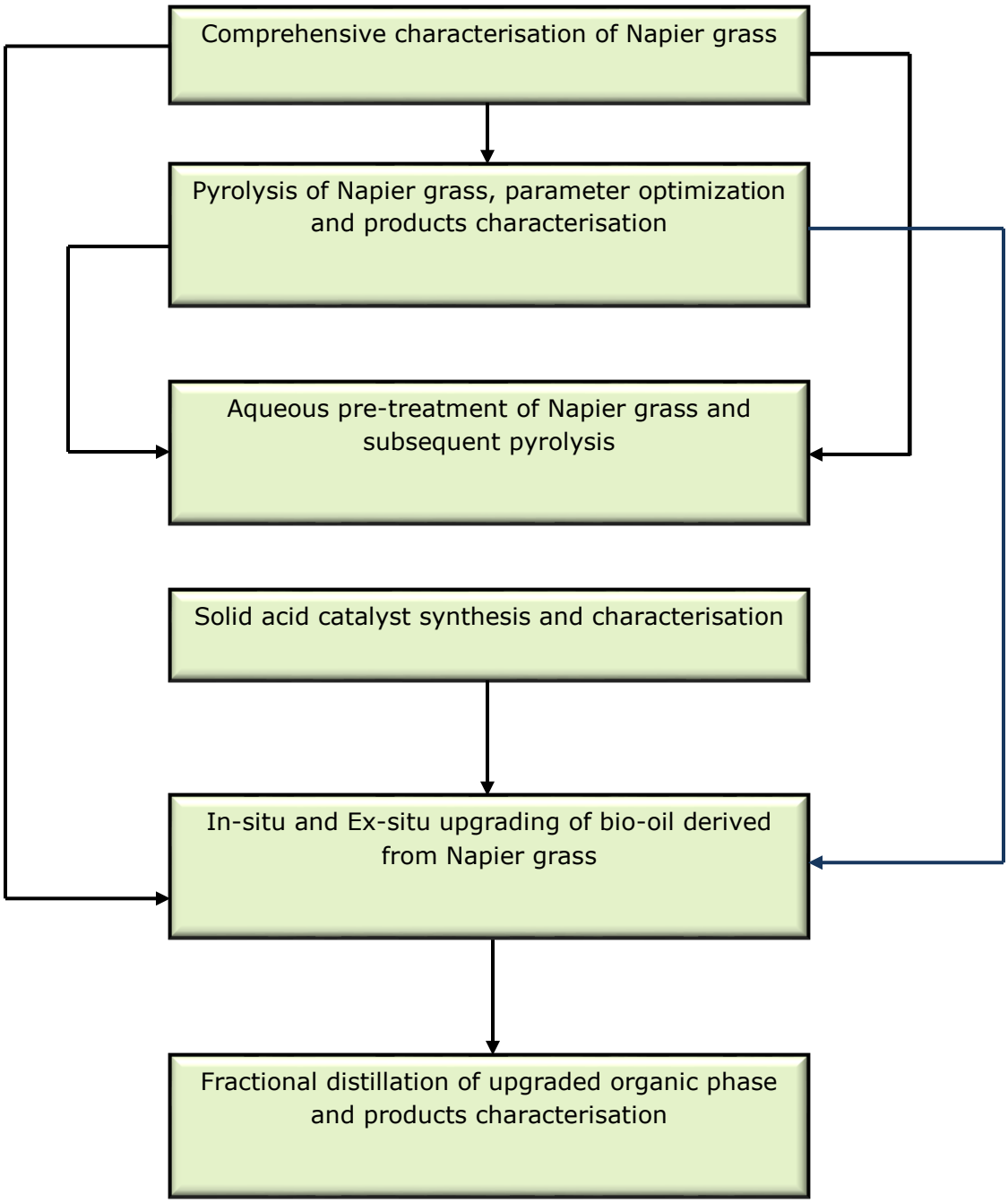

Figure 3.6: Experimental methodology flow chart

3.4 Statistical and Uncertainty Analyses

Response surface methodology (RSM) is a statistical and mathematical technique for designing experiments to provide reliable measurements of the desired response which may be affected by many variables. A mathematical model with the best fit is usually developed using data from the experimental design and the optimal value of the variables that produces maximum or minimum response are determined. In this study, the RSM was used following the face central composite design (FCCD) method with the aid of design expert software (Version 6.0.6, Stat-Ease Inc., USA). The CCD consists factorial points, axial points and number of replicates. These factors determine the number of experimental runs as given by equation (3.15). After the experiment, results are fitted to second-degree polynomial model as shown in the equation (3.16). The adequacy of the final model is tested using both graphical and numerical analysis and the experimental data are analysed statistically using analysis of variance (ANOVA).

$$N = 2^n + 2n + n_c \qquad (3.15)$$

$$Y = \beta_o + \sum_{i=1}^{n} \beta_i X_i + \sum_{i=1}^{n} \beta_{ii} X_i^2 + \sum_{i=1}^{n} \sum_{j>1}^{n} \beta_{ij} X_i X_j \qquad (3.16)$$

Where N is the number of experiments, n is the number of factors and n_c is the number of replicates at the centre point. Y is the predicted response, β_o, β_i, β_{ii} and β_{ij} is regression coefficients for the constant, linear, quadratic and interaction terms, respectively. X_i and X_j are the coded independent factors.

Uncertainties associated with the use of analytical units are computed from the standard deviation of each the unit specified by the manufacturer using square root of the sum of squares of the relative standard deviations as presented in equation (3.17)

$$\frac{\sigma_x}{\bar{x}} = \sqrt{\left[\left(\frac{\sigma_i}{\bar{x}_i}\right)^2 + \left(\frac{\sigma_j}{\bar{x}_j}\right)^2 + \left(\frac{\sigma_k}{\bar{x}_k}\right)^2 + ...\right]} \qquad (3.17)$$

Where σ_x, $\bar{x}$, σ_i and $\bar{x}_i$ represent random error of the analytical units used, average value of the final analytical result, error in a specific piece of measuring equipment and value of the measured parameter respectively. In the course of establishing calibration graphs, particularly during the determination of biomass mineral composition, regression analysis was used. The corresponding uncertainties were computed using the following equations.

$$S_{x/y} = \sqrt{\frac{\Sigma(y_i - y_{ic})^2}{n-2}} \qquad (3.18)$$

$$S_m = \frac{S_{x/y}}{\sqrt{\Sigma(x_i - x_{av})^2}} \qquad (3.19)$$

$$S_c = S_{x/y} \times \sqrt{\frac{\Sigma x_i^2}{n \times \Sigma(x_i - x_{av})^2}} \qquad (3.20)$$

Where $S_{y/x}$ is the regression error, y_i and y_{ic} represent the measured parameter from the equipment and calculated parameter using generated regression equation

respectively. S_m and S_c is the uncertainty in the regression line gradient and intercept in that order.

3.5 Conclusion

Comprehensive methods for characterization of materials and products have been outlined in this chapter. Experimental procedures follow standard protocol of British Standard Institution, American Society for Testing and Materials, and National Renewable Laboratory. It gives detail description of analytical equipment for the characterization materials and products such as oxygen bomb calorimeter, thermogravimetric analyser, elemental analyser, atomic absorption spectrometer, scanning electron microscopy, energy dispersive x-ray, physisorption analyser, chemisorption analyser, x-ray diffraction, Fourier-transform infra-red. It provides details of pyrolysis systems and bio-oil upgrading rig. These techniques were employed in the subsequent chapters for material characterization and modification, bio-oil production and upgrading, and products quantification and analysis.

CHAPTER FOUR

4. PYROLYSIS OF NAPIER GRASS AND PRODUCTS CHARACTERIZATION

4.1 Introduction

This chapter provides detail characterization of Napier grass as a feedstock for thermochemical conversion. It gives information on intermediate pyrolysis of Napier grass in a fixed bed reactor. It examines impact of pyrolysis temperature, heating rate and nitrogen flow rate collectively on product distributions. Subsequently, it dicusses optimization of pyrolysis process variables for optimum bio-oil yield using response surface methodology (RSM) based on a central composite design (CCD) and evaluates characteristics of pyrolysis products, comprehensive mass and energy analysis of the process.

4.2 Characteristics of Napier Grass

The characteristics of Napier grass feedstock used in this study are summarized in Table 4.1. The proximate analysis result obtained showed significant difference relative to similar properties of Napier grass (NG) reported in the literature. Higher volatile matter and lower ash contents were recorded and compared to the values reported by Strezov et al. (2008), Lee et al. (2010), Braga et al. (2014) and De Conto et al. (2016). Higher heating value (HHV) was 18.05 MJ/kg relative to 15.61 MJ/kg and 15.77 MJ/kg reported by Braga et al. (2014) and De Conto et al. (2016). These variations in the proximate analysis result are attributed to the post-harvest treatment of the NG sample used. The results of ultimate and structural analyses (Table 4.1) showed good agreement with the literature values.

Table 4.1: Characteristics of Napier grass biomass

Standard used	Property	**This study**	Strezov et al. (2008)	Lee et al. (2010)	Braga et al. (2014)	Sousa et al. (2016)	De Conto et al. (2016)
			Proximate analysis (wt %)				
BS EN 14774-1	Moisture Content[a]	75.27 ± 0.21	12.40	9.43	10.04	-	10.63
BS EN 15148	Volatile Matter[b]	81.51 ± 0.26	66.90	72.58	65.00	-	72.54
BS EN 14775	Ash Content[b]	1.75 ± 0.04	2.90	9.68	6.90	-	8.26
	Fixed Carbon[c]	16.74 ± 0.05	-	-	14.66	-	19.20
BS EN 14918	HHV(MJ/kg)	18.05 ± 0.07	-	-	15.61	-	15.77
			Ultimate analysis (wt%) dry basis				
	Carbon (C)	51.61 ± 0.24	41.6	42.4	44.5	41.85	39.63
	Hydrogen (H)	6.01 ± 0.02	4.83	5.96	5.4	6.77	6.31
	Nitrogen (N)	0.99 ± 0.01	0.43	1.71	1.4	0.72	1.70
	Sulphur (S)	0.32 ± 0.01	-	0.09	-	48.64	0.20
	Oxygen (O)[c]	41.07 ± 0.02	-	45.32	31.8	-	52.16
	O/C (atomic ratio)	0.80	-	-	-	-	-
	H/C (atomic ratio)	0.12	-	-	-	-	-
NREL/TP-510-42618			Structural composition (wt %)				
	Cellulose	38.75 ± 2.30		66.59	39.14	-	30.37
	Hemicellulose	19.76 ± 1.68			19.9	-	31.31
	Lignin	26.99 ± 1.29		26.72	6.18	-	26.02
	Extractives	12.07 ± 0.32		-		-	14.86
BS EN 15290			Atomic absorption analysis of ash (mg/kg)				
	Sodium (Na)	12.85±1.05	-	-	-	-	-
	Potassium (K)	3079.51±224.80	-	-	-	-	-
	Calcium (Ca)	206.71±13.20	-	-	-	-	-
	Aluminium (Al)	64.67±4.66	-	-	-	-	-
	Iron (Fe)	38.93±4.01	-	-	-	-	-
	Silicon (Si)	206.0±25.13	-	-	-	-	-

Notes: [a] as received at harvest; [b] dry basis; [c] by difference. Values are the means (n =3) ± standard deviations

Comparing the structural characteristics of NGS with that of switchgrass and miscanthus, from the work of Imam and Capareda (2012) and Rena et al. (2016), switchgrass has lower cellulose (32-34 wt%) and lignin (18.8 wt%) contents. Similarly, miscanthus has lower lignin content (12.00-12.58 wt%) but higher cellulose (50.34-52.13wt%) and hemicellulose (24.83-25.76wt%) contents as reported by Brosse et al. (2012) and Shemfe et al. (2016). Studies on the detail mineral composition of NG biomass are rarely reported. This characteristic is very important for biomass thermochemical conversion. For pyrolysis, it has been reported that mineral composition of biomass has great influence on both product yield and bio-oil composition (Mohammed et al., 2016b). Most researchers employed x-ray fluorescence (XRF), energy dispersive x-ray (EDX) in determining the mineral composition of biomass. These techniques provide elemental composition at a specific point within the sample instead of the mineral distribution in the whole sample. Strezov et al. (2008) reported silicon (Si), potassium (K), magnesium (Mg), calcium (Ca), iron (Fe), aluminium (Al) and sodium (Na) using XRF as the major elements present in the Napier grass biomass. In this study, the major elements recorded in the feedstock using atomic absorption spectrometer (AAS) showed similar mineralogical composition (Na, K, Ca, Al, Fe and Si).

The thermogravimetric profile of NGS is presented in Figure 4.1. The TG/DTG showed four distinct regions at temperature around 200 ^{o}C, 229-285 ^{o}C, 326 ^{o}C and 373-540 ^{o}C. Visible peak at about 200 ^{o}C was observed, which is due to the decomposition of extractives. This could also be due to further dehydration of the biomass through cleavage of hydroxyl groups in the hemicellulose, cellulose and lignin (Van de Velden et al., 2010; Collard and Blin, 2014). The total weight loss recorded under this region

was 12.58 wt%. A shoulder is observed at temperature between 229 and 285 °C and is ascribed to the fast decomposition of hemicellulose as a result of cleavage of the glyosidic bond between the monomeric units.

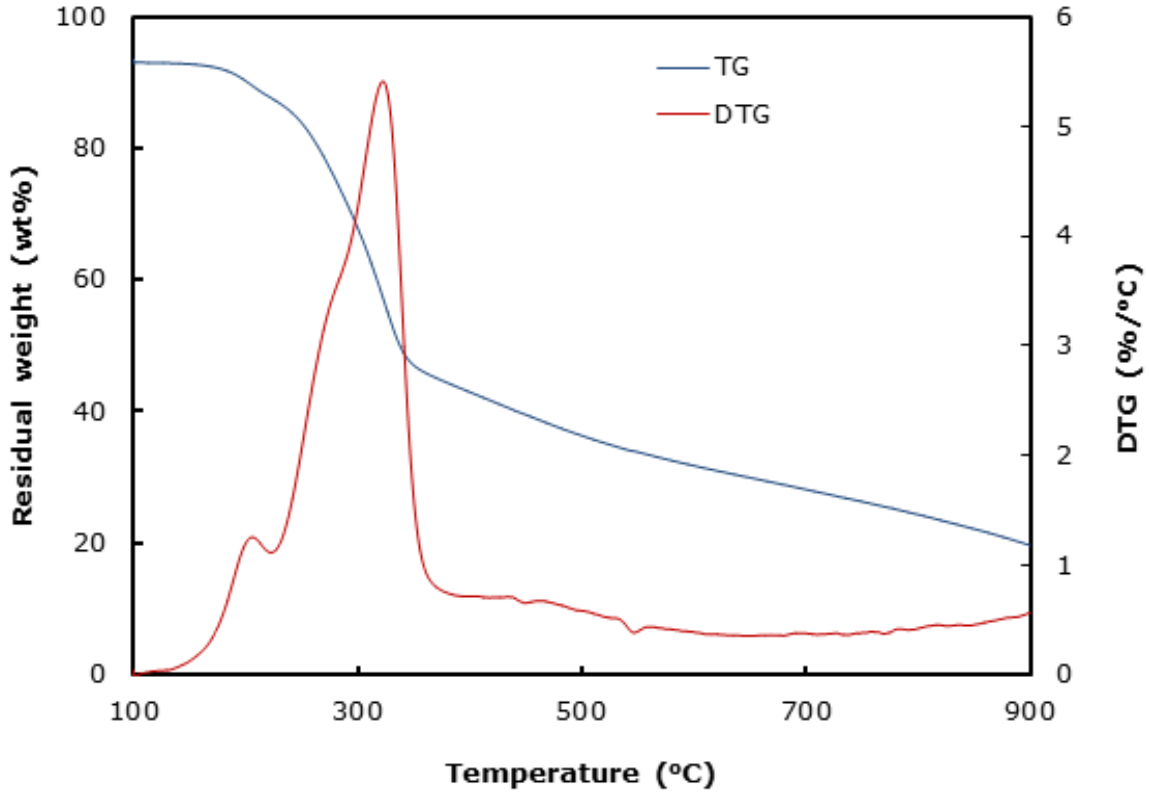

Figure 4.1: Thermogravimetric profile of Napier grass stem (TG and DTG). Sample particle size (0.2 mm); Nitrogen flow (20 mL/min); heating rate (10 °C/min)

Depolymerisation of cellulose to active cellulose is also expected within this temperature range (Van de Velden et al., 2010; Collard and Blin, 2014). The corresponding weight loss of 13.66 wt% was recorded. The main characteristic peak was observed at 326 °C. This is attributed to cellulose decomposition and had a

maximum weight loss of 35.74 wt%. Temperature between 373 and 540 °C represent degradation of lignin, which resulted in 10.78 % weight loss. Temperature beyond 540 °C represent transformation of the remaining solid (char) through aromatization and demethylation (Patwardhan et al., 2011; Collard and Blin, 2014). Similar decomposition profile of NG has also been reported by Braga et al. (2014). They ascribed peaks observed at temperature range of 180-300 °C, 300-380°C and 380-530 °C to the decomposition of hemicellulose, cellulose and lignin respectively. Similarly, De Conto et al. (2016) studied thermogravimetrics of NG and reported decomposition of cellulose at 318 °C and lignin with 350-500 °C. These decomposition temperature ranges has also been reported in the literature for other lignocellulosic biomass (Gómez et al., 2016)

4.3 Effect of Process Variables on Pyrolysis Products Distribution

Impact of temperature 450-750 °C), heating rate (10-50 °C) and carrier gas (nitrogen) flow rate (5-25 L/min) on intermediate pyrolysis of NGS in a vertical fixed bed reactor were evaluated through different levels were used as summarized in Table 4.2. The range of temperature and nitrogen flow were chosen to allow complete thermal decomposition of structural components of Napier grass particularly, the lignin which has high thermal stability and to ensure that the vapor residence time in the reactor was between 10-30 s, a requirement for the intermediate pyrolysis.

Table 4.2: Range of independent variables and experimental levels

	Experimental levels		
Variables	-1	0	+1
Temperature (°C): A	450	600	750
Nitrogen flow (L/min): B	5	15	25
Heating rate (°C/min): C	10	30	50

Central composite experimental design matrix and Bio-oil, bio-char and non-condensable gas yields (responses) collected are presented in Table 4.3. Individual response was fitted in to second order polynomial models (equation 4.1, 4.2 and 4.3).

Table 4.3: Central composite experimental design matrix and response

	Variables			Response (wt %)		
Runs	A (°C)	B (L/min)	C (°C/min)	Bio-oil	Bio-char	Non-condensable
1	600	25	30	48.12	21.67	30.21
2	750	25	10	37.11	19.61	43.28
3	600	15	30	48.67	22.96	28.37
4	600	15	10	46.13	23.18	30.70
5	750	5	10	38.87	19.23	41.90
6	600	15	30	49.42	22.89	27.69
7	450	5	10	30.11	41.29	28.61
8	750	5	50	39.37	18.79	41.83
9	450	25	10	29.99	46.41	23.60
10	600	15	30	49.88	21.13	28.98
11	450	25	50	38.37	42.83	18.79
12	600	15	30	48.97	21.89	29.14
13	600	5	30	52.06	21.89	26.05
14	600	15	30	49.20	20.44	30.36
15	600	15	30	50.16	20.83	29.01
16	750	15	30	37.85	20.59	41.57
17	450	5	50	37.09	42.09	20.81
18	450	15	30	34.22	43.89	21.89
19	600	15	50	50.89	19.22	29.89
20	750	25	50	36.92	19.42	43.66

Responses are the average values (n= 2)

$$Y_{oil} = 49.37 + 2.03A - 0.70B + 2.04C - 13.31A^2 + 0.75B^2 - 0.83C^2 - 0.67AB - 1.88AC + 0.09BC \quad (4.1)$$

$$Y_{char} = 21.78 - 11.89A + 0.66B - 0.73C + 10.32A^2 - 0.14B^2 - 0.72C^2 - 0.61AB + 0.27AC - 0.52BC \quad (4.2)$$

$$Y_{char} = 28.85 + 9.85A + 0.04B - 1.31C + 2.99A^2 - 0.61B^2 + 1.55C^2 + 1.28AB + 1.61AC + 0.43BC \quad (4.3)$$

From analysis of variance (ANOVA), of bio-oil yield, the Model F-value of 171.60 (Table 4.4) implies the model is significant. Lack of Fit F-value of 3.18 indicates that it is not significant relative to the pure error, which is desirable. For the bio-char and non-condensable gas yields, similar trends are observed. Model F-value of 151.22 (Table 4.5) and 69.74 (Table 4.6) with the corresponding lack of fit F-value of 1.47 and 3.41 are recorded. Values of "Prob > F" less than 0.0500 shows model terms are significant while values greater than 0.1000 indicate the model terms are not significant. In the case of bio-oil, the significant model terms are A, B, C, A^2, AB, AC, with the corresponding F-value of 62.92, 7.46, 63.59, 741.20, 5.52, and 43.12. It can also be observed that the most significant model term on the bio-oil yield obeyed the following order A^2>A>C>AC>B>AB while the quadratic terms B^2, C^2 and the interaction BC does not have a significant impact on the bio-oil yield. For bio-char, the significant model terms are A and A^2 with the linear term having the largest significance due to higher F-value of 1006.27 (Table 4.5). The significant model terms for the non-condensable gas are A, C, A^2, AB, AC, with A being the most significant term having F-value of 557.41 (Table 4.6). The coefficient of determination, R^2 for the bio-oil, bio-char and non-condensable gas model is 0.9936, 0.9927 and 0.9843 (Table 4.4-4.6). Another regression parameter considered is the adjusted R^2, which improves the coefficient of determination (R^2) in relation to the sample size and the model terms, the corresponding values are 0.9878, 0.9861 and 0.8903. Another regression parameter considered is the adjusted R^2, which improves the coefficient of determination (R^2) in relation to the sample size and the model terms, the corresponding values are 0.9878, 0.9861 and 0.8903.

Table 4.4: ANOVA test for bio-oil response model and respective model term

Source	Sum of squares	df	Mean square	F-value	prob >F	Remark
Model	1014.97	9	112.77	171.60	< 0.0001	significant
A	41.35	1	41.35	62.92	< 0.0001	significant
B	4.90	1	4.90	7.46	0.0211	significant
C	41.79	1	41.79	63.59	< 0.0001	significant
A^2	487.13	1	487.13	741.20	< 0.0001	significant
B^2	1.55	1	1.55	2.36	0.1556	
C^2	1.91	1	1.91	2.91	0.1187	
AB	3.63	1	3.63	5.52	0.0407	significant
AC	28.34	1	28.34	43.12	< 0.0001	significant
BC	0.06	1	0.06	0.10	0.7642	
Residual	6.57	10	0.66			
Lack of Fit	5.00	5	1.00	3.18	0.1151	not significant
Pure Error	1.57	5	0.31			
Cor Total	1021.54	19				
Std. Dev.	0.81		R-Squared	0.9936		
Mean	42.67		Adj R-Squared	0.9878		
C.V.	1.90		Pred R-Squared	0.9518		
PRESS	49.28		Adeq Precision	36.4925		

Table 4.5: ANOVA test for bio-char response model and respective model term

Source	Sum of squares	df	Mean square	F-value	prob >F	Remark
Model	1911.12	9	212.35	151.22	< 0.0001	significant
A	1413.01	1	1413.01	1006.27	< 0.0001	significant
B	4.42	1	4.42	3.15	0.1065	
C	5.40	1	5.40	3.84	0.0784	
A^2	292.88	1	292.88	208.58	< 0.0001	significant
B^2	0.05	1	0.05	0.04	0.8491	
C^2	1.42	1	1.42	1.01	0.3380	
AB	2.94	1	2.94	2.09	0.1788	
AC	0.58	1	0.58	0.41	0.5361	
BC	2.14	1	2.14	1.53	0.2450	
Residual	14.04	10	1.40			
Lack of Fit	8.35	5	1.67	1.47	0.3421	not significant
Pure Error	5.69	5	1.14			
Cor Total	1925.16	19				
Std. Dev.	1.18		R-Squared	0.9927		
Mean	26.51		Adj R-Squared	0.9861		
C.V.	4.47		Pred R-Squared	0.9411		
PRESS	113.31		Adeq Precision	32.8072		

Table 4.6: ANOVA test for non-condensable gas response model and respective model term

Source	Sum of squares	df	Mean square	F-value	prob >F	Remark
Model	1093.29	9	121.48	69.74	< 0.0001	significant
A	970.91	1	970.91	557.41	< 0.0001	significant
B	0.01	1	0.01	0.01	0.9339	
C	17.15	1	17.15	9.85	0.0105	significant
A^2	24.57	1	24.57	14.11	0.0037	significant
B^2	1.03	1	1.03	0.59	0.4601	
C^2	6.64	1	6.64	3.81	0.0795	
AB	13.09	1	13.09	7.52	0.0208	significant
AC	20.83	1	20.83	11.96	0.0061	significant
BC	1.47	1	1.47	0.85	0.3794	
Residual	17.42	10	1.74			
Lack of Fit	13.47	5	2.69	3.41	0.1020	not significant
Pure Error	3.95	5	0.79			
Cor Total	1110.71	19				
Std. Dev.	1.32		R-Squared	0.9843		
Mean	30.82		Adj R-Squared	0.9702		
C.V.	4.28		Pred R-Squared	0.8903		
PRESS	121.87		Adeq Precision	27.3167		

Another regression parameter considered is the adjusted R^2, which improves the coefficient of determination (R^2) in relation to the sample size and the model terms, the corresponding value is 0.9878, 0.9861 and 0.8903. The R^2 and adjusted R^2 values for the individual model are high enough and comparable, which indicate that the selected quadratic response surface model for the pyrolysis products sufficiently describe the experimental data within the selected operating conditions. Predicted R^2 value of the bio-oil, bio-char and the non-condensable gas model is 0.9518, 0.9411 and 0.8903, which is in good agreement with the respective adjusted R^2 values. Adequate precision (Adeq Precision) is a measure of signal to noise ratio and a ratio greater than 4 is desirable. In this study, the value of Adeq precision is 36.4925,

32.8072 and 27.3167 for the bio-oil, bio-char and non-condensable gas model. These high values indicate adequate signal and the models can be used to navigate the design space. Coefficient of variation (CV), which is a measure of the reliability of the experiment, it expresses the overall experimental error as a percentage of the overall mean. The CV value recorded for all the pyrolysis products are less than 4.5, hence, this experiment can be said to be reliable since the lower the CV value, the higher is the reliability of the experiment.

Diagnostic plots (normal % probability against studentized and outlier T against a number of runs), which measure the adequacy of the quadratic models in fitting the experimental data are presented in Figure 4.2. Points in the probability plots are distributed approximately on a straight line along the diagonal for each of the pyrolysis product models. This trend depicts that the error terms are normally distributed and independent of each. In the outlier plots on the other hand, the points are randomly distributed around zero between +3.5 and -3.5, which connote homoscedasticity. Consequently, the respective model is suitable and successfully establish the relationship between the pyrolysis process variables studied and the product distribution.

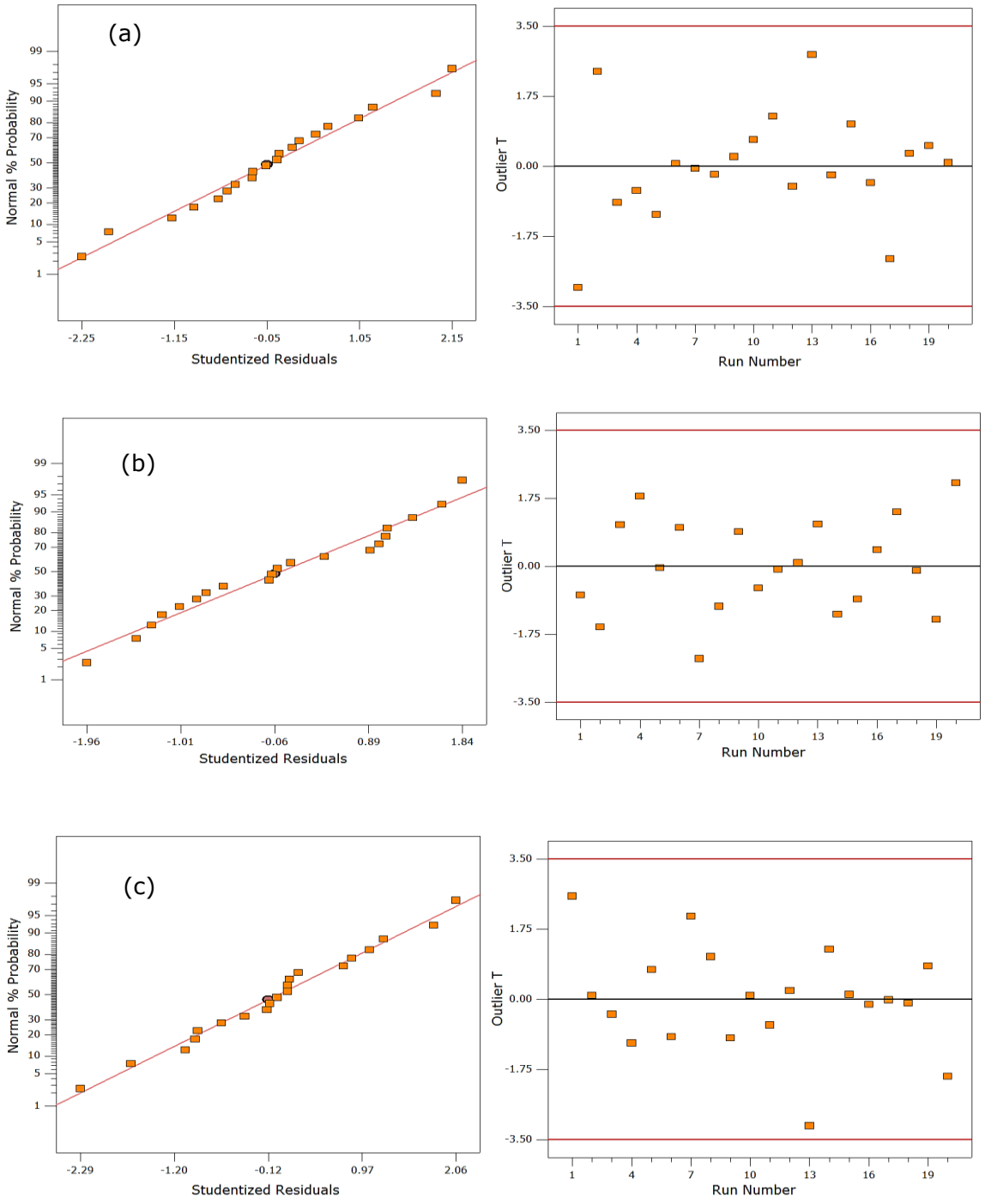

Figure 4.2: Diagnostics of models (a) Bio-oil (b) bio-char Normal (c) non-condensable gas.

4.3.1 Effect of process variables on bio-oil yield

In order to examine the effect of the pyrolysis process variables on the yields, interaction and 3D surface plots are used. Although, it is not possible to present the effects of all the parameters studied on the same 3D, as such, the response surface plots are presented by varying two factors and keeping one factor constant. The interaction between the nitrogen flow and temperature at a constant heating rate (30 ^{o}C/min) on the bio-oil yield (Figure 4.3a) shows that increase in the nitrogen flow rate from 5 L/min to 25 L/min and temperature from 450 ^{o}C to 600 ^{o}C increased the bio-oil yield. The oil yield became maximum at 600 ^{o}C for both nitrogen levels but at a different amount. Lower nitrogen level (5 L/min) produced 52.06 wt% oil compared to 49.20 wt% oil yield at 25 L/min nitrogen flow at the same 600 ^{o}C. The decreased oil yield at the higher nitrogen flow rate could be as a result of more uncondensed volatiles leaving as part of non-condensable gas due to short vapour residence time in the condenser. Declines in the oil yields were observed at temperature above 600 ^{o}C. The bio-oil yield trend recorded with temperature from 450 ^{o}C to 600 ^{o}C and above 600 ^{o}C can be respectively ascribed to degradation of more lignin, and secondary reactions of pyrolysis vapour and more decomposition of bio-char at the elevated temperature (Soetardji et al., 2014). The effect of heating rate and temperature on the bio-oil yield at a constant nitrogen flow rate (15 L/min) is presented in Figure 4.3b. Increasing temperature from 450 to 600 ^{o}C and heating rate between 10 and 50 ^{o}C/min increased the oil yield from 29.26 to 46.13 wt% and 37.12 to 50.89 wt%. The yield of more bio-oil at 50 ^{o}C/min relative to 10 ^{o}C/min under the same pyrolysis temperature is attributed to rapid depolymerization of the biomass to primary volatiles at the higher heating rate. (Yorgun and Yildz, 2015). The oil yield decreased to 37.10 wt% at both heating rates under the same temperature (750 ^{o}C) and nitrogen flow (15 L/min) due

to secondary reactions at such a high temperature. Combined effects of heating rate and nitrogen flow rate at a pyrolysis temperature of 600 °C on the bio-oil yield is shown in Figure 4.3c. As the nitrogen flow increased from 5 L/min to 25 L/min, bio-oil yield at 50 °C/min heating rate remained higher compared to the oil collected at 10 °C/min but no significant impact of nitrogen flow was observed in both cases. Bio-oil yield at 50 °C/min was between 50.72 and 51.94 wt% relative to 46.45-48.03 wt% oil recorded at 10 °C/min.

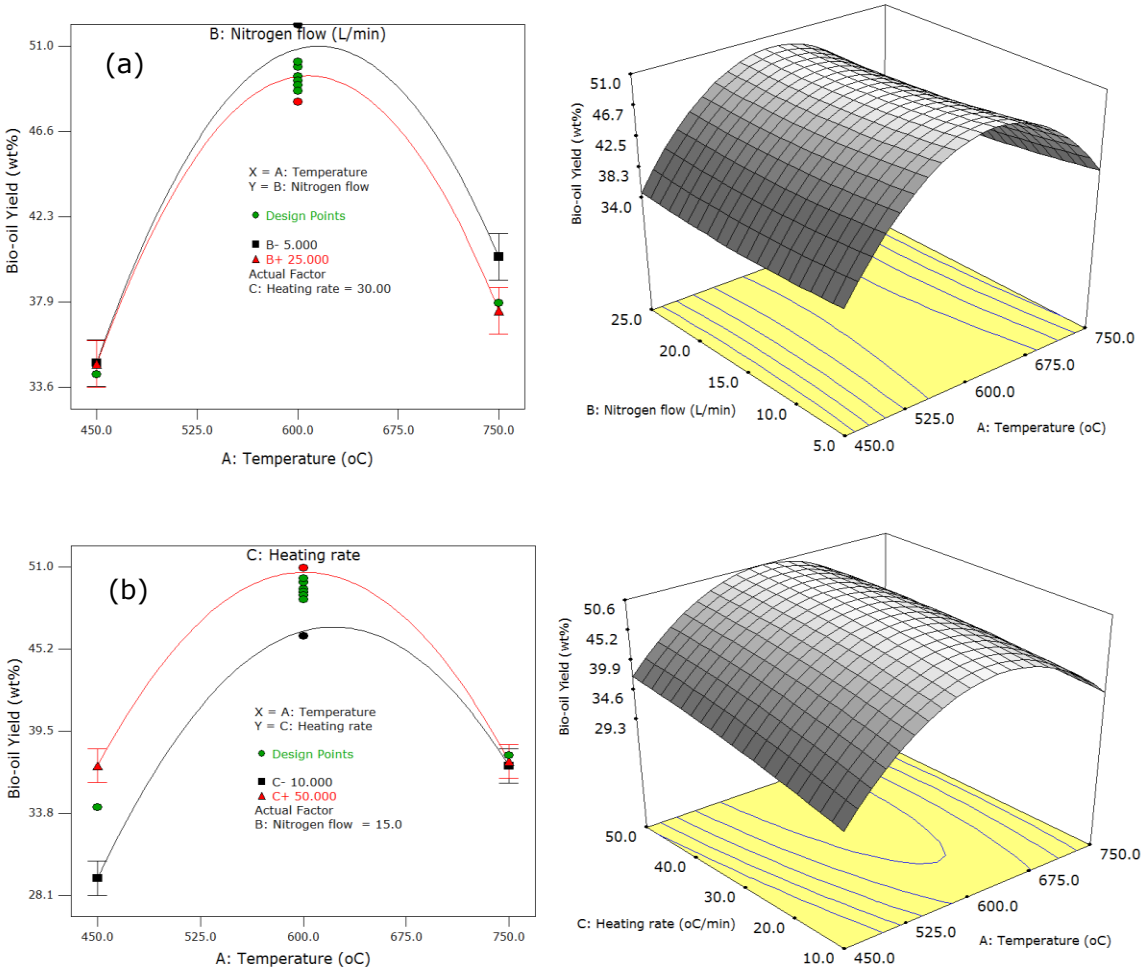

Figure 4.3 continued

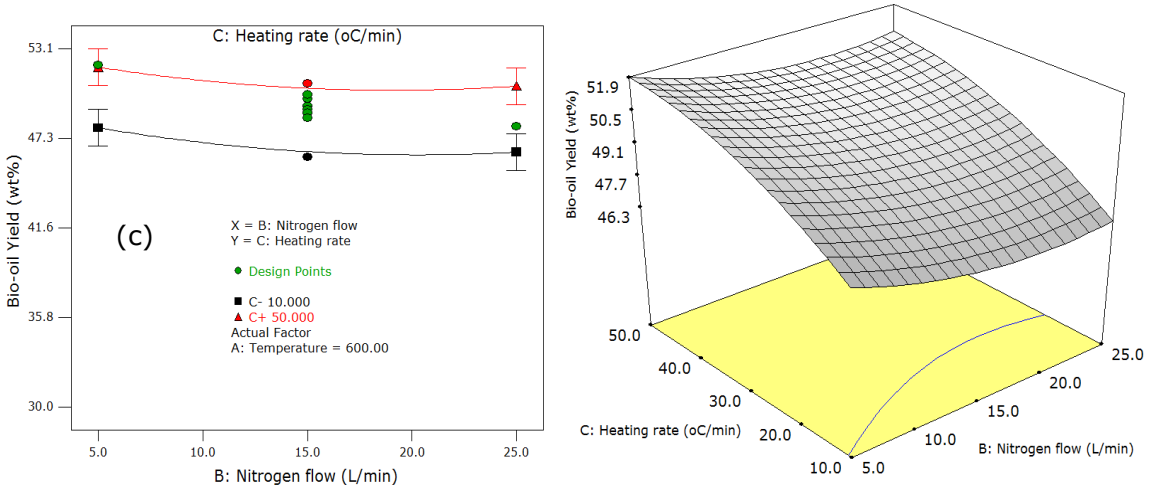

Figure 4.3: Interaction graphs and the corresponding surface response plots for the combined effects of process variables parameters on bio-oil yield. (a) Effect of nitrogen flow and temperature at 30 °C/min; (b) effect of heating rate and temperature at 15 L/min N_2; (c) effect heating rate and nitrogen flow at 600 °C

4.3.2 Effect of process variables on bio-char yield

Interactions between temperature and nitrogen flow (Figure 4.4a) reveals that the temperature had great influence on the bio-char yield compared to the nitrogen flow rate. A general decline in the bio-char yield was recorded with increasing temperature at both 5 L/min and 25 L/min nitrogen flow rates, which is attributed to devolatilization more organic materials as dehydration of hydroxyl groups and decomposition of lignocellulose structure progresses with increasing temperature (Mohammed et al., 2015b). This clearly demonstrated that bio-char yield is governed by the pyrolysis temperature. The impact of temperature also dominated interaction between temperature and heating rates on the bio-char yield (Figure 4.4b). There was no considerable difference between the bio-char yields at 10 °C/min and 50 °C/min throughout the investigated temperature range. Bio-char yields recorded were 44.27

and 42.27 wt% at 450 °C, and 20.59 and 19.03 wt% at 750 °C for 10 °C/min and 50 °C/min heating rate respectively. The slightly lower value of bio-char recorded at 50 °C/min could also be attributed to rapid degradation of biomass. Influence of heating rate and nitrogen flow on the bio-char yield is presented in Figure 4.4c. Both factors did not significantly impacted on the char yield. As nitrogen flow increased from 5 L/min to 25 L/min, bio-char yield at 50 °C/min remained the same (around 20 wt%) while between 20.48 to 22.84 wt% char yield was recorded at 10 °C/min under the same nitrogen flow regime. These observations indicated that the range of nitrogen flow rates used in this study was sufficient in preventing secondary reaction such as condensation which normally favoured char formation (Yorgun and Yildz, 2015).

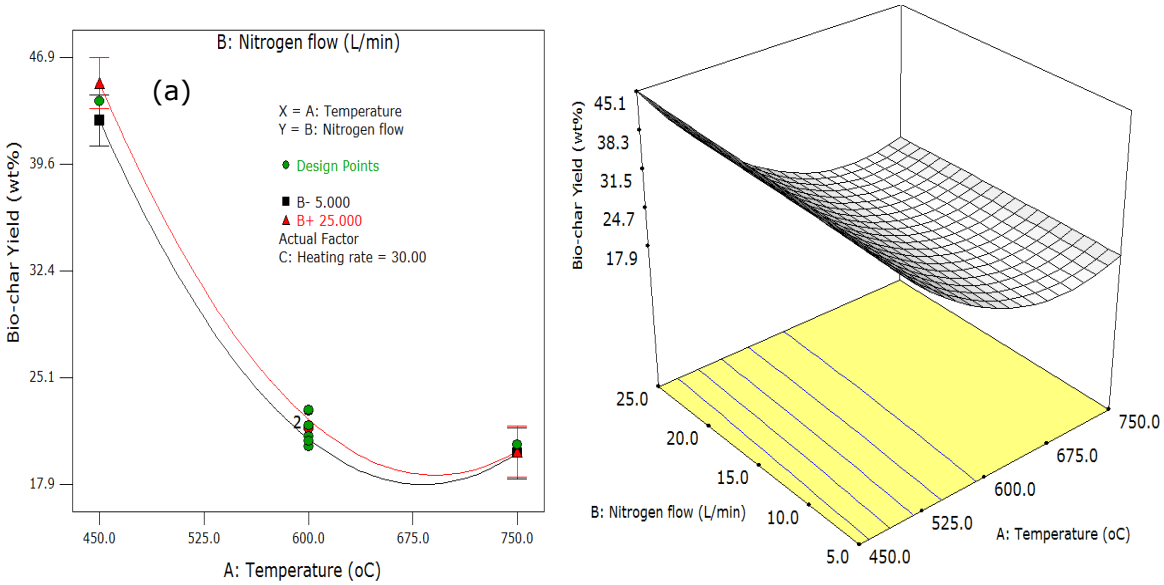

Figure 4.4 continued

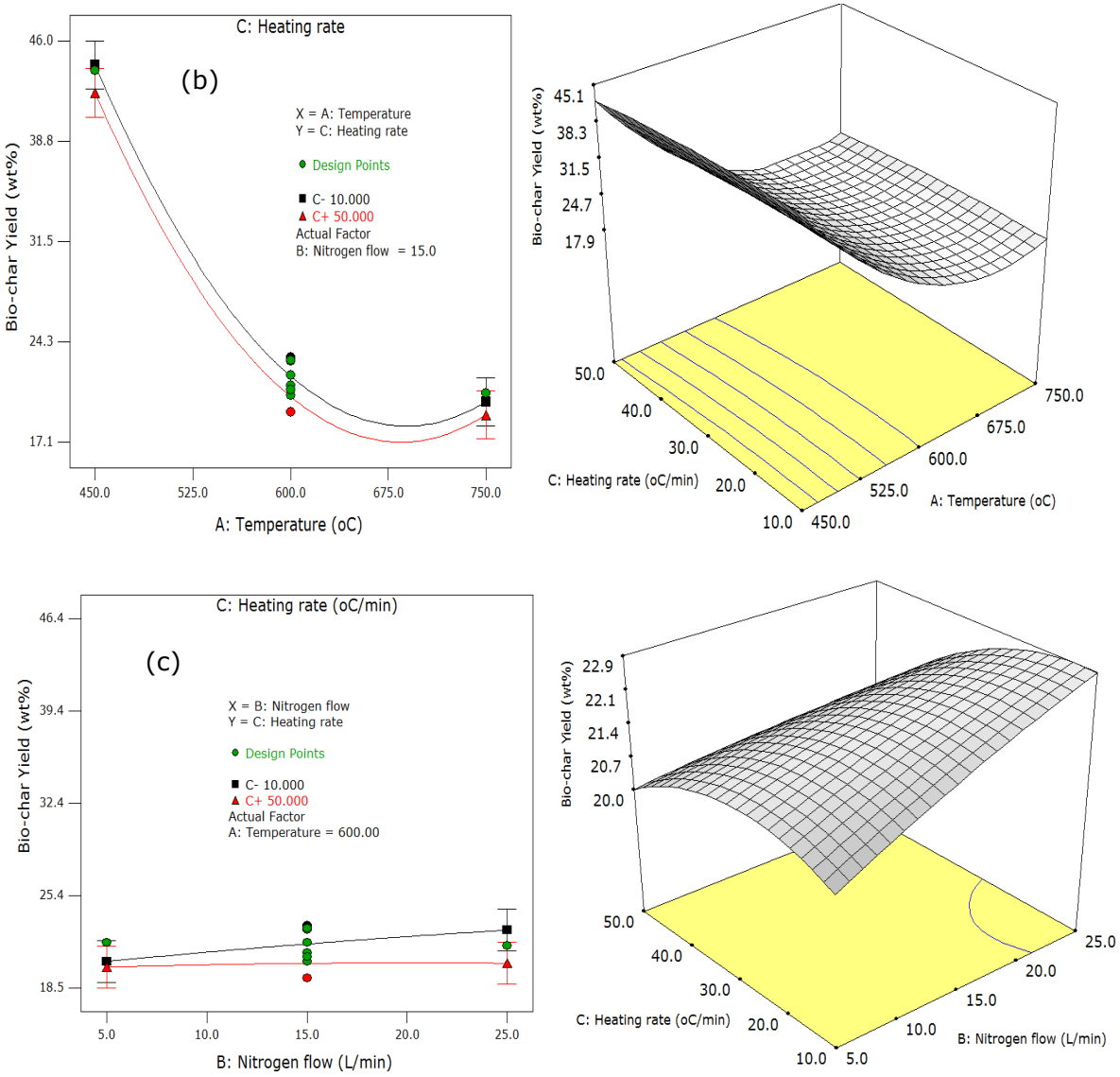

Figure 4.4: Interaction graphs and the corresponding surface response plots for the combined effects of process variables bio-char yield. (a) Effect of nitrogen flow and temperature at 30 °C/min; (b) effect of heating rate and temperature at 15 L/min N_2; (c) effect heating rate and nitrogen flow at 600 °C

4.3.3 Effect of process variables on non-condensable gas yield

Impacts of process variables on the production of non-condensable gas are shown in Figure 4.5 (a-c). Interaction between temperature and nitrogen flow (Figure 4.5a) shows that non-condensable gas yield increased with temperature at both nitrogen flow levels. As the temperature progressed from 450 to 600 ^{o}C, increase in the gas yield was not significant under 5 L/min nitrogen flow. This indicates the most of the volatiles generated during the pyrolysis are effectively captured in the condenser, which eventually ended up in the bio-oil as rightly identified in the bio-oil yield section above. The change in the gas yield recorded under 25 L/min nitrogen flow between 450 and 600 ^{o}C is mainly due to shorter vapour residence time in the condenser compared to the 5 L/min nitrogen flow rate. With increasing temperature above 600 ^{o}C, the gas yield increased rapidly in both nitrogen flow regimes, which can be ascribed to further thermal decomposition of pyrolysis vapour in addition to some uncondensed volatiles leaving the pyrolysis system as part of non-condensable gas, particularly at the higher flow rate. 30.21-42.40 wt% gas yield was recorded with 25 L/min nitrogen flow relative to 26.05-39.77 wt% gas yield using 5 L/min. The combined effects of temperature and heating rate on the yield of non-condensable gas are shown in (Figure 4.5b), it also reveals that the temperature has great influence on the gas yield. With increasing temperature from 450-750 ^{o}C, the non-condensable gas yield increased from 26.46 to 42.94 wt% and 20.62 to 43.55 wt% at 10 ^{o}C/min and 50 ^{o}C/min respectively. This trend is believed to be as a result of secondary cracking of volatiles and further decomposition of bio-char at higher temperatures (Yorgun and Yildz, 2015). On the other hand, nitrogen flow and the heating rate seem to have no considerable impact on the yield of non-condensable gas (Figure 4.5c). As the nitrogen flow rate increased from 5 L/min to 25 L/min, the change in the yield of non-

condensable gas was insignificant at both 10 °C/min and 50 °C/min. Gas yield of 28.02-28.95 wt% and 30.71-31.50 wt% were recorded with 10 and 50 °C/min heating rate throughout the carrier gas flow range used in this study.

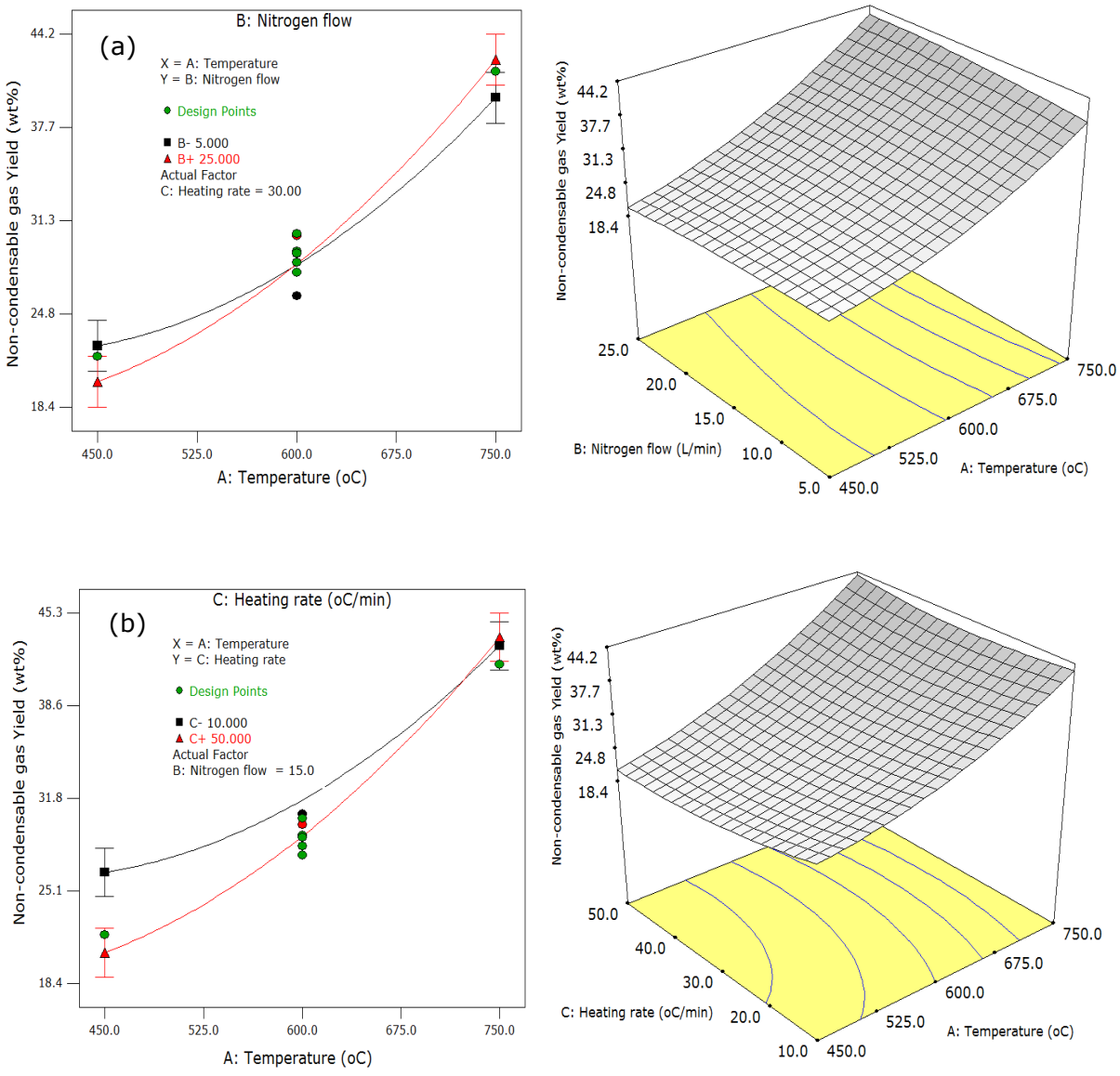

Figure 4.5 continued

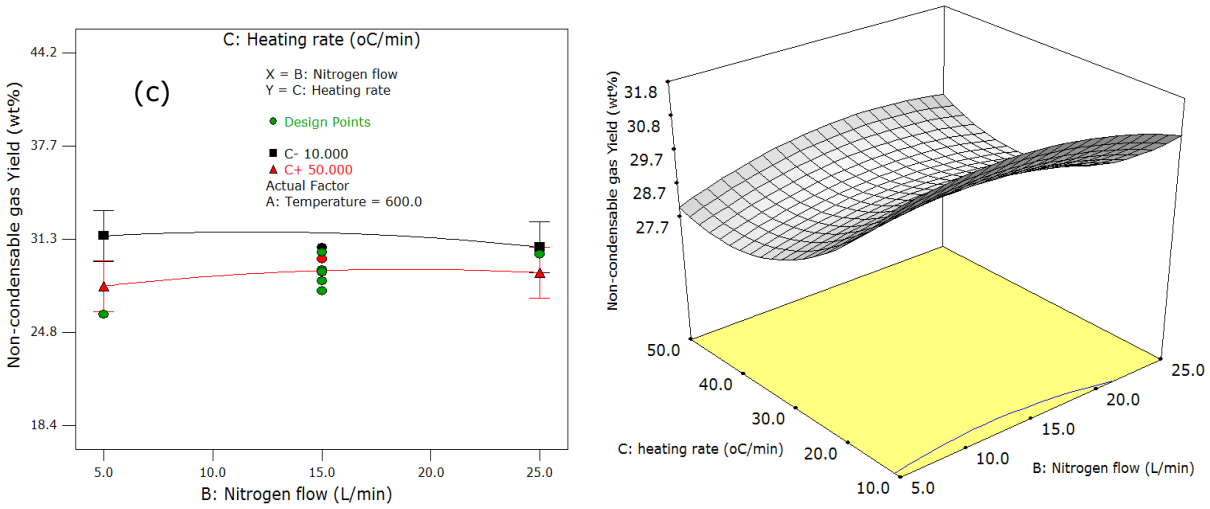

Figure 4.5: Interaction graphs and the corresponding surface response plots for the combined effects of process variables on non-condensable gas yield. (a) Effect of nitrogen flow and temperature at 30 °C/min; (b) effect of heating rate and temperature at 15 L/min N_2; (c) effect heating rate and nitrogen flow at 600 °C

4.3.4 Optimization and validation of result

In order to maximize the bio-oil yield, the process variables parameters considered in this study were optimized. Pyrolysis temperature, heating rate, and nitrogen flow rate were maintained within the range of experimental condition studied while the bio-char and non-condensable gas responses were minimized (Table 4.7). Based on these conditions, eight (8) solutions were generated by the software as presented in Table 4.7. Solution number one (1) with the highest desirability was chosen. This indicates that the pyrolysis temperature of around 600 °C, 5 L/min nitrogen flow rate, and 50 °C/min heating rate was sufficient to produce optimum bio-oil of 51.94 wt%. This result was validated by performing further experiments under the optimized process condition. The experiment was repeated in triplicates and the results are shown in

Table 4.8. The average value of bio-oil yield recorded (50.57 wt%) sufficiently agree with the predicted value. Consequently, this validation confirms the adequacy of the developed quadric model for bio-oil yield.

Table 4.7: Optimization condition (constrain) and solutions

Constraints		Lower	Upper	
Name	Goal	Limit	Limit	Importance
Temperature (A)	is in range	450	750	3
Nitrogen flow (B)	is in range	5	25	3
Heating rate (C)	is in range	10	50	3
Bio-oil Yield	maximize	29.99	52.06	5
Bio-char Yield	minimize	18.79	46.41	1
Non-condensable gas Yield	minimize	18.79	43.66	1

Solutions

Number	A (°C)	B(L/min)	C(°C/min)	Bio-oil	Bio-char	N/gas	Desirability
1	**599.68**	**5.00**	**50.00**	**51.94**	**20.06**	**28.00**	**0.9260**
2	599.80	5.00	49.38	51.93	20.11	27.96	0.9258
3	595.63	5.00	47.74	51.85	20.55	27.60	0.9244
4	590.77	25.00	50.00	50.70	21.13	28.18	0.8817
5	591.73	25.00	49.71	50.70	21.08	28.22	0.8814
6	594.45	25.00	49.71	50.71	20.84	28.45	0.8812
7	591.70	25.00	49.32	50.68	21.13	28.18	0.8812
8	578.88	25.00	49.99	50.52	22.26	27.21	0.8782

N/gas: non-condensable gas

Table 4.8: Bio-oil yield predicated at optimized condition and experimental value

Run	Temperature (°C)	Nitrogen flow (L/min)	Heating rate (°C/min)	Bio-oil Yield (wt %) Experimental	Predicted
1	600	5	50	51.56	51.94
2	600	5	50	48.14	51.94
3	600	5	50	52.02	51.94
Average				**50.57**	**51.94**

The bio-oil yield from NGS observed at the optimized condition (600 °C, 5 L/min N_2 and 50 °C/min) in this study is comparable to the pyrolysis oil yield reported by Strezov et al. (2008) from NG. They observed 54.37 wt% bio-oil yield at 50 °C/min and 900 °C final pyrolysis temperature under argon atmosphere. Similarly, the result of pyrolysis study of NG by De Conto et al. (2016) showed a total bio-oil yield of 52.99 wt% at 700 °C, 25 °C/min and 1 L/min nitrogen flow. Sousa et al. (2016) also reported a total liquid product of 48.2 wt% from the pyrolysis of NGS at 540 °C. Report by Lee et al. (2010) on NG pyrolysis showed a lower oil yield of 36 wt% at 500 °C and 150 °C/min heating rate under nitrogen atmosphere. These variations in the yield of bio-oil from NG biomass can be linked to the characteristic of the feedstock used, heating and heat transfer rates of the reactor, and the difference in the pyrolysis condition (temperature, inert gas flow). The optimum condition established is used in the subsequent pyrolysis study.

Comparing bio-oil from NG with other herbaceous biomass materials, Corton et al.(2016) reported 46.61 wt% bio-oil yield from pyrolysis of Miscanthus in a fluidised system at 500 °C. Pyrolysis product distribution from switchgrass reported by Imam and Capareda (2012) showed a maximum bio-oil yield of 37 wt% at 600 °C. These bio-oil yields are approximately 9.4 and 38 % respectively lower relative to the optmimum bio-oil yield recorded from NG in this study. Similarly, studies by Ren et al. (2016) on pyrolysis of switchgrass in an auger reactor showed a total bio-oil yield of 50-54 wt% at 500 °C. This value is similar to the bio-oil yield (51 wt%) recorded from NG in this study. However, only 15-22% of the total bio-oil yield was organic phase as reported by the authors compared to the NG bio-oil with 31.40 % of the total bio-oil

representing the organic phase. Consequently, NG biomass has potential for higher organic phase bio-oil yield, an important feedstock for biofuel production.

4.4 Properties of Bio-oil

4.4.1 Physicochemical characteristics of bio-oil

The bio-oil product collected throughout this study was two-phase liquid, the organic phase (high molecular weight component) and aqueous phase (low molecular weight component). The organic fractions are usually water-insoluble derived mostly from lignin component of the feed biomass while the light fractions consist predominantly water (originates from both moisture in the feed biomass and pyrolysis reaction), acids, ketones, aldehydes, small fraction of phenols and other water-soluble organics (Resende et al., 2015). The physicochemical characteristics of the oil produced at optimized condition are summarized in Table 4.9. Both the organic and aqueous phases present an acidic characteristics with corresponding pH values of 3.71 and 2.09. This property is attributed to presence of organic acids and phenolics in the bio-oil. The presence of water in the pyrolysis oil is mainly from moisture in the feed biomass and product of dehydration during the pyrolysis reaction (Resende et al., 2015; Mohammed et al., 2015b). In this study, the biomass feedstock used was bone dry and, therefore, the water content of the oil could be said to have originated from the pyrolysis reaction. Despite a careful separation of the aqueous phase, 7.24wt% water remained in the organic phase. Total solid content of less than 0.01wt% (0.008-0.009) was recorded. Other characteristics of the organic phase such as density, viscosity, ash content and calorific value reasonably conform to the ASTM specifications for pyrolysis oil. Consequently, the organic phase bio-oil from NGS can be regarded as ASTM-Grade D bio-oil. Carbon and oxygen contents from the ultimate analysis revealed that the

organic phase bio-oil has higher carbon (51.14 wt %) and lower oxygen (41.66 wt %) compared to the value reported by Lee et al. (2010) (6.04 wt%-carbon); Sousa et al. (2016) (41.85 wt%-carbon). High carbon content in the organic phase connotes presence carbon-rich organic molecules, which have resulted in the higher heating value (HHV) of 26.42MJ/kg.

Table 4.9: Physicochemical properties of bio-oil produced at optimized condition compared with the ASTM D7544-12 specifications

Property	Organic phase	ASTM-Grade G	ASTM-Grade D	Aqueous phase
Appearance	Black	-	-	Dark brown
pH	3.71±0.01	Report	Report	2.09±0.01
Water content (wt %)	7.24±0.21	30 max.	30 max.	62.44±0.25
Density (g/cm^3)[1]	0.981±0.0	1.1-1.3	1.1-1.3	1.052±0.0
Viscosity (cSt)[2]	2.04±0.17	125 max.	125 max.	1.20±0.14
Solid (wt%)[3]	<0.100	2.5 max.	0.25 max	0.00
Ash (wt %)	0.012±0.0	0.25 max	0.15 max	-
Carbon (wt %)	51.14±1.72	-	-	15.27±1.43
Hydrogen (wt %)	6.22±0.07	-	-	13.80±0.09
Nitrogen (wt %)	0.78±0.01	-	-	1.45±0.03
Sulphur (wt %)	0.20±0.01	0.05 max.	0.05 max.	0.10±0.01
Oxygen (wt%)[4]	41.66±1.01	-	-	69.38±1.27
HHV (MJ/kg)	26.42±0.10	15 min.	15 min.	14.55±0.10

[1]Measured at 20°C; [2]Measured at 40°C; [3]ethanol insoluble (0.1µm filter); [4]by difference. Max: maximum value; Min: minimum value. Values are the means (n =3) ± standard deviations (SD)

4.4.2 Fourier-transform infra-red (FTIR)

FTIR spectra of chemical species in the bio-oil samples are shown in Figure 4.6. The common broad peak around 3439 cm^{-1} implies that the samples contain chemical compounds with hydroxyl group (O – H) such as water, alcohols and phenol (Bordoloi et al., 2015). The peak at a frequency around 2970 cm^{-1} is due C – H stretching vibration indicating the presence of saturated hydrocarbon in the organic phase while

the peak at a frequency around 2100 cm^{-1} common to both phases is ascribed to the $C \equiv C$ functional group (Guo et al., 2015). Vibration observed between 1625 cm^{-1} and 1707 cm^{-1} are attributed to $C = O$, which signifies the presence of aldehydes, ketones or carboxylic acids. The vibration around 1462 cm^{-1} is ascribed to $C = H$ indicating the presence of alkenes/aromatic hydrocarbons while the peak between 1388 and 1364 cm^{-1} in both cases is due to $C - H$ bond (Yorgun and Yildz, 2015). The sharp band around 1269, 1016 and 1092 cm^{-1} are due to $C - O$ vibration indicating the presence of alcohol and esters. The fingerprint between 900 and 620 cm^{-1} are ascribed to aromatic $C - H$ bending vibrations (Pan et al. 2012).

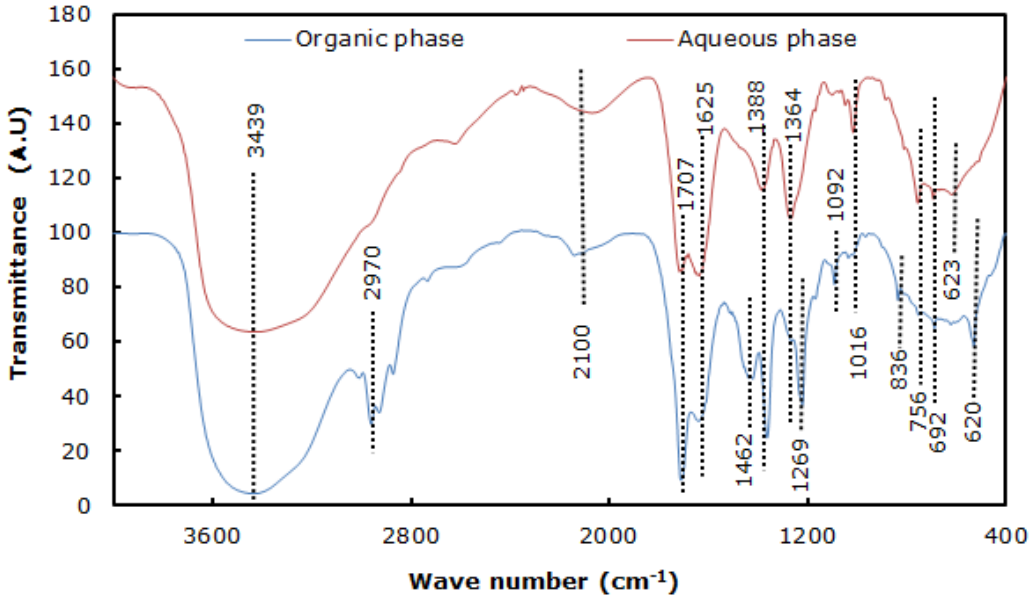

Figure 4.6: Averaged FTIR spectra (auto-smoothed and auto-baseline corrected) of bio-oil obtained at optimized condition

4.4.3 Thermogravimetric analysis of organic phase bio-oil

Thermogravimetric analysis (TGA) of bio-oil provides data on weight loss by evaporation as sample is heated over a certain temperature range. The resulting information

similar to the distillation data, which can be used to estimate amount of bio-oil that will distil into specific fuel products. In this study, TGA analysis of commercial fossil premium motor spirit (PMS), kerosene and diesel were performed as standards. The organic bio-oil was subjected to the same thermal treatment. From Figure 4.7(a), final evaporation temperature of PMS, kerosene and diesel was found to be 126, 185 and 291°C. Using the final evaporation temperature, by extrapolation, the organic phase bio-oil constitutes (Figure 4.7b) about 70 wt% volatile fraction. The mass loss above 300 °C can be attributed to thermal decomposition of the residue. About 68 wt% of the oil has boiling range similar to that of diesel. Similarly, approximately 53 wt% of the bio-oil is made up of kerosene boiling fraction while 35 wt% has boiling characteristic comparable to that of PMS. Information from the TGA simulated distillation can also be used as an indicator for selecting temperature condition for GC-S analysis of the oil. Based on the injection temperature selected (250 °C) for the bio-oil characterization, only about 62 wt% of the oil can be analysed by the GC-MS.

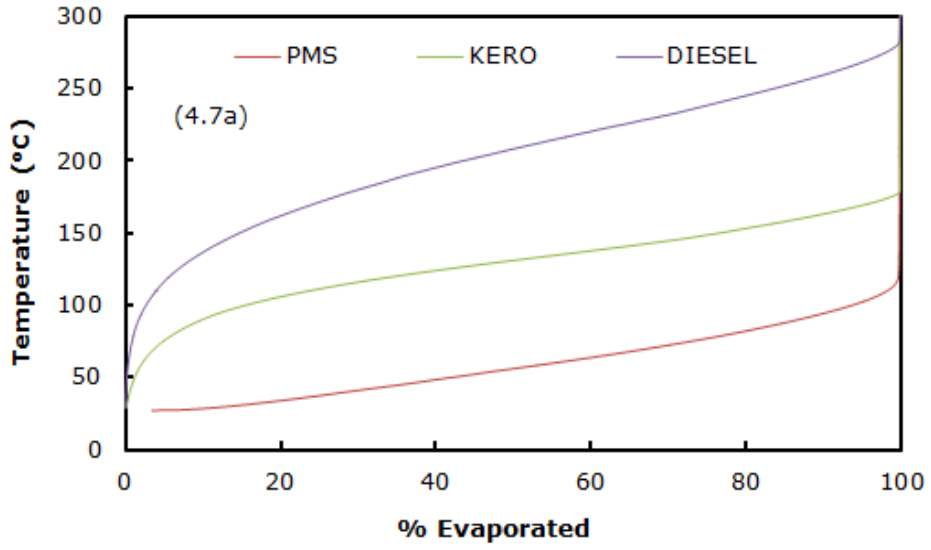

Figure 4.7 continued

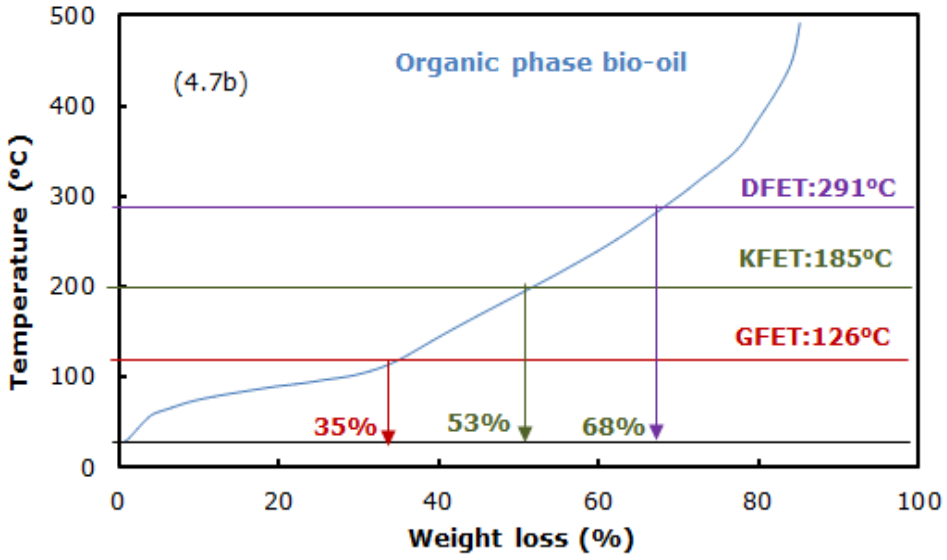

Figure 4.7: Simulated Distillation using TGA. (a) Premium motor sprit-PMS, kerosene and diesel (b) organic phase bio-oil. DFET, KFET and PMSFET: diesel, kerosene and PMS final evaporation temperature.

4.4.4 GC-MS analysis of bio-oil

Identification of detail chemical compounds in the bio-oil samples was carried out by GC-MS. Library search of twenty (20) most abundant compounds using MS NIST library 2011 showed that the organic phase consists predominantly benzene derivatives such as phenols, methyl-phenol, ethyl-phenol, methoxy-phenols, methoxy-benzene, benzaldehyde and benzene carboxylic acid, which accounted for approximately 70 % of the total organic phase. Other compounds identified are dimethylcyclohexene and ethylbiphenyl. The compounds were further grouped into acids, aldehydes and ketones (AAK); hydrocarbons (HC); benzene derivatives (BD); value added chemicals (VAC) as shown in Figure 4.8. These together can be processed to fuels and valuable chemicals via upgrading step, which is one of the focus of this study. The composition of organic phase bio-oil in this study is similar to the result of

GC-MS analysis reported by Strezov et al. (2008). The oil analysed by the author consisted large amount of benzene derivatives (24.46 wt %). Aqueous phase (Figure 4.8) comprised mainly organic acids, esters, ketones, aldehydes and oxygenated aromatics. The composition of bio-oil reported by Lee et al. (2010) was made up of 27.2 % organic acids, 7.9 % phenols, which is comparable to the aqueous phase composition recorded in this study.

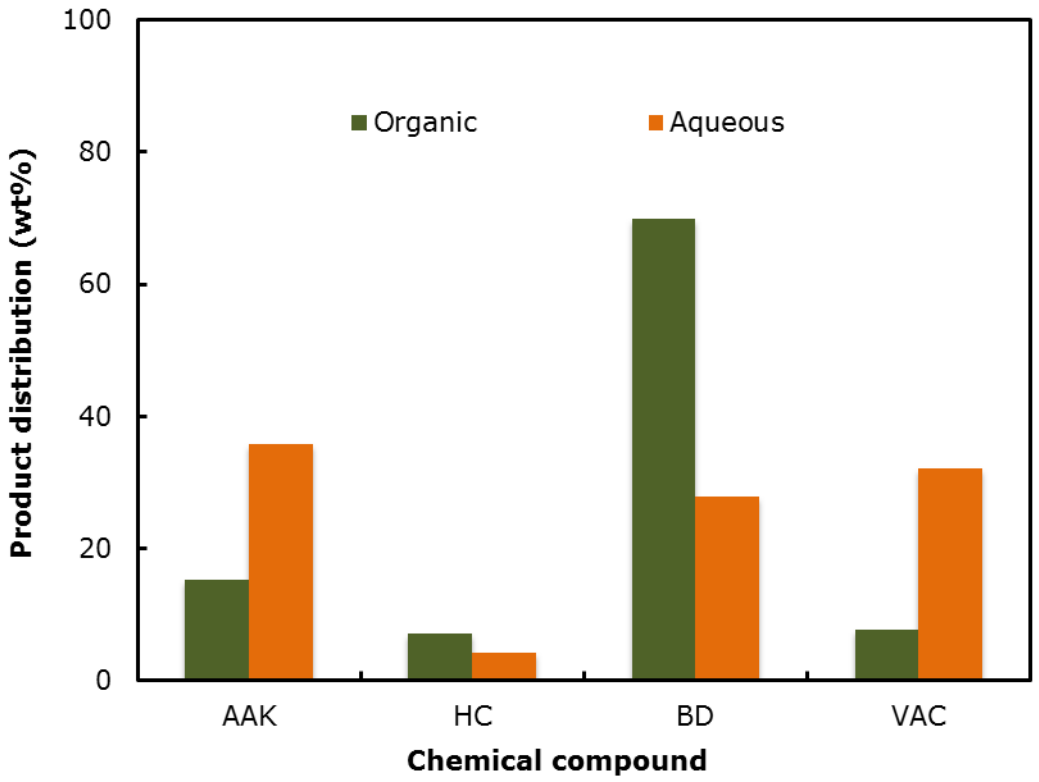

Figure 4.8: Group of chemical compounds identified. (AAK) acids, aldehydes and ketones; (HC) hydrocarbons; (BD) benzene derivatives; (VAC) value added chemicals

Generally, the bio-oil aqueous phase is considered less important and often discarded as pyrolysis by-products due to lack of specific applications. However, recent studies have proposed production of hydrogen *via* catalytic aqueous, and steam reforming

processes from this stream (Resende et al., 2015; Chan et al., 2015). Yet, these processes require complex system, which calls for further studies to understand the reaction mechanisms. Imidazole, the third most abundant component in the bio-oil aqueous phase is an important material in polymer industry. There has been growing interest in the synthesis and application of imidazole based polymer, *N*-vinylimidazole. This is because homo- and copolymers of *N*-vinylimidazole belong to a rapidly emerging class of polymeric materials. Beletskaya et al. (2010) employed *N*-vinylimidazole for catalyzing Michael addition of uracil, 1*H*-1,2,4-triazole, succinimide, 3,5-dimethyl-1*H*-1,2,4-triazole, and oxazolidin-2-one to methyl acrylate, but-3-en-2-one, cyclohex-2-en-1-one, and methyl vinyl sulfone. This is interesting considering the minimal energy requirement for the reaction, conducted in water, and at room temperature. Poly (N-vinylimidazole also serves as indicator in chemical reactions that produce oxygen, which explains its usefulness as biosensors for phenolic compounds, and biomarkers for biomass smoke exposure. Metal ion binding properties of imidazole and poly (1-vinylimidazole) have been reported by Takafuji et al. (2004).

4.5 GC-TCD Analysis of Non-condensable Gas

Samples of non-condensable gas were collected at different temperature (450, 600 and 750 ^{o}C) under the pyrolysis condition of 50 ^{o}C/min and 5 L/min N_2 as shown in Figure 4.9. The gas composition (nitrogen free basis) detected include hydrogen (H_2), carbon monoxide (CO), carbon dioxide (CO_2) and methane (CH_4). At 450 ^{o}C, the main components of the gas were CO_2 (16.42 vol %), H_2 (15.44 vol %) and CO (9.79 vol %). The high amount of CO_2 and H_2 together with the release of CO are attributed to fragmentation and subsequent transformation of unstable carbonyl and carboxyl groups from depolymerization of holocellulose (hemicellulose and cellulose) and the

resulting char transformation (Collard and Blin, 2014). The trace of CH_4 (0.84 vol %) detected at this temperature is mainly due to demethylation of char from hemicellulose and fragmentation of methoxy group of lignin. As the temperature increased, the amount of CO_2 declined considerably due to the fact that fragmentation of glyosidic bonds in the holocellulose must have been completed. This observation is in strong agreement with the biomass TG/DTG result. A total of 14.04 and 12.56 vol% CO_2 was recorded at 600 and 750 ^oC. The amount of CO_2 recorded at 450^oC (16.42 vol %) in this study is similar to the value (18.5 % CO_2) reported by Strezov et al. (2008) during the pyrolysis of NG at 500 ^oC. Decline in the amount of CO_2 with increasing pyrolysis temperature has been reported by De Conto et al. (2016). The authors recorded CO_2 value of about 42.25 vol% at 500 ^oC, which declined substantially to around 12 vol % at 600^oC and then to about 9.vol% at 700 ^oC. The continuous rise in the CO, H_2 and CH_4 components of the non-condensable gas with pyrolysis temperature can be ascribed to carbon-carbon scission within the lignin and demethylation of final residue from the sample. This can also be attributed to the pyrolysis secondary reactions usually promoted by mineral elements in the biomass, particularly the alkali and alkali element (K, Ca) (Mohammed et al., 2016b). At 600 ^oC, the amount of H_2, CO and CH_4 recorded was 25.32, 13.60 and 3.36 vol%. This value increased to 35.45, 23.12 and 6.55 vol% at 750 ^oC. The ratio of H_2/CO (vol%/vol %) increased from 1.58 to 1.86 at 450 to 600 ^oC and there after decreased to 1.53 at 750 ^oC. This indicate that the non-condensable gas from NGS pyrolysis is a suitable feedstock for Fischer-Tropsch (FT) synthesis, where the syngas can be further processed into liquid fuel (Pirola et al., 2014; De Conto et al., 2016). However, presence of hydrogen sulphide (H_2S) in bio-syngas is a common characteristic of a non-condensable gas from biomass pyrolysis due to the presence of sulphur in the feedstock (Mohammed et al., 2015b). Catalyst

used in the FT synthesis are highly sensitive to H_2S even at part per million level (Yamamoto et al., 2015). Gas cleaning is therefore need prior to the FT process. H_2S can be selectively removed from gas stream by absorption with the aid of selexol solvent (Mohammed et al., 2014a).

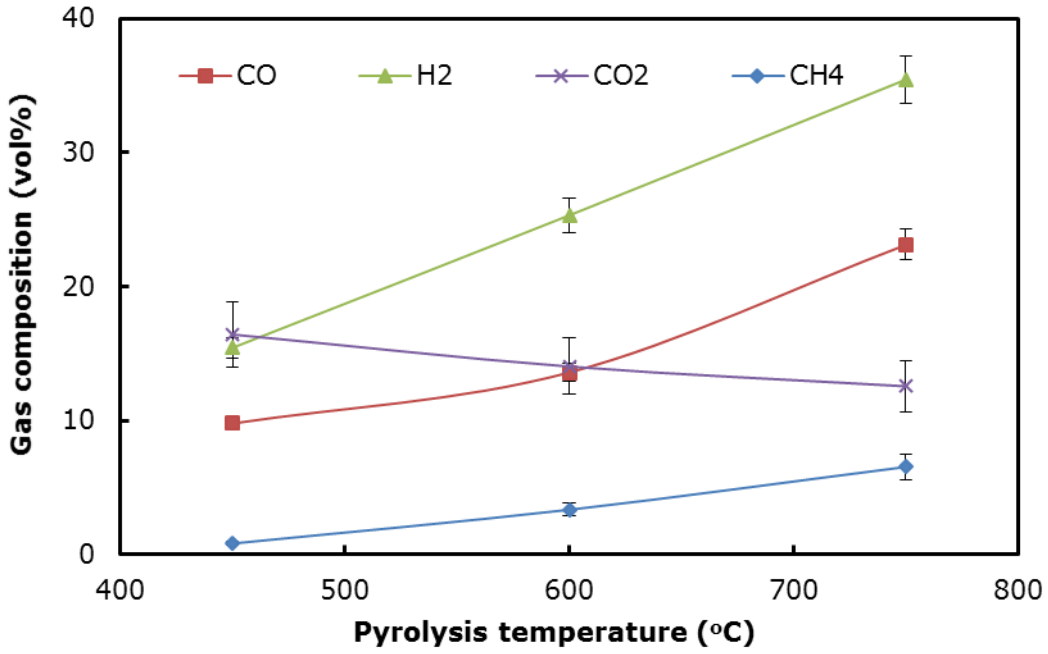

Figure 4.9: Composition of non-condensable gas collected (N_2 free basis) at 50 °C/min and 5 L/min N_2 at different pyrolysis temperature. Values are the means (n = 2) ± SD

4.6 Characteristics of produced bio-char

4.6.1 Physicochemical properties of produced bio-char

Physicochemical properties of NGS bio-char produced at different temperature and 50 °C/min and 5 L/min nitrogen flow are summarized in Table 4.10. Volatile matter (VM) and heating value of the bio-char decreased with increasing pyrolysis temperature while the ash content (AC) and fixed carbon (FC) increased. This means that with increasing temperature, more VM is released and highly thermal stable and non-

volatile components of the source biomass are left within the remaining solid. Reduction in the heating value is attributed to the increased AC, which is non-combustible and generally has negative impact on the solid fuel (Mohammed et al., 2014b). Ultimate analysis showed increased carbon content (C) with pyrolysis temperature while oxygen (O), and hydrogen (H) decreased (Table 4.10). This can be attributed to structural transformation of char via scission and cracking of weak bond within the bio-char structure. Similarly, nitrogen (N) and sulphur (S) content also declined with pyrolysis temperature. This shows that N and S compounds are released during pyrolysis (De Conto et al., 2016), which is responsible for the sulfur and nitrogenous compounds detected in the bio-oil (Appendix I).

Table 4.10: Physicochemical properties of NGS bio-char produced at 50 oC/min and 5 L/min nitrogen flow at different pyrolysis temperature

Property	450°C	600°C	750°C
Proximate analysis (wt%) dry basis			
Ash	10.47±0.29	13.40±0.31	14.49±0.30
Volatile matter (VM)	19.41±0.21	15.09±0.17	12.70±0.13
Fixed carbon (FC)	70.12±0.51	71.51±0.51	72.81±0.50
FC/(VM+FC)	0.78	0.83	0.85
HHV (MJ/kg)	29.06±0.01	27.60±0.01	26.71±0.01
Ultimate analysis (wt%) dry basis			
Carbon (C)	72.21±0.41	79.78±0.44	85.86±0.42
Hydrogen (H)	5.20±0.01	3.61±0.01	2.67±0.01
Nitrogen (N)	1.16±0.01	0.98±0.00	0.66±0.00
Sulphur (S)	0.30±0.00	0.18±0.00	0.11±0.00
Oxygen (O)	21.13±0.22	15.45±0.20	10.70±0.21
O/C (mole ratio)	0.22	0.15	0.09

Values are the means (n =3) ± standard deviations (SD)

4.6.2 Thermal stability of produced bio-char

Thermal stability of bio-char can be evaluated from the proximate, ultimate and TGA analyses. De Conto et al. (2016) reported that the ratio of FC to the sum of FC and VM

[FC/ (VM+FC)] of bio-char is an indicator of thermal stability. A ratio between 0.78 and 0.85 was recorded in this study, which indicates high thermal stability of organic matter in the bio-char. Spokas (2010) reported that there is connection between bio-char stability and O/C molar ratio. The author stated that O/C ratio below 0.2 signifies a minimum bio-char half-life of 1000 years. O/C mole ratio of 0.22, 0.15 and 0.09 was recorded for the bio-char produced at 450, 600 and 750°C. Similarly, Harvey et al. (2012) proposed a recalcitrance index (R_{50}) for evaluating bio-char suitability for carbon sequestration. They defined R_{50} as the ratio of temperature of bio-char ($T_{50\ bio-char}$) to temperature of graphite ($T_{50\ graphite}$) at which both materials decompose 50% initial weight under oxygen atmosphere. They grouped bio-char based on the R_{50} value into class A ($R_{50} \geq 0.70$), B ($0.50 \leq R_{50} < 0.70$) or C ($R_{50} < 0.50$) where class A, B and C represent carbon sequestration potential similar to graphite, intermediate sequestration potential and carbon sequestration potential similar to the biomass plant. Thermal decomposition of the produced bio-char in oxygen atmosphere (50 mL/min) was carried out from ambient to 900 °C at 10 °C/min (Figure 4.10). Thermal stability increased with pyrolysis temperature. Decomposition of the bio-char produced at pyrolysis temperature of 450, 600 and 750 °C commenced at 250, 309 and 320 °C respectively. The corresponding $T_{50\ bio-char}$ was 380, 385 and 392 °C. Using 886 °C for $T_{50\ graphite}$ (Harvey et al., 2012), the equivalent R_{50} value was 0.43, 0.43 and 0.44. Hence, the bio-chars from NGS in this study are class C and have potential carbon sequestration similar to the uncharred biomass plant. The TGA result indicate that the char can be used in processes under moderate temperature up to 300 °C. Residue (non-combustible) from the TGA profile (Figure 4.10) increased with temperature pyrolysis temperature. This observation is in good agreement with the proximate

analysis results particular the increased ash content observed with pyrolysis temperature.

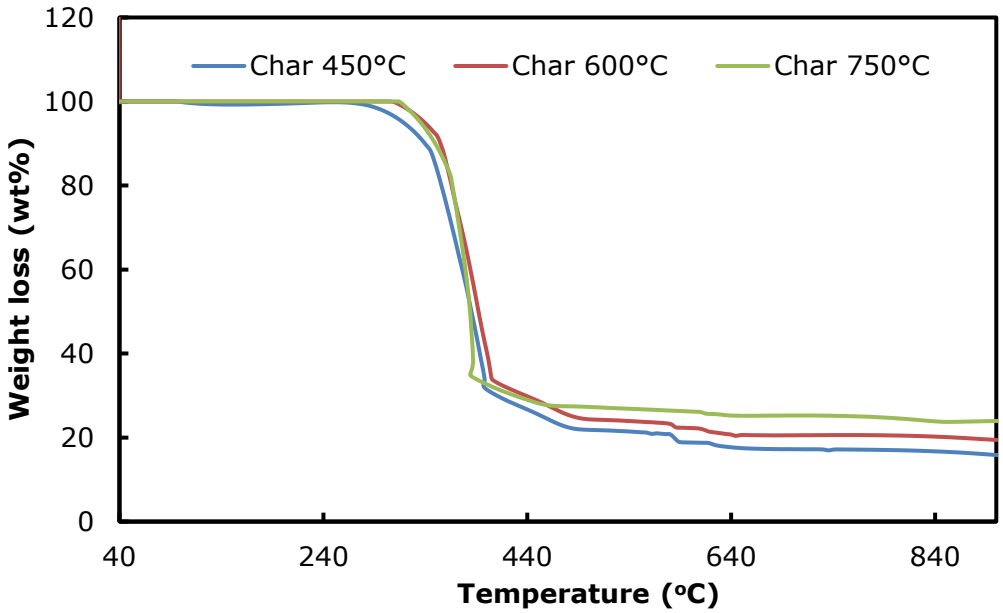

Figure 4.10: Combustion profile of NGS bio-char produced at different pyrolysis temperature. Condition: 10 mg sample, 50 mL/min oxygen and 10 °C/min heating rate

4.6.3 Morphology and mineral composition of produced bio-char

Scanning electron micrograph and elemental mapping of the bio-char (Figure 4.11) showed that the materials have porous structures, which increased with pyrolysis temperature. This result was further confirmed by the result of physisorption analysis (Table 4.11). The specific surface area recorded for the bio-char produced at 450, 600 and 750 °C was 0.014, 0.126 and 0.293 m^2/g and the corresponding pore volume of 0.08, 010 and 0.13cm^3/g was observed. From elemental mapping of the bio-char (Figure 4.11), potassium (K), calcium (Ca), magnesium (Mg), phosphorus (P) and chlorine (Cl) constitute the major mineral elements in the bio-char, which originated

from the source biomass. K, Ca, Mg and P are macronutrients needed for most plant growth. The nature of these minerals was confirmed by XRD analysis. XRD diffractogram of bio-char (Figure 4.12) shows disappearance of the cellulose peak ($2\theta=22.16^{o}$) present in the source NGS biomass in all the bio-char. With increasing pyrolysis temperature, the peak broadened and became almost flat at pyrolysis temperature of 750°C. New peaks were observed at 2θ value of 28.46, 40.66 and 50.32°, which are evidence of crystalline system in the char. XRD search and match using PANalytical X'Pert High Score Plus software program revealed that the produced bio-char samples consisted predominantly sylvite (KCl) with a crystal system corresponding to those of the new peaks identified (Yuan et al., 2011). Sylvite is a good candidate for fertilizer production. Bio-char can therefore be applied as a source of macronutrient for agricultural production. Traces of various barium cerates ($BaCeO_3$) were also detected. This material is an important ingredient in the development of fuel cells (Ketzial et al., 2013; Medvedev et al., 2014). Further investigation is needed in order to utilize the bio-char as an alternative source of barium cerate in fuel cell application. Summary of pyrolysis product application is shown in Figure 4.13.

Table 4.11: Pore characteristics of NGS bio-char

Physisorption analysis			
Surface area (BET) (m^2/g)	0.014	0.126	0.293
Pore volume (cm^3/g)	0.008	0.100	0.130

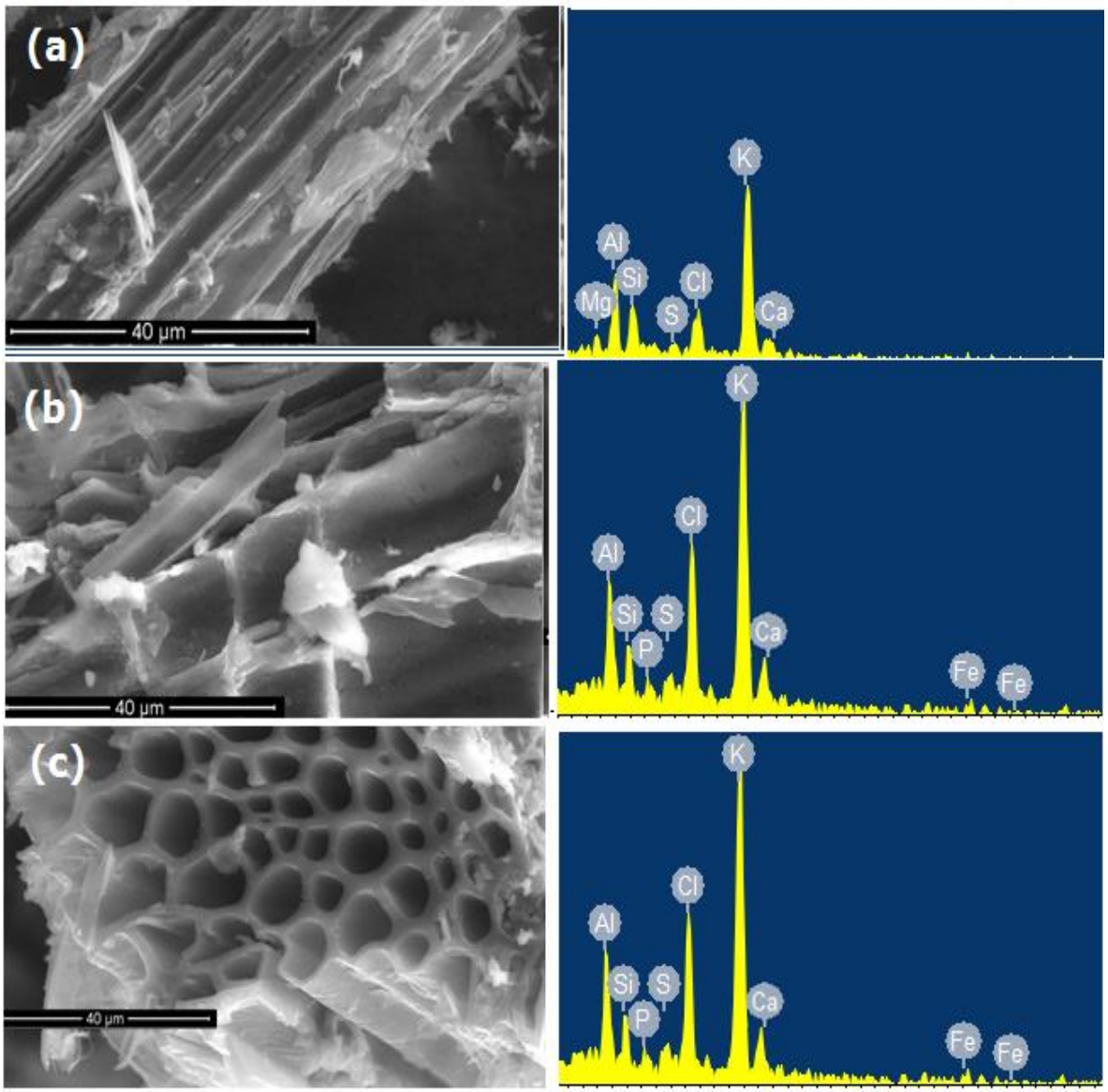

Figure 4.11: SEM-EDX of biochar obtained at (a) 450 °C, (b) 600 °C and (c) 750 °C from NGS biomass

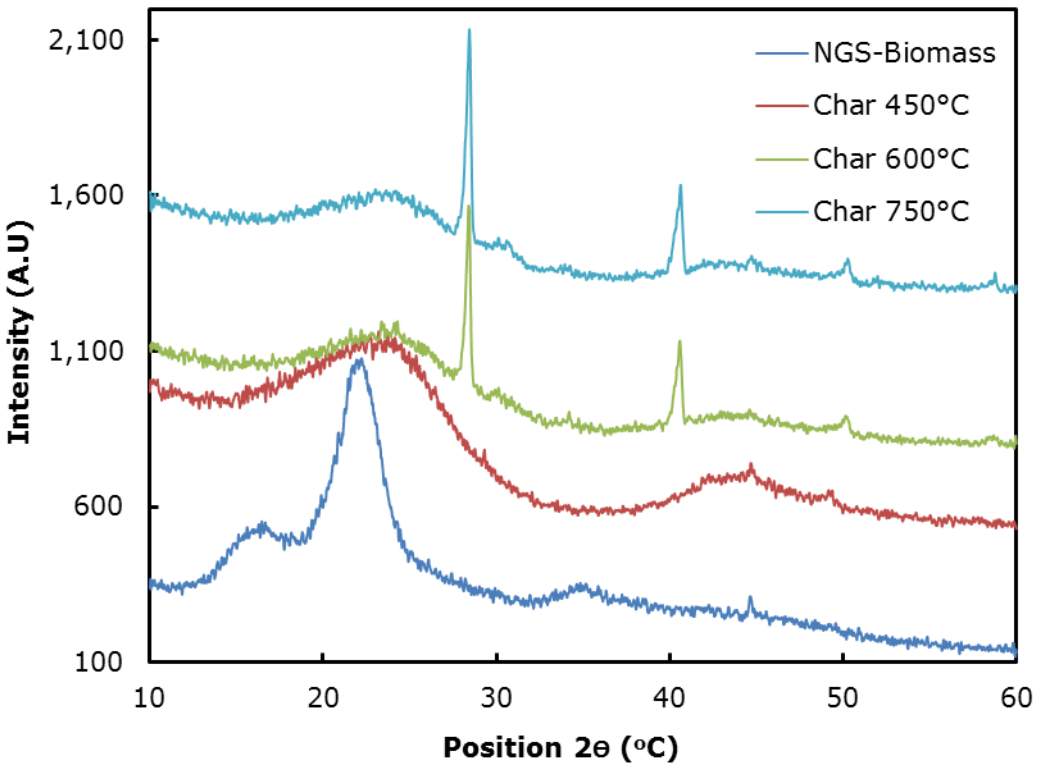

Figure 4.12:X-ray diffractogram of NGS biomass and corresponding bio-char produced at 450, 600 and 750 °C

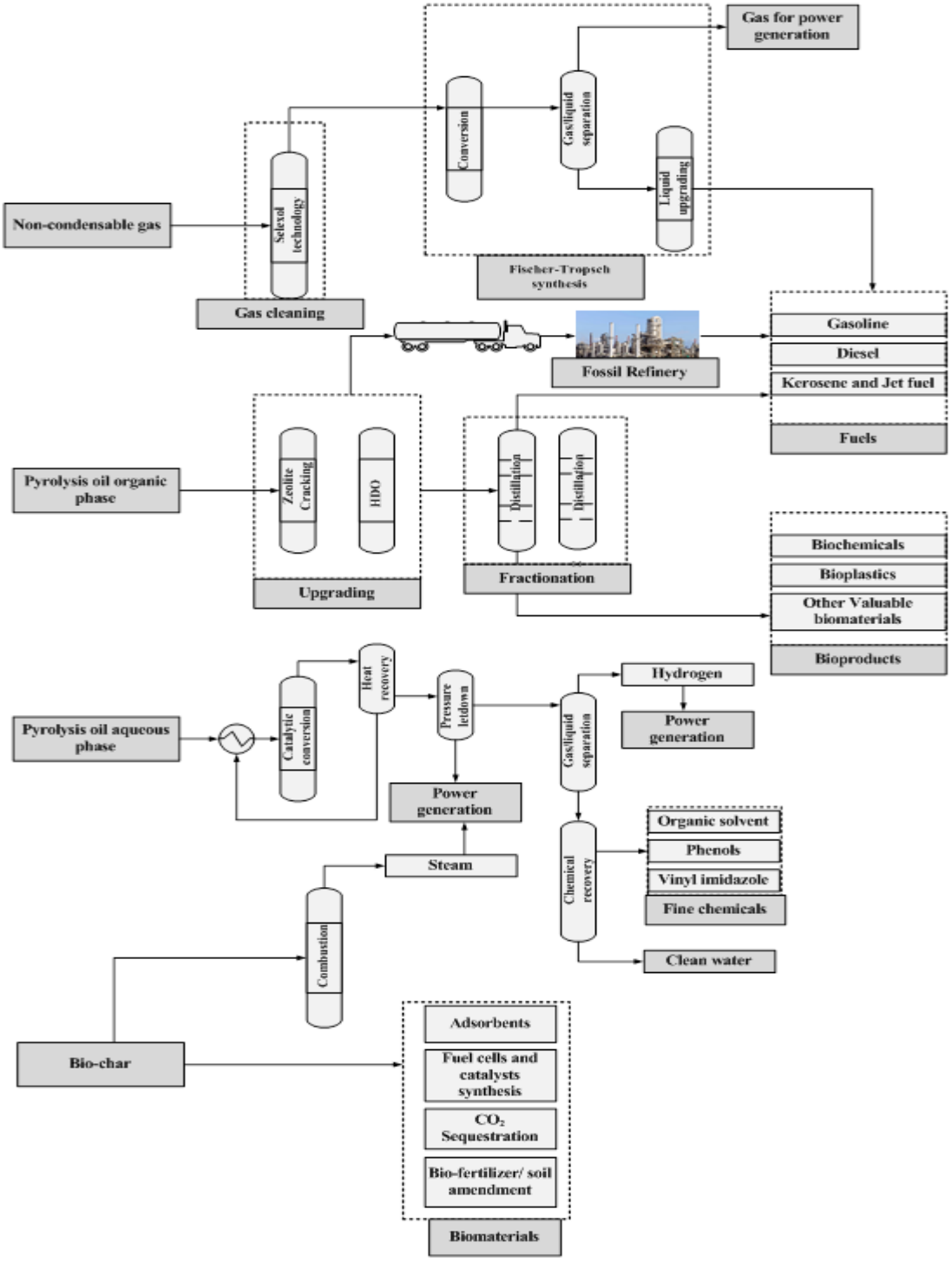

Figure 4.13: Schematic diagram of possible application of pyrolysis products

4.7 Energy Analysis of Napier Grass Pyrolysis Process

4.7.1 Energy yield of pyrolysis product

Energy yield of pyrolysis product is obtained from mass flow and higher heating values of the organic phase bio-oil, bio-char and non-condensable gas with respect to that of the feedstock. Figure 4.14 shows the mass flow collected at optimized condition and the corresponding heating values of each stream. The energy yield of the organic phase bio-oil was about 26 % compared to 31 % and 47 % for the bio-char and non-condensable gas. This is attributed to lower mass production of the organic phase since the higher heating value on dry basis is higher relative to other product streams. Higher energy yield from the non-condensable gas is not surprising due to the stream high mass flow, which is 9 wt% higher than the mass flow of bio-char and approximately two-folds the mass flow of organic phase. Study on pyrolysis of poplar wood in a fixed bed reactor at 600 ^{o}C and 50 ^{o}C/min reported by Chen et al. (2016) showed that energy yield from bio-char was 46.69 % while bio-oil and non-condensable gas had 31.84% and 22.34 % yield respectively. They attributed the higher energy yield recorded from the bio-char to higher heating value (32.10 MJ/kg) despite the lower mass yield while the relatively lower energy yield from the bio-oil was ascribed to lower calorific value (13.93 MJ/kg) in spite of the higher mass yield (41.67 wt%). Although, the authors did not state the portion of the bio-oil used in the energy analysis.

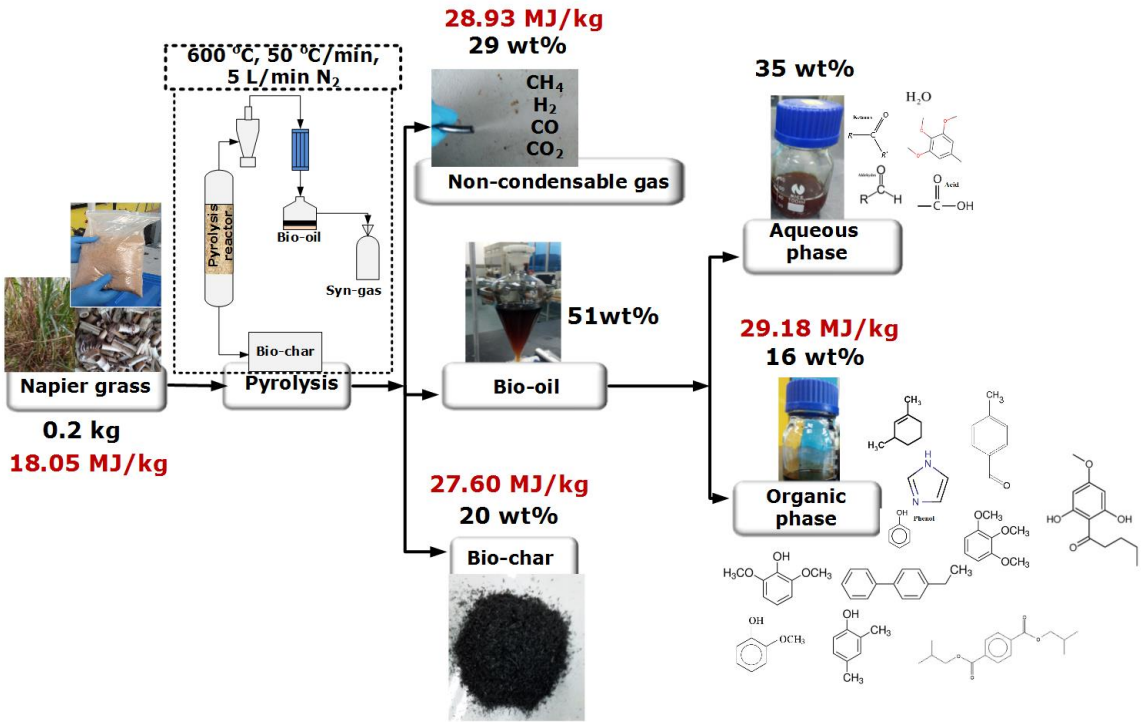

Figure 4.14: Mass and flow of Napier grass pyrolysis in a fixed bed reactor

4.7.2 Pyrolysis process energy evaluation

Energy consumption in the pyrolysis process can be related to the overall energy yield of the pyrolysis products, which can be used as an indicator of pyrolysis process energy efficiency. In this study, the total energy input such as energy consumption during pre-processing (drying and grinding) and pyrolysis stage (pyrolysis reactor and cooling) is summarized in Table 4.12. Napier grass was bone dried in an electrical oven for 12 h. For 1.0 kg bone dried biomass processing, 1 h chiller and pyrolysis reactor operation, the total electrical energy consumption was 82.67 MJ (22.96 kWh). The ratio of energy output to energy input recorded is 0.22. This indicates that the total energy produced from the process is far less than the energy input. The highest

contributor to the energy consumption is the drying stage, consuming approximately 84 % of the total energy input. Pyrolysis stage, which is the heart of the process consumed only about 15.4 % of the total energy consumption. This mean that the energy efficiency of the process can be improved by reducing the energy consumption at drying stage. Combustion of bio-char and non-condensable gas can generate steam and hot air, which could be used for drying the biomass. This would definitely reduce the energy requirement significantly and make the process more energy efficient.

Table 4.12: Energy evaluation of Napier grass pyrolysis process in a fixed bed reactor

	Energy (MJ)		
Process Stage	Input	output	output/input ratio
Drying	69.12	-	-
Grinding	0.81	-	-
Pyrolysis reactor	5.83	-	-
cooling water	6.91	-	-
Organic bio-oil	-	4.67	-
Bio-char	-	5.52	-
Non-condensable gas	-	8.39	-
Total	**82.67**	**18.58**	**0.22**

4.8 Conclusion

Pyrolysis of Napier grass was carried out in a vertical fixed bed tubular reactor. Optimization of process variables such as temperature, heating rate and nitrogen flow rate was performed by means of central composite design approach. The individual model equation for bio-oil, bio-char and non-condensable gas yield was developed using set of experimental data and analysis of variance. Temperature, nitrogen flow rate and heating rate had significant impact on the bio-oil and non-condensable gas yield while the bio-char yield was mainly affected by the pyrolysis temperature. The

oil yield was maximized by optimizing the process variables and optimum bio-oil yield of 51.94 wt% was predicted at 600 °C, 50 °C/min and 5 L/min nitrogen flow. This result was further validated through multiple experiments and the average value of the experimental results was in good agreement with the predicted value. The optimum bio-oil yield recorded in this study is higher than the pyrolysis oil yield derived from Napier grass reported in the literature. The bio-oil obtained throughout was two-phase liquid, the organic phase (high molecular weight component) and aqueous phase (low molecular weight component). Both phases collected at optimized condition were characterized using standard analytical techniques. The results revealed that the organic phase consist mainly of various benzene derivatives and hydrocarbons which can be further processed into fuels and valuable chemicals through upgrading step, which is discussed in the subsequent chapters. The aqueous phase was predominantly water, acids, ketones, aldehydes and some phenolics and other water-soluble organics. The non-condensable gas was made-up of methane, hydrogen, carbon monoxide and carbon dioxide with high hydrogen/carbon monoxide ratio suitable for Fischer-Tropsch (FT) synthesis. Biochar collected was a porous carbonaceous material, rich in mineral elements, which may be used as adsorbent, solid fuel or source of macronutrient for agricultural production. The bio-char also possessed potential for carbon sequestration. This study demonstrated that Napier grass biomass is a potential feedstock for production of high-value bioenergy precursors.

CHAPTER FIVE

5. IMPROVING QUALITY OF BIO-OIL DERIVED FROM NAPIER PYROLYSIS VIA BIOMASS PRETREATMENT

5.1 Introduction

This chapter evaluates pre-treatment of Napier grass using three different aqueous solvents. It gives experimental results on impact of sulfuric acid, sodium hydroxide and deionized water on the resulting pre-treated sample, pyrolysis product distribution and characteristics bio-oil. It discusses result of analysis of leachate from the pre-treatment process and their possible application.

5.2 Ash removal, Mass and Energy Yields

Severity factor (Ro) varies exponentially with pre-treatment temperature and values between 0.4 and 2.7 with maximum temperature of 38 ^{o}C were used to reduce the energy cost of the pretreament using deionized water, while dillte (0.5-2.5 %w/w) NaOH and H_2SO_4 were used to allow possible downstream application of effluent. Improvement in the characteristics of pre-treated NGS is observed with increasing pre-treatment Ro from 0.4 to 2.7 (Figure 5.1) in neutral solvent. Mass yield decreased from 84.12 to 80.61 % while the energy yield increased from 84.12 to 85.33 % which account for about 1.21 %. The rise in energy was attributed to the level of ash extraction achieved during the pre-treatment (Figure 5.2) while the reduction in mass yield was due to the removal of extractives and solubilization of some parts of the hemicellulose (Eom et al., 2011; Asadieraghi and Wan Daud, 2014). Although the value of energy rise appeared to be less significant due to the loss in the mass yield, but this suggests that mass loss has a great impact on the energy recovery. However, the mass loss was relatively low as more than 80 % of the initial mass of the sample was recovered after the pre-treatment. Ash extraction under this treatment condition was 20 to 64.29 % (Figure 5.2).

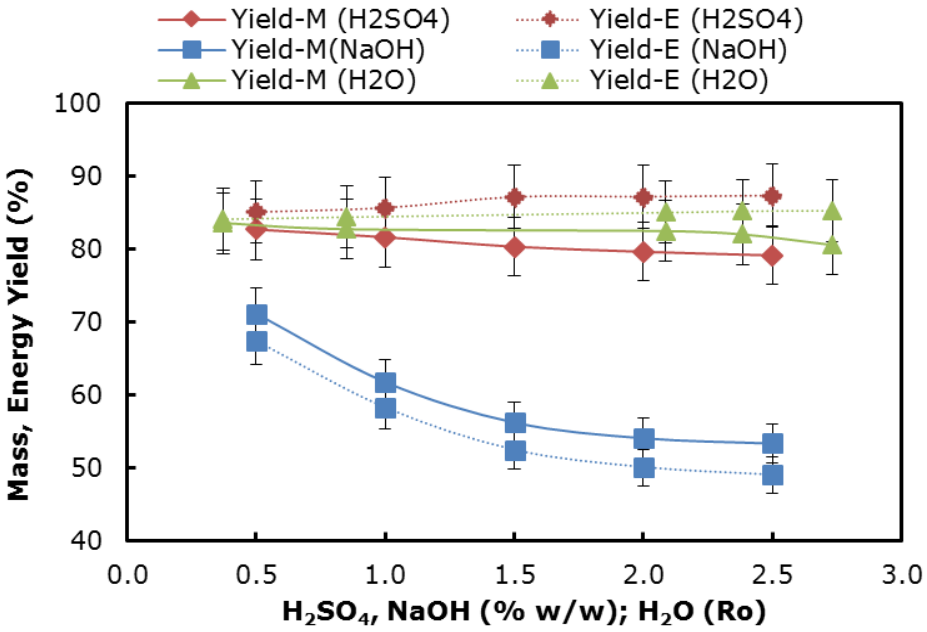

Figure 5.1: Mass and energy yield of pre-treated samples. (YM) mass yield, (YE) energy yield

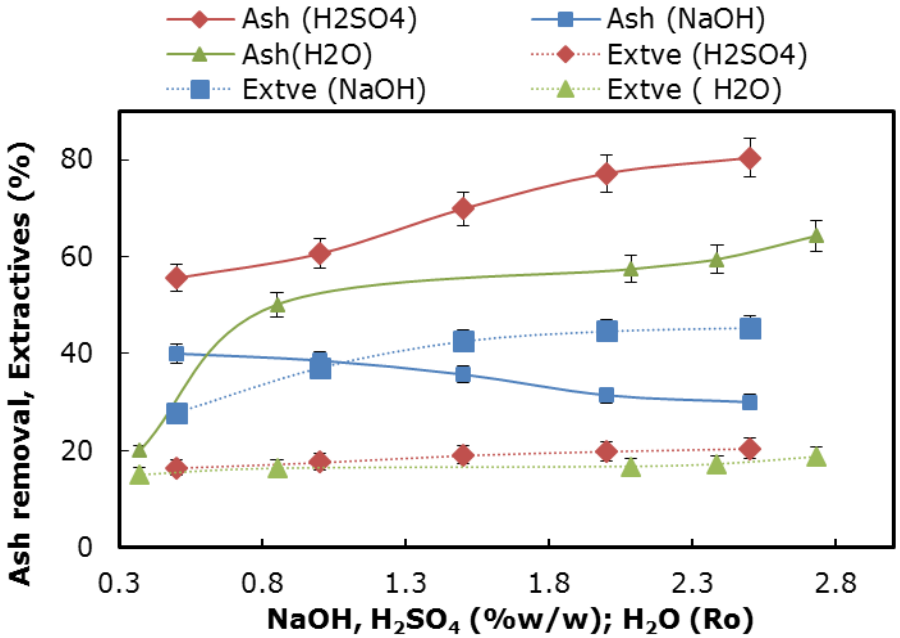

Figure 5.2: Effect of pre-treatment solvents on ash and extractives removal from NGS

For an efficient and effective pre-treatment process, a compromise between the energy and mass yield, percentage ash extraction and most importantly, the duration of pre-treatment is needed. In large scale process, a lower pre-treatment time will facilitate several treatments per day, which will in turn impact positively on bio-oil production. Catalytic activities of biomass ash is said to have high impact on the bio-oil quality when the ash content of the source biomass is more than 1.0 wt% (Carpenter et al., 2014). Ro value around 0.9 corresponds to an hour operation and yielded more than 83 % mass and 84 % energy with ash extraction above 50 %. This translates to about 0.87 wt% ash (Appendix II) in the pre-treated NGS compared to the raw NGS with 1.75 wt% ash. Therefore, Ro value of 0.9 can be regarded as optimum condition for pre-treatment of NGS biomass using neutral solvent. Sample treated at this condition was used for further analysis.

Pre-treatment of NGS with sulfuric acid (0.5 to 2.5 %w/w concentration) results in decrease in mass yield from 82.78 to 79.18 % with corresponding energy yield from 84.42 to 87.35 % (Figure 5.1). The decline in the mass yield is attributed to high solubilization of extractives, hemicellulose while the rise in the energy yield was due to high improvement in the heating value of the pre-treated sample (Eom et al., 2011; Carpenter et al., 2014) brought by the level of ash extraction recorded (Figure 5.2). Generally, among the components of lignocellulosic material, hemicellulose is prone to hydrolytic attack due to resistance to hydrogen bond formation by some of its component such as glucuronic acid and acetic acid (Cuvilas and Yang, 2012). Acid concentrations from 0.5 to 1.5 w/w% (Figure 5.1) showed a sharp increase in energy yield from 85.06 to 87.17% and thereafter remain relatively stable. The mass yield under this condition was within 80 %. Similarly, about 70 % ash extraction was

recorded which is equivalent to 0.53 wt% ash (Appendix 2) in the pre-treated sample. This satisfies the ash requirement of below 1.0 wt% for high yield and quality bio-oil production. Thus, NGS sample treated at 1.5 w/w% acid concentration was further analysed.

Pre-treatment using NaOH (0.5-2.5 w/w %) showed more impact on both mass and energy yields with continuous decline from 71.20 to 53.38 % and 67.50 to 49.04 % (Figure 5.1). The decrease in mass yield was as a result of high removal of lignin, extractives, and some hemicellulose and cellulose (Menon and Rao, 2012; Yang et al., 2015). The ash removal (Figure 5.2) declined with increasing alkaline concentration, which in addition to lignin removal, lower the higher heating values of the pre-treated samples. The combine effect of this is responsible for the decrease in the energy yield. Alkaline pre-treatment cannot be considered suitable for a pyrolysis process since large portion lignin is removed, which is an important component of the feedstock in the pyrolysis process. In addition, lower ash extraction recorded throughout this process with pre-treated samples having ash content more than 1.0 wt% (Appendix II) is an indication that the pyrolysis process will be affected by catalytic activity of the biomass ash (Carpenter et al., 2014). For the purpose of comparison with other solvents (H_2O and H_2SO_4), sample pre-treated with 1.5 w/w% NaOH was further examined.

5.3 Effect of Pre-treatment on Mineral Composition

Mineral compositions of NGS for both raw and pre-treated samples are summarized in Table 5.1. Potassium (K) constitutes the most abundant metal in the raw NGS compared to other metals such as sodium (Na), calcium (Ca), Aluminium (Al), iron (Fe) and silicon (Si). This could be attributed to the nature of treatment or nutrient uptake during the cultivation of the Napier grass. Leaching of the individual element

in the biomass varied with solvent. High removal of alkaline metals such as sodium (Na) and potassium (K) were recorded with neutral solvent, which increased with pre-treatment Ro. The corresponding removal efficiency recorded was 90 % and 74 %. This suggests that considerable amount of the Na and K in the NGS are present in form of water soluble salts such as salt of chlorides, nitrates, carbonates and phosphates. For other elements, slight declines were observed in calcium (Ca), aluminium (Al), iron (Fe) and silicon (Si) content after the treatment. The Ca, Al and Fe minerals can be said to be in cation form bound to reactive sites of the NGS biomass which can be removed substantially through ion exchange (Jiang et al., 2013**;** Carpenter et al., 2014; Wigley et al., 2015). The small reduction in Si content suggest that NGS biomass is made up of two forms of silica, the amorphous silica, which is normally deposited on the outer walls of epidermal cells and dissolved in water as $Si(OH)_4$ while the second type of Si is physiologically bond to the plant tissue and cannot be removed by the neutral solvent (Deng et al., 2013; Gudka et al., 2015).

Table 5.1: Mineral composition of raw NGS and pre-treated samples using NaOH, H_2SO_4 and deionized water

Pre-treatment		Mineral Composition (mg/kg)					
	Ro	Na	K	Ca	Al	Fe	Si
Raw	0.0	12.85±1.05	3079.51±224.80	206.71±13.20	64.67±4.66	38.93±4.01	206.0±25.13
H_2O	0.4	4.63±0.34	1299.02±94.83	182.51±5.28	57.27±1.96	35.80±1.63	187.19±21.62
	0.9	2.67±0.22	1120.98±81.83	168.74±4.40	53.61±1.72	33.57±1.40	182.39±21.03
	2.1	2.40±0.15	1099.02±80.23	163.03±4.03	53.20±1.72	33.35±1.38	181.91±20.97
	2.4	1.99±0.12	974.63±71.14	147.56±3.04	52.98±1.72	31.74±1.21	180.47±20.80
	2.7	1.28±0.08	800.49±58.44	136.67±2.35	52.88±1.75	29.57±0.99	179.99±20.74
H_2SO_4	(w/w%)						
	0.5	4.10±0.24	988.20±62.56	166.15±3.80	51.18±1.44	33.65±2.90	219.22±30.62
	1.0	2.08±0.17	733.88±55.11	152.55±2.90	45.80±1.65	28.32±2.11	247.29±31.24
	1.5	1.48±0.14	483.88±27.21	105.33±2.10	39.98±1.35	24.99±1.90	253.78±31.37
	2.0	1.26±0.10	278.22±15.89	89.55±2.90	33.33±1.31	18.25±1.77	282.44±35.65
	2.5	0.47±0.07	142.88±12.63	52.75±2.90	30.78±1.28	16.75±1.69	338.79±38.85
NaOH	(w/w%)						
	0.5	387.14±24.33	873.35±34.76	169.51±3.20	57.61±1.66	32.65±2.80	78.78±2.85
	1.0	431.29±27.17	565.78±31.17	142.94±2.78	40.75±1.28	30.32±2.41	51.39±2.55
	1.5	459.56±26.14	334.15±23.14	123.81±2.40	29.38±1.15	27.99±2.00	36.69±2.19
	2.0	557.22±27.10	322.76±20.10	88.21±2.03	20.33±1.11	23.25±1.97	31.81±2.05
	2.5	593.20±28.07	290.48±18.07	53.67±1.40	14.13±1.08	21.75±1.59	26.42±1.99

5.4 FTIR of Raw and Pre-treated NGS Samples

Functional group distribution in the NGS before and after the aqueous pre-treatment was evaluated. Peaks were identified at different frequency as shown in Figure 5.3. The spectra showed two distinct regions with frequencies between 3750-2916 cm^{-1} and 1753-615 cm^{-1}. The band between 3750 and 3421 cm^{-1} are attributed to different hydroxyl group (alcohol/phenol) stretching vibrations (Xu et al., 2013; Nhuchhen et al., 2014). The band at 3750 cm^{-1} in the RNGS became wider in WTNGS sample due to the stretching of the H-bonded hydroxyl functional group (Lupoi et al., 2014). The broad peak at 3405 cm^{-1} in the RNGS shifted to a higher wave number, 3656 cm^{-1} and became enhanced in the ACTNGS and ALTNGS samples due to attenuation of hydrogen bonds between cellulose molecules by the acid and alkaline solvents (Das et al., 2015). The band at 2937 cm^{-1} is as a result of aliphatic saturated C-H stretching vibrations (asymmetric and symmetric methyl and methylene stretching groups) from extractives which almost disappeared in all the pre-treated samples, confirming the removal of extractives. In the fingerprint region (1753- 615 cm^{-1}), the band around 1600 cm^{-1} in the RNGS due to the ring-conjugated C=C bonds of lignin (Nhuchhen et al., 2014; Lupoi et al., 2014) shifted to around 1750 cm^{-1} in the pre-treated samples. The band became improved in the WTNGS and ACTNGS while it almost levelled completely in the ALTNGS, which confirms the removal of lignin in the alkaline process. New peak appeared in the WTNGS and ACTNGS samples around 1450 cm^{-1} which is ascribed CH_3 bending vibration in the lignin (Lupoi et al., 2014). The band observed at 1200 cm^{-1} is an indication of O-H bending in the cellulose and hemicellulose (Nhuchhen et al., 2014; Lupoi et al., 2014) which remained in the WTNGS but diminished in ACTNGS and ALTNGS samples suggesting removal of more hemicellulose. The frequency at 1050 cm^{-1} is ascribed to C-O and C=C, and C-C-O stretching in cellulose,

hemicelluloses and lignin, which diminished in the following order WTNGS>ACTNGS>ALTNGS. This trend is attributed to removal of some hemicellulose and lignin in the WTNGS and ACTNGS, and ALTNGS respectively. Frequency between 800 and 600 cm^{-1} is attributed to aromatic C-H bending vibrations from the lignin (Li et al., 2015) in the samples which disappeared completely in the ALTNGS.

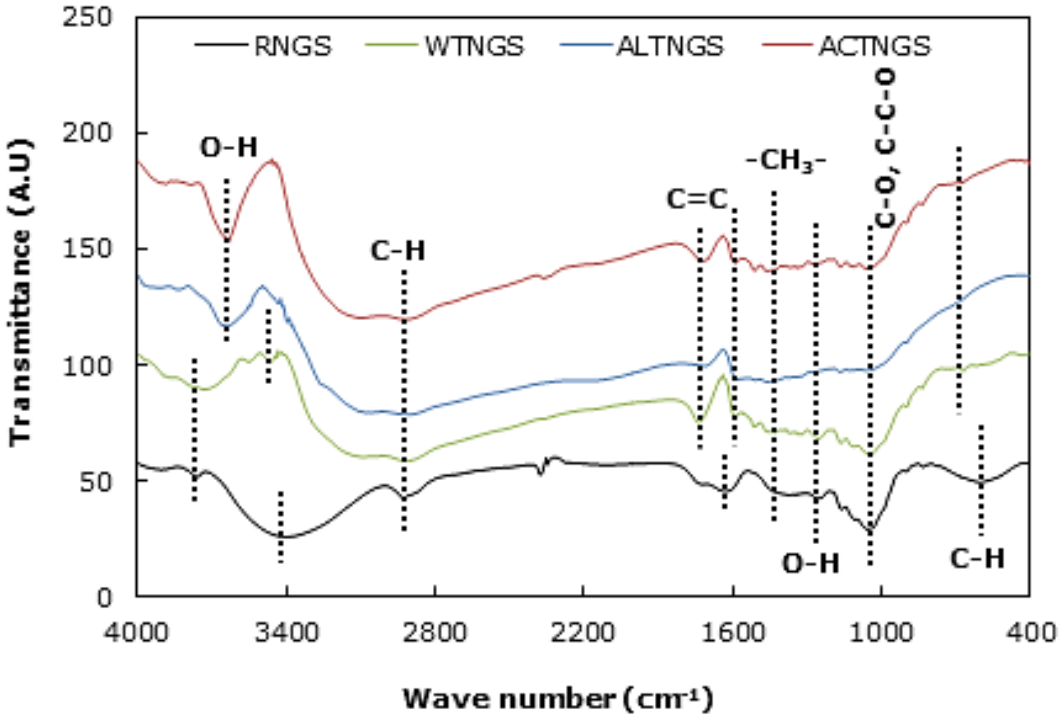

Figure 5.3: Averaged FTIR spectra (auto-smoothed and auto-baseline corrected) of Napier grass samples (RNGS, WTNG-0.9, ALTNGS-1.5% and ACTNGS-1.5%)

5.5 Thermogravimetric Analysis

Thermal decomposition characteristics of pre-treated samples were compared with the raw sample as presented on DTG curves in Figure 5.4. Extractive peak (e) of RNGS

around 200 °C disappeared in the all pre-treated samples. Hemicellulose peak (h) of RNGS at around 270 °C shifted to around 298 °C in WTNGS sample. The peak tends toward cellulose decomposition region, which is an indication improved thermal stability due to partial solubilization during the pre-treatment. Hemicellulose decomposition peak was not detected in ACTNGS and ALTNGS samples. The disappearance of the peak in ACTNGS confirms substantial removal of hemicellulose during the acid pre-treatments. For ALTNGS sample, it can be attributed to the alteration of the hemicellulose structure and removal acetyl groups by the alkaline solvent (Sebestyén et al., 2011). Cellulose degradation peak (c) around 326 °C in the RNGS shifted to 350 °C and 338 °C in WTNGS and ACTNGS samples respectively, indicating improved thermal stability. Higher cellulose reaction intensity of 10.52 %/°C in WTNGS and 12.29 %/°C in ACTNGS was recorded compared to 5.5 %/°C of cellulose in the RNGS. This can be related to reduction in the ash content and its minerals during the pre-treatment particularly the alkaline and alkaline earth metals, which tend to reduce the cellulose decomposition rate during pyrolysis (Biswas et al., 2011). High cellulose decomposition rate (9.79 %/°C) was also recorded in the ALTNGS sample but at a lower temperature (322 °C) compared to the RNGS (326 °C). This observation can be attributed to level of lignin removal recorded during the pre-treatment. Characteristics of all the samples were similar in lignin decomposition region (*l*). No noticeable peak was observed due to low thermal decomposition characteristic of lignin which spans over a wide temperature range.

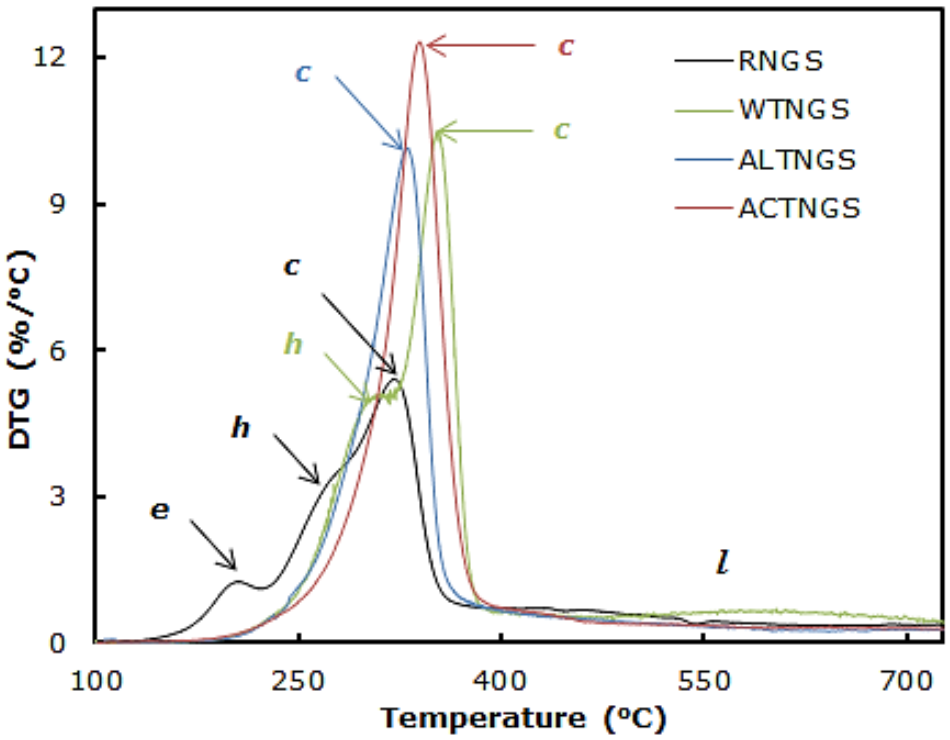

Figure 5.4: DTG of RNGS, ACTNGS and ALTNGS on dry basis. (*e*) Extractives; (*h*) Hemicellulose; (*c*) Cellulose; and (*l*) lignin decompositions. Condition: nitrogen atmosphere (20 mL/min), heating rate (10 °C/min).

5.6 Preliminary Analysis of Leachate and Possible Application

In aqueous pre-treatment of biomass, secondary effluents are generated which consists mostly fine particles and parts of biomass that was solubilized during the pre-treatment such as extractives, sugars, hemicellulose, lignin. This pre-treatment coproduct is seldom utilized and generally discharged as waste effluent (Tyrone et al., 2015). Generally, a good pre-treatment system is expected to require low energy, low capital and operational costs and should be conducted in such a way that coproducts have valuable downstream applications. Therefore further processing of pre-treatment

effluent and utilization to generate value added products become very important. Characteristic of leachate from the pure water, alkaline and acid pre-treatment Napier grass is summarized in Table 5.2. Leachate from the neutral solvent had pH value between 3.9 and 4.02 and sugar concentration from 31.47 to 34.35 g/L. The stream can be channel to other process such as biochemical conversion process for bioethanol production. Fine suspended solids were also observed in the leachate. This can serve as ethanol substrate in addition to the leachate to increase the ethanol concentration. Acid tolerant microbes having been developed which shows high ethanol yield under low pH condition between 2.8 and 4.7 (Mitsumasu et al., 2014). Ethanol produced from this process can be used as fuel and for bio-oil stabilization during bio-oil storage and upgrading strategy. Leachate from acid pre-treatment consist high concentration of sugar between 157.79 and 162.74 g/L. This present high potential for bioethanol production. However, the extreme acid condition of the effluent remains a serious challenge to microbes in biochemical process. Neutralization of effluent under extreme acid condition has been linked to formation of high salinity leachate which deters tricarboxylic acid cycle glycolysis pathways of fermenting microorganism (Zhang et al., 2007). In alkaline process, black liquor known as lignin with some sugar content was obtained. The presence of sugar is believed to have originated from extractives and partial solubilization of hemicellulose. In bio-refining integration, alkaline pre-treatment may be useful where lignin separated from biomass can be upgraded directly to fuel and chemicals via catalytic process (Beauchet et al., 2012; Ma et al., 2014) and the residue rich in cellulose converted to ethanol through biochemical process.

Table 5.2: Characteristics of leachate from aqueous pre-treatment of NGS

Solvent		Leachate Property			
		pH	Spgr at 20 °C	Sugar Concentration	
				(°Bx)	g/L
H_2O	Ro				
	0.37	4.02	1.0120	3.11	31.47
	0.85	3.91	1.0130	3.36	34.04
	2.09	3.94	1.0126	3.26	33.01
	2.38	3.90	1.0126	3.26	33.01
	2.73	3.94	1.0131	3.39	34.35
H_2SO_4	Conc. (w/w%)				
	0.5	1.30	1.0602	14.88	157.79
	1.0	1.20	1.0610	15.07	159.70
	1.5	1.09	1.0615	15.18	161.16
	2.0	0.92	1.0617	15.23	161.73
	2.5	0.55	1.0621	15.32	162.74
NaOH	Conc. (w/w%)				
	0.5	13.70	1.0276	7.04	72.35
	1.0	13.72	1.0280	7.14	73.41
	1.5	13.92	1.0285	7.26	74.67
	2.0	>14.00	1.0287	7.31	75.20
	2.5	>14.00	1.0289	7.36	75.73

Spgr: Specific gravity

5.7 Pyrolysis Product Distribution

Pyrolysis products distribution obtained from the pre-treated samples pyrolyzed at 600 °C reaction temperature, 30 °C /min heating rate and 30 mL/min nitrogen flow rate were compared with the product yield from the raw sample under the same condition as shown in Figure 5.5. Higher bio-oil yield was recorded from ACTNGS (38.71 wt %) and WTNGS (33.28 wt %) while ALTNGS produced lower yield (29.27 wt %) compared to the yield from RNGS (32.06wt %). The corresponding bio-char yield from the pre-treated samples was 24.21 wt %, 28.05 wt % and 32.15wt %. The increase in bio-oil and reduction in bio-char yields from ACTNGS and WTNGS samples can be linked to the removal of ash and its composition, particularly the alkaline and alkaline earth

metals during the pre-treatment. This is also true for the opposite trend recorded from ALTNGS sample since Na from NaOH has been reported to convert to irrecoverable salts and get incorporated in the biomass by the pre-treatment reactions during pre-treatment (Wang et al., 2011; Cuvilas and Yang, 2012). This tends to favour char formation during pyrolysis. Non-condensable gas yield was between 37.08 and 38.58 wt%. This indicates that pre-treatment has less impact on the gas yield. High non-condensable gas yield during pyrolysis is generally attributed to secondary cracking of pyrolysis vapour and further decomposition of bio-char at higher pyrolysis temperature.

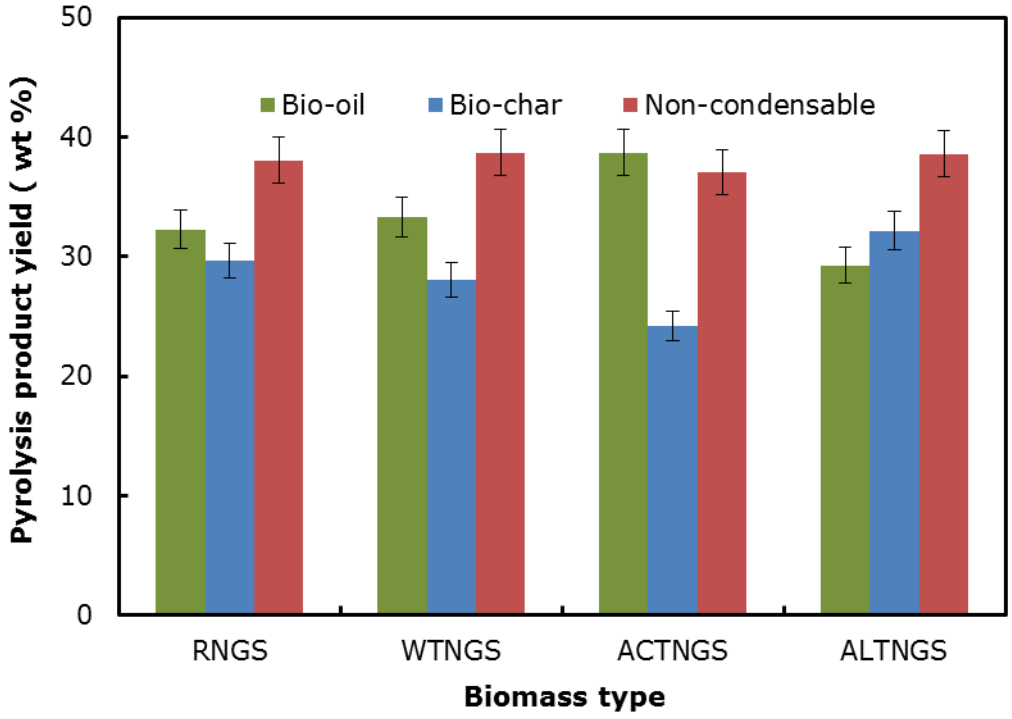

Figure 5.5: Pyrolysis products distribution from the raw and pre-treated Napier grass samples. Biomass condition: 30 g bone dry, 0.2 to 2 mm particle size; heating rate: 30 °C/min, nitrogen flow rate: 30 mL/min; pyrolysis temperature: 600 °C. Values are the means (n =3) ± SD

5.8 Physicochemical Properties of Bio-oil

Property of bio-oil from each sample is summarized in Table 5.3. The bio-oil collected from the all samples was a single phase dark black homogeneous liquid. The pH of the bio-oil from RNGS, WTNGS, ACTNGS and ALNGS sample was 2.95, 2.92, 2.68 and 3.26 respectively. The bio-oil from ALTNGS sample is less acidic relative to all the bio-oil from other samples. This is due to the removal organic acid forming groups such as acetyl group and uronic acid substitution on hemicellulose during the alkaline pre-treatment (Wang et al., 2011; Qian et al., 2013). Phenolics, which originate from lignin are also acidic and usually contribute to pH value of bio-oil. Therefore, Delignification could also be responsible for the less acidity of the oil. Water content of the oil produced from WTNGS and ACTNGS samples was about 21.14 and 33.28 wt% (Table 5.3) lower compared to moisture content recorded in the oil from RNGS. On the other hand, 5.57 wt% moisture increase in the bio-oil from ALTNGS sample was noted. This observation can be related to the level of demineralization recorded in the pre-treatment step prior to the pyrolysis. Generally, ash content above 1.0 wt% in the biomass tends to catalyse pyrolysis reaction toward formation of reaction water during pyrolysis (Le et al., 2015). ALTNGS used in the pyrolysis had 1.13 wt% ash content with increased Na composition incorporated by the NaOH compared to the RNGS (Table 5.1). Elemental compositions of the bio-oil products from both raw and pre-treated samples showed similar oxygen content. One would have expected that the solubilization of hemicellulose and extractives component of biomass will lead to drastic reduction in oxygen content of the product bio-oil but that was not the case. Therefore, formation of oxygenated compound during the pyrolysis does not only originate from hemicellulose and extractive but also from the cellulose and lignin component of the biomass.

Table 5.3: Physicochemical characteristics of bio-oil from raw and pre-treated NGS samples.

Property	Bio-oil			
	RNGS	WTNGS	ACTNGS	ALTNGS
Appearance	Dark black homogeneous liquid			
pH	2.95±0.01	2.92±0.01	2.68±0.01	3.26±0.01
Water content (wt %)	26.01±0.22	20.52±0.24	17.36±0.221	27.47±0.25
Density (g/cm^3)[1]	1.057±00	1.080±00	1.092±00	1.035±00
Viscosity (cSt)[2]	2.10±0.13	2.10±0.16	2.20±0.17	1.70±0.15
Solid (wt%)[3]	0.20	0.20	0.21	0.19
HHV (MJ/kg)	20.97±0.10	22.22±0.10	27.96±0.10	21.94±0.10
Carbon (wt %)	45.32±0.81	46.01±0.82	48.95±0.82	45.12±0.79
Hydrogen (wt %)	7.17±0.13	6.59±0.12	6.02±0.11	7.39±0.11
Nitrogen (wt %)	0.81±0.03	0.77±0.03	0.72±0.03	0.95±0.03
Sulphur (wt %)	0.10±0.00	0.11±0.00	0.15±0.00	0.11±0.00
Oxygen (wt%)[4]	46.60±0.78	46.52±0.75	44.16±0.76	46.43±0.76

[1]Measured at 20°C; [2]Measured at 40°C; [3]ethanol insoluble (0.1µm filter); [4]by difference. Values are the means (n =3) ± SD

5.9 GC-MS Analysis of Bio-oil

Group of compound detected in bio-oil collected from all the samples is shown in Figure 5.6. In order to elucidate the effect of the pre-treatment on the distribution of chemical compounds in the oil, the compounds were further classified as hydrocarbons (HC); value added chemical (VAC); acids and ketones (AK); esters and other organic compounds (EOC); nitrogenous and sulphur containing compounds (NS). Highest HC content was recorded in the bio-oil from ALTNGS follow by the oil from RNGS, WTNGS and the least was obtained in the oil from ACTNGS. Generally, HCs are formed during pyrolysis either from the product of partial pyrolysis or from volatile compounds of the source biomass (Deshmukh et al., 2015). The high percentage of HC recorded in the

oil from ALTNGS could be attributed to selective removal of lignin during the pre-treatment, which makes other volatile components of the biomass readily available for conversion during the pyrolysis. While the lower composition of HC in the oil from WTNGS and ACTNG was due to removal of some hydrocarbon component by the water and acid solvent at the pre-treatment stage. The VAC chemicals constitute phenols, alcohols, furans, furfural and levoglucosan. These bio-oil components increased with pre-treatment in the following order ACTNGS>WTNGS>ALNGS>RNGS. Phenolics in the bio-oil are generally product of lignin degradation during the pyrolysis and lower value recorded in the oil from ALTNGS compared to ACTNGS and WTNGS is linked to the lignin removal by the alkaline solvent during the pre-treatment. Furan, furfural and levoglucosan are degradation product of cellulose and hemicellulose (Adrados et al., 2015; Bordoloi et al., 2015). Lower level of furfural in the oil from ALTNGS and ACTNGS compared to the oil from WTNGS sample was due to the removal of hemicellulose recorded during the pre-treatment which was also evident in the thermogravimetric result and sugar concentration in the leachate. In the case of oil from RNGS, it can be attributed to the high ash level in the raw sample, which favours side reactions that lead to formation of organic acids (Deshmukh et al., 2015). Levoglucosan was present only in the bio-oil from WTNGS and ACTNGS feedstocks. It can also be stated that pre-treatment of NGS with deionized water and sulfuric acid favour formation of cellulose structure, which lead to the production and faster withdrawal levoglucosan in the pyrolysis vapour product stream (Stephanidis et al., 2011; Bordoloi et al., 2015; Deshmukh et al., 2015). Reduction of AK content in the bio-oil from the pre-treated samples was observed, which is attributed solely to the ash removal recorded during the pre-treatment since studies have shown that elimination of hemicelluloses from biomass does not significantly reduce content the

AK content in the bio-oil (Stephanidis et al., 2011; Adrados et al., 2015). Esters and other organic compounds such as pentamethoxyflvone, propanenitrile were also detected (Appendix II) in the bio-oil from RNGS, ALTNGS, ACTNGS and WTNGS respectively. NS detected in the bio-oil can be attributed to nitrogen and sulphur content in the parent biomass.

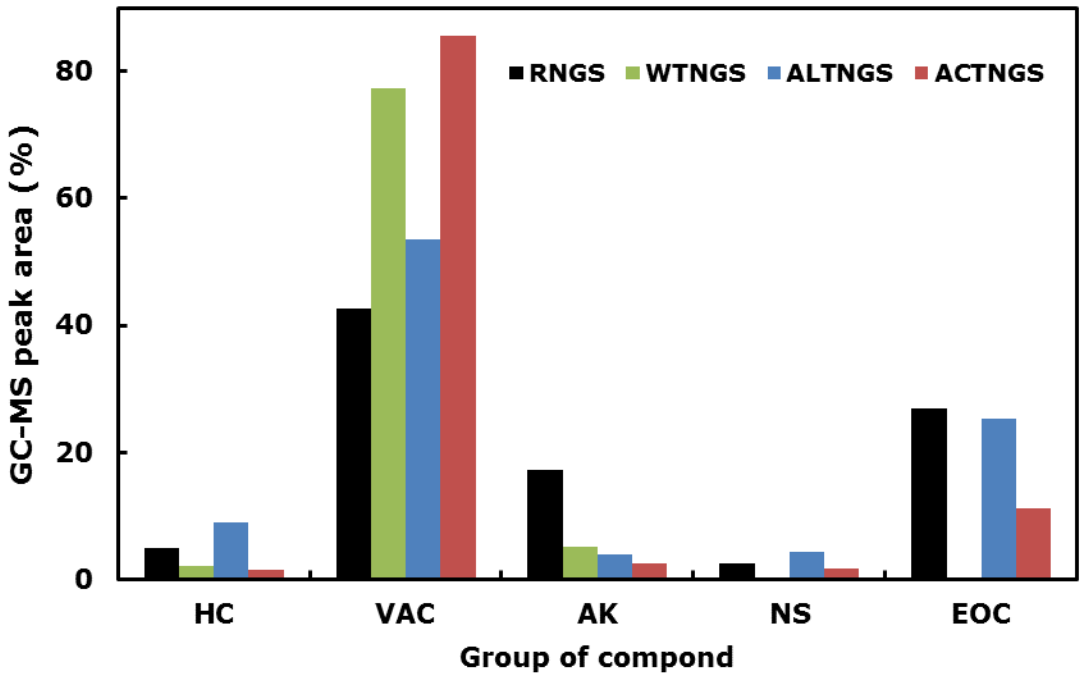

Figure 5.6: Group of chemical compounds detected in bio-oil from raw and pre-treated NGS samples

5.10 Conclusion

Pre-treatment of Napier grass was carried out with deionized water, sodium hydroxide and sulfuric acid. The pre-treated samples were subsequently pyrolyzed in a fixed bed reactor. Deionized water and sulfuric acid significantly reduced the ash content in the

Napier grass with about 64 and 80% ash reduction respectively. Deionized water was effective in leaching Na and K while sulfuric acid substantially reduced Na, K, Ca, Al and Fe. For sodium hydroxide, 40% ash removal was recorded initially but decreased as the concentration increased. This solvent was effective for the removal Si and Al. Some reduction in K and Ca were also noted but more Na element was incorporated in the sample. All the solvents obviously removed the extractives component of the Napier grass. Partial solubilization of hemicellulose was also observed with deionized water while substantial removal of hemicellulose was detected with sulfuric acid. Sodium hydroxide was highly effective for lignin removal. Though, it appeared that some hemicelluloses were also solubilized

Sulfuric acid produced high acidic leachate which will require neutralization. The neutralization of highly acidic leachate can be very challenging in large scale system. Sodium hydroxide generated high lignin reach leachate that can be further upgraded to fuel and chemicals which could be a very good option for bio-refinery integration. Effluent from the neutral solvent has relatively high pH. The stream can be channelled back to the pre-treatment process or biochemical conversion process to convert the sugar to bioethanol. Pre-treatment using sulfuric acid and deionized water increased bio-oil yield while sodium hydroxide promoted bio-char formation. All the pre-treatment methods did not show a significant reduction in oxygen content of the resulting bio-oil. However, some decrease in organic acid and ketone content of the bio-oil from all the pre-treated samples were observed. Acid and water pre-treated samples produced bio-oil with high value added chemicals.

Pre-treatment with the neutral solvent can be considered appropriate for the pyrolysis process as good quality bio-oil can be produced in addition to its environmental

friendliness, high generation of value added chemicals and possible practical application of its effluent.

CHAPTER SIX

6. IN-SITU UPGRADING OF BIO-OIL DERIVED FROM NAPIER GRASS

6.1 Introduction

This chapter deals with in situ upgrading of bio-oil derived from Napier grass. The chapter consists of two sections, in-situ catalytic upgrading and non-catalytic upgrading. The former involves application of microporous and mesoporous ZSM-5 catalysts in pyrolysis of Napier grass towards improving bio-oil quality. It evaluates effect of process variables such catalyst-biomass ratio and catalyst type. The latter assesses catalytic activities of biomass mineral composition (ash) on the quantity and quality of bio-oil. It investigates synergism between Napier grass mineral elements and other biomass ash during pyrolysis and resulting impact on the bio-oil quality.

6.2 In situ Catalytic Upgrading of Bio-oil

6.2.1 Characteristics of catalysts

Diffractogram of the catalysts is shown in Figure 6.1. Both the parent ZSM-5 and mesoporous ZSM-5 samples (0.2HZSM-5 and 0.3HZSM-5) exhibited main peaks at around 2θ between 20° and 25°, which are typical characteristic peaks for ZSM-5. Although the intensity of the modified ZSM-5 decreased with increased NaOH concentration, but this observation shows a loss of crystallinity due to desilication, which could also be linked to the formation of mesoporous structures in the material (Zhang et al., 2015b; Wei et al., 2016). Physisorption analysis (Figure 6.2) of ZSM-5 displayed a type I isotherm according to the IUPAC classification. The isotherm showed a very strong adsorption in the initial region and a plateau at high relative pressure (>0.9). This pattern indicates that ZSM-5 is a microporous material (Ibáñez et al., 2014). Both 0.2HZSM-5 and 0.3HZSM-5 displayed a combination of type I and IV isotherms with a low slope region at the middle which shows the presence of few multilayers and a

hysteresis loop at relative pressures above 0.4, which could be linked to capillary condensation in a mesoporous material (Na et al., 2013; Li et al., 2014a). With increasing NaOH concentration, the hysteresis loop became more pronounced and could also be related to the level of mesoporous structure formed in the sample after the desilication.

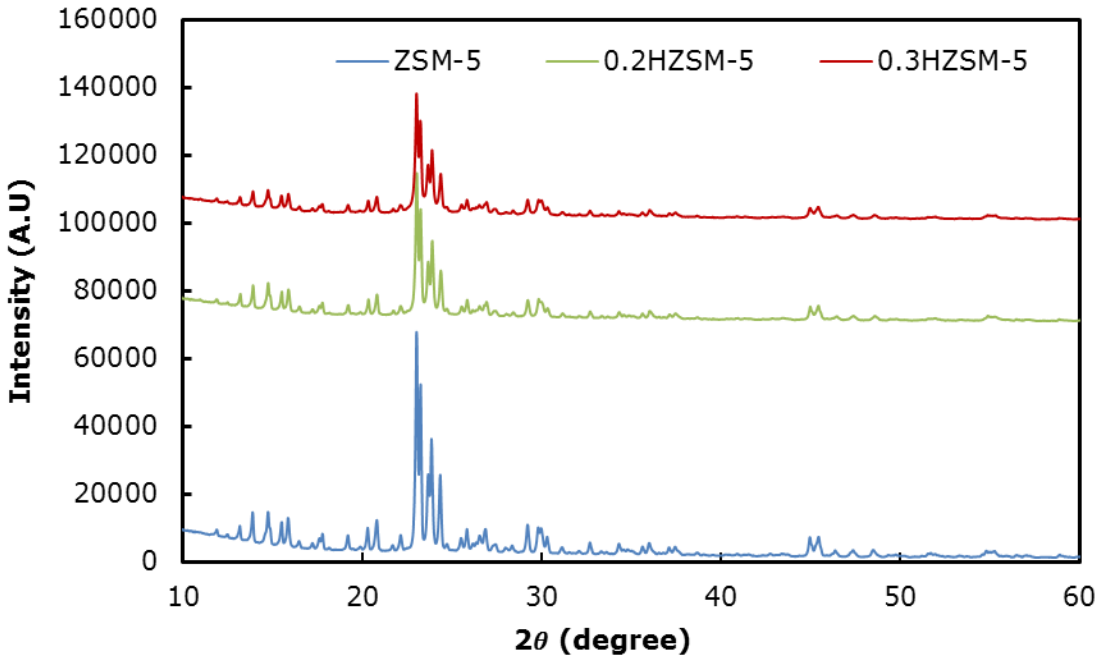

Figure 6.1: XRD Diffractogram of parent and modified ZSM-5

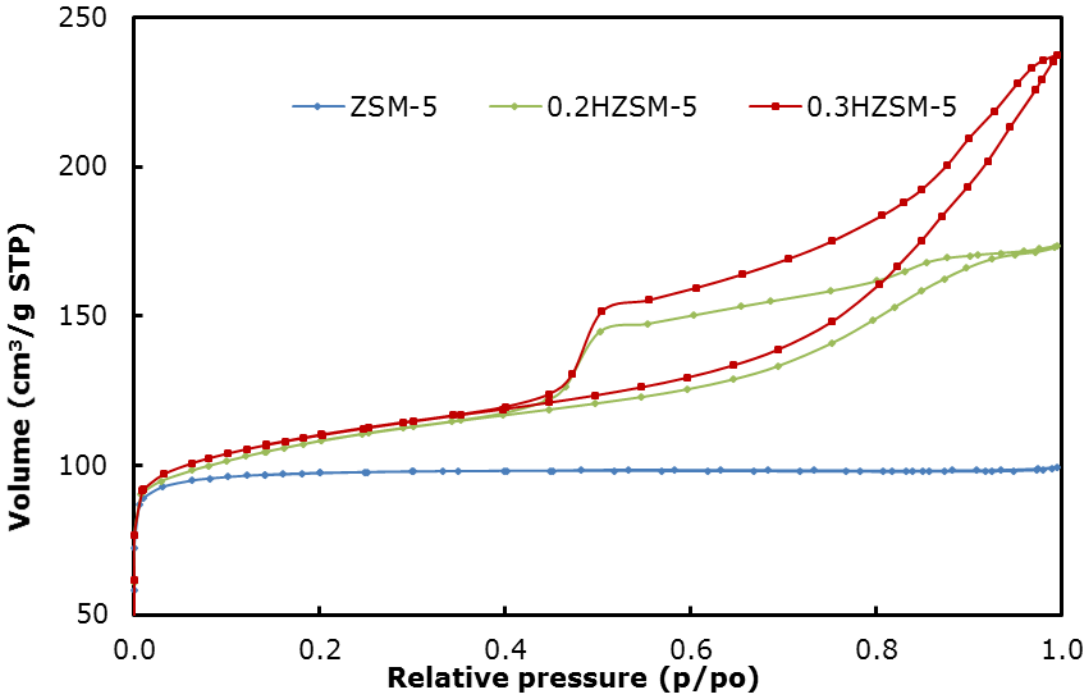

Figure 6.2: Isotherms of N_2 adsorption/desorption of the catalysts

Other characteristics of catalysts from the physisorption analysis are summarized in Table 6.1. Comparing ZSM-5 and modified ZSM-5, as expected, the Si/Al ratio decreased between 34-40 % after desilication. Similarly, reduction in Brunauer Emmet Teller (BET) specific surface area (S_{BET}), S_{micro} and V_{micro} were also observed in the modified ZSM-5. This observation shows that some of the micropores in the parent ZSM-5 have been converted to mesoporous structures after the desilication, which have contributed to the resulting mesoporosity in the modified ZSM-5 (Na et al., 2013). Increasing NaOH concentration for desilication from 0.2 M to 0.3 M produced a more mesopore with 17 % increase in surface (S_{meso}) and 37 % increase in total pore volume while the acidity remained within 1% difference. The significant increase in the

pore volume can be responsible for the enlarged hysteresis loop observed in sample treated with 0.3 M NaOH.

Table 6.1: Treatment condition and characteristics of zeolite ([a]determined by X-ray fluorescence; [b]Brunauer–Emmett–Teller method; [c]t-plot method; [d]Vmeso=Vpore -Vmicro)

Catalyst	C_{NaOH}	(Si/Al)[a]	$(S_{BET})^b$	$(S_{micro})^c$	$(S_{meso})^c$	(V_{pore})	$(V_{micro})^c$	$(V_{meso})^d$	total acidity
	(mol/L)	(mol/mol)	surface area (m^2/g)			volume (cm^3/g)			(mmol/g)
ZSM-5	0.00	20.76	385.20	356.54	28.66	0.1540	0.1383	0.0157	3.8085
0.2HZSM-5	0.20	13.79	369.43	274.66	114.76	0.2685	0.1039	0.1646	3.0036
0.3HZSM-5	0.30	12.51	374.88	240.23	134.65	0.3670	0.1114	0.2556	2.9635

Ammonia-temperature programmed desorption (NH_3-TPD) analysis (Figure 6.3) displayed two peaks in the parent ZSM-5 at temperatures around 219 and 435 °C while single peaks around 206 and 258 °C were observed 0.2HZSM-5 and 0.3HZSM-5 respectively. The high temperature peak represents the desorption of NH_3 from strong acid sites while those observed at temperatures between 206 and 258 °C is ascribed to the desorption of NH_3 from weak acid sites (Li et al., 2014a; Saad et al., 2015). Disappearance of the strong acid sites in the modified ZSM-5 is attributed to decreased silica content in the respective samples (Na et al., 2013; Li et al., 2014a). Total surface acidity obtained from the area under each peak was found to be 3.8085, 3.0036 and 2.9635 mmol/g for ZSM-5, 0.2HZSM-5 and 0.3HZSM-5 respectively. The SEM-EDX (Figure 6.4) revealed that ZSM-5 is highly crystalline, with hexagonal prismatic morphology and different particle size of less than 500 nm. Both 0.2HZSM-5 and 0.3HZSM-5 had morphological characteristic similar to the parent ZSM-5 indicting that the morphological integrity of the catalyst was not affected by desilication.

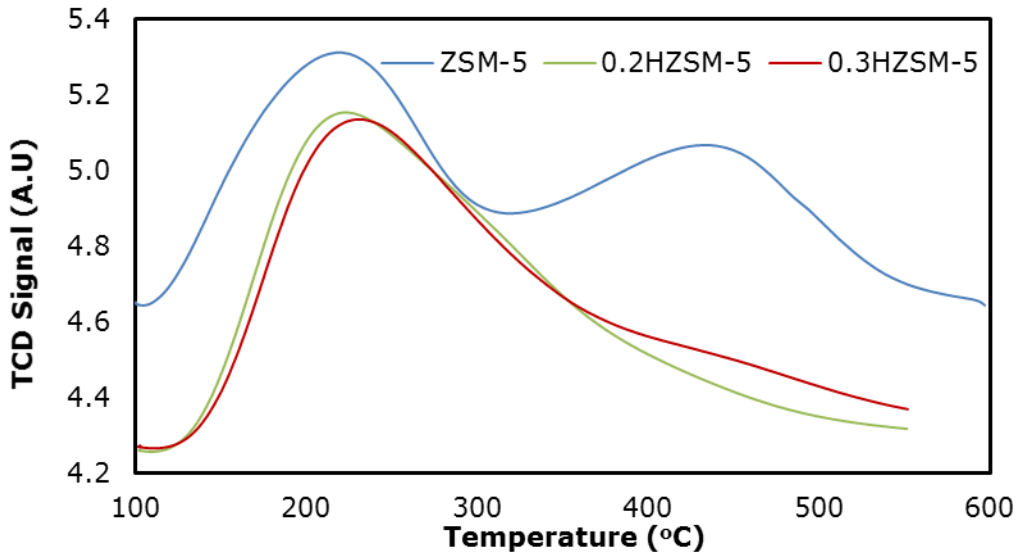

Figure 6.3: NH_3-TPD temperature-programmed desorption curves

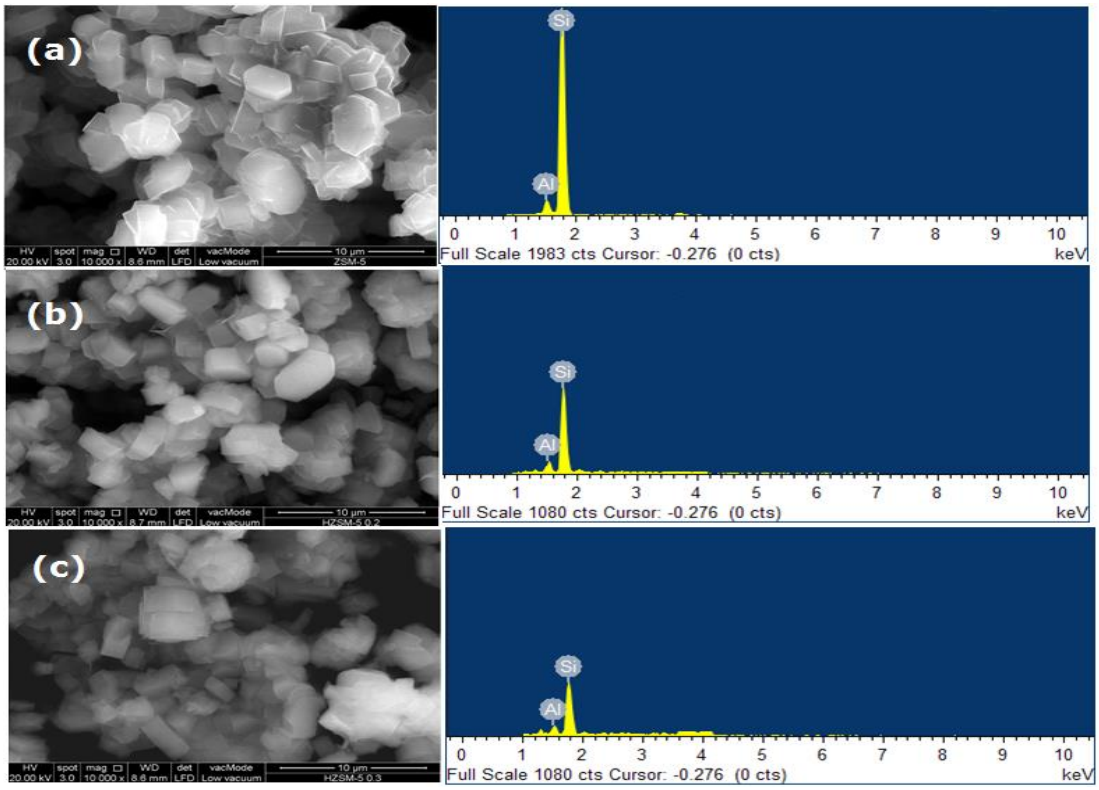

Figure 6.4: SEM-EDX images of (a) ZSM-5, (b) 0.2HZSM-5 and (c) 0.3HZSM-5

6.2.2 Pyrolysis product distribution

Pyrolysis was conducted at 600 ^{o}C, 5 L/min N_2 flow and 50 ^{o}C/min heating rate. The effect of ZMS-5/biomass ratio (CBR: 0.0-3.0) on pyrolysis product distribution relative to non-catalytic pyrolysis (NCP) (catalyst/biomass ratio: 0.0 wt %) is shown in Figure 6.5. The CBR range employed in this study was to allow high yield of organic phase since high CBR generally lead to high gas production. Total bio-oil (organic and aqueous phase) collected under NCP was 49.20 wt%, which decreased to 47.04, 45.24, 38.08 and 37.13 wt% at CBR of 0.5, 1.0, 2.0 and 3.0 wt%. The organic phase collected was 15.69, 13.99, 13.18, 11.70 and 9.11 wt% at CBR of 0.0-3.0 wt%. Increasing CBR between 0.5-1.0 wt% showed no significant decrease in the organic phase yield, which could be attributed to the generation of less reactive pyrolysis vapour via simultaneous dehydration, decarboxylation, and decarbonylation reactions. Under this condition, the aqueous phase yield decreased from 33.05-32.06 wt% compared to 28.02-26.38 wt% recorded at CBR of 2.0-3.0 wt%. Non-condensable gas yield recorded at CBR of 0.5-1.0 wt% was 30.86-32.57 wt% relative to 36.14-36.67 wt% at 2.0-3.0 wt% CBR. This indicates that dehydration reaction was more prevalent at CBR of 0.5-1.0 wt% compared to CBR of 2.0-3.0 wt% where the decarboxylation and decarbonylation reaction appeared to be dominant due to high gas generation. Solid yield was approximately 22.0 wt% at 0.0-1.0 wt% CBR compared to 25.78-26.20 wt% recorded at 2.0-3.0 wt% CBR, which be linked to formation of core or coke precursors. This observation is in good agreement with the literature (Wang et al., 2012; Mohammed et al., 2016a) Comparing with the existing literature, most researchers employed CBR which generally lead to less liquid yield and more gas production (Wang et al., 2012; Du et al., 2014; Jae et al., 2014). Studies involving catalyst loadings similar to the ones used in this study, particularly between 0.5 and 1.0 wt %, are seldom carried

out. Research conducted by Park et al. (2012) on catalytic pyrolysis of Miscanthus with ZSM-5 using a catalyst to biomass ratio of 0.1 and a reaction temperature of 450 °C in a fixed bed reactor resulted in a high yield of organic phase (21.5 wt %). Similarly, the work of Elordi et al. (2011) on catalytic pyrolysis of polyethylene with ZSM-5 using a catalyst/biomass ratio of 0.03 at 500 °C in a spouted bed reactor generated about 25 wt % organic product. Degree of deoxygenation (DOD) of 20.51 % was recoded in organic phase with 0.5 wt% CBR. This value increased by 8, 13 and 16 % with CBR of 1.0, 2.0 and 3.0. Similarly, a continuous increase in the higher heating value (HHV) was recorded with increasing CBR, which is attributed to the DOD achieved. Other physicochemical properties of bio-oil are summarized in Appendix III-Table 1

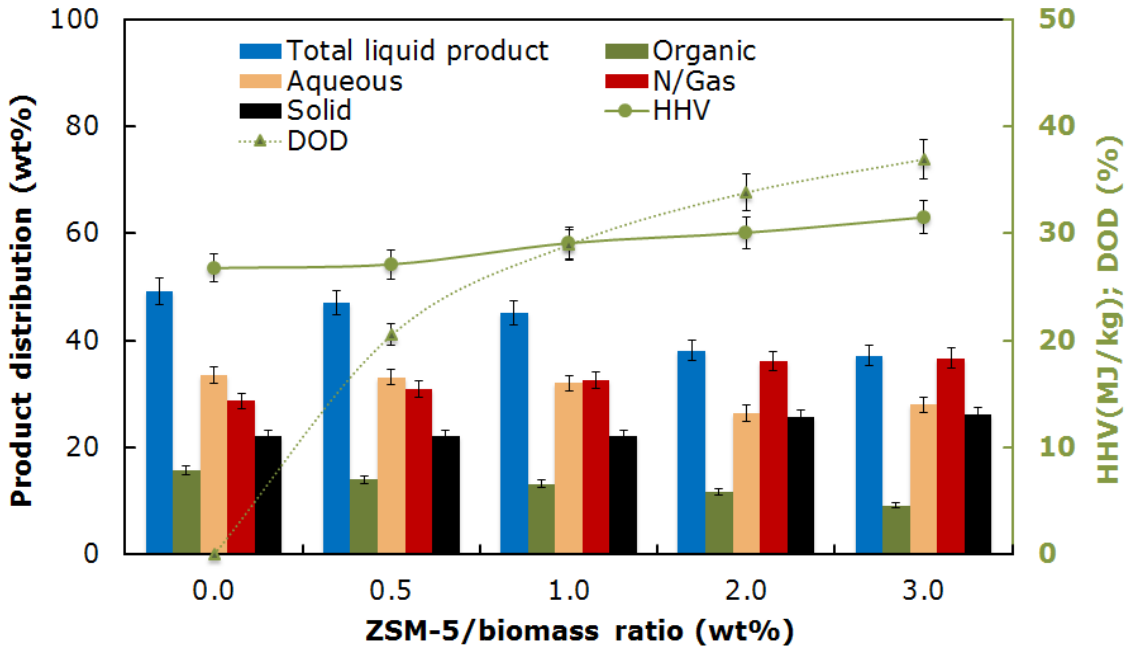

Figure 6.5: Effect of ZSM-5/biomass ratio on pyrolysis product distribution, degree of deoxygenation (DOD) and higher heating value (HHV). N/gas: non-condensable gas. Solid: coke and char. Values are the means (n =3)

Impact of mesoporous 0.2HZSM-5 on pyrolysis product distribution is shown in Figure 6.6. Production of organic and aqueous phases decreased from 15.69-13.28 wt% and 33.51-24.83 wt% as the CBR increased form 0.0-3.0 wt%. Significant increase in the yield of non-condensable gas was observed. At 0.0 CBR, the non-condensable gas recorded was 28.74 wt%. This increased to 34.13, 35.51, 36.64 and 38.78 wt% at 0.5, 1.0, 2.0 and 3.0 wt% CBR, which are evidence deoxygenation reaction. The solid yield remained at approximately 23.0 wt%. Comparing with the performance of ZSM-5 (Figure 6.5), the organic phase recorded with 0.2HZSM-5 was 4.90-45.80 % higher, which can be linked to the improved pore characteristics. Similarly, higher non-condensable gas yield in the range of 1.38-10.60% recorded with 0.2HZSM-5 relative to ZSM-5 is an indication of superior catalytic activity. Decrease in aqueous phase bio-oil with 0.2HZSM-5 from 33.51 wt% at 0.0 wt% CBR to 27.77, 27.40, 26.49 and 24.83 wt% at 0.5, 1.0, 2.0 and 3.0 wt% CBR suggest that the reaction proceeds via decarbonylation or decarboxylation reaction, which is also in agreement with the increased non-condensable gas yield recorded with CBR. DOD and HHV increased with increasing CBR. 3.0 wt% 0.2HZSM-5 CBR yielded highest values of DOD (39.42 %) and HHV (37.34 MJ/kg) compared to 36.92 % and 31.51 MJ/kg recorded at 3.0 wt% ZSM-5 CBR.

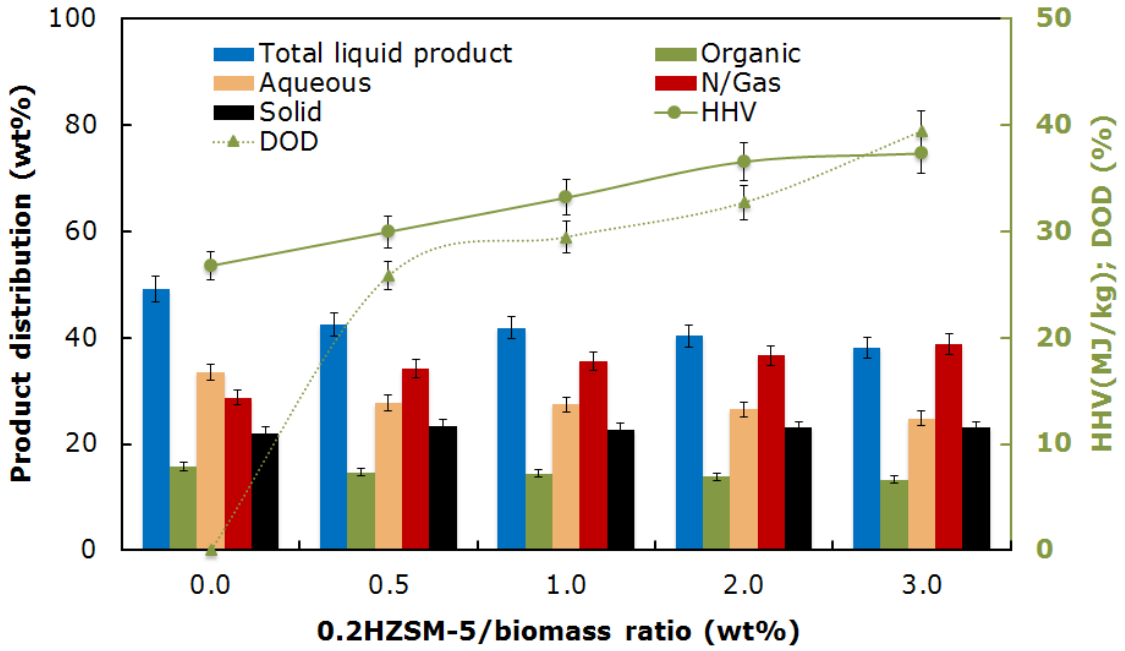

Figure 6.6: Effect of 0.2HZSM-5/biomass ratio on pyrolysis product distribution, degree of deoxygenation (DOD) and higher heating value (HHV). N/gas: non-condensable gas. Solid: coke and char. Values are the means (n =3)

Pyrolysis product distribution over 0.3HZSM-5 is shown in Figure 6.7. Organic phase produced over 0.3HZSM-5 decreased from 15.69 wt% to 14.18 wt% at CBR of 0.5 wt% and subsequently to 13.66, 13.08 and 12.58 wt% at 1.0, 2.0 and 3.0 wt% CBR. These values are not significantly different (3.33-5.27 %) from the organic phase yield recorded over 0.2HZSM-5 under the same CBR condition but higher than the organic yield collected over ZSM-5 in the range of 3.64-38.09 % at CBR of 1.0-3.0 wt%. Substantial decrease in aqueous phase (25.43 to 20.09 wt %) and significant increase in non-condensable gas (38.18 to 47.20 wt %) recorded with 0.3HZSM-5 as CBR increased from 1.0 to 3.0 wt% is an evidence of high selective deoxygenation through either decarbonylation or decarboxylation reaction. Highest DOD and HHV of the organic phase recorded with 0.3HZSM-5 at 3.0 wt% CBR was 43 % and 38.71 MJ/kg,

which is approximately 6 % and 23 % respectively higher than the highest DOD and HHV recorded in the organic phase produced over ZSM-5.

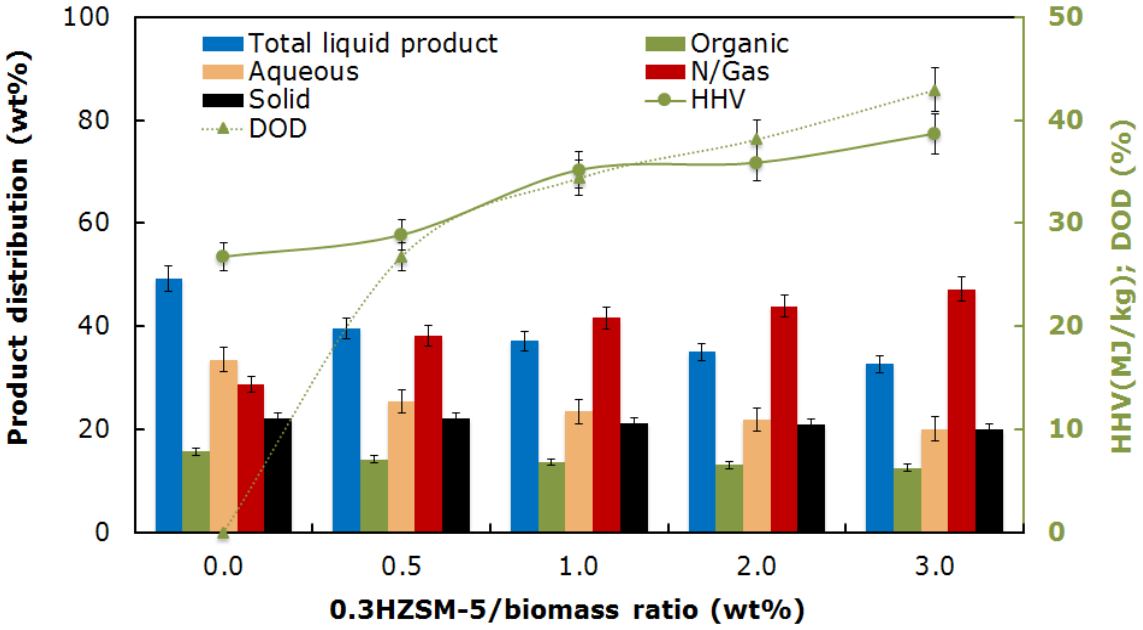

Figure 6.7: Effect of 0.3HZSM-5/biomass ratio on pyrolysis product distribution, degree of deoxygenation (DOD) and higher heating value (HHV). Solid: coke and char. Values are the means (n =3)

6.2.3 GC-MS analysis of organic phase product

Twenty most abundant organic compounds identified in the bio-oil samples consist various HCs, PHOL, ARHCs, MEST and OVAC, which are summarized in Table 6.2. Increasing ZSM-5 CBR promoted production of HCs, which could be linked to the deoxygenation of holocellulose derived oxygenates such as AAK and cracking of long chain organic molecules. Increasing ZSM-5 CBR from 1.0-3.0 wt% decreased the amount of AAK by 50, 90 and 96 % while HCs increased in 3.5, 5.0 and 6.0 folds respectively relative to 0.0 wt% CBR. This suggest that the AAK are small enough to enter the micropore of the ZSM-5, which has sufficient surface area and active sites.

Study by Li et al. (2014) showed that microporous ZSM-5 can effectively converts small oxygenates. The authors recorded complete conversion of carbohydrate-derived oxygenates during catalytic fast pyrolysis of beech wood, which was attributed to the efficient mass transfer of oxygenates into the micropore due to their small size and followed by subsequent conversion. The HCs detected were mainly olefins. This observation can be attributed to the acidity of the ZSM-5 catalyst which is known for the selective production of olefins through cracking of oxygenated compounds at higher temperatures similar to the temperature (600 °C) used in this study (Zhang et al., 2013; Liu et al. 2015). Similarly, the production of ARHCs increased with increasing CBR relative to 0.0 wt% CBR. The nature of ARHCs detected was with ZSM-5 were mainly poly aromatic hydrocarbons (PAH) (naphthalene) at 1.0 wt% CBR, which is mainly the product of condensed fragments from the surface active cites of the ZSM-5. While methyl benzene and ethyl benzenes constituted main ARHCs detected at CBR of 2.0 and 3.0 wt% (Appendix III-Table 2). These compounds are produced via a series of complex chemical reactions such as cracking, oligomerization, dehydrogenation, and aromatization promoted by the Brønsted acid cites of the ZSM-5 (Mohammed et al., 2016a). In this study, production of ARHCs may have originated from conversion of MPHOL to MARHCs and subsequently to ARHCs. Although, only 23-29 % decrease in MPHOL and about 1.2-15.3 increase in MAHCs were recorded while there was no significant changes in the PHOL with increasing CBR. This suggests that PHOL, MPHOL and MARHCs are too bulky to be transferred into the micropores of ZSM-5, as such only pre-cracked species at the external surface small enough diffused into the micropores to form ARHCs.

Table 6.2: Group of organic compound in the deoxygenated bio-oil over ZSM-5, 0.2HZSM-5 and 0.3HZSM-5

Composition (%)	ZSM-5 CBR (wt %)			
	0.00	1.00	2.00	3.00
HC	4.67	16.30	22.88	28.89
ARHC	2.53	15.19	11.17	15.69
MARHC	2.18	3.41	17.48	9.93
PHOL	28.15	18.71	33.10	29.55
MPHOL	37.87	14.51	11.30	9.13
AAK	16.88	5.94	1.77	0.69
MEST	4.68	6.33	1.23	0.00
OVAC	3.05	19.62	1.07	6.12
	0.2HZSM-5 CBR (wt %)			
	0.00	1.00	2.00	3.00
HC	4.67	15.46	14.62	12.18
ARHC	2.53	2.60	8.31	14.16
MARHC	2.18	1.20	5.99	0
PHOL	28.15	57.95	54.50	61.41
MPHOL	37.87	4.92	0	0
AAK	16.88	2.18	2.90	5.75
MEST	4.68	4.60	4.13	5.45
OVAC	3.05	11.08	9.56	1.05
	0.3HZSM-5 CBR (wt %)			
	0.00	1.00	2.00	3.00
HC	4.67	9.25	11.55	7.19
ARHC	2.53	8.98	6.31	24.72
MARHC	2.18	9.21	3.09	4.30
PHOL	28.15	61.01	58.14	45.03
MPHOL	37.87	3.83	4.64	0.00
AAK	16.88	0.00	4.31	2.84
MEST	4.68	4.40	0.00	5.84
OVAC	3.05	3.33	11.96	10.08

(HC) hydrocarbons, (ARHC) aromatic hydrocarbons, (MARHC) methoxy aromatics, (PHOL) phenol, (MPHOL) methoxy phenol, (AAK) acids, aldehydes and ketones, (MEST) methyl ester and (OVAC) other value added chemical.

Significant conversion of AAK to HCs was also achieved with 0.2HZSM-5 and 0.3HZSM-5. The composition of HCs was a mixture of olefins and saturated hydrocarbons (Appendix III-Table 3 & 4), which is an indication of possible hydrogenation reaction. Maximum ARHCs detected at 3.0 wt% over 0.2HZSM-5 was similar to that recorded with ZSM-5 but differs in composition. Monoaromatic hydrocarbons (MAH) such as alkyl benzenes were the ARHCs detected. ARHCs produced with 0.3HZSM-5 at CBR of 3.0 wt% was approximately 10 % higher the values recorded for 0.2HZSM-5 and ZSM-5 and constituted trimethylbenzene, ethylbenzene, toluene and p-xylene (Appendix 3). PHOL content of oil collected over 0.2HZSM-5 and 0.3HZSM-5 was 26-38 % higher than the PHOL content of the oil produced over ZSM-5, suggesting formation of ARHCs proceeded via conversion of MPHOL to PHOL and MARHCs, and then to ARHCs. Study have shown that cracking of MPHOL proceeds through formation of methyl radical resulting in hydoxyphenoxy radical, which subsequently decarbonylates to cyclopentadienyl radical. Radical-radical reaction between methyl and cyclopentadienyl lead to the formation of phenols (Scheer et al., 2011). MPHOL were completely eliminated with both 0.2HZSM-5 and 0.3HZSM-5 at CBR 0f 3.0 wt%. This can be attributed to the improved pore characteristics of the catalysts, which enhanced mass transport of the molecules to active sites. Higher content of PHOL in the final bio-oil produced over 0.2HZSM-5 and 0.3HZSM-5 relative to ZSM-5 suggests that PHOL molecules are too small and thus flow through the mesopore rather than attaching to the pore for subsequent conversion (Li et al., 2014).

6.2.4 GC-TCD analysis of non-condensable gas

Composition of non-condensable gas collected is at 0.0 and 3.0 wt% CBR is summarized in Table 6.3. High levels of H_2 in the non-condensable gas at 0.0 wt%

CBR is due to thermal cracking, which generally produce small organic molecules during the pyrolysis. Higher composition of CO and CO_2 in the non-condensables from the catalytic process relative the gas product at 0.0 wt% CBR is an indication of catalytic reactions (Gamliel et al. 2015). Gas collected over 0.2HZSM-5 and 0.3HZSM-5 had higher percentages of CO and CO_2 relative to gas produced with ZSM-5, which is an indication of higher degree of decarbonylation and decarboxylation reactions. Reduction in H_2 content in the gas produced with 0.2HZSM-5 and 0.3HZSM-5 is a confirmation that some of the H_2 generated during catalytic reaction are subsequently consumed in the process, which could be responsible for hydrogenation of some olefins to alkanes as observed in the liquid product distribution.

Table 6.3: Composition of non-condensable gas collected at 3.0 wt% CBR

Catalyst Type	CBR (wt %)	Gas Composition (vol %) N_2-free basis			
		CH_4	H_2	CO	CO_2
Raw	0.0	3.36	25.32	13.60	14.04
ZSM-5	3.0	2.34	10.36	22.14	27.95
0.2HZSM-5	3.0	3.26	8.31	33.97	30.32
0.3HZSM-5	3.0	3.01	7.94	37.67	28.07

6.2.5 SEM-EDX analysis of bio-char

Pyrolysis is an energy intensive process. Energy analysis in the previous chapter has shown that the challenge of high energy requirement may be compensated through efficient utilization of other pyrolysis products (bio-char and non-condensable gas). SEM-EDX of the produced bio-char is shown in Figure 6.8. The micrograph showed that bio-char obtained from the catalytic process contained spent catalyst, which cannot be easily separated. The corresponding EDX spectrum revealed increased

amount of inorganic metals such as Si and Al, which originated from the catalyst. Application of this bio-char for energy production such as combustion can lead to emission of alumina and silica dust, which can affect the ecosystem.

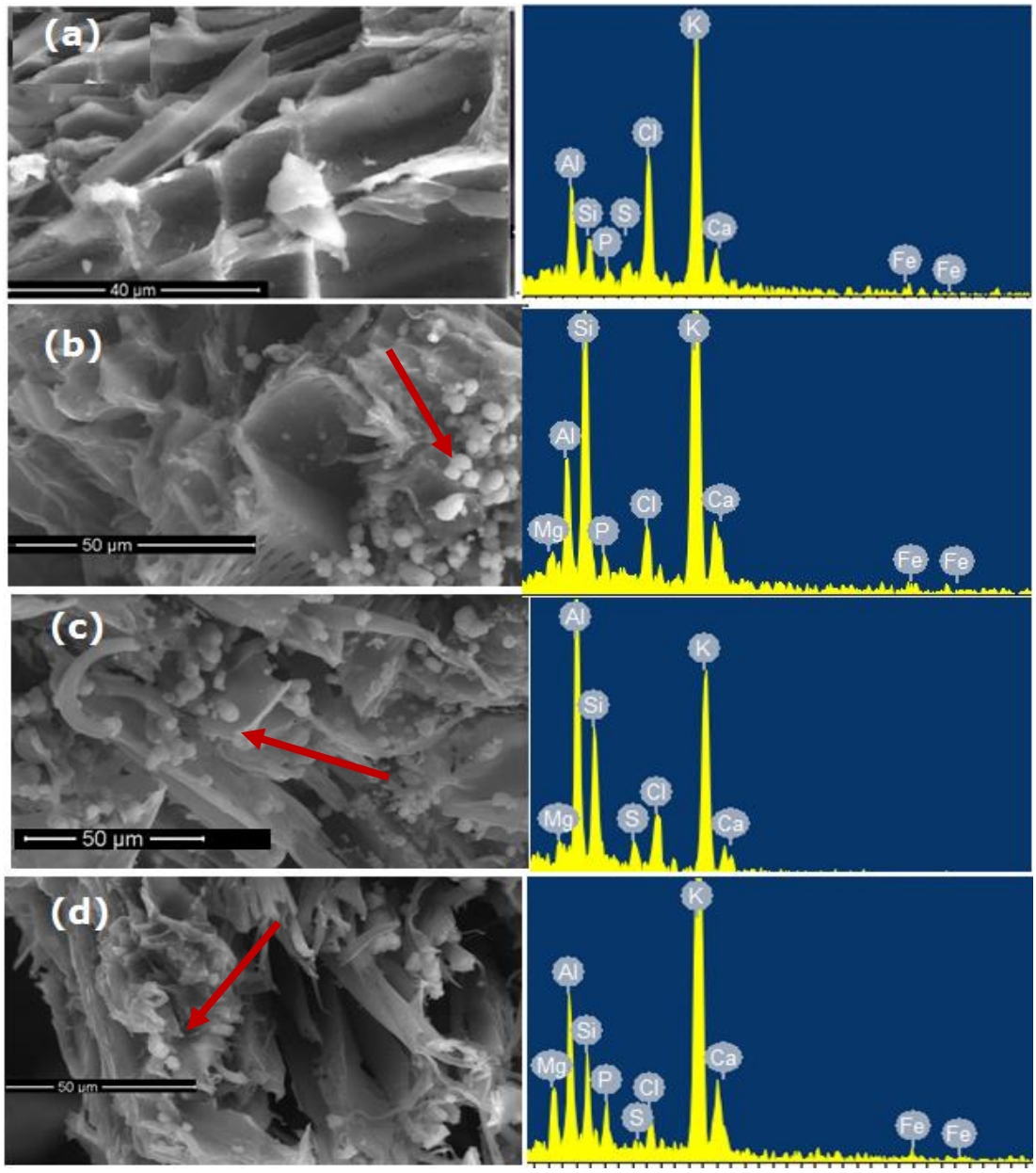

Figure 6.8: SEM-EDX of bio-char. (a) CBR: 0.0wt%; (b) ZSM-5 CBR: 3.0 wt%; (c) 0.2HZSM-5 CBR: 3.0 wt%; (d) 0.3HZSM-5 CBR: 3.0 wt%

6.3 In situ Non-catalytic Upgrading of Bio-oil

6.3.1 Feedstock characteristics

Characteristics of the individual and assorted biomass are summarized in Table 6.4. From the proximate analysis, it can be seen that the assorted samples have 4-8 folds higher ash content and 2-9% lower volatile matter content relative to the scenario 1 (pure NGS), which can be linked to the lower heating values recorded for the samples. The major inorganic element in the ash such as potassium (K), calcium (Ca) and silicon (Si) determined using atomic absorption spectrometer (AAS) (Table 6.5) showed that proportion of the elements in the ash are in the following order K>Ca>Si, Si>K>Ca and Ca>Si>K for the case study 1 and 5, 2 and 3 while Si>K>Ca was recorded for the remaining case studies. The result of TGA analysis of the samples is shown in Figure 6.9. The DTG curves showed distinct regions at temperature around 200 ^{o}C, 229-285 ^{o}C, 326 ^{o}C and 373-540 ^{o}C. Case study 1 displayed noticeable peaks at the first three regions, which is due to decomposition of extractives, hemicellulose, and cellulose while the last region was a uniform decomposition trend for lignin. Case study 2 had hemicellulose, cellulose and lignin decomposition sections while the pure SGW (case study) exhibited only cellulose and lignin degradation profile. Both case study 2 and 3 have uniform lignin decomposition similar to that of case 1, which indicate that the lignin component of the individual biomass species have similar thermal decomposition pathways. On the other hand, the visible extractive decomposition peak observed in the case study 1 (pure NGS) around 200 ^{o}C diminished considerably in all the assorted feedstock (case study 4, 5 and 6). Similarly, the hemicellulose degradation shoulder at 229-285 ^{o}C visible in the case study 1 and 2 completely aligned with the cellulose decomposition peak. Intensity of the cellulose peak in all the assorted biomass increased from 5.5 %/^{o}C in case study 1 to 5.9, 8.0 and 6.7 %/^{o}C in case study 4, 5

and 6, which is an evidence of increased cellulose decomposition rate resulting from synergistic effect of mineral element in the feedstock (Biwas et al., 2011; Mohammed et al., 2015a). The Lignin degradation profile of all the assorted biomass species was a non-uniform broader peak between 450 and 680 °C compared to the lignin profile observed in the individual biomass, which can also be attributed to interaction between various mineral elements in biomass.

Table 6.4: Characteristics of feedstock

Property	Case study					
	1	2	3	4	5	6
	Proximate analysis (wt%) dry basis					
AC	1.75±0.04	13.16±0.58	10.82±0.46	7.45±0.33	6.69±0.32	9.27±0.42
VM	81.51±0.26	72.27±0.22	79.97±0.26	76.89±0.24	77.74±0.24	75.33±0.25
FC	16.74±0.05	14.57±0.04	9.21±0.03	15.66±0.04	10.97±0.03	15.40±0.04
HHV (MJ/kg)	18.05±0.07	16.56±0.05	17.02±0.06	17.30±0.06	17.88±0.07	17.76±0.06
	Ultimate analysis (wt%) dry basis					
C	51.61±0.24	40.67±0.23	44.62±0.23	46.14±0.23	45.63±0.23	43.65±0.23
H	6.01±0.02	6.79±0.02	6.67±0.02	6.40±0.02	6.31±0.02	6.50±0.02
N	0.99±0.01	0.44±0.01	0.19±0.01	0.71±0.01	0.59±0.01	0.53±0.01
S	0.32±0.01	0.87±0.01	0	0.60±0.01	0.16±0.01	0.44±0.01
O	41.07±0.02	51.23±0.04	48.52±0.03	46.15±0.02	47.31±0.03	48.88±0.03

(AC): Ash content; (VM): volatile matter; (FC): fixed carbon; (C): carbon; (H): hydrogen; (N): nitrogen; (S): sulphur; (O): oxygen; (HHV): higher heating value. Values are the means (n=3) ± standard deviation

Table 6.5: Mineral composition of the ash

	Mineral (mg/kg)		
Case study	K	Ca	Si
1	3079.51±224.80	206.71±13.20	206.0±25.13
2	174.08±3.23	31.91±2.36	2641.57±116.59
3	474.98±9.11	1247.40±69.63	860.55±21.03
4	1077.85±81.10	80.01±4.22	1835.45±66.21
5	1314.13±30.22	859.40±20.86	444.11±16.37
6	673.241±38.34	144.79±12.67	2030.35±95.71

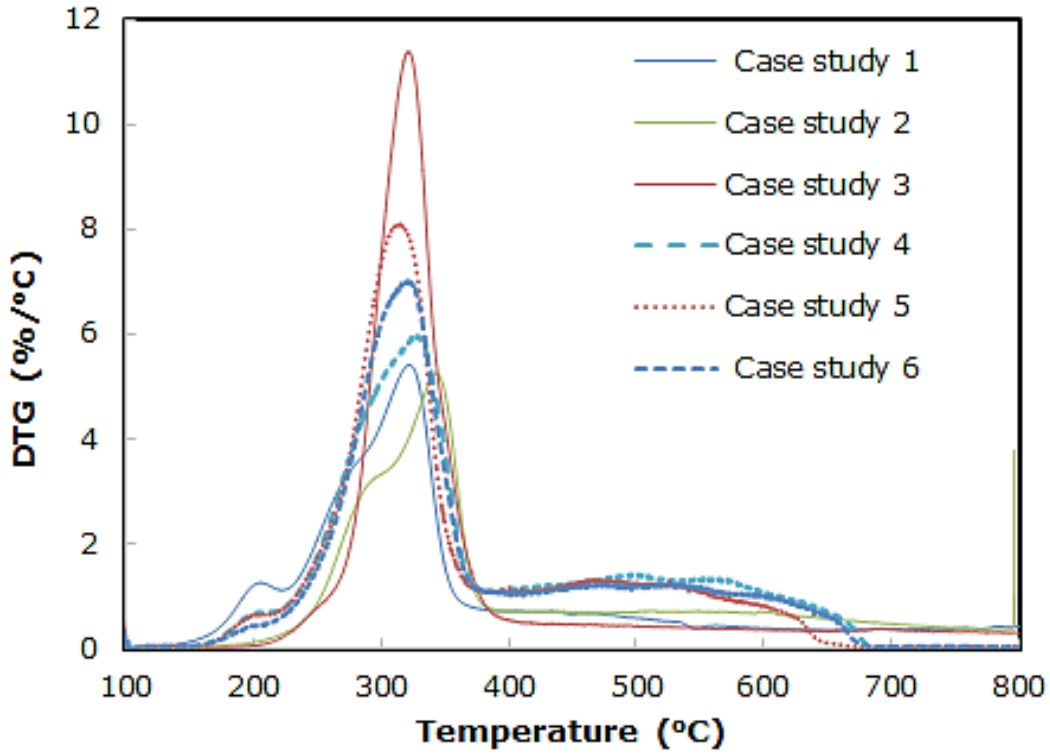

Figure 6.9: DTG profile of the feedstock. Condition: nitrogen atmosphere (20 mL/min), 10 °C/min heating rate.

6.3.2 Pyrolysis product distribution

Pyrolysis study was carried out at 600 °C, 5 L/min N_2 flow and 50 °C/min heating rate. The product distribution is shown in Figure 6.10. The total bio-oil (organic and aqueous) yield recorded from the assorted biomass was 42.89, 43.72 and 32.44 wt% for the case study 4, 5 and 6, which corresponds to 6.0, 5.5 and 16.8 wt% lower relative to the total bio-oil yield in case study 1 (pure NGS). Similarly, the organic phase recorded from the assorted biomass, case study 4, 5 and 6 was approximately 7.0, 4.0 and 6.0 wt% lower than the organic phase yield in case study 1 while production of aqueous was similar except in the case study 6, where about 10.0 wt%

lower aqueous phase was recorded. The non-condensable gas yield recorded in case study 5 is similar to gas obtained in case study 1 while case study 4 and 6 had lower and higher gas production respectively. The trend observed in the product distribution from the assorted biomass compared to the product from the individual biomass is an evidence of synergistic effect during the co-pyrolysis, which can be related to the characteristic of the biomass feed, particularly the biomass ash and its composition. The declined trend observed in the bio-oil organic phase from the assorted biomass relative to case study 1 is attributed to higher ash content. High biomass ash generally produce more solid materials as evident in Figure 6.10. Ash is non-combustible and will remain in the solid product after the pyrolysis (Mohammed et al., 2016b). It is interesting to note that among the assorted biomass, case study 5 produced more organic phase bio-oil (11.70 wt %), which can be connected to the feedstock mineral composition particularly the alkaline and alkaline earth metals. Ash composition of the feedstock constituted a total of 2173.53 mg/kg alkaline and alkaline earth metals (Table 6.5) with potassium (K) accounting for 60 % while the remaining 40 % represents calcium (Ca). These elements tend to catalyse pyrolysis reactions which usually lead to degradation and polymerization of the intermediate products. Studies have shown that the addition of Ca promotes the formation of liquid product during pyrolysis (Wang et al., 2010; Lin et al., 2010). Although, case study 3 had the highest Ca content among all the feedstock but the organic phase yield (7.03 wt %) was lower than that produced from case study 5. Therefore, the increased organic phase bio-oil observed in scenario 5 can be attributed to combined catalytic activity of the Ca and K mineral in the ash.

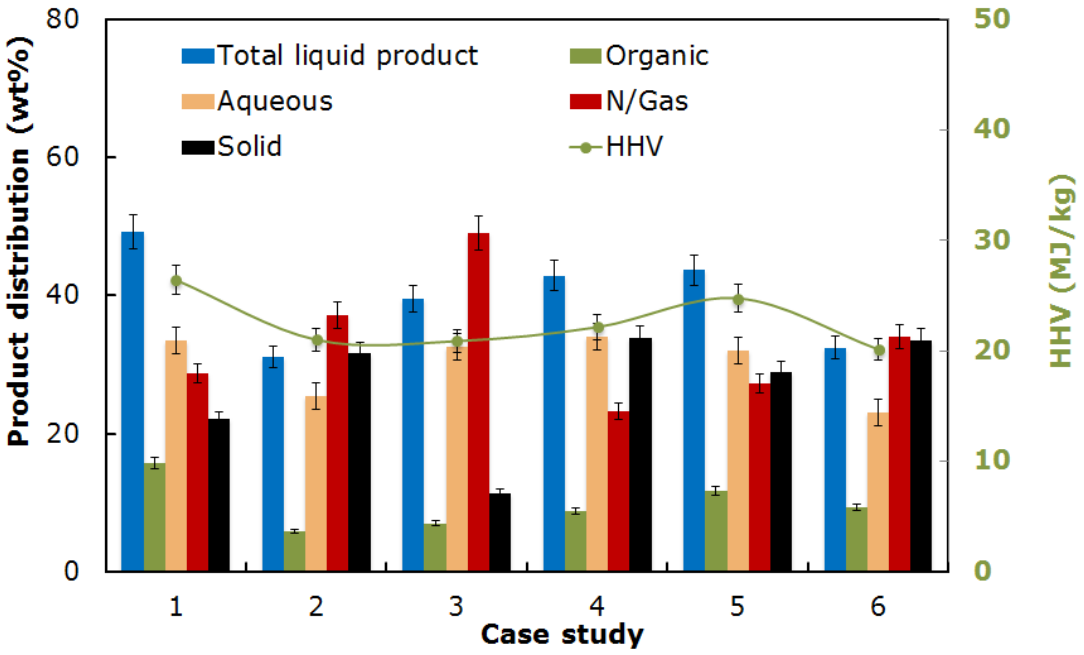

Figure 6.10: Pyrolysis product distribution (600 °C, 5 L/min N_2 flow and 50 °C/min heating rate). N/gas: non-condensable gas. Solid: Bio-char. HHV: higher heating value. Values are the means (n = 3) ± SD

6.3.3 GC-MS analysis of organic phase product

The most abundant group of organic compound present in the bio-oil collected are summarized in Table 6.6. Impact of co-pyrolysis was more on the distribution of MARHC, PHOL, MPHOL and AAK. MARHC was not detected in case study 5 and 6 while MPHOL reduced approximately by 18 and 23 % respectively relative to case study 1, which could be responsible for about 37-44 % increase in the PHOL content recorded. Production of PHOL may have proceeded via demethoxylation of MARHC and MPHOL promoted by the catalytic activities of K and Ca in the feedstock. Similarly, about 34 and 81 % reduction in AAK was recorded in scenario 5 and 6 while MEST, a component of biodiesel increased by 34 and 81%. The reduction of AAK in the oil can also be

attributed to the synergism between K and Ca minerals in the ash, which have aided decarboxylation and decarbonylation reactions. Consequently, Co-pyrolysis oil obtained from case study 5 and 6 showed a superior quality compared to bio-oil from case study 1 (pure NGS), which can serve as a good precursor for production of fuel, valuable chemicals and consumer products.

Table 6.6: Group of compound in the organic phase bio-oil

Composition (%)	Case study					
Organic	1	2	3	4	5	6
HC	4.67	0.00	3.19	0.00	4.24	0.00
ARHC	2.53	0.00	0.00	0.00	2.31	3.24
MARHC	2.18	2.60	2.26	2.08	0.00	0.00
PHOL	28.15	28.71	45.82	29.46	40.50	38.70
MPHOL	37.87	29.49	20.49	42.92	30.93	29.20
AAK	16.88	13.16	15.40	21.35	11.12	3.20
MEST	4.68	4.29	5.47	2.19	7.82	13.50
OVAC	3.05	21.75	7.36	2.00	3.07	12.17

(HC) hydrocarbons, (ARHC) aromatic hydrocarbons, (MARHC) methoxy aromatics, (PHOL) phenol, (MPHOL) methoxy phenol, (AAK) acids, aldehydes and ketones, (MEST) methyl ester and (OVAC) other value added chemical.

6.4 Conclusion

In-situ catalytic and non-catalytic upgrading of bio-oil derived from Napier grass was carried out. Increasing catalyst-biomass ratio during the catalytic process with microporous structure reduced production of organic phase bio-oil by approximately 10.83-42.94 % compared to organic phase yield from the non-catalytic process. Using mesoporous catalyst promoted nearly 54.0 % higher organic yield relative to microporous catalyst, which translate to only about 6.44-19.82 % reduction in organic phase compared to the yield of organic phase from the non-catalytic process. Maximum degree of deoxygenation of about 36.9 % was recorded with microporous catalyst compared to the mesoporous catalysts, which had between 39 and 43 %.

Mesoporous catalysts promoted production olefins and alkanes, normal phenol, monoaromatic hydrocarbons while microporous catalyst favoured the production of alkenes and polyaromatic hydrocarbons. There was no significant increase in the production of normal phenols over microporous catalyst due to its inability to transform the methoxyphenols and methoxy aromatics. On the other hand, in-situ non-catalytic upgrading revealed that co-pyrolysis of Napier grass with calcium reach feedstock favoured production of normal phenol and methyl esters without significant reduction in the organic phase yield. The oil from co-pyrolysis showed a superior quality compared to the raw bio-oil from pure Napier grass and can be transformed to fuel, valuable chemicals and other consumer products. All the pyrolysis products from this process can be further utilized compared to the bed mixing of catalyst and biomass of the in-situ catalytic process, where bio-char application seem not possible due difficulty in separating the spent catalyst from the resulting bio-char.

CHAPTER SEVEN

7. EX-SITU CATALYTIC UPGRADING OF BIO-OIL DERIVED FROM NAPIER GRASS

7.1 Introduction

This chapter deals with Ex-situ catalytic upgrading of bio-oil derived from Napier grass. It consists of catalytic upgrading studies and fractional distillation of upgraded organic phase oil. The upgrading studies evaluate effect microporous and hierarchical mesoporous ZSM-5 (modified ZSM-5) on upgraded products distribution and composition of organic phase product. It further examines impact of temperature, catalyst loading and reaction time on the product yield and characteristics. At the end, it provides distribution of fractional liquid products and composition from distillation of upgraded organic phase.

7.2 Effects of Microporous and Mesoporous ZSM-5 on Bio-oil Upgrading

7.2.1 Products distribution and characteristics

Characteristics of the catalysts have been presented in Chapter 6. Catalytic performance of ZSM-5 and modified ZSM-5 in the upgrading of bio-oil under 60 min reaction time at 400 ^{o}C and catalyst loading of 2.0 wt% is presented in Figure 7.1. Thermal condition (0.0 wt% catalyst loading) was used as control and total liquid, gas and solid product collected was 76.6, 22.5 and 0.9 wt%. Total liquid yield decreased to 51.10, 50.30 and 47.40 wt% while the gas increased to 32.90, 37.10 and 43.30 wt% when ZSM-5, 0.2HZSM-5 and 0.3HZSM-5 was applied. The lower liquid yield and increased gas production with the catalysts is attributed to several catalytic reactions such as dehydration, decarbonylation and decarboxylation (Mohammed et al., 2016a). Increase in solid product was recorded with the catalysts relative to the control. Comparing between the catalysts, ZSM-5 produced highest solid product (16.0 wt %) while 0.3ZSM-5 had lowest solid yield (9.30 wt %). Vitolo et al. (2001) reported total solid content of about 11.0wt% during upgrading of pyrolysis oil over ZSM-5. Similarly,

in a separate study by Saad et al. (2015), a total solid content of 29.2 wt% was recorded. The high yield of solid with ZSM-5 is attributed diffusion resistance of large oxygenated compounds or coke precursors in the raw bio-oil, which undergo polymerization and polycondensation reactions and finally deposited on the catalyst surface. Consequently, the lower solid yield recorded with modified ZSM-5 can be linked to the improved pore structures in the modified ZSM-5. This observation is contrary to the report of Puertolas et al. (2015). The authors observed increase in solid yield and reduction in total liquid product over the hierarchical zeolites. This dissimilarity could be attributed to differences in pore and acidity of the hierarchical zeolites. Organic phase from the catalytic process was lower compared to the thermal process. Mesoporous ZSM-5 produced 15-16 wt% higher organic phase compared to the bulk ZSM-5, which produced more aqueous phase. This observation indicates that bulk ZSM-5 favoured dehydration reaction while the modified ZSM-5 promoted more decarbonylation and decarboxylation, which substantiated the higher gas yield recorded with the modified catalyst. Higher heating value (HHV) of the organic phase (Figure 7.1) increased from 29.18 MJ/kg (raw bio-oil dry basis) to 35.90 MJ/kg after the thermal treatment, which accounted for about 23 % increase. Upgrading over ZSM-5, 0.2HZSM-5 and 0.3HZSM-5 produced organic phase with HHV of 40.46, 43.43 and 42.08 MJ/kg. These values accounted 39-49 % increase in the HHV relative to the raw bio-oil. Degree of deoxygenation (DOD) (Figure 7.1) was 19.24 % after thermal treatment, which increased significantly to 48.58 % with ZSM-5. The modified ZSM-5 produced more deoxygenated organic phase with DOD of about 57 %. The high DOD recorded with the catalysts is therefore responsible for the improved HHV.

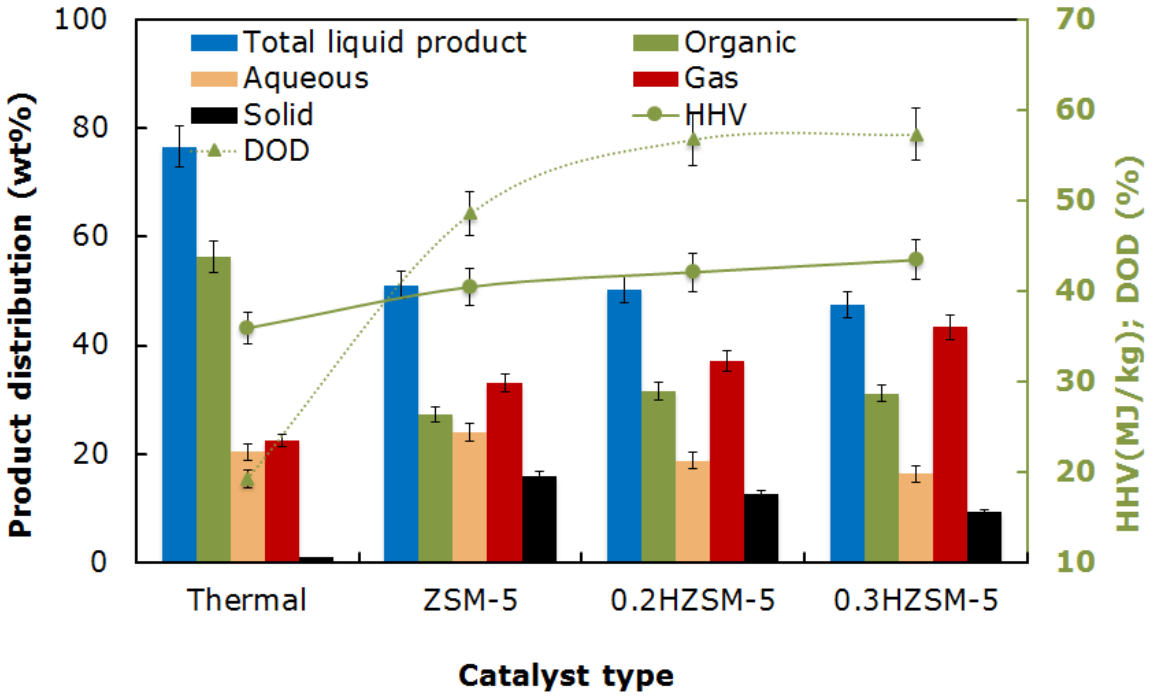

Figure 7.1: Effect of catalyst on deoxygenation of bio-oil at 400 °C. Feed: 30g bio-oil, catalyst loading: 2.0 wt%, reaction time: 60 min. Solid: char and tar. Values are the means (n =3)

Puertolas et al. (2015) reported 34 % DOD of bio-oil over bulk ZSM-5 while DOD recorded with hierarchical mesoporous ZSM-5 was 42%. Maximum HHV of 35.3 MJ/kg was also recorded, which was attributed the higher DOD achieved with the mesoporous ZSM-5. Similar improvement in DOD and HHV of upgraded bio-oil over mesoporous ZSM-5 has been reported by Veses et al. (2016). The authors recorded 7.1% DOD with thermal upgrading while 39% DOD was recorded with mesoporous ZSM-5. The corresponding HHV was 27.3 and 32.5 MJ/kg. Other physicochemical properties of bio-oil are summarized in Table 7.1. There was no clear trend in pH value of the upgraded bio-oil. Although, slight decrease in acidity of the upgraded bio-oil was

observed (3.88-3.92) relative to the raw bio-oil (3.71) except for the thermally upgraded bio-oil, which had pH value of 3.6. The decrease in the acidity of the oil produced over the catalyst is an indication of reduction of organic acids and phenolic compound through carboxylation and decarbonylation reactions (Mohammed et al., 2016).

Table 7.1: Physicochemical properties of raw and upgraded bio-oil

Property	Raw	Thermal	ZSM-5	0.2HZSM-5	0.3HZSM-5
Density (g/cm^3)	0.98±0.0	0.95±0.0	0.91±0.0	0.9±0.0	0.9±0.0
pH	3.71±0.01	3.6±0.01	3.92±0.01	3.88±0.01	3.92±0.01
HHV (MJ/kg)	29.18±0.10	35.90±0.10	40.46±0.10	42.08±0.10	43.43±0.10
C (wt %)	53.87±1.71	60.93±1.72	72.86±1.70	74.82±1.73	74.75±1.72
H (wt %)	6.45±0.07	7.50±0.10	7.36±0.09	8.62±0.11	8.55±0.10
N (wt %)	1.35±0.01	1.10±0.01	0.34±0.01	0.39±0.01	0.24±0.01
S (wt %)	0.76±0.01	0.13±0.01	0.12±0.01	0.14±0.01	0.22±0.01
O*(wt %)	37.57±1.01	30.34±1.01	19.32±1.01	16.24±1.01	16.03±1.01

Value are the mean (n =3) ± standard deviation. *by difference

7.2.2 Thermogravimetric analysis of upgraded bio-oil

TGA analysis of commercial fossil premium motor spirit (PMS), kerosene and diesel were performed as standards. Organic raw bio-oil feedstock and upgraded samples were subjected to the same thermal treatment. From Figure 7.2a, final evaporation temperature of PMS, kerosene and diesel was found to be 126, 185 and 291 ^{o}C respectively. Using the final evaporation temperature, by extrapolation, the raw organic bio-oil constitutes (Figure 7.2b) nearly 70 wt% volatile fraction. The weight loss above 300^{o}C can be attributed to thermal decomposition of residue. About 68 wt% of the oil had boiling range similar to that of diesel. Similarly, approximately 48 wt% of the bio-oil is made up of kerosene boiling fraction while 35 wt% had boiling characteristic comparable to that of PMS. Evaporation profile of thermally upgraded

bio-oil revealed increase in diesel and kerosene boiling fractions to 75 and 50 wt% respectively, while volatile fraction with PMS boiling characteristics decreased to 31 wt% relative to the raw bio-oil. Upgraded bio-oil over bulk ZSM-5 had about 77, 53 and 34 wt% diesel, kerosene and PMS boiling fraction respectively. Reduction in PMS boiling fraction recorded with thermal and ZSM-5 compared to the raw bio-oil could be attributed to thermal and catalytic cracking of light fractions originally present in the bio-oil feedstock. Bio-oil upgrading over modified ZSM-5 produced about 78-84 wt%, 57-67 wt% and 43-50 wt% volatile organic fraction with boiling point comparable to that of diesel, kerosene and PMS respectively. The increased volatile fraction recorded with modified ZSM-5 could be ascribed to cracking of heavy molecular fractions and subsequent transformation.

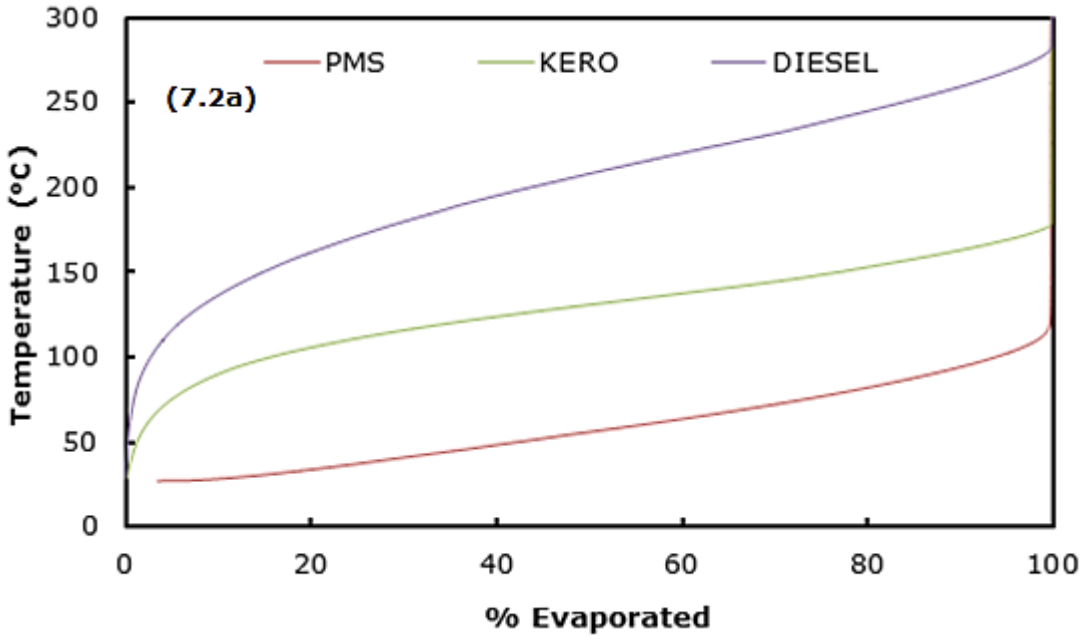

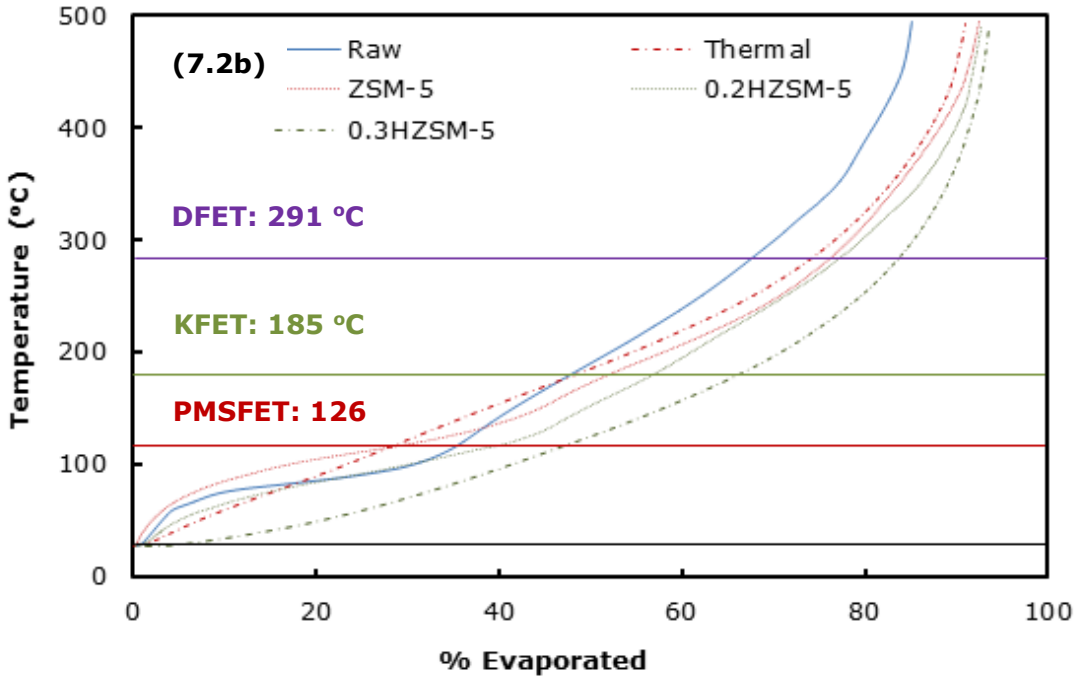

Figure 7.2: Simulated distillation using TGA. (a) Premium motor sprit-PMS, kerosene and diesel (b) Raw and upgraded organic phase bio-oil. DFET, KFET and PMSFET: diesel, kerosene and PMS final evaporation temperature.

7.2.3 GC-MS analysis of upgraded bio-oil

Compounds identified in the raw and upgraded bio-oil are grouped into hydrocarbons (HC), aromatic hydrocarbons (ARHC), methoxy aromatics (MARHC), phenol (PHOL), methoxy phenol (MPHOL), acids, aldehydes and ketones (AAK), methyl ester (MEST) and other value added chemicals (OVAC). The amounts of each component is expressed in percentage (%) based on the relative area from GC-MS analysis as summarized in Table 7.2 Noticeable changes were observed in the composition of the upgraded bio-oil. Increase in PHOL content was recorded in thermally upgraded bio-oil relative to the raw bio-oil. This is ascribed to thermal decomposition of MPHOL

which decreased considerably. The process involves formation of methyl radical resulting in hydoxyphenoxy radical, which subsequently decarbonylates to cyclopentadienyl radical. Radical-radical reaction between methyl and cyclopentadienyl lead to the formation of phenols (Scheer et al., 2011). High formation of phenol has also been reported by Veses et al. (2016). They recorded about 21.32 % phenol content in the blank test relative to 14.66-18.41 % obtained with catalyst.

Table 7.2: Group of organic compound in the deoxygenated bio-oil at 400 °C, 60 min and 2.0 wt% catalyst loading.

Composition	Raw	Thermal	ZSM-5	0.2HZSM-5	0.3HZSM-5
			Organic phase (%)		
HC	4.67	5.20	20.67	13.56	3.94
ARHC	2.53	0.00	13.33	20.40	26.87
MARHC	2.18	10.34	3.56	0.00	0.00
PHOL	28.15	65.91	41.25	43.12	47.70
MPHOL	37.87	5.03	0.00	0.00	0.00
AAK	16.88	4.35	12.69	3.71	2.01
MEST	4.68	9.18	8.50	11.75	11.00
OVAC	3.05	0.00	0.00	7.46	8.48

(HC) hydrocarbons, (ARHC) aromatic hydrocarbons, (MARHC) methoxy aromatics, (PHOL) phenol, (MPHOL) methoxy phenol, (AAK) acids, aldehydes and ketones, (MEST) methyl ester and (OVAC) other value added chemical

Thermal cracking of MPHOL to MARHC may have occurred, which is responsible to the increased composition of MARHC in the thermally upgraded bio-oil relative to the feedstock and other upgraded oil. Significant reduction in AAK was also recorded with thermal cracking. Similarly, the percentage of hydrocarbon (1, 3-dimethyl-1-cyclohexene) in the feedstock increased from 4.67 to 5.2 % but a new hydrocarbon structure, 1 3 5-cycloheptatriene was observed after the upgrading (Appendix IV). Benzene originally present in the feedstock was not detected in the product after

thermal treatment. Therefore, cycloheptatriene may have originated from transformation of benzene and the cyclohexene and subsequent rearrangement and ring expansion. Bio-oil upgraded over bulk ZSM-5 and modified ZSM-5 produced oil with less PHOL, AAK and complete elimination of MPHOL through series of reactions such as dehydration, decarbonylation and decarboxylation. The presence of MARHC in the upgraded bio-oil over ZSM-5 indicates that deoxygenation proceeds via formation MARHC and subsequent conversion to aromatic. Significant amount of HC and ARHC were recorded with the catalysts, which can be linked to conversion of oxygenates. Modified ZSM-5 produced high amount of aromatics relative to parent ZSM-5, suggesting high degree of conversion of MARHC while formation of other HC compounds declined with hierarchical mesoporous ZSM-5. It is interesting to note that most of the HCs produced with parent ZSM-5 are cyclic olefins, which decreased with modified ZSM-5. Selectivity of olefins and aromatics by the catalysts is shown Figure 7.3. It can be seen that the parent ZSM-5 produced more olefins and polyaromatic hydrocarbon (PAH) while the opposite trend was recorded with the modified ZSM-5. It can therefore be inferred that the high amount of solid earlier recorded with the parent ZSM-5 was due to evolution of PAH at acid sites, which serves as coke precursors and eventually result in the solid yield. The nature of aromatics recorded with modified ZSM-5 were mainly alkyl benzenes, which suggests that hierarchical mesoporous ZSM-5 favoured ring alkylation reaction. This trend seems to have correlation with Si/Al ratio. With decreasing Si/Al ratio, more alkyl benzenes were produced. Similar observation has been reported by Foster et al. (2012). The authors observed that decrease in Si/Al ratio promote production of aromatics. They also reported that mesoporous ZSM-5 favoured the production of alkylated monoaromatic hydrocarbons. It is worthy to note that the content of esters in the raw bio-oil increased significantly

in all the upgraded bio-oil. These compounds are believed to have formed through transesterification reaction. Decomposition of methanol-imidazole present in the raw bio-oil to release methanol is expected, which may have further reacted with organic acids and could responsible for the increased ester content recorded. Methyl esters are biodiesel component, which is another valuable renewable products.

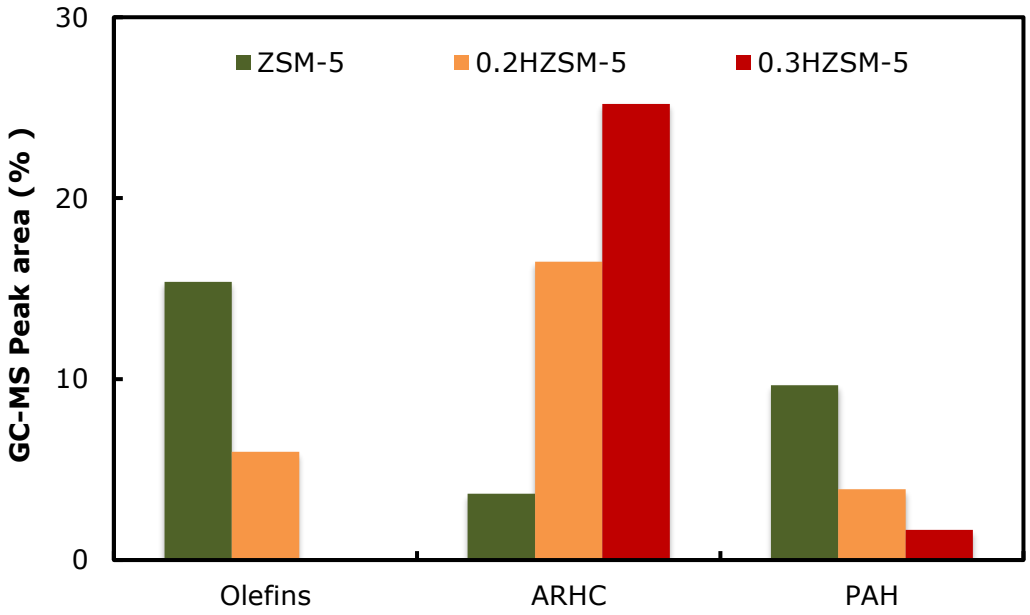

Figure 7.3: Selectivity of olefins and aromatic hydrocarbons at 400 °C, 60 min and 2 w% catalyst loading

7.2.3 GC-TCD analysis of gas composition

Composition of gas as determined by the GC is summarized in Table 7.3. The component identified includes hydrogen (H_2), carbon monoxide (CO), carbon dioxide (CO_2) and methane (CH_4). Thermal cracking produced gas with highest CH_4 content (33.42 vol %), suggesting production of small organic molecules. Similarly, significant amount of CO in the gas from thermal cracking is an evidence of some decarbonylation

reaction, which confirmed the formation of cyclopentadienyl radical as previously stated in the mechanism of phenol formation from thermal decomposition of methoxyphenol. The principal composition gases from the catalytic upgrading process were CO and CO_2, which are indications of decarboxylation and decarbonylation reactions. With modified ZSM-5, the CH_4 composition decreased relative to ZSM-5. This can be linked to the alkylation reaction observed with the hierarchical ZSM-5. It can therefore be stated that the alkyl group generated during upgrading reacted with the aromatic pool within the system and subsequently result in alkyl benzenes as observed in the previous section above. Considerable increase in the amount of CO and CO_2 were recorded with the mesoporous ZSM-5 relative to bulk ZSM-5, indicating higher degree of decarboxylation and decarbonylation. This observation is in good agreement with the result of GC-MS analysis. Preferential decarbonylation and decarboxylation reactions with hierarchical mesoporous ZSM-5 has been reported in the literature (Veses et al., 2016). A summary of possible reaction pathways during upgrading is shown in Figure 7.4. Effects of other process parameters such reaction temperature, catalyst loading, reaction time and catalyst stability on deoxygenation of bio-oil were further evaluated with 0.3HZSM-5, being the best performing catalyst recorded in this study

Table 7.3: Gas composition from GC-TCD analysis

Composition (vol %)	Thermal	ZSM-5	0.2HZSM-5	0.3HZSM-5
H_2	1.35	1.61	1.51	1.42
CH_4	33.42	24.66	17.14	12.18
CO	25.34	27.72	32.92	36.88
CO_2	9.03	28.01	30.43	32.35

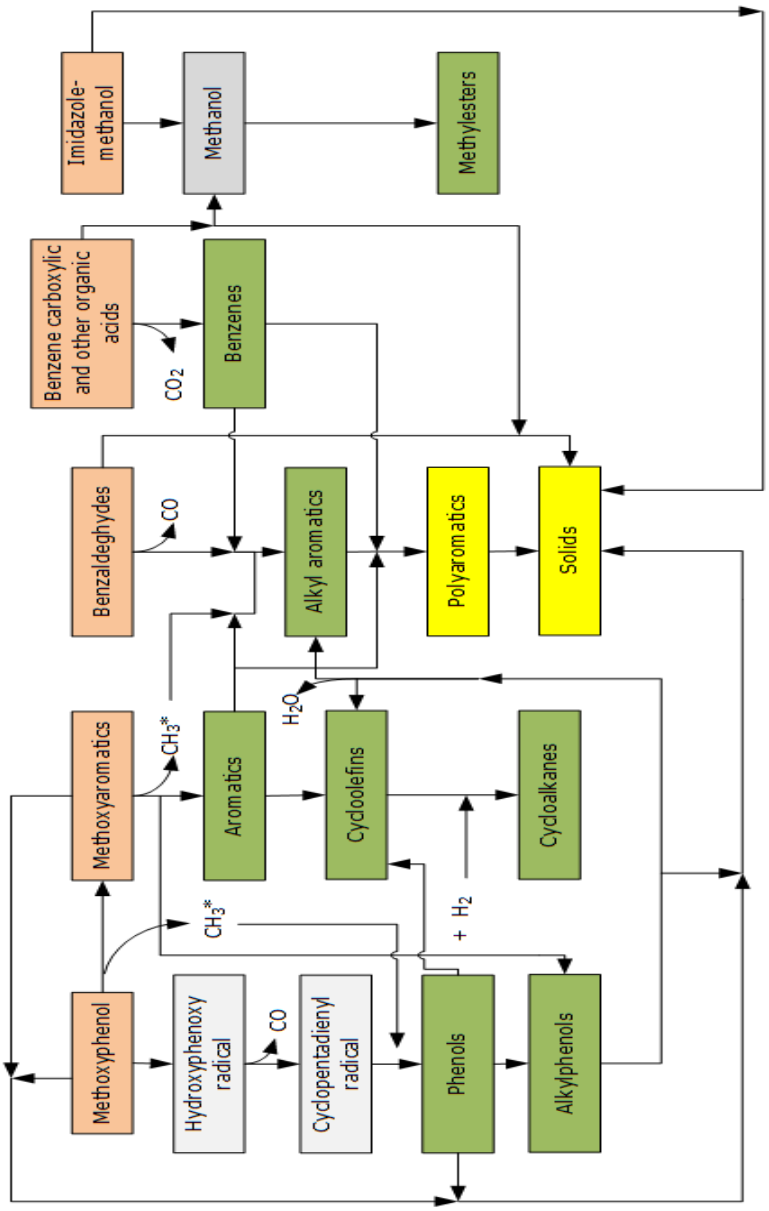

Figure 7.4: Possible reaction pathways of thermal and catalytic ex-situ upgrading of bio-oil. Component in the raw bio-oil, intermediate products, unwanted products and desired products

7.3 Effect of Reaction Temperature on Deoxygenation of Bio-oil Over Mesoporous Zeolite

Temperature is one of the most imoportant variables in catalytic cracking process as it controls product distribution. Temperature between 375 and 425 °C was employed in this study to minimize gas production. Performance of 0.3HZSM-5 (2.0 wt %) on deoxygenation of bio-oil was evaluated at 375, 400 and 425 °C under 60 min. Figure 7.5 showed impact of temperature on the production distribution. Total liquid yield of 51.20 wt% was recorded at 375 °C, which decreased to 47.40 wt% at 400 °C and subsequently to 39.7 wt% at 425 °C. Similar declining trend was recorded in the total solid yield while increasing gas production was observed with temperature. At 375 °C, solid yield was approximately two folds higher compared to the solid yield at 400 and 425 °C whereas the gas production at 400 and 425 °C was 38 and 69 wt % respectively higher than the gas production at 375 °C.

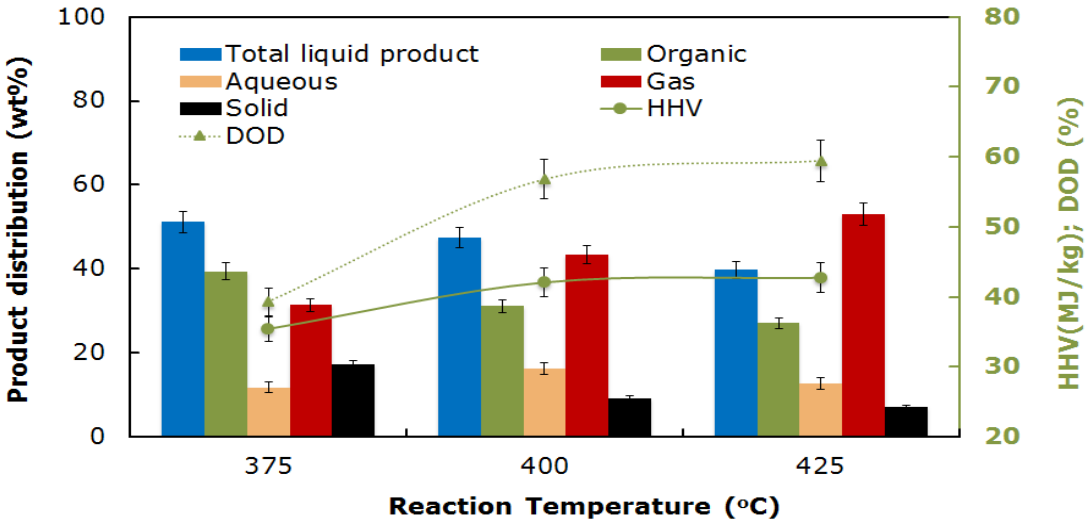

Figure 7.5: Effect of reaction temperature on deoxygenation of bio-oil at 2.0 wt% 0.3HZSM-5 and 60 min. Feed: 30g bio-oil. Solid: char and tar. Values are the means (n =3)

High solid production at lower temperature could be attributed to polymerization of heavy fractions while decomposition of large organic molecules, which generally occur at high temperature is responsible for the high gas production. Similarly, decrease in the yield of organic phase was recorded with increasing temperature. Wei et al. (2016) reported that higher temperature promotes production of small gas molecules, which eventually result in lower liquid yield. They further stated that upgrading of raw bio-oil with zeolite catalyst at low temperature, particularly below 400 °C, produce more solid products. Furthermore, there was no significant difference between the aqueous phase produced at 375 (11.80 wt %) and 425 °C (12.6 wt %). These values are lower relative to 16.30 wt% aqueous phase recorded at 400 °C. The lower gas production at 375 °C is an indication of less deoxygenation activity. Both dehydration, decarboxylation and decarbonylation reactions may have occurred but at low severity. Higher dehydration reaction can be suspected at 400 °C compared to 425 °C reaction temperature where severe cracking reactions are likely. HHV and DOD recorded at 400 and 425 °C were 21 and 44-51 % higher relative to the values recorded at 375 °C.

Composition of organic phase is summarized in Table 7.4. MARHC, MPHOL and AAK were the main oxygenates detected in the organic phase produced at 375 °C. These groups of organic compounds were significantly reduced in the oil upgraded at 400 and 425 °C. Amount of normal PHOL recorded at 375 °C was 58.62 %, which is about 19-20 % higher than the phenol content in the oil upgraded at 400 and 425 °C. On the other hand, the ARHC content in the oil upgraded at 400 and 425 °C was approximately 3 and 4 times higher relative to the ARHC content of the oil produced at 375 °C. Nature of ARHC recorded at 375 °C was mainly PAH (naphthalene), accounting for about 73 % of the total ARHC, while the total ARHCs recorded at 400 and 425 °C were

predominantly alkyl benzenes and benzenes (less than 10 % PAH). Production of monoaromatic (benzene) was prevalent in the oil upgraded oil at 425 °C relative to oil production at 400 °C, which constituted majorly, the alkyl aromatics. Similar trend was also recorded in the yield of HCs. Heptadecane, 9-hexyl- and octadecane, 3-ethyl-5-(2-ethylbutyl)- were detected at 400 °C compared to heptane and cyclopentane obtained at 420 °C.

Table 7.4: Effect of reaction temperature on the organic phase and gas compositions at 2.0 wt% 0.3HZSM-5 loading and 60 min

Composition	Reaction Temperature (◦C)		
	375	400	425
Organic phase liquid (%)			
HC	2.14	3.94	8.05
ARHC	8.13	26.87	33.67
MARHC	5.20	0.00	0.00
PHOL	58.62	47.70	46.43
MPHOL	16.36	0.00	0.00
AAK	4.58	2.01	3.30
MEST	2.82	11.00	5.09
OVAC	2.16	8.48	3.46
Gas composition (vol %)			
H_2	1.78	1.42	1.51
CH_4	6.66	12.18	16.02
CO	25.76	36.88	38.98
CO_2	26.55	32.35	33.02

HC) hydrocarbons, (ARHC) aromatic hydrocarbons, (MARHC) methoxy aromatics, (PHOL) phenol, (MPHOL) methoxy phenol, (AAK) acids, aldehydes and ketones and (MEST) methyl ester

Result of gas analysis (Table 7.4) revealed no significant changes in H_2 content of the gases collected at different temperature tested in this study. Substantial increase in CH_4 and CO in the gas composition were recorded. About 6.66 vol% CH_4 was obtained in the gas collected at 375 °C, which increased to 12.18 and 16.02 vol% at 400 and 425 °C respectively. Increase in CH_4 observed at higher reaction temperature is an

indication of cracking reactions. This means that large hydrocarbon molecules undergo scission, resulting in the production of small organic molecules and light gas hydrocarbons. This explains the significant amount of normal benzene and small chain HCs recorded in the oil upgraded at 425 °C. Production of CO increased significantly with temperature compared to CO_2, signifying more decarbonylation reactions, a typical characteristic of mesoporous ZSM-5. Therefore, it can be stated that catalytic upgrading of bio-oil over mesoporous ZSM-5 at high temperature above 400 °C proceeded via cracking of long chain hydrocarbons, decarbonylation, decarboxylation and dehydration reactions, which promotes production of small organic molecules at the expense of organic liquid yield. Consequently, further evaluation of impact of process variables such as reaction time and catalyst loading on bio-oil deoxygenation over the hierarchical mesoporous zeolite (0.3HZSM-5) was carried out at 400 °C

7.4 Effects of Catalyst Loading on Deoxygenation of Bio-oil Over Mesoporous Zeolite

Impacts of catalyst loading on deoxygenation of bio-oil over 0.3HZSM-5 were investigated using 1-4 wt % catalyst at 400 °C and 60 min. From Figure (7.6), increase in catalyst loading increased gas and solid production while decline trend was recorded in the yield of organic phase product. 38.10 wt% organic phase was recorded at 1.0 wt% catalyst loading. This value decreased to 31.2, 27.7 and 25.5 wt% at 2.0, 3.0 and 4.0 wt% catalyst loading. 18.2 wt% aqueous phase was obtained at 1.0 wt% catalyst loading, which decreased to approximately 16.0 wt% when 2.0, 3.0 and 4.0 wt% was applied. Increasing catalyst loading implied an increase in the number of acid site of the catalyst. Therefore, the trend observed in the organic phase depicts a typical characteristic of a mesoporous ZSM-5, which usually promotes selective

decarbonylation or decarboxylation reaction. This was also evidenced in the increased gas production from 38.0 to 46.0 wt%. Gradual increase in solid yield from 5.8 wt% to 11.90 wt% suggests possible polymerization of small organic molecules during reactor cooling. DOD and HHV increased significantly from 45.38-56.77 % and 40.31-42.08 MJ/kg as catalyst loading increased from 1.0 to 2.0 wt%. Subsequently, at 3.0 and 4.0 wt% catalyst loading, DOD and HHV values revolved between 59-60 % and approximately 43 MJ/kg.

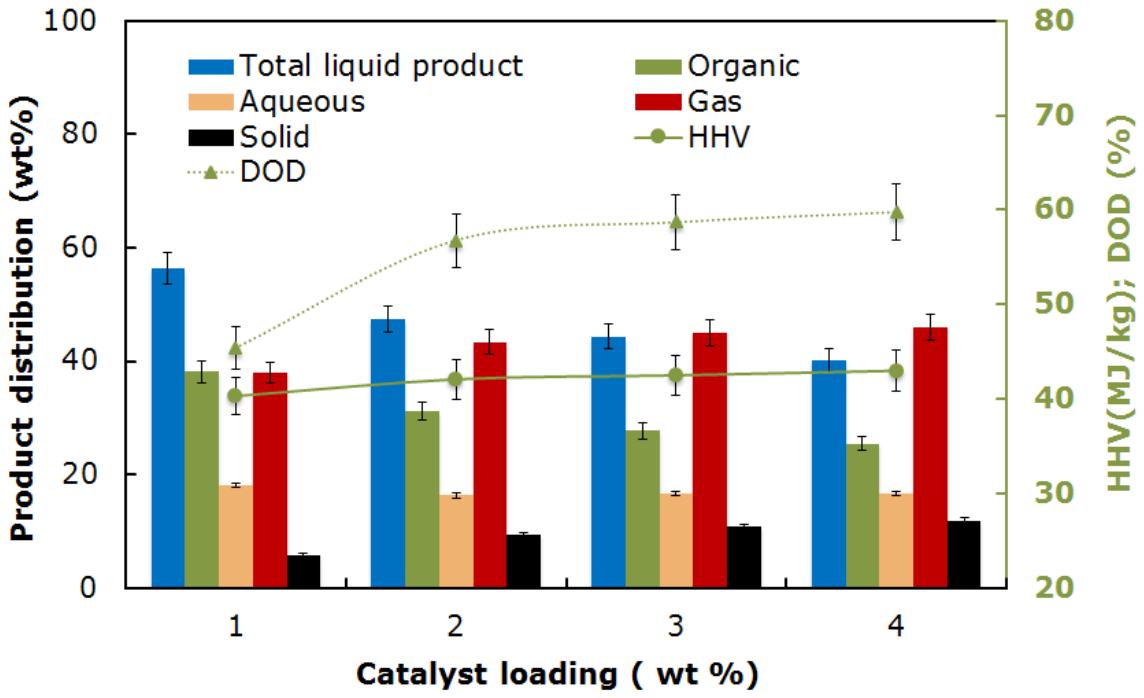

Figure 7.6: Effect of 0.3HZSM-5 catalyst loading on deoxygenation of bio-oil at 400 °C and 60 min. Feed: 30g bio-oil. Solid: char and tar. Values are the means (n =3)

Composition of organic phase collected at each catalyst loading is summarized in Table 7.5. MARHC and MPHOL were detected in organic phase produced with 1.0 wt%

catalyst loading. These oxygenated organic compounds were not identified in the upgraded oil produced with 2.0, 3.0 and 4.0 wt% catalyst. This explains the significant increase in DOD and HHV observed above as the catalyst loading increased from 1.0 to 2.0 wt%. Increasing trends in the production of HCs and ARMHCs were recorded with increased catalyst loading. Cyclo olefins (cycloheptatriene and cyclopentadiene) constituted the major HCs at 1.0 wt% catalyst loading whereas more saturated HCs such as heptanes and cyclopentanes were detected as the catalyst loading increased from 2.0 to 4.0 wt%. Similarly, benzocycloheptatriene and trimethylnaphthalene were among the ARMHCs detected at 1.0 wt% catalyst loading while the oil produced with catalyst loading between 2.0 and 4.0 wt% constituted alkyl benzenes as the major component of ARHCs. It is also interesting to note that MEST content of the upgraded bio-oil decreased with catalyst loading. At 1.0 wt% catalyst, 18.90 % MEST was recorded. This value decreased by 42-63 % when catalyst loadings between 2.0 and 4.0 wt% were applied. More than 54 % total MEST recorded at 1.0 wt% catalyst loading was C32 while the compositions of MEST obtained between 2.0 and 4.0wt% catalyst loading were C19 and below. These observations suggest that increase in catalyst loading promoted formation of small organic molecules.

Result of gas analysis (Table 7.5) showed significant changes in CO and CO_2 contents, which are indications of increased decarbonylation and decarboxylation reactions respectively. Increase in the catalyst loading from 1.0 to 2.0 wt% increased CO and CO_2 content by 28 and 31 %. This observation justifies the significant improvement in the quality of upgraded bio-oil observed under this catalyst loading. As catalyst loading increased from 2.0 to 4.0 wt%, only slight increase in CO (3-4%) content was recorded. CO_2 was between 32-33 vol %. This observation indicates that increase in

catalyst loading between 2.0 and 4.0 have similar deoxygenation activity but increased cracking of large organic molecules to short chain HCs. Similar observation has been reported by Cheng et al. (2014). The authors observed increase in alkanes and alkenes in the upgraded bio-oil with increasing ZSM-5 loading, which was attributed to selective decomposition long ester and hydrocarbon molecules, which disappeared with increasing catalyst loading.

Table 7.5: Effect of 0.3HZSM-5 catalyst loading on the organic phase and gas compositions at 400 °C and 60 min

Composition	0.3HZSM-5 loading (wt %)			
	1.00	2.00	3.00	4.00
	Organic phase (%)			
HC	1.70	3.94	6.92	7.32
ARHC	14.16	26.87	32.81	40.94
MARHC	7.90	0.00	0.00	0.00
PHOL	48.22	47.70	46.11	44.70
MPHOL	6.30	0.00	0.00	0.00
AAK	2.82	2.01	1.56	0.00
MEST	18.90	11.00	8.27	7.04
OVAC	0.00	8.48	4.33	0.00
	Gas composition (vol %)			
H_2	1.22	1.42	1.34	1.23
CH_4	10.56	12.18	12.26	12.78
CO	26.55	33.88	34.76	35.22
CO_2	24.78	32.53	32.88	31.87

(HC) hydrocarbons, (ARHC) aromatic hydrocarbons, (MARHC) methoxy aromatics, (PHOL) phenol, (MPHOL) methoxy phenol, (AAK) acids, aldehydes and ketones and (MEST) methyl ester

7.5 Effects of Reaction time on Deoxygenation of Bio-oil Over Mesoporous Zeolite

Effect of reaction time on the deoxygenation of bio-oil was evaluated between 30 and 90 min at 400 ^{o}C and 2.0 wt% 0.3HZSM-5 catalyst loading. From Figure 7.7, increasing reaction time showed a continuous decline in the organic phase while aqueous phase and gas yields increased. After 30 min, 38.8 wt% organic product was recorded, which decreased approximately by 24 % and 34 % at the end of 60 and 90 min. Whereas the aqueous phase and gas product increased from 14.8-19.9 wt% and 35.9-48.0 wt% when the reaction time varied from 30-90 min. Production of solid was found to decrease from 10.50 wt% after 30 min to 8.90 and 6.30 wt% at the end of 60 and 90 min. The trends in product distribution suggest that increase in reaction time promoted series of chemical reactions. Cracking of long chain organic molecules to small components could be responsible for the decrease in the organic phase and increased gas production, which eventually led to more aqueous phase in addition to dehydration reaction. Cheng et al. (2014) reported that increase in reaction time during upgrading of crude bio-oil over ZSM-5 produces more gas and aqueous phase at expense of upgraded organic phase. Similarly, Ahmad et al. (2016) stated that increase in reaction time during cracking of organic liquid over zeolite catalyst promotes scission of heavy molecular weight compounds to small molecules. From the physicochemical point of view, DOD and HHV (Figure 7.7) of organic phase increased considerably with reaction time. 37.82 % DOD was recorded at end of 30 min, which increased about 1.5 and 1.6 times after 60 and 90 min. HHV of 38.39 MJ/kg was obtained after 30 min but increased to 42.08 and 42.54 MJ/kg after 60 and 90 min.

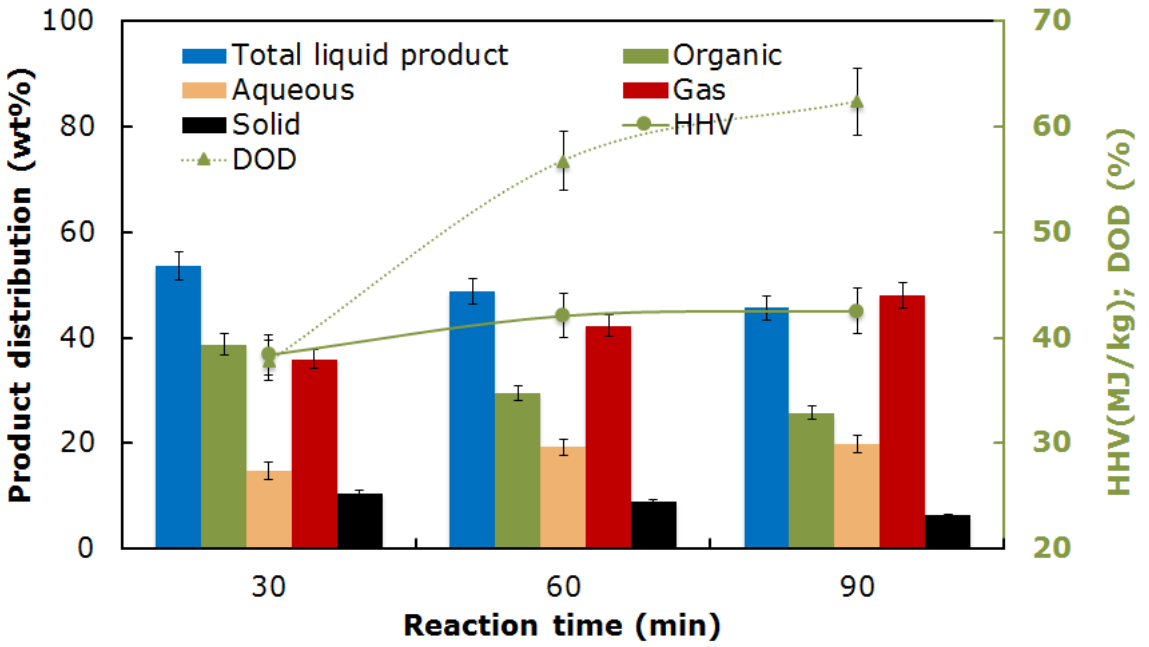

Figure 7.7: Effect reaction time on deoxygenation of bio-oil over 0.3HZSM-5 at 400 °C. Feed: 30g bio-oil. Catalyst loading: 2.0 wt%. Solid: char and tar. Values are the means (n =3)

Chemical composition of upgraded organic phase is summarized in Table 7.6. The organic phase collected after 30 min reaction time was mainly ARHCs PHOL. MARHC and MPHOL were also detected in the oil in addition to AAK, which justifies the lower DOD and HHV recorded. The oil collected after 60 and 90 min relative to 30 min reaction time had 27 and 32 % reduction in PHOL content while ARHC content approximately doubled and tripled. The phenolics recorded at end of 90 min were single alkyl phenols compared to multiple alkyl phenols detected after reaction time of 30 and 60 min. Dealkylation of multiple alkyl aromatics may have also occurred due to the presence of monoaromatics such as benzene, toluene and xylene (BTX) as the major components of the ARMHCs in the upgraded oil after 90 min. Similarly, the

amount of HCs was 2.8 and 2.3 times higher compared to the HCs recorded after 30 and 60 min. This observation can be attributed to cracking of long chain HCs.

Compositions of gas collected (Table 7.6) were mainly CO and CO_2 due to decarbonylation and decarboxylation reactions, which increased with increasing reaction time. Substantial increase in CH_4 content was also recorded with increasing reaction time. This shows that long reaction time increases generation light hydrocarbon gases.

Table 7.6: Effect reaction time on the organic phase and gas compositions at 400 °C and 2.0 wt% 0.3HZSM-5 catalyst loading

Composition	Reaction time (min)		
	30	60	90
Organic phase liquid (%)			
HC	3.31	3.94	9.15
ARHC	12.48	26.87	40.94
MARHC	6.36	0.00	0.00
PHOL	65.75	47.70	44.70
MPHOL	3.59	0.00	0.00
AAK	4.12	2.01	0.00
MEST	4.40	11.00	5.22
OVAC	0.00	8.48	0.00
Gas composition (vol %)			
H_2	1.80	1.42	2.78
CH_4	2.36	12.18	16.55
CO	23.06	36.88	39.98
CO_2	20.1	32.35	33.44

(HC) hydrocarbons, (ARHC) aromatic hydrocarbons, (MARHC) methoxy aromatics, (PHOL) phenol, (MPHOL) methoxy phenol, (AAK) acids, aldehydes and ketones and (MEST) methyl ester

7.6 Reusability of Mesoporous Zeolite

Stability of 0.3HZSM-5 in the upgrading of bio-oil was evaluated. Upgrading experiments were conducted in four consecutive cycles. After each experiment, the spent catalyst was regenerated in air at 550 °C for 6 h at 10 °C/min heating rate. A

portion of the regenerated catalyst was subsequently characterized. Catalyst loading (4.0 wt %), temperature (400 °C) and reaction time (60 min) were kept constant to ensure similar contact time. From Figure 7.8, reusability of modified 0.3HZSM-5 showed no significant impact on the total liquid, gas and solid yields but rather have considerable impact on the production of organic and aqueous phases. First cycle produced 29.5 wt% organic phase, which decreased to 25 wt% in the second cycle. The corresponding aqueous phase recorded was 10.6 wt% and 16.9 wt%. There was no significant difference between organic yield in the second and third cycles but thereafter decreased to 21.2 wt% in the fourth cycle.

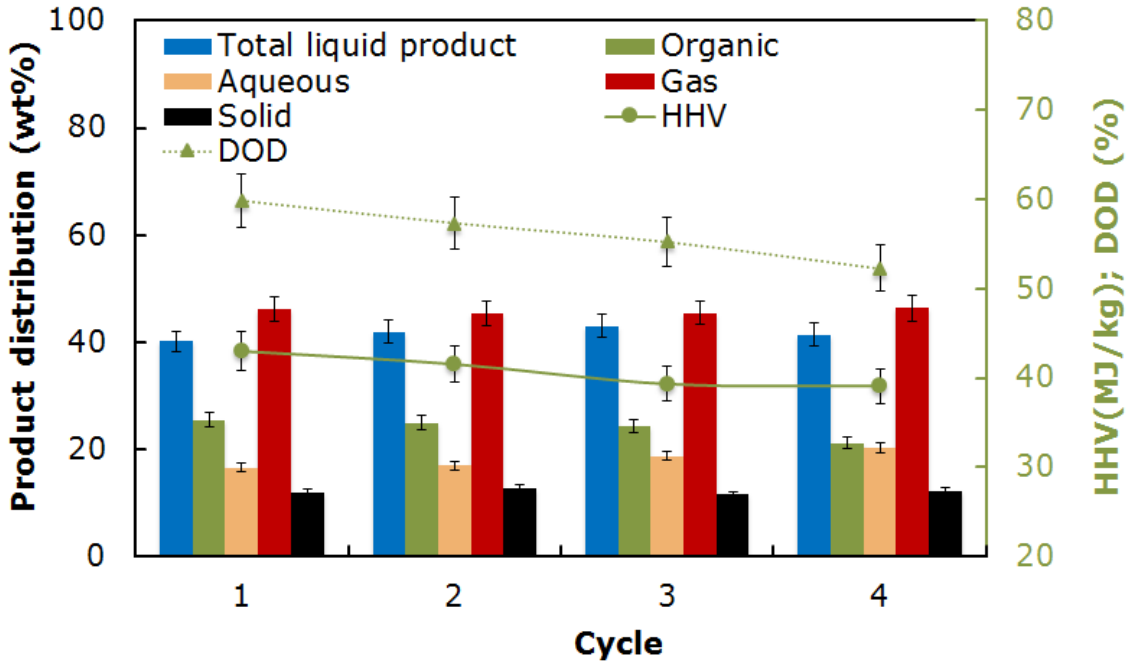

Figure 7.8: Reusability of 0.3HZSM-5 on deoxygenation of bio-oil at 400 °C and 60 min. Catalyst loading (catalyst/bio-oil): 4 wt%

Increase in the aqueous phase was recorded after each cycle. This observation suggests that regenerated catalyst promoted dehydration reaction. From the physicochemical analysis, a continuous decline in HHV and DOD were observed with catalyst in the consecutive cycles (Figure 7.8), which are indications of loss of catalytic activity probably due to chemisorption of poisons such as nitrogen or sulphur containing compounds on the active sites (Argyle and Bartholomew, 2015). Puertolas et al. (2015) reported that the ratio of organic to aqueous phase in the upgraded bio-oil over regenerated mesoporous ZSM-5 decreased and was attributed to decrease in the acid sites. Chemical composition of upgraded bio-oil and gas collected over regenerated catalyst are summarized in Table 7.7. In consistent with the physicochemical properties, significant decrease in ARMHCs was observed in the bio-oil after each cycle with corresponding increase in PHOL content. AAK and MARHC compounds were detected in the upgraded oil after the first cycle. Study by Wei et al. (2016) revealed that zeolite reusability has impact on the composition of organic phase. They reported decrease in hydrocarbon yield and production of polyaromatic hydrocarbons with reused catalyst, which was attributed to thermal polymerization of monoaromatics. In this study, polyaromatic hydrocarbons were not detected. This dissimilarity in organic product composition can be linked to the nature of zeolite catalyst used. Microporous ZSM-5 was used by the authors, which is generally prone to coke formation via polymerization of heavy molecules due its micro channels compared to mesoporous ZSM-5 employed in this study, which has improved pore characteristics that enhances mass transfer of large molecules. From the gas analysis result (Table 7.7), a decline trend in the CO contents was observed after each cycle, which is an evidence of decreased decarbonylation reaction.

Table 7.7: Organic phase and gas compositions collected at 400 °C, 60 min over regenerated 0.3HZSM-5 catalyst. Catalyst loading: 4 wt%

Composition (%)	Cycle			
	1st	2nd	3rd	4th
HC	7.32	6.46	8.59	2.50
ARHC	40.94	25.40	12.58	10.42
MARHC	0.00	2.89	10.33	12.66
PHOL	44.70	50.12	62.28	63.32
MPHOL	0.00	0.00	0.00	2.46
AAK	0.00	3.38	2.81	5.03
MEST	7.04	11.75	3.41	3.61
Gas composition (vol %)				
H_2	1.23	1.29	1.21	1.30
CH_4	12.78	12.08	12.41	12.80
CO	35.22	33.78	30.44	29.53
CO_2	31.87	30.01	30.82	28.77

HC) hydrocarbons, (ARHC) aromatic hydrocarbons, (MARHC) methoxy aromatics, (PHOL) phenol, (MPHOL) methoxy phenol, (AAK) acids, aldehydes and ketones and (MEST) methyl ester

Characteristics (BET, XRD and SEM-EDX) of fresh and regenerated catalyst are shown in Table 7.8 and Figure 7.9. From the physisorption analysis result (Table 7.8), all the properties of the regenerated catalyst decreased after four consecutive cycles except the mesopore surface area, which increased by 12 %. BET surface area decreased by 44% while micro surface area and pore volumes are approximately three-folds lower relative to the original value.

Table 7.8: Characteristic of fresh and regenerated 0.3HZSM-5 after 4 cycle. [a]Brunauer–Emmett–Teller method; [b] t-plot method; [c]$V_{meso}=V_{pore}-V_{micro}$)

Catalyst	$(S_{BET})^a$	$(S_{micro})^b$	$(S_{meso})^b$	(V_{pore})	$(V_{micro})^b$	$(V_{meso})^c$
	surface area (m^2/g)			volume (cm^3/g)		
Fresh 0.3HZSM-5	374.88	240.23	134.65	0.37	0.11	0.26
Regenerated 0.3HZSM-5	208.95	88.47	150.96	0.14	0.04	0.10

SEM-EDX images (Figure 7.9b) displayed new peak for carbon and sulphur, suggesting thermal and chemical deactivation. As earlier stated, sulphur containing compounds are among the chemical species that result in catalyst poisoning. After regeneration, the catalyst composition was similar to that of fresh catalyst (Figure 7.9c). Although the SEM image showed some disruption of original hexagonal prismatic structure in the regenerated catalyst, which is an indication of partial collapse in the catalyst morphology, but this observation could be responsible for the reduction in surface and pore characteristics recorded. Similarly, from the diffractogram (figure 7.9d), the regenerated catalyst after four consecutive cycles displayed characteristic peaks similar to that of fresh catalyst, indicating high stability. However, the intensity of the peaks in the regenerated catalyst were considerably lower than that of the fresh catalyst. This means that crystallinity of 0.3HZSM-5 decreased with reusability. The changes observed in the catalyst properties after regeneration, particularly the surface area, which is directly proportional to the number of active sites, can be attributed to the declined performance recorded after each cycle (Vitolo et al., 2001 and Puertolas et al., 2015).

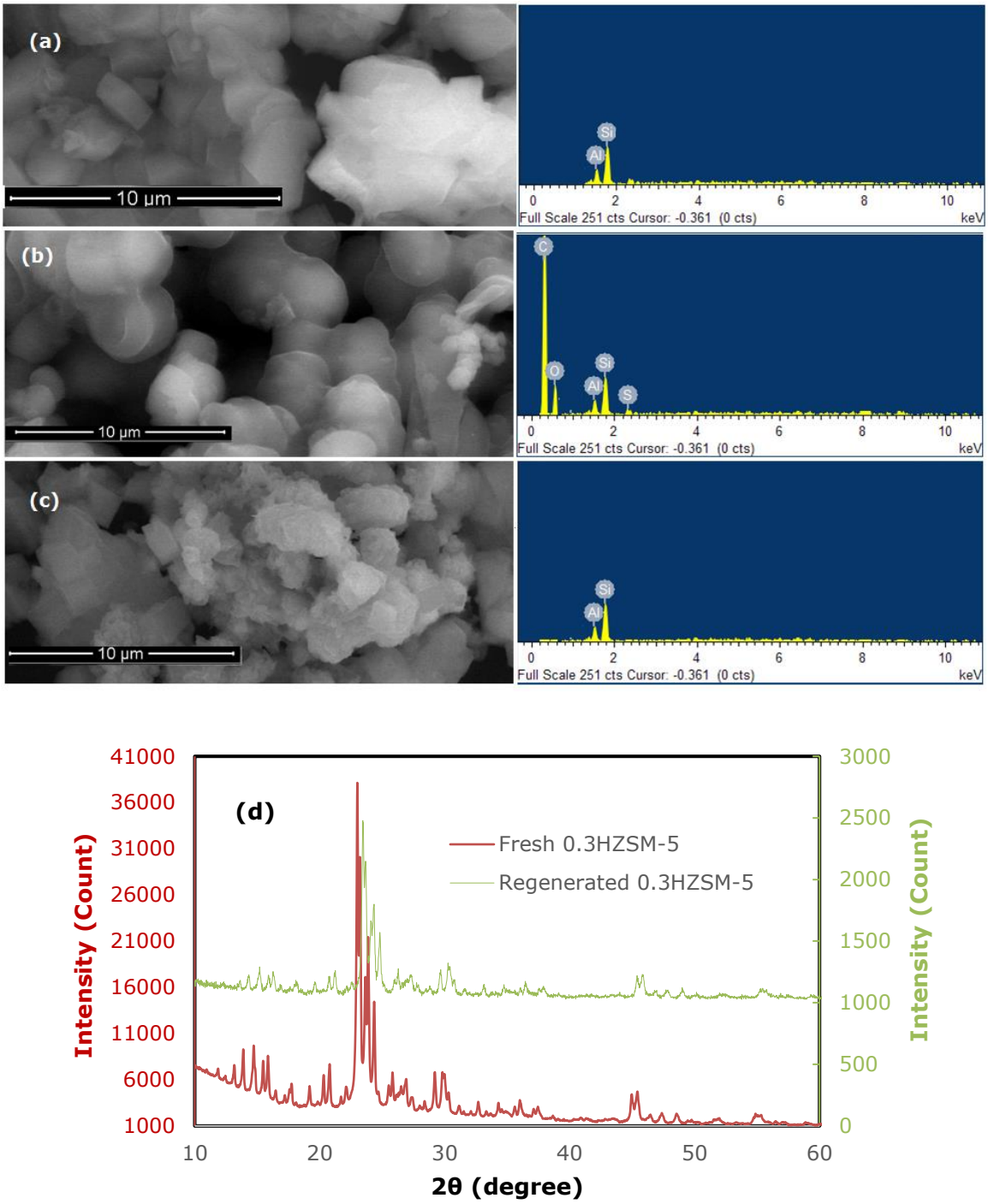

Figure 7.9: Characteristics of 0.3HZSM-5 catalyst. SEM-EDX: (a) fresh catalyst, (b) spent catalyst (c) regenerated catalyst after 4 cycle, (d) diffractogram of fresh and regenerated sample.

7.7 Optimization of Process Variables

Organic phase product has potential to be converted into different fuel fractions and therefore, it is important to evaluate interaction between the catalyst loading and reaction time for optimum yield. Response surface methodology with central composite design was used and range of independent variables and experimental levels are summarized in Table 7.9. Experiments were conducted accordingly at 400 °C and the response is presented in Table 7.10.

Table 7.9: Range of independent variables and experimental levels

	Experimental levels		
Variables	**-1**	**0**	**+1**
Catalyst loading (wt%): A	1	2.5	4
Reaction time (min): B	30	60	90

Table 7.10: Central composite experimental design matrix and response

Runs	**Coded level factors**		**Response**
	A (wt %)	B (min)	Organic phase (wt %)
1	0	0	28.17
2	-1	0	38.12
3	1	1	26.06
4	-1	-1	44.98
5	-1	1	33.28
6	0	-1	36.76
7	0	0	29.67
8	0	0	30.30
9	0	1	26.30
10	0	0	30.45
11	1	0	30.47
12	1	-1	38.27
13	0	0	30.67

Response is the average values (n=2)

Response was fitted to a second-degree polynomial as shown in equation 6.1 and analysis of variance (ANOVA) was performed (Table 7.11).

$$Y_{organic} = 30.07 - 3.60A - 5.73B + 4.18A^2 + 1.42B^2 - 0.13AB \qquad (6.1)$$

Table 7.11: ANOVA test for response model and respective model term

Source	Sum of Squares	DF	Mean Square	F-value	Prob > F
Model	352.16	5	70.43	202.23	< 0.0001
A	77.62	1	77.62	222.86	< 0.0001
B	196.88	1	196.88	565.30	< 0.0001
A^2	48.31	1	48.31	138.72	< 0.0001
B^2	5.55	1	5.55	15.93	0.0052
AB	0.07	1	0.07	0.19	0.6787
Residual	2.44	7	0.35		
Lack of Fit	0.91	3	0.30	0.80	0.5562
Pure Error	1.53	4	0.38		
Cor Total	354.60	12			
Std. Dev.	0.59		R-Squared	0.9931	
Mean	32.65		Adj R-Squared	0.9882	
C.V.	1.81		Pred R-Squared	0.9676	
PRESS	11.48		Adeq Precision	47.6599	

The R^2 and adjusted R^2 values (Table 7.11) for the model are high enough and comparable, which indicates that the selected quadratic response surface model for the organic phase product suitably describe the experimental data within the selected operating conditions. The predicted R^2 value is in good agreement with the adjusted R^2 values. Adequate precision (Adeq Precision) is a measure of signal to noise ratio and a ratio greater than 4 is desirable. In this case, the value of Adeq precision is 47.6599, which shows adequate signal and the models can be used to navigate the design space. Adequacy of the quadratic model in fitting the experimental data was further evaluated. From the plot of normal % probability versus studentized (Figure

7.10a), the points are distributed approximately on a straight line along the diagonal, which illustrates that the error terms are normally distributed and independent of each. Outlier T versus a number of runs (Figure 7.10b) shows that the points are randomly distributed around zero on the outlier T axis and between +3.5 and -3.5. Consequently, it can be concluded that the model is suitable and successfully establish the relationship between the catalyst loading and reaction time studied and the organic phase product.

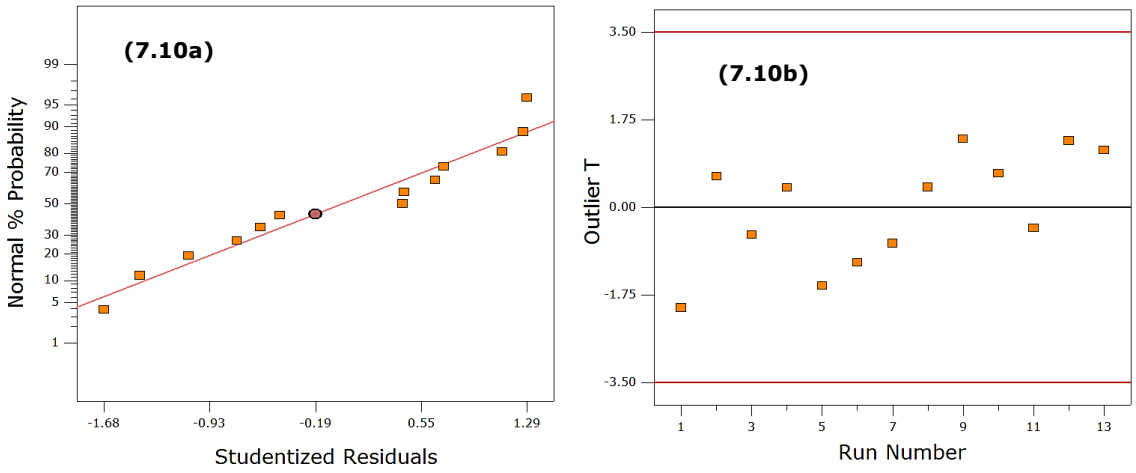

Figure 7.10: Diagnostics of models (a) Normal % probability versus studentized residuals (b) Outliers T versus run number

Interaction and 3D surface plots (Figure 7.11) show the combined effect of catalyst loading and reaction time on the yield of organic product. Comparing the response trend with respect to reaction time, it is clear that at any catalyst loading, production of more organic phase is achieved at 30 min relative to 90 min reaction time during catalytic upgrading of bio-oil over mesoporous 0.3HZSM-5 at 400 °C. This may be at the expense of degree of deoxygenation as earlier observed. Similarly, increase in

catalyst loading at both reaction time (30 and 90 min) reduced the yield of organic phase due to increased number of active sites, which propagates more deoxygenation reactions.

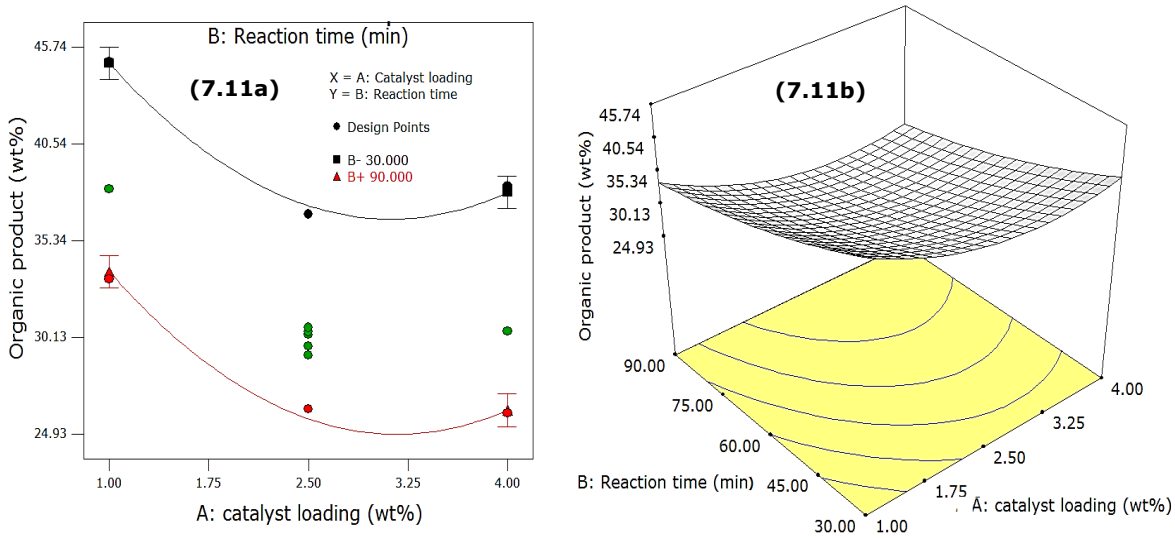

Figure 7.11: Interaction graph (a) and surface response plot (b) for the combined effects of catalyst loading and reaction time on the yield of organic product

To maximize the yield of organic product, catalyst loading and reaction time were optimized. Optimization conditions are summarized in Table 7.12. Catalyst loading within 1-4 wt% and minimum reaction time were used as constraints. Four solutions was generated by the software (Table 7.12) and based on the characteristics of organic phase analysed previously, solution number four (4) was selected. This implies that catalyst loading of approximately 3.0 wt% and reaction time of 30 min is sufficient to produce optimum organic liquid of 36.62 wt%. The result was validated by performing other repeated experiments using the optimized condition and the responses are displayed in Table 7.13. Average value of organic product collected (31.69 wt %) was lower than the predicted yield. However, the standard deviation between the two

values is approximately within 3%. Therefore, the quadratic equation adequately modelled the organic phase yield from catalytic upgrading of bio-oil over mesoporous 0.3HZSM-5.

Table 7.12: Optimization conditions and predicted solutions

Constraints	Goal	lower Limit	Upper Limit	Importance
Catalyst loading	is in range	1	4	3
Reaction time	minimize	30	90	3
Organic	maximize	26.06	44.98	5
		Solutions		
Number	Catalyst loading (wt %)	Reaction time (min)	Organic product (wt %)	Desirability
1	1.00	30.00	44.87	1.0
2	1.15	30.00	43.73	1.0
3	3.99	30.00	37.88	0.7
4	**2.87**	**30.00**	**36.62**	**0.7**

Table 7.13: Organic product yield predicated at optimized condition and experimental value

Run	Catalyst loading (wt %)	Reaction time (min)	Organic product (wt %)	
			Experimental	Predicted
1	3.0	30	33.09	36.62
2	3.0	30	30.26	36.62
3	3.0	30	31.71	36.62
Average			**31.69**	**36.62**

7.8 Fractional Distillation of Organic Liquid

Organic liquid produced at optimized condition over mesoporous 0.3HZSM-5 was fractionated into light, middle and heavy fractions at temperature from ambient -100 ^{o}C, 100-200 ^{o}C and above 200 ^{o}C respectively. Approximately 30.0 g of organic liquid was used as feed for the distillation and fractions collected are shown in Figure 7.12.

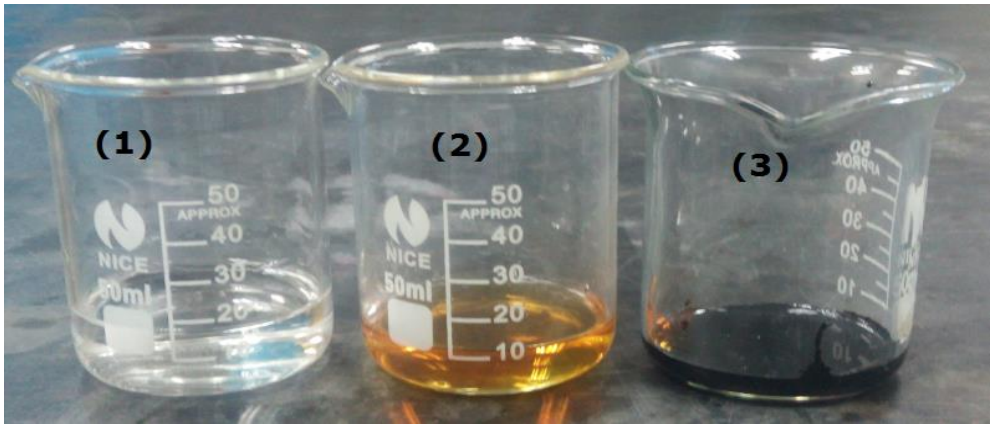

Figure 7.12: Distillates from organic liquid. (1) Light fraction, (2) middle fraction (3) heavy bottom

About 50 wt% of the organic liquid can be converted to middle distillate while an average of 37.60 wt% is transformed to light fraction (Table 7.14). Distribution of the fractions collected is synonymous to the result of simulated distillation of organic liquid produced over the mesoporous 0.3HZSM-5 in section 7.2.2. Evaporation characteristics of the distillates were compared with that of commercial fossil kerosene and premium motor spirit (PMS). 50 wt% of the light fraction and PMS evaporated at the same temperature, 56 ^{o}C (Figure 7.13). 90 wt% weight loss of light fraction occurred at 68 ^{o}C compared to PMS with 90 wt% evaporation at 94 ^{o}C. Final evaporation temperature of the light fraction was 72 ^{o}C relative to 126 ^{o}C recorded for the PMS. This observation shows that light fraction constitutes about 50 % components with boiling characteristic similar to that of PMS. On the other hand, the middle distillate consists of lower boiling fractions compared to kerosene. 50 wt%, 90 wt% and final evaporation of middle distillate was 73, 95 and 100 ^{o}C receptively relative to 130, 163 and 185 ^{o}C recorded for kerosene.

Table 7.14: Yield of light, middle and heavy bottom from fractional distillation of organic liquid. Feed: 30.0 g of organic liquid produced at 3.0 wt% 0.3HZSM-5, 400 °C and 30 min reaction time

Run	light fraction		middle fraction		heavy bottom		loss
	(g)	(wt %)	(g)	(wt %)	(g)	(wt %)	(wt %)
1	11.28	37.60	14.54	48.47	2.09	6.97	6.97
2	11.92	39.73	14.15	47.17	1.84	6.13	6.97
3	10.86	36.20	14.96	49.87	2.23	7.43	6.50
4	11.06	36.87	13.98	46.60	2.17	7.23	9.30
Average	**11.28**	**37.60**	**14.41**	**48.03**	**2.08**	**6.94**	**7.43**
SD	**-**	**1.53**	**-**	**1.46**	**-**	**0.57**	**-**

SD: Standard deviation

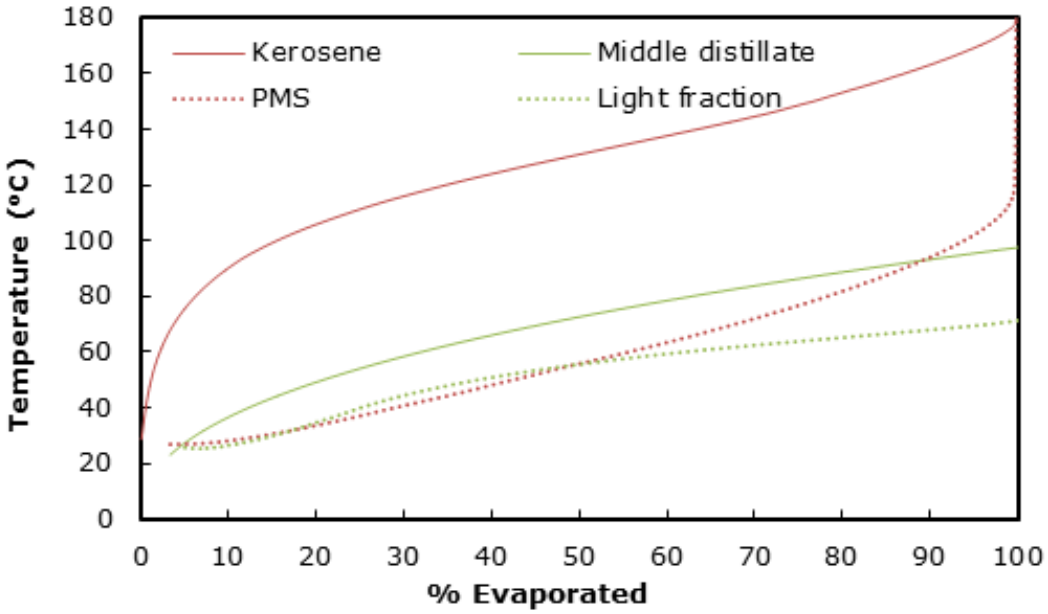

Figure 7.13: Thermogravimetric evaporation profile of distillates from organic liquid and fossil kerosene and PMS under nitrogen atmosphere (20mL/min) at 10 °C/min.

Figure 7.14 gives group of compounds identified in each fraction. Distribution of chemical compound in the light fraction is similar to that of PMS. In both cases, HCs

constituted the largest fractions. ARHCs content of light fraction was three folds higher compared to PMS. MEST and other compounds such as 1,5-Cyclooctanediol diacetate and 4-(Aminomethyl) pyridine, Pyridine, 5-ethenyl-2-methyl-, 2,4-Bis(diazo) were detected in the PMS, which are fuel additives (ATC, 2013). Therefore, the light fraction collected can be used as bio-gasoline or formulated with additives to have comparable characteristics with PMS. Composition of HC and ARHC in middle distillate was 31 and 47 % lower while MEST was approximately two-fold higher relative to fossil kerosene. This fraction can be applied as cooking fuel, particularly in rural areas where access to fossil kerosene is a serious challenge. Heavy bottom constituted mainly PHOL and MEST, which is a good feedstock for biomaterial processing.

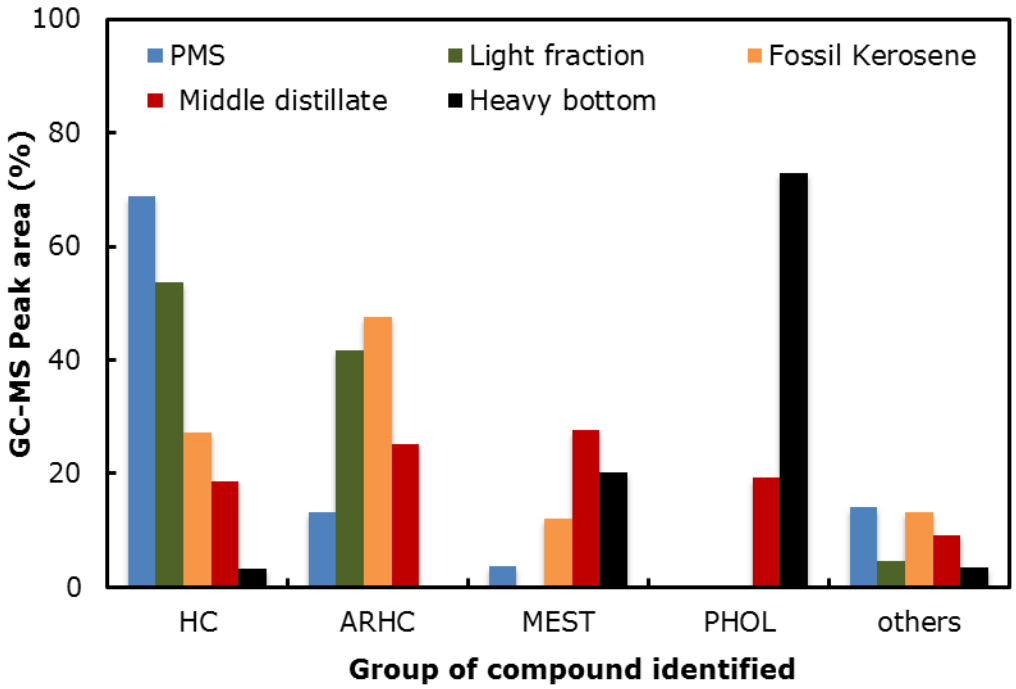

Figure 7.14: Group of compounds in the distillates identified by GC-MS. (HC) hydrocarbons, (ARHC) aromatic hydrocarbons, (PHOL) phenol, (MEST) methyl ester and others

7.9 Conclusion

Ex-situ upgrading of bio-oil derived from Napier grass over microporous zeolite (ZSM-5) and hierarchical mesoporous zeolite (0.2HZSM-5 and 0.3HZSM-5) was carried out in a high pressure reactor. Upgrading over microporous ZSM-5 produced more solid and aqueous phase liquid while 0.2HZSM-5 and 0.3HZSM-5 favoured production of organic phase liquid with higher degree of deoxygenation. GC-MS analysis of organic phase collected revealed high transformation of methoxyphenol and methoxyaromatics in the feed bio-oil. Microporous ZSM-5 produced cyclic olefins and polyaromatic hydrocarbons compared to 0.2HZSM-5 and 0.3HZSM-5, which were selective toward cycloalkanes and alkyl monoaromatcs. Result of gas analysis showed that hierarchical mesoporous zeolite favoured decarboxylation and decarbonylation reactions relative to ZSM-5, which promoted dehydration reaction. 0.3HZSM-5 was found to be the best-performing catalyst and its reusability was tested over four consecutive cycles. Composition of aromatic hydrocarbon in the oil collected over regenerated catalyst decreased while increase in phenol content was recorded relative to the oil composition from the fresh catalyst. Degree of deoxygenation and higher heating value were found to decrease after each cycle, which are attributed to the loss catalyst active sites. Effects of process variable such temperature (375 ^{o}C, 400 ^{o}C, 425 ^{o}C), catalyst loading (1.0-4.0 wt %) and reaction time (30, 60 and 90 min) on bio-oil upgrading over fresh 0.3HZSM-5 was evaluated. Increasing reaction time, temperature and catalyst loading produced high quality organic phase at the expense of yield. Catalyst loading and reaction time were further optimized at 400 ^{o}C and optimum organic liquid yield was recorded at 30 min and 3.0 wt% 0.3HZSM-5 loading. Organic phase collected at optimized condition was fractionated into high grade bio-

fuel. This study showed that bio-oil derived from Napier grass can be transformed to that high-grade bio-oil via catalytic upgrading over hierarchical mesoporous ZSM-5.

CHAPTER EIGHT

8. CONCLUSIONS AND RECOMMENDATION FOR FUTURE STUDIES

8.1 Summary

To date, production of bio-oil from Napier grass via pyrolysis is limited to very few classical studies. This thesis articulates valorisation of Napier grass via pyrolysis into high energy precursors. It investigates impact of aqueous pre-treatment of Napier grass on bio-oil quality and subsequent evaluates conversion of bio-oil derived from the Napier grass into high-grade biofuel through in-situ non-catalytic and in-situ catalytic upgrading, and ex-situ catalytic upgrading. From the experimental results and interpretation of analysed data as discussed, some conclusions can be made together with future recommendations.

8.2 Research Conclusions

In conclusion, the key findings of this research work are summarized as follows:

- Comprehensive characterization of Napier grass for thermochemical conversion was successfully carried out. Up to 51 wt% bio-oil can be produced from Napier grass in a fixed bed reactor at 600 ^{o}C, 5 L/min N_2 flow rate and 50 ^{o}C/min. This value is relatively higher than the bio-oil yield from Napier grass reported in the literature, which are produced even at higher temperature (700-900 ^{o}C). Bio-char (20 wt%) derived from Napier grass was a dry porous material rich in minerals suitable for carbon sequestration, energy and agricultural applications. The non-condensable gas (29 wt%) from Napier grass has high hydrogen/carbon monoxide ratio suitable for liquid fuel production via Fischer-Tropsch (FT) synthesis.
- Aqueous pre-treatment of Napier grass biomass prior to pyrolysis was successfully carried out using deionized water, sodium hydroxide and sulfuric acid as solvents. Bio-oil yield from samples pre-treated with deionized water

and sulphuric acid increased by 3.2 and 20.0 % respectively while about 9.3 % reduction in oil yield was recorded from sample pre-treated with sodium hydroxide. All the pre-treatment methods did not show significant reduction in oxygen content of the resulting bio-oil. However, between 71 and 85 % reduction in the organic acid and ketone content was achieved in the bio-oil produced from the pre-treated samples.

- In-situ catalytic and non-catalytic upgrading of bio-oil from Napier grass was successfully carried out. In-situ upgrading over microporous zeolite decreased oil yield and promoted production of olefins and polyaromatic hydrocarbons while the mesoporous zeolites produced about 54 % more oil yield, favoured production of alkanes and monoaromatic hydrocarbons compared to the microporous zeolite. On the other hand, in-situ non-catalytic upgrading revealed that co-pyrolysis of Napier grass with calcium reach feedstock favoured production of normal phenol and methyl esters without significant reduction in the organic phase yield. The oil from co-pyrolysis showed a superior quality compared to the raw bio-oil from pure Napier grass and can be transformed into fuel, valuable chemicals and other consumer products.
- Ex-situ upgrading of Napier grass bio-oil was successfully carried out in a high pressure reactor. The upgraded bio-oil over mesoporous zeolite can be converted to about 37.60 wt% light fraction and 48.03 wt% middle distillate with chemical composition comparable to fossil premium motor spirit and kerosene respectively.

The findings suggest that valorisation of Napier grass to bio-oil and subsequent upgrading in to high-grade biofuel has been achieved. The results from this research

contributes to the body of knowledge for biofuel development from lignocellulosic biomass via pyrolysis and catalytic upgrading.

8.3 Recommendations for Future Work

Pyrolysis of Napier grass to bio-oil and subsequent upgrading to high-grade fuel presents a high prospect for bio-gasoline and bio-kerosene production. The pyrolysis and upgrading system used in this research was a fixed bed reactor and high pressure batch reactor, the following recommendations can be considered as a way forward for further research.

- Production of bio-oil from Napier grass should be carried out in a continuous pyrolysis system and optimization of process variables.
- Upgrading study should be carried out in a continuous catalytic system.
- Techno-economic study of bio-gasoline and bio-kerosene production from Napier grass through a continuous pyrolysis and catalytic upgrading system should be carried out.
- Testing of bio-gasoline should be carried out in internal combustion engines and compare its performance with fossil gasoline.
- Extraction of valuable chemicals from aqueous phase bio-oil derived from Napier grass through catalytic upgrading or reduced pressure distillation should be carried out to increase valorisation of Napier grass.

REFERENCES

Abnisa, F., Daud, W. M. A. W. (2014) "A review on co-pyrolysis of biomass: An optional technique to obtain a high-grade pyrolysis oil" Energy Conversion and Management 87, 71-85

Adrados, A., DeMarco, I., Lopez-Urionabarrenechea, A., Solar, J., Caballero, B. (2015) "Avoiding tar formation in biocoke production from waste biomass" Biomass and Bioenergy 74, 172-179

Agbor, V.B., Cicek, N., Sparling, R., Berlin, A., Levin, D.B. (2011) "Biomass pretreatment: Fundamentals toward application" Biotechnology Advances 29, 675–685

Ahmadi, A., Yuan, Z., Rohani, S., Xu, C. (2016) "Effects of nano-structured CoMo catalysts on hydrodeoxygenation of fast pyrolysis oil in supercritical ethanol" Catalysis Today 269, 182-194

Aho, A., Käldström, M., Fardim, P., Kumar, N., Eränen, K., Salmi, T., Holmbon, B., Hupa, M. and Murzin, D.Y., (2010) "Catalytic deoxygenation of cellulose pyrolysis vapours over mesoporous materials. Cellul. Chem. Technol 44, 89-96.

American Coal Council (2014). "Biomass Co-firing with Coal as an Emissions Reduction Strategy" http://www.americancoalcouncil.org/?page=biomass. Accessed 2 June 2015

Amutio, M., Lopez, G., Alvarez, J, Moreira, R., Duarte, G., Nunes, J., Olazar, M., Bilbao, J. (2013)" Flash pyrolysis of forestry residues from the Portuguese Central Inland Region within the framework of the BioREFINA-Ter project" Bioresource Technology 129, 512–518

Anca-Couce, A. (2016) "Reaction mechanisms and multi-scale modelling of lignocellulosic biomass pyrolysis" Progress in Energy and Combustion Science 53, 41-79

Anex, R. P., Aden, A., Kazi, F. K., Fortman, J., Swanson, R. M., Wright, M. M., Satrio, J.A., Brown, R.C., Daugaard, D.E., Platon, A., Kothandaraman, G., Hsu, D.D., Dutta, A. (2010) "Techno-economic comparison of biomass-to-transportation fuels via pyrolysis, gasification, and biochemical pathways" Fuel 89, S29–S35

Argyle, M.D., Bartholomew, C.H. (2015) "Heterogeneous Catalyst Deactivation and Regeneration: A Review" Catalysts 5,145-269

Asadieraghi, M., Wan Daud, W.M.A. (2014) "Characterization of lignocellulosic biomass thermal degradation and physiochemical structure: Effects of demineralization by diverse acid solutions" Energy Conversion and Management 82, 71–82

Asadullah, M. (2014) "Barriers of commercial power generation using biomass gasification gas: A review" Renewable and Sustainable Energy Reviews 29, 201–215

Baeyens, J., Kang, Q., Appels, L., Dewil, R., Lv, Y., Tan, T. (2015) "Challenges and opportunities in improving the production of bio-ethanol" Progress in Energy and Combustion Science 47, 60-88

Balat, M. (2011) "Production of bioethanol from lignocellulosic materials via the biochemical pathway: A review. Energy Convers Manage 52, 858–875.

Beauchet, R., Monteil-River, F., Lavoie, J.M. (2012) "Conversion of lignin to aromatic-based chemicals (L-chems) and biofuels (L-fuels)" Bioresource Technology 121, 328–334

Beletskaya, I.P., Tarasenko, E.A., Khokhlov, A.R., Tyurin, V.S. (2010) "Poly (N-vinylimidazole) as an efficient and recyclable catalyst of the Aza-Michael reaction in water" Russian Journal of Organic Chemistry 46(4), 461-467.

Bertero, M., Puente, G., Sedran, U. (2012) "Fuels from bio-oils: Bio-oil production from different residual sources, characterization and thermal conditioning" Fuel 95, 263–271

Bertero, M., Puente, G., Sedran, U. (2012) "Fuels from bio-oils: Bio-oil production from different residual sources, characterization and thermal conditioning" Fuel 95, 263–271.

Biopower Factsheet (2000). "Biomass Cofiring: A Renewable Alternative for Utilities" National Renewable Laboratory at: http://www.nrel.gov/docs/fy00osti/28009.pdf . Accessed: 2nd June, 2015

Biswas, A.K., Umeki, K., Yang, W., Blasiak, W. (2011) "Change of pyrolysis characteristics and structure of woody biomass due to steam explosion pretreatment" Fuel Processing Technology 92, 1849–1854

Bordoloi, N., Narzari, R., Chutia, R.S., Bhaskar, T., Kataki, R. (2015) "Pyrolysis of Mesua ferrea and Pongamia glabra seed cover: Characterization of bio-oil and its sub-fractions" Bioresource Technology 178, 83–89

Botas, J., Serrano, D.P., García, A., Ramos, R. (2014) "Catalytic conversion of rapeseed oil for the production of raw chemicals, fuels and carbon nanotubes

over Ni-modified nanocrystalline and hierarchical ZSM-5" Applied Catalysis B 145, 205–215

Braga, R. M., Melo, D. M. A., Aquino, F. M., Freitas, J. C. O., Melo, M. A. F., Barros, J. M. F., Fontes, M. S. B. (2014) "Characterization and comparative study of pyrolysis kinetics of the rice husk and the elephant grass" Journal of Thermal Analysis and Calorimetry 115 (2), 1915 - 1920.

Braga, R.M., Melo, D.M., Sobrinho, E.V., Barros, J.M., Melo, M.A., Carvalho, A.F., Maria do Socorro, B.F. and Freitas, J.C., (2016) "Catalytic upgrading of Elephant grass (Pennisetum purpureum Schum) pyrolysis vapor using WO3 supported on RHA and RHA-MCM-41" Catalysis Today, in press http://dx.doi.org/10.1016/j.cattod.2016.06.003

Bridgwater, A.V. (2012) "Review of Fast Pyrolysis of biomass and product upgrading" Biomass Bioenergy 38, 68–94.

Brinchi, L., Cotana, F., Fortunati, E., Kenny, J.M. (2013) "Production of nanocrystalline cellulose from lignocellulosic biomass: Technology and applications. Review" Carbohydrate Polymers 94, 154– 169

Burhenne, L., Messmer, J., Aicher, T., Laborie, M-P. (2013) "The effect of the biomass components lignin, cellulose and hemicellulose on TGA and fixed bed pyrolysis" Journal of Analytical and Applied Pyrolysis 101, 177–184

Cadoux, S., Riche, A.B., Yates, N. E., Machet, J-M. (2012) "Nutrient requirements of Miscanthus x giganteus: Conclusions from a review of published studies" Biomass and Bioenergy 38, 14-22

Cai, Y., Fan, Y., Li, X., Chen, L., Wang, J. (2016) "Preparation of refined bio-oil by catalytic transformation of vapors derived from vacuum pyrolysis of rape straw over modified HZSM-5" Energy 102, 95-105

Candelier, K., Chaouch, M., Dumarçay, S., Pétrissans, A., Pétrissans, M., Gérardin, P. (2011) "Utilization of thermodesorption coupled to GC–MS to study stability of different wood species to thermodegradation" Journal of Analytical and Applied Pyrolysis 92, 376–383

Caputo, A. (2014) "Trends in European bioenergy law: problems, perspectives and risks" Journal of Culture, Politics and Innovation 1-2, DOI: 10.12893/gjcpi.2014.1-2.10

Carpenter, D., Westover, T.L., Czernik, S., Jablonski, W. (2014) "Biomass feedstocks for renewable fuel production: a review of the impacts of feedstock and

pretreatment on the yield and product distribution of fast pyrolysis bio-oils and vapors" Green Chemistry 16, 384–406

Carraretto, C., Macor, A., Mirandola, A., Stoppato, A., Tonon, S., (2004) Biodiesel as alternative fuel: experimental analysis and energetic evaluations. Energy 29, 2195–2211.

Chadwick, D.T., McDonnell, K.P., Brennan, L.P., Fagan, C.C., Everard, C.D. (2014) "Evaluation of infrared techniques for the assessment of biomass and biofuel quality parameters and conversion technology processes: A review" Renewable and Sustainable Energy Reviews 30, 672–681

Chaiwat, W., Gunawan, R., Gholizadeh, M., Li, X., Lievens, C., Hu, X., Wang, Y., Mourant, D., Rossiter, A., Bromly, J., Li, C-Z. (2013) "Upgrading of bio-oil into advanced biofuels and chemicals. Part II. Importance of holdup of heavy species during the hydrotreatment of bio-oil in a continuous packed-bed catalytic reactor" Fuel 112, 302–310.

Chan, W.R., Kelbon, M., Krieger, B.B., (1985) "Modelling and experimental verification of physical and chemical processes during pyrolysis of large biomass particle" Fuel 64, 1505–1513

Chen, D., Li, Y., Cen, K., Luo, M., Li, H. and Lu, B. (2016) "Pyrolysis polygeneration of poplar wood: Effect of heating rate and pyrolysis temperature" Bioresource Technology 218, 780-788.

Chen, W., Shi, S., Zhang, J., Chen, M., Zhou, X. (2016) "Co-pyrolysis of waste newspaper with high-density polyethylene: Synergistic effect and oil characterization" Energy Conversion and Management 112, 41-48

Chen, W-H., Liu, S-H., Juang, T-T., Tsai, C-M., Zhuang, Y-Q. (2015) "Characterization of solid and liquid products from bamboo torrefaction" Applied Energy 160 (15), 829-835

Cheng, D., Wang, L.J., Shahbazi, A., Xiu, S., Zhang, B. (2014) "Catalytic cracking of crude bio-oil from glycerol-assisted liquefaction of swine manure" Energy Conversion and Management 87, 378-384.

Cherubini, F. (2010) "The biorefinery concept: using biomass instead of oil for producing energy and chemicals" Energy Conversion and Management 51, 1412–21.

Collard, F.X., Blin, J. (2014) "A review on pyrolysis of biomass constituents: Mechanisms and composition of the products obtained from the conversion of

cellulose, hemicelluloses and lignin" Renewable and Sustainable Energy Reviews 38, 594–608

Corton, J., Donnison, I. S., Patel, M., Bühle, L., Hodgson, E., Wachendorf, M., Bridgwater, A., Allison, G., Fraser, M. D. (2016) "Expanding the biomass resource: sustainable oil production via fast pyrolysis of low input high diversity biomass and the potential integration of thermochemical and biological conversion routes" Applied Energy 177, 852-862.

Cuvilas, C.A., Yang, W. (2012) "Spruce Pretreatment for Thermal Application: Water, Alkaline, and Diluted Acid Hydrolysis" Energy and Fuel 26, 6426−6431

Damartzis, T., Zabaniotou, A. (2011) "Thermochemical conversion of biomass to second generation biofuels through integrated process design—A review" Renewable and Sustainable Energy Reviews 15, 366–378

Das, S., Bhattacharya, A., Haldar, S., Ganguly, A., Gu, S., Ting, Y.P., Chatterjee, P.K. (2015) "Optimization of enzymatic saccharification of water hyacinth biomass for bio-ethanol: Comparison between artificial neural network and response surface methodology" Sustainable Materials and Technologies 3, 17-28.

De Conto, D., Silvestre, W.P., Baldasso, C., Godinho, M. (2016) "Performance of Rotary Kiln Reactor for the Elephant Grass Pyrolysis. Bioresource Technology 218, 153-160

Demirbas, A. (2011) "Competitive liquid biofuels from biomass" Applied Energy 88, 17–28

Deng, L., Zhang, T., Che, D. (2013) "Effect of water washing on fuel properties, pyrolysis and combustion characteristics, and ash fusibility of biomass" Fuel Processing Technology 106, 712–720

Deshmukh, Y., Yadav, V., Nigam, N., Yadav, A., Khare, P. (2015) "Quality of bio-oil by pyrolysis of distilled spent of Cymbopogon flexuosus" Journal of Analytical and Applied Pyrolysis 115, 43-50

Di Blasi C. (2008) "Modeling chemical and physical processes of wood and biomass pyrolysis. Progress in Energy and Combustion Science 34, 47–90

Di Blasi C. (2002) "Modeling intra- and extra-particle processes of wood fast pyrolysis" AIChE Journal 48 (10), 2386–2397.

Di Blasi, C., Branca, C. (2001) "Kinetics of primary product formation from wood pyrolysis" Industrial and Engineering Chemistry Research 40, 5547–5556.

Di-Blasi, C. (2008) "Modeling chemical and physical processes of wood and biomass pyrolysis" Progress in Energy and Combustion Science 34(1), 47-90

Doherty, W.O., Mousavioun, P., Fellows, C.M. (2011) "Value-adding to cellulosic ethanol: lignin polymers" Ind. Crop. Prod 33, 259–276.

Du, S., Sun, Y., Gamliel, D.P., Valla, J.A., Bollas, G.M. (2014) "Catalytic pyrolysis of miscanthus × giganteus in a spouted bed reactor" Bioresource Technology 169, 188–197

Duan, C., Zhang, X., Zhou, R., Hua, Y., Zhang, L., Chen, J. (2013) "Comparative studies of ethanol to propylene over HZSM-5/SAPO-34 catalysts prepared by hydrothermal synthesis and physical mixture" Fuel Processing Technology 108, 31–40

Duku, M. H., Gu, S., Hagan, E. B. (2011) "A comprehensive review of biomass resources and biofuels potential in Ghana" Renewable and Sustainable Energy Reviews 15, 404–415

Elliott, D.C., Biller, P., Ross, A.B., Schmidt, A.J., Jones, S.B. (2015) "Hydrothermal liquefaction of biomass: Developments from batch to continuous process" Bioresource Technology 178, 147-156

Elordi, G., Olazar, M., Lopez, G., Castaño, P., Bilbao, J. (2011) "Role of pore structure in the deactivation of zeolites (HZSM-5, Hb and HY) by coke in the pyrolysis of polyethylene in a conical spouted bed reactor" Applied Catalysis B: Environmental 102, 224–231.

Eom, I.Y., Kim, J.Y., Lee, S.M., Cho, T.S., Yeo, H., Choi, J.W. (2012) "Comparison of pyrolytic products produced from inorganic-rich and demineralized rice straw (Oryzasativa L.) by fluidized bed pyrolyzer for future biorefinery approach" Bioresource Technology 128, 664–672

Eom, I-Y., Kim, K-H., Kim, J-Y., Lee, S-M., Yeo, H-M., Choi, I-G., Choi, J-W. (2011) "Characterization of primary thermal degradation features of lignocellulosic biomass after removal of inorganic metals by diverse solvents" Bioresource Technology 102 (3), 3437-3444

Flores, R. A., Urquiaga, S., Alves, B.J.R., Collier, L.S., Boddey, R. M. (2012) "Yield and quality of elephant grass biomass produced in the cerrados region for bioenergy" Engenharia Agrícola 32(5), 831-839.

Floudas, C. A., Elia, J. A., Baliban, R. C. (2012) "Hybrid and single feedstock energy processes for liquid transportation fuels: A critical review" Computers and Chemical Engineering 41, 24– 51

Font, R., Marcilla, A., Verdu, E., Devesa, J., (1990) "Kinetics of the Pyrolysis of Almond Shells and Almond Shells Impregnated with CoC12 in a Fluidized Bed Reactor and in a Pyroprobe 100. Industrial and Engineering Chemistry Research 1990, 29 (9) 1846–1855

Fontes, M.D.S.B., Melo, D.M.D.A., Barros, J.M.D.F., Braga, R.M. and Rodrigues, G. (2014) "Kinetic study of the catalytic pyrolysis of elephant grass using Ti-MCM-41" Materials Research 17, 216-221.

Foster, A.J., Jae, J., Cheng, Y.T., Huber, G.W. and Lobo, R.F. (2012) "Optimizing the aromatic yield and distribution from catalytic fast pyrolysis of biomass over ZSM-5" Applied Catalysis A: General 423, pp.154-161.

Gamliel, D. P., Cho, H. J., Fan, W., & Valla, J. A. (2016) "On the effectiveness of tailored mesoporous MFI zeolites for biomass catalytic fast pyrolysis" Applied Catalysis A: General, 522, 109-119.

Gamliel, D.P.; Du, S.; Bollas, G.M.; Valla, J.A. (2015) "Investigation of in situ and ex situ catalytic pyrolysis of miscanthus-giganteus using a PyGC–MS microsystem and comparison with a bench-scale spouted-bed reactor" Bioresource Technology 191, 187–196.

García, J.R., Bertero, M., Falco, M., Sedran, U. (2015) "Catalytic cracking of bio-oils improved by the formation of mesopores by means of Y zeolite desilication" Applied Catalysis A: General 503, 1-8.

Gayubo, A., Valle, B., Aguayo, A., Olazar, M., Bilbao, J. (2010) "Pyrolytic lignin removal for the valorization of biomass pyrolysis crude bio-oil by catalytic transformation" Journal of chemical technology and biotechnology 85, 132–144

Gebreslassie, B.H., Slivinsky, M., Wang, B., You, F. (2013)" Life cycle optimization for sustainable design and operations of hydrocarbon biorefinery via fast pyrolysis, hydrotreating and hydrocracking" Computers and Chemical Engineering 50, 71– 91

Gerhard, K. (2010) "Biodiesel and renewable diesel: a comparison" Progress in Energy and Combustion Science 36, 364–73.

Ghayal, M.S., Pandya, M.T. (2013) "Microalgae biomass: a renewable source of energy" International Conference on Sustainable Energy Engineering and Application Energy Procedia 32, 242 – 250

Ghobadian, B. (2012) "Liquid biofuels potential and outlook in Iran" Renewable and Sustainable Energy Reviews 16, 4379–4384

Gudka, B., Jones, J.M., Lea-Langton, A.R., Williams, A., Saddawi, A. (2015) "A review of the mitigation of deposition and emission problems during biomass combustion through washing pre-treatment" Journal of the Energy Institute 1-13

Haafiz, M.K.M., Eichhorn, S.J., Hassan, A., Jawaid, M. (2013) "Isolation and characterization of microcrystalline cellulose from oil palm biomass residue" Carbohydrate Polymers 93, 628– 634

Hayter, S., Tanner, S. (2004). "Biomass Co-firing in Coal-Fired Boilers" National Renewable Laboratory at: http://www.nrel.gov/docs/fy04osti/33811.pdf . Accessed: 2nd June, 2015

Heidenreich, S., Foscolo, P. U. (2015) "New concepts in biomass gasification" Progress in Energy and Combustion Science 46, 72-95

Heitner, C., Dimmel, D.R., Schmidt, J.A. (2010) "Lignin and Lignans" Advances in Chemistry, CRC Press, Boca Raton, USA, 1–10

Hellsmark, H., Jacobsson, S. (2009) "Opportunities for and limits to Academics as System builders—The case of realizing the potential of gasified biomass in Austria" Energy Policy 37, 5597–5611

Hew, K.L., Tamidi, A.M., Yusup, S., Lee, K.T., Ahmad, M.M. (2010) "Catalytic cracking of bio-oil to organic liquid product (OLP)" Bioresource technology 101(22), 8855-8858.

Hosoya, T., Kawamoto, H., Saka, S. (2007) "Cellulose-hemicellulose and cellulose-lignin interactions in wood pyrolysis at gasification temperature" Journal of Analytical and Applied Pyrolysis 80,118–25.

Huang, Y., Wei, Z., Qiu, Z., Yin, X., Wu, C. (2012) "Study on structure and pyrolysis behavior of lignin derived from corncob acid hydrolysis residue" Journal of Analytical and Applied Pyrolysis 93, 153-159

Huber, G.W., Corma, A. (2007) "Synergies between bio- and oil refineries for the production of fuels from biomass" Angewandte Chemie International Edition 46(38), 7184-7201.

Ibáñez, M., Artetxe, M., Lopez, G., Elordi, G., Bilbao, J., Olazar, M., Castaño, P. (2014) "Identification of the coke deposited on an HZSM-5 zeolite catalyst during the sequenced pyrolysis-cracking of HDPE" Applied Catalysis B: Environmental 148, 436–445.

Imam,T., Capareda, S. (2012) ”Characterization of bio-oil, syn-gas and bio-char from switchgrass pyrolysis at various temperatures” Journal of Analytical and Applied Pyrolysis 93, 170-177

Jae, J., Coolman, R., Mountziaris, T.J., Huber, G.W. (2014) “Catalytic fast pyrolysis of lignocellulosic biomass in a process development unit with continual catalyst addition and removal” Chemical Engineering Science 108, 33–46.

Jae, J., Tompsett, G.A., Foster, A.J., Hammond, K.D., Auerbach, S.M., Lobo, R.F., Huber, G.W. (2011) “Investigation into the shape selectivity of zeolite catalysts for biomass conversion” Journal of Catalysis 279, 257–268.

Jahirul, M.I., Rasul, M.G., Chowdhury, A.A., Ashwath, N. (2012) “Biofuels production through biomass pyrolysis—a technological review. Energies 5(12), 4952-5001

Jakeria, M.R., Fazal, M.A., Haseeb, A.S.M.A. (2014) “Influence of different factors on the stability of biodiesel: A review” Renewable and Sustainable Energy Reviews 30, 154–163

Jiang, L., Hu, S., Sun, L-S., Su, S., Xu, K., He, L-M., Xiang, J. (2013) “Influence of different demineralization treatments on physicochemical structure and thermal degradation of biomass” Bioresource Technology 146, 254–260

Johnston, C. M. T., Van Kooten, G.C. (2015) “Economics of co-firing coal and biomass: An application to Western Canada” Energy Economics 48, 7–17

Kan, T., Strezov, V., Evans, T.J. (2016) “Lignocellulosic biomass pyrolysis: A review of product properties and effects of pyrolysis parameters” Renewable and Sustainable Energy Reviews 57, 1126–1140

Karimi, E., Teixeira, I. F., Gomez, A., De Resende, E., Gissane, C., Leitch, J., Jollet, V., Aigner, I., Berruti, F., Briens, C., Fransham, P., Hoff, B., Schrier, N., Lago, R. M., Kycia, S. W., Heck, R., Schlaf, M. (2014) “Synergistic co-processing of an acidic hardwood derived pyrolysis bio-oil with alkaline Red Mud bauxite mining waste as a sacrificial upgrading catalyst” Applied Catalysis B: Environmental 145, 187– 196

Kebelmann, K., Hornung, A., Karsten, U., Griffiths, G. (2013) “Intermediate pyrolysis and product identification by TGA and Py-GC/MS of green microalgae and their extracted protein and lipid components” Biomass Bioenergy 49, 38–48.

Ketzial, J., Radhika, D., and Nesaraj, A S. (2013). “Low-temperature preparation and physical characterization of doped BaCeO3nanoparticles by chemical precipitation” International Journal of Industrial Chemistry 4(1), 18.

Khan, A.A., Jonga, W.D., Jansens, P.J., Spliethoff, H. (2009) "Biomass combustion in fluidized bed boilers: potential problems and remedies" Fuel Processing Technology 90, 21–50

Kim, B-S., Kim, Y-M., Jae, J., Watanabe, C., Kim, S., Jung, S-C., Kim, S.C., Park, Y.K. (2015) "Pyrolysis and catalytic upgrading of Citrus unshiu peel" Bioresource Technology 194, 312–319.

Kim, K H., Eom, I Y., Lee, S.M., Choi, D., Yeo, H., Choi, I-G., Choi, J.W. (2011) "Investigation of physicochemical properties of biooils produced from yellow poplar wood (Liriodendron tulipifera) at various temperatures and residence times" Journal of Analytical and Applied Pyrolysis 92, 2–9

Kim, K., Ryoo, R., Jang, H-D., Choi, M. (2012) "Spatial distribution, strength, and dealumination behavior of acid sites in nanocrystalline MFI zeolites and their catalytic consequences" Journal of Catalysis 288, 115–123

Kim, Y., Mosier, N.S., Ladisch, M.R. (2009) "Enzymatic digestion of liquid hot water pretreated hybrid poplar" Biotechnology Progress 25, 340-348

Kshirsagar, M.P., Kalamkar, V.R. (2014) "A comprehensive review on biomass cookstoves and a systematic approach for modern cookstove design" Renewable and Sustainable Energy Reviews 30, 580-603

Kubicka, D., Kikhtyanin, O. (2015) "Opportunities for zeolites in biomass upgrading—Lessons from the refining and petrochemical industry" Catalysis Today 243, 10–22

Kumar, M., M.P. Sharma, M. P. (2015) "Assessment of potential of oils for biodiesel production" Renewable and Sustainable Energy Reviews 44, 814–823

Le, Roux. E., Chaouch, M., Diouf, P.N., Stevanovic, T. (2015) "Impact of a pressurized hot water treatment on the quality of bio-oil produced from aspen" Biomass and Bioenergy 81, 202-209

Lee, H. W., Park, S. H., Jeon, J. K., Ryoo, R., Kim, W., Suh, D. J., & Park, Y. K. (2014) "Upgrading of bio-oil derived from biomass constituents over hierarchical unilamellar mesoporous MFI nanosheets" Catalysis Today 232, 119-126.

Lee, M.-K., Tsai, W.-T., Tsaic, Y.-L., Lin, S.-H. (2010) "Pyrolysis of Napier grass in an induction-heating reactor" Journal of Analytical and Applied Pyrolysis 88, 110–116.

Leibbrandt, N.H., Knoetze, J.H., Gorgens, J.F. (2011) "Comparing biological and thermochemical processing of sugarcane bagasse: An energy balance perspective" Biomass and bioenergy 35, 2117-2126

Li, F., Yuan, Y., Huang, Z., Chen, B. and Wang, F. (2015) "Sustainable production of aromatics from bio-oils through combined catalytic upgrading with in situ generated hydrogen" Applied Catalysis B: Environmental 165, 547-554.

Li, J., Li, X., Zhou, G., Wang, W., Wang, C., Komarneni, S., & Wang, Y. (2014b) "Catalytic fast pyrolysis of biomass with mesoporous ZSM-5 zeolites prepared by desilication with NaOH solutions" Applied Catalysis A: General 470, 115-122.

Li, T., Duan, A., Zhao, Z., Liu, B., Jiang, G., Liu, J., Wei, Y., Pan, H. (2014a) "Synthesis of ordered hierarchically porous L-SBA-15 material and its hydro-upgrading performance for FCC gasoline" Fuel 117, 974–980.

Li, W., Wang, W., Xu, P., Xu, P., Zhao, X., Wang, Y. (2015) "Pretreatment of Miscanthus stalk with organic alkali guanidine and amino-guanidine" Bioresource Technology 179, 606-610

Liew, W.H., Hassim, M.H., Ng, D.K.S. (2014) Review of evolution, technology and sustainability assessments of biofuel production, Journal of Cleaner Production 17, 11-29

Lim, J.S., Abdul-Manan, Z., Wan-Alwi, S.R., Hashim, H. (2012) "A review on utilisation of biomass from rice industry as a source of renewable energy" Renewable and Sustainable Energy Reviews 16, 3084– 3094.

Lin, Y.Y., Zhang, C., Zhang, M.C., Zhang, J.A. (2010) "Deoxygenation of bio-oil during pyrolysis of biomass in the presence of CaO in a fluidized-bed reactor" Energy Fuels 24, 5686–5695

Liu, G., Wright, M.M., Zhao, Q., Brown, R.C. (2015) "Catalytic fast pyrolysis of duckweed: Effects of pyrolysis parameters and optimization of aromatic production" Journal of Analytical and Applied Pyrolysis 112, 29–36.

Lupoi, J.S., Singh, S., Simmons, B.A., Henry, R.J. (2014) "Assessment of lignocellulosic biomass using analytical spectroscopy: an evolution to high-throughput techniques" Bioenergy Research 7(1), 1–23

Ma, X., Tian, Y., Hao, W., Ma, R., Li, Y. (2014) "Production of phenols from catalytic conversion of lignin over a tungsten phosphide catalyst" Applied Catalysis A: General 481, 64–70

Mahfud, F.H., Ghijsen, F., Heeres, H.J. (2007) "Hydrogenation of fast pyrolysis oil and model compounds in a two-phase aqueous organic system using homogeneous ruthenium catalysts" Journal of molecular catalysis A: Chemical 264, 227–36.

Mahmood, A.S.N., Brammer, J.G., Hornung, A., Steele, A., Poulston, S. (2013) "The inter-mediate pyrolysis and catalytic steam reforming of Brewers spent grain" Journal of Analytical and Applied Pyrolysis 103, 328–342.

Makibar, J., Fernandez-Akarregi, A.R., Amutio, M., Lopez, G., Olazar, M. (2015) "Performance of a conical spouted bed pilot plant for bio-oil production by poplar flash pyrolysis" Fuel Processing Technology 137, 283–289

Mante, O.D., Agblevor, F., Oyama, S., McClung, R. (2014) "Catalytic pyrolysis with ZSM-5 based additive as co-catalyst to Y-zeolite in two reactor configurations" Fuel 117, 649–659

Margeot, A., Hahn-Hagerdal, B., Edlund, M., Slade, R., Monot, F. (2009) "New improvements for lignocellulosic ethanol" Curr Opin Biotechnol 20, 372–80

Maya, J. J., Sabu, T. (2008) "Biofibres and biocomposites" Carbohydrate Polymers 71, 343–364.

Medvedev, D., Murashkina, A., Pikalova, E., Demin, A., Podias, A., and Tsiakaras, P. (2014). "BaCeO3: Materials development, properties and application" Progress in Materials Science 60, 72-129.

Menon, V., Rao, M. (2012) "Trends in bioconversion of lignocellulose: Biofuels, platform chemicals & biorefinery concept" Progress in Energy and Combustion Science 38, 522-550

Ming, Z., Ximei, L., Yulong, L., Lilin, P. (2014) "Review of renewable energy investment and financing in China: Status, mode, issues and countermeasures" Renewable and Sustainable Energy Reviews 31, 23–37

Mirmoshtaghi, G., Li, H., Thorin, E., Dahlquist, E. (2016) "Evaluation of different biomass gasification modeling approaches for fluidized bed gasifiers" Biomass and Bioenergy 91, 69-82

Mitsumasu, K., Liu, Z-S., Tang, Y-Q., Akamatsu, T., Taguchi, H., Kida, K. (2014) "Development of industrial yeast strain with improved acid- and thermo-tolerance through evolution under continuous fermentation conditions followed by haploidization and mating" Journal of Bioscience and Bioengineering 118(6), 689-695

Mizsey, P., Racz, L. (2010) "Cleaner production alternatives: Biomass utilisation options" Journal of Cleaner Production 18 (8), 767-770

Mohammed, I.Y., Abakr, Y.A., Kazi, F.K., Yusup, S., Alshareef, I., Chin, S.A. (2015a) "Comprehensive Characterization of Napier Grass as a Feedstock for Thermochemical Conversion" Energies 8(5), 3403-3417.

Mohammed, I.Y., Abakr, Y.A., Kazi, F.K., Yusup, S., Alshareef, I., Chin, S.A., (2015b). Pyrolysis of Napier Grass in a Fixed Bed Reactor: Effect of Operating Conditions on Product Yields and Characteristics" BioResources

10 (4), 6457–6478.

Mohammed, I.Y., Kazi, F. K., Yusup, S., Abakr, Y.A. (2016b) "Effects of Pretreatments of Napier Grass with Deionized Water, Sulfuric Acid and Sodium Hydroxide on Pyrolysis Oil Characteristics" Waste and Biomass Valorization DOI: 10.1007/s12649-016-9594-1, in press

Mohammed, I.Y., Kazi, F.K., Yusup, S., Alaba, P.A., Sani, Y.M., Abakr, Y.A. (2016a) "Catalytic Intermediate Pyrolysis of Napier Grass in a Fixed Bed Reactor with ZSM-5, HZSM-5 and Zinc-Exchanged Zeolite-A as the Catalyst" Energies 9 (4), 246.

Mohammed, I.Y., Lim, C.H., Kazi, F. K., Yusup, S., Lam, H.L., Abakr, Y.A. (2016c) "Co-pyrolysis of Rice Husk with Underutilized Biomass Species: A Sustainable Route for Production of Precursors for Fuels and Valuable Chemicals" Waste and Biomass Valorization. DOI: 10.1007/s12649-016-9599-9, in press

Mortensen, P.M., Grunwaldt, J.D., Jensen, P.A., Jensen, A.D. (2016) "Influence on nickel particle size on the hydrodeoxygenation of phenol over Ni/SiO2" Catalysis Today 259 (Part 2), 277-284

Mortensen, P.M., Grunwaldt, J.D., Jensen, P.A., Knudsen, K.G., Jensen, A.D. (2011) "A review of catalytic upgrading of bio-oil to engine fuels" Applied Catalysis A: General 407, 1– 19.

Mu, W., Ben, H., Ragauskas, A., Deng, Y. (2013) "Lignin pyrolysis components and upgrading – technology review" BioEnergy Research 6, 1183–1204

Na, K., Choi, M., Ryoo, R. (2013) "Recent advances in the synthesis of hierarchically nanoporous zeolites" Microporous Mesoporous Material 166, 3–19.

Ndibe, C., Grathwohl, S., Paneru, M., Maier, J., Scheffknecht, G. (2015) "Emissions reduction and deposits characteristics during cofiring of high shares of torrefied biomass in a 500 kW pulverized coal furnace" Fuel 156, 177–189

Nhuchhen, D.R., Basu, P., Acharya, B.A. (2014) "Comprehensive Review on Biomass Torrefaction" International Journal of Renewable Energy & Biofuels 1-56

Nigam, P.S., Singh, A. (2011) "Production of liquid biofuels from renewable resources" Progress in Energy and Combustion Science 37 52–68.

Ning, S-K., Hung, M-C., Chang, Y-H., Wan, H-P., Lee, H-T., Shih, R-F. (2013) "Benefit assessment of cost, energy, and environment for biomass pyrolysis oil" Journal of Cleaner Production 59, 141-149

Ojha, D.K., Vinu, R. (2015) "Resource recovery via catalytic fast pyrolysis of polystyrene using zeolites" Journal of Analytical and Applied Pyrolysis 113, 349–359.

Olofsson, K., Bertilsson, M., Lidén, G.A. (2008) "Short review on SSF – an interesting process option for ethanol production from lignocellulosic feedstocks" Biotechnology for Biofuels 1, 1-14

Parasuram, K. V., Reddy, K. O., Shukla, M., Marwala, T. (2013). "Morphological, structural and thermal characterization of acetic acid modified and unmodified napier grass fiber strands" 7th International Conference on Intelligent Systems and Control (ISCO), 506-510

Park, H.J., Park, K.-H., Jeon, J.-K., Kim, J., Ryoo, R., Jeong, K.-E., Park, S.H., Park, Y.-K. (2012) "Production of phenolics and aromatics by pyrolysis of Miscanthus" Fuel 97, 379–384.

Park, S.R., Pandey, A.K., Tyagi, V.V., Tyagi, S.K. (2014) "Energy and exergy analysis of typical renewable energy systems" Renewable and Sustainable Energy Reviews 30, 105–123

Park, Y.K., Yoo, M.L., Jin, S.H., Park, S.H. (2015) "Catalytic fast pyrolysis of waste pepper stems over HZSM-5" Renewable Energy 79, 20–27.

Patel, M., Kumar, A. (2016) "Production of renewable diesel through the hydroprocessing of lignocellulosic biomass-derived bio-oil: A review" Renewable and Sustainable Energy Reviews 58, 1293-1307

Patwardhan, P.R., Brown, R.C., Shanks, B.H. (2011) "Product distribution from the fast pyrolysis of hemicellulose" ChemSusChem 4(5), 636–643.

Pérez-Ramírez, J., Mitchell, S., Verboekend, D., Milina, M., Michels, N-L., Krumeich, F., Marti, N., Erdmann, M. (2011) "Expanding the Horizons of Hierarchical Zeolites: Beyond Laboratory Curiosity towards Industrial Realization" ChemCatChem 3, 1731–1734.

Puértolas, B., Veses, A., Callén, M. S., Mitchell, S., García, T., & Pérez-Ramírez, J. (2015) "Porosity–Acidity Interplay in Hierarchical ZSM-5 Zeolites for Pyrolysis Oil Valorization to Aromatics" ChemSusChem 8(19), 3283-3293.

Qian, K., Kumar, A., Patil, K., Bellmer, D., Wang, D., Yuan, W., Raymond, L., Huhnke, R.L. (2013) "Effects of biomass feedstocks and gasification conditions on the physiochemical properties of char" Energies 6, 3972–3986

Reddy, K.O., Maheswari, C.U., Reddy, D.J.P., Rajulu, A.V. (2009) "Thermal properties of Napier grass fibers" Materials Letters 63, 2390–2392.

Reddy, K.O., Maheswari, C.U., Shukla, M., Rajulu, A.V. (2012) "Chemical composition and structural characterization of Napier grass fibers" Materials Letters 67, 35–38.

Ren, S., Yea, X. P., Borole, A.P., Kimc, P., Labbé, N. (2016) "Analysis of switchgrass-derived bio-oil and associated aqueous phase generated in a semi-pilot scale auger pyrolyzer" Journal of Analytical and Applied Pyrolysis 119, 97–103

Renewables global status report (RGSR) (2015). https://cleanenergysolutions.org/sites/default/files/documents/150716_gsr2015_cesc-webinar_rad.pdf. Accessed 26 June 2016

Report of the Paris Conference on Climate Change (COP21) (2015) .http://ec.europa.eu/clima/policies/international/negotiations/paris/index_en.htm. Accessed 15 May 2016

Resende, F.L.P. (2016) "Recent advances on fast hydropyrolysis of biomass" Catalysis Today 269, 148-155.

Richter, G.M., Riche, A.B., Dailey, A.G., Gezan, S.A., Powlson, D.S. (2008) "Is UK biofuel supply from Miscanthus water-limited?" Soil Use Manage 24, 235–245.

Ridzuan, M. J. M., Majid, A., Afendi, M., Aqmariah Kanafiah, S. N., Nuriman, M. B. M. (2015) "Effects of alkaline concentrations on the tensile properties of Napier grass fibre" Applied Mechanics and Materials 786, 23-27

Saad, A., Ratanawilai, S., Tongurai, C. (2015) "Catalytic Cracking of Pyrolysis Oil Derived from Rubberwood to Produce Green Gasoline Components" BioResources 10(2), 3224-3241.

Said, N., El-Shatoury, S.A., Díaz, L.F., Zamorano, M. (2013) "Quantitative appraisal of biomass resources and their energy potential in Egypt" Renewable and Sustainable Energy Reviews 24, 84–91

Saidura, R., Abdelaziza, E.A., Demirbasb, A., Hossaina, M.S., Mekhilef, S. (2011) "A review on biomass as a fuel for boilers" Renewable and Sustainable Energy Reviews 15, 2262–2289

Samson, R., Mani, S., Boddey, R. (2005) "The potential of C4 perennial grasses for developing a global bioheat industry" Critical Review in Plant Science 24, 461–495.

Sawatdeenarunat, C., Surendra, K.C., Takara, D., Oechsner, H., Khanal, S.K. (2015) "Anaerobic digestion of lignocellulosic biomass: Challenges and opportunities" Bioresource Technology 178, 178–186

Scheer, A.M., Mukarakate, C., Robichaud, D.J., Nimlos, M.R. and Ellison, G.B., 2011. "Thermal decomposition mechanisms of the methoxyphenols: formation of phenol, cyclopentadienone, vinylacetylene, and acetylene" The Journal of Physical Chemistry A, 115(46), 13381-13389.

Sebestyén, Z., May, Z., Réczey, K., Jakab, E. (2011) "The effect of alkaline pretreatment on the thermal decomposition of hemp" Journal of Thermal Analysis and Calorimetry 105, 1061-1069

Serapiglia, M.J., Mullena, C.A., Boatenga, A.A., Cortese, L.M., Bonos, S.A. Hoffman, L. (2015) "Evaluation of the impact of compositional differences in switchgrass genotypes on pyrolysis product yield" Industrial Crops and Products 74, 957–968

Shaaban, M., Petinrin, J.O. (2014) "Renewable energy potentials in Nigeria: Meeting rural energy needs" Renewable and Sustainable Energy Reviews 29, 72–84

Shemfe, M.B., Whittaker, C., Gu, S., Fidalgo, B. (2016) "Comparative evaluation of GHG emissions from the use of Miscanthus for bio-hydrocarbon production via fast pyrolysis and bio-oil upgrading" Applied Energy 176, 22–33

Shen, D.K., Gu, S. (2009) "The mechanism for thermal decomposition of cellulose and its main" Bioresource Technology 100, 6496–6504

Shen, D.K., Gu, S., Bridgwater, A.V. (2010a) "Study on the pyrolytic behaviour of xylan-based hemicellulose using TG-FTIR and Py-GC-FTIR" Journal of Analytical and Applied Pyrolysis 87, 199–206

Shen, D.K., Gu, S., Luo, K.H., Wang, S.R., Fang, M.X. (2010b) "The pyrolytic degradation of wood-derived lignin from pulping process" Bioresource Technology 101, 6136–6146

Sousa, J.F., Bezerra, M.B.D., Almeida, M.B.B., Moure, G.T., Mesa-Perez, J.M., Caramao, E.B. (2016) "Characteristics of Bio-oil from the Fast Pyrolysis of Elephant Grass (Pennisetum purpureum Schumach) in a Fluidized Bed Reactor" American Chemical Science Journal 14(2), 1-10

Srirangan, K., Akawi, L., Moo-Young, M., Chou, C.P. (2012) "Towards sustainable production of clean energy carriers from biomass resources" Applied Energy 100, 172–186

Starink, M. (2003) "the determination of activation energy from linear heating rate experiments: a comparison of the accuracy of isoconversion methods. Thermochimica Acta 404, 163-176

Stedile, T., Ender, L., Meier, H.F., Simionatto, E.L., Wiggers, V.R. (2015) "Comparison between physical properties and chemical composition of bio-oils derived from lignocellulose and triglyceride sources" Renewable and Sustainable Energy Reviews 50, 92–108

Stephanidis. S., Nitsos, C., Kalogiannis, K., Iliopoulou, E.F., Lappas, A.A., Triantafyllidis, K.S. (2011) "Catalytic upgrading of lignocellulosic biomass pyrolysis vapours: Effect of hydrothermal pre-treatment of biomass" Catalysis Today 167, 37–45

Stephenson, A.L., Dennis, J.S., Scott, S.A. (2008) "Improving the sustainability of the production of biodiesel from oilseed rape in the UK" process safety and environment protection 86, 427–440

Strezov, V., Evans, T.J., Hayman, C. (2008) "Thermal conversion of elephant grass (Pennisetum Purpureum Schum) to bio-gas, bio-oil and charcoal" Bioresource Technology 99, 8394–8399.

Swanson, R.M., Platon, A., Satrio, J.A., Brown, R. C. (2010) "Techno-economic analysis of biomass-to-liquids production based on gasification" Fuel 89, S11–S19

Takafuji, M., Ide, S., Ihara, H., Xu. Z. (2004). Preparation of Poly (1-vinylimidazole)-grafted magnetic nanoparticles and their application for removal of metal ions. Chemistry of materials 16(10), 1977-1983.

Takase, M., Zhao, T., Zhang, M., Chen, Y., Liu, H., Yang, L., Wu, X. (2015) "An expatriate review of neem, jatropha, rubber and karanja as multipurpose non-edible biodiesel resources and comparison of their fuel, engine and emission properties" Renewable and Sustainable Energy Reviews 43, 495–520

Tan, H., Wang, S. (2009) "Experimental study of the effect of acid-washing pretreatment on biomass pyrolysis" Journal of Fuel Chemistry and Technology 37(6), 668-672

Technical committee of petroleum additive manufacturers in Europe (ATC) https://www.atc-europe.org/public/Doc113%202013-10-01.pdf (2013). Accessed 25 August 2016.

Thangalazhy-Gopakumar, S., Adhikari, S., Gupta, R.B., Tu, M., Taylor, S. (2011) "Production of hydrocarbon fuels from biomass using catalytic pyrolysis under helium and hydrogen environments" Bioresource Technology 102, 6742–6749.

Tian, Q., Liu, Z., Zhu, Y., Dong, X., Saih, Y., Basset, J.M., Sun, M., Xu, W., Zhu, L., Zhang, D. and Huang, J., (2016) "Beyond Creation of Mesoporosity: The Advantages of Polymer-Based Dual-Function Templates for Fabricating Hierarchical Zeolites" Advanced Functional Materials 26, 1881-1891

Toor, S.S., Rosendahl, L., Rudolf, A. (2010) "Hydrothermal liquefaction of biomass: A review of subcritical water technologies" Energy 36 (5), 2328-2342

Tripathi, M., Sahu, J.N., Ganesan, P. (2016) "Effect of process parameters on production of biochar from biomass waste through pyrolysis: A review" Renewable and Sustainable Energy Reviews 55, 467–481.

Tsai, W.T. and Tsai, Y.L. (2016) "Thermochemical characterization of Napier grass as an energy source and its environmental and economic benefit analysis" Energy Sources, Part B: Economics, Planning, and Policy 11(2), 130-136.

Tumuluru, J. S., Sokhansanj, S., Wright, C. T., Boardman, R. D., & Yancey, N. A. (2011) "A Review on Biomass Classification and Composition, Co-Firing Issues and Pretreatment Methods" In Proceedings of the 2011 ASABE annual international meeting. Louisville, Kentucky, USA, 7-10.

Tyrone, W., Wei, Z., Ragauskas, A. (2015) "Bioconversion of lignocellulosic pretreatment effluent via oleaginous Rhodococcus opacus DSM 1069" Biomass and bioenergy 72, 200 -205

Van de Velden, M., Baeyens, J., Brems, A., Janssens, B., Dewil, R. (2010) "Fundamentals, kinetics and endothermicity of the biomass pyrolysis reaction" Renewable Energy 35, 232–242.

Vassilev, S.V., Baxter, D., Andersen, L.K., Vassileva, C.G. (2010) "An overview of the chemical composition of biomass" Fuel, 89 913–933

Vassilev, S.V., Baxter, D., Andersen, L.K., Vassileva, C.G., Morgan, T.J. (2012) "An overview of the organic and inorganic phase composition of biomass" Fuel 94, 1–33

Veses, A., Puértolas, B., López, J. M., Callén, M. S., Solsona, B., & García, T. (2016) "Promoting Deoxygenation of Bio-Oil by Metal-Loaded Hierarchical ZSM-5 Zeolites" ACS Sustainable Chemistry & Engineering 4(3), 1653-1660

Vichaphund, S., Aht-ong, D., Sricharoenchaikul, V., Atong, D. (2014) "Catalytic upgrading pyrolysis vapors of Jatropha waste using metal promoted ZSM-5 catalysts: An analytical PY-GC/MS" Renewable Energy 65, 70-77

Vitolo, S., Bresci, B., Seggiani, M., Gallo, M.G. (2001) "Catalytic upgrading of pyrolytic oils over HZSM-5 zeolite: behaviour of the catalyst when used in repeated upgrading–regenerating cycles" Fuel 80 (1), 17-26.

Vyazovkin, S., Burnham, A.K., Criado, J.M., Pérez-Maqueda, L.A., Popescu, C., Sbirrazzuoli, N. (2011) "ICTAC Kinetics Committee recommendations for performing kinetic computations on thermal analysis data" Thermochimica Acta 520 1-19

Wang, H., Srinivasan, R., Yu, F., Steele, P., Li, Q., Mitchell, B. (2011) "Effect of Acid, Alkali, and Steam Explosion Pretreatments on Characteristics of Bio-Oil Produced from Pinewood" Energy Fuels 25, 3758–3764

Wang, L., Lei, H., Ren, S., Bu, Q., Liang, J., Wei, Y., Liu, Y., Lee, G.S.J., Chen, S., Tang, J. and Zhang, Q. (2012). Aromatics and phenols from catalytic pyrolysis of Douglas fir pellets in microwave with ZSM-5 as a catalyst. Journal of Analytical and Applied Pyrolysis, 98, 194-200.

Wang, S., Chen, J., Cai, Q., Zhang, F., Wang, Y., Ru, B., Wang, Q. (2016) "The effect of mild hydrogenation on the catalytic cracking of bio-oil for aromatic hydrocarbon production" International Journal of Hydrogen Energy in press

Wang, S.R., Guo, X.J., Wang, K.G., Luo, Z.Y. (2011) "Influence of the interaction of components on the pyrolysis behavior of biomass" Journal of Analytical and Applied Pyrolysis 91, 183–9.

Wang, Y., He, T., Liu, K., Wua, J., Fang, Y. (2012) "From biomass to advanced bio-fuel by catalytic pyrolysis/hydro-processing: Hydrodeoxygenation of bio-oil derived from biomass catalytic pyrolysis" Bioresource Technology 108, 280–284

Wang, Z., Wang, F., Cao, J., Wang, J. (2010) "Pyrolysis of pine wood in a slowly heating fixed-bed reactor: potassium carbonate versus calcium hydroxide as a catalyst" Fuel Processing Technology 91 (8), 942–950

Wei, Y., Lei, H., Zhu, L., Zhang, X., Liu, Y., Yadavalli, G., Zhu, X., Qian, M., Yan, D. (2016) "Hydrocarbon produced from upgrading rich phenolic compound bio-oil with low catalyst coking" Fuel 178, 77-84

White, J.E., Catallo, W.J., Legendre, B.L. (2011) "Biomass pyrolysis kinetics: a comparative critical review with relevant agricultural residue case studies Journal of Analytical and Applied Pyrolysis 91, 1–33.

Widayatno, W. B., Guan, G., Rizkiana, J., Yang, J., Hao, X., Tsutsumi, A., Abudula, A. (2016) "Upgrading of bio-oil from biomass pyrolysis over Cu-modified β-zeolite catalyst with high selectivity and stability" Applied Catalysis B: Environmental 186, 166-172.

Wigley, T., Yip, A.C.K., Pang, S. (2015) "The use of demineralisation and torrefaction to improve the properties of biomass intended as a feedstock for fast pyrolysis" Journal of Analytical and Applied Pyrolysis 113, 296–306

Wiinikka, H., Carlsson, P., Johansson, A-C., Gullberg, M., Ylipää, C., Lundgren, M., Sandström, L. (2015) "Fast Pyrolysis of Stem Wood in a Pilot-Scale Cyclone Reactor" Energy & Fuels 29 (5), 3158-3167

Wu, Z., Wang, S., Zhao, J., Chen, L., Meng, H. (2016) "Thermochemical behavior and char morphology analysis of blended bituminous coal and lignocellulosic biomass model compound co-pyrolysis: Effects of cellulose and carboxymethylcellulose sodium" Fuel 171, 65-73

Xin, D., Yang, Z., Liu, F., Xu, X., Zhang, J. (2015) "Comparison of aqueous ammonia and dilute acid pretreatment of bamboo fractions: Structure properties and enzymatic hydrolysis" Bioresource Technology 175, 529–536

Xu, F., Shi, Y-C., Wang, D. (2013a) "X-ray scattering studies of lignocellulosic biomass: A review" Carbohydrate Polymers 94, 904– 917

Xu, F., Yu, J., Tesso, T., Dowell, F., Wang, D. (2013b) "Qualitative and quantitative analysis of lignocellulosic biomass using infrared techniques: A mini-review" Applied Energy 104, 801–809

Yakub, M.I., Abdalla, A.Y., Feroz, K.K., Suzana, Y., Ibraheem, A., Chin, S.A., (2015) "Pyrolysis of Oil Palm Residues in a Fixed Bed Tubular Reactor" Journal of Power Energy Engineering 3, 185–193

Yakub, M.I., Mohamed, S., Danladi, S.U. (2014) "Technical and Economic Considerations of Post-combustion Carbon Capture in a Coal Fired Power Plant" International Journal of Advances in Engineering & Technology 7(5), 1549–1581.

Yan, H., Le Van Mao, R. (2010) "Hybrid catalysts used in the catalytic steam cracking process (CSC): influence of the pore characteristics and the surface acidity properties of the ZSM-5 zeolite-based component on the overall catalytic performance" Applied Catalysis A: General 375, 63–69.

Yan, Y., Li,X., Wang,G., Gui,X., Li,G., Su,F., Wang,X., Liu, T. (2014) "Biotechnological preparation of biodiesel and its high-valued derivatives: A review" Applied Energy 113, 1614–1631

Yang, X., Choi, H-S., Park, C., Kim, S-W. (2015) "Current states and prospects of organic waste utilization for biorefineries" Renewable and Sustainable Energy Reviews 49, 335–349

Yildiz, G., Ronsse, F., Venderbosch, R., Van Duren, R., Kersten, S.R.A., Prins, W. (2015) "Effect of biomass ash in catalytic fast pyrolysis of pine wood" Applied Catalysis B: Environmental 168–169, 203–211.

Yorgun, S., Yıldız, D. (2015) "Slow pyrolysis of paulownia wood: Effects of pyrolysis parameters on product yields and bio-oil characterization" Journal of Analytical and Applied Pyrolysis 114, 68-78

Yu, F. W., Ji, D. X., Nie, Y., Luo, Y., Huang, C. J., & Ji, J. B. (2012) "Study on the pyrolysis of cellulose for bio-oil with mesoporous molecular sieve catalysts" Applied biochemistry and biotechnology 168(1), 174-182.

Yuan, J.-H., Xu, R.-K., and Zhang, H. (2011). "The forms of alkalis in the biochar produced from crop residues at different temperatures" Bioresource Technology 102(3), 3488-3497

Zaafouri, K., Trabelsi, A.B.H., Krichah, S., Ouerghi, A., Aydi, A., Claumann, C. A., Wüst, Z. A., Naoui, S., Bergaoui, L., Hamdi, M. (2016) "Enhancement of biofuels production by means of co-pyrolysis of Posidonia oceanica (L.) and frying oil wastes: Experimental study and process modeling" Bioresource Technology 207, 387-398

Zhang, B., Zhong, Z.P., Chen, P., Ruan, R. (2015b) "Microwave-assisted catalytic fast pyrolysis of biomass for bio-oil production using chemical vapor deposition modified HZSM-5 catalyst" Bioresource Technology 197, 79–84

Zhang, B., Zhong, Z.P., Wang, X.B., Ding, K., Song, Z.W. (2015a) "Catalytic upgrading of fast pyrolysis biomass vapors over fresh, spent and regenerated ZSM-5 zeolites" Fuel Processing Technology 138, 430–434.

Zhang, B., Zhong, Z.P., Wang, X.B., Ding, K., Song, Z.W. (2015a) "Catalytic upgrading of fast pyrolysis biomass vapors over fresh, spent and regenerated ZSM-5 zeolites" Fuel Processing Technology 138, 430–434.

Zhang, H., Cheng, Y-T., Vispute, T.P., Xiao, R., Huber, G.W. (2011) "Catalytic conversion of biomass-derived feedstocks into olefins and aromatics with ZSM-5: the hydrogen to carbon effective ratio" Energy Environmental Science 4, 2297–2307.

Zhang, H., Luo, M., Xiao, R., Shao, S., Jin, B., Xiao, G., Zhao, M., Liang, J. (2014) "Catalytic conversion of biomass pyrolysis-derived compounds with chemical liquid deposition (CLD) modified ZSM-5" Bioresource Technology 155, 57–62.

Zhang, H., Xiao, R., Jin, B., Xiao, G., Chen, R. (2013) "Biomass catalytic pyrolysis to produce olefins and aromatics with a physically mixed catalyst" Bioresource Technology 140, 256–262.

Zhang, H.P., Ding, S.Y., Mielenz, J.R., Elander, R.T., Laser, M., Himmel, M.E., McMillan, J.R., Lynd, L.R. (2007) "Fractionating recalcitrant lignocellulose at modest reaction conditions" Biotechnology and Bioengineering 97(2), 214–223

Zhou, Y., Jiang, J., Peng, Z., Wang, Q., Xiong, D. (2012) "Ecosystem Management in the Natural Rubber Industry" Journal of Resources and Ecology 3(3), 230-235

APPENDICES

APPENDIX I

Table 1(a): GC-MS analysis of organic phase bio-oil obtained at optimized condition

RT (min)	Compound	Formula	Area%
	Organic Phase		
3.85	1,3-DIMETHYL-1-CYCLOHEXENE	C_8H_{14}	4.67
4.03	1H-IMIDAZOLE-2-METHANOL	$C_4H_6ON_2$	3.05
5.13	PHENOL	C_6H_6O	8.43
5.76	PHENOL, 2-METHYL-	C_7H_8O	4.06
5.93	PHENOL, 3-METHYL-	C_7H_8O	4.96
6.06	PHENOL, 2-METHOXY-	$C_7H_8O_2$	7.65
6.51	PHENOL, 2,4-DIMETHYL-	$C_8H_{10}O$	2.50
6.64	PHENOL, 3-ETHYL-	$C_8H_{10}O$	8.20
6.86	CREOSOL	$C_8H_{10}O_2$	3.68
7.03	BENZALDEHYDE, 4-METHYL-	C_8H_8O	13.41
7.47	PHENOL, 4-ETHYL-2-METHOXY-	$C_9H_{12}O_2$	5.39
7.73	2-METHOXY-4-VINYLPHENOL	$C_9H_{10}O_2$	6.74
7.96	PHENOL, 2,6-DIMETHOXY-	$C_8H_{10}O_3$	8.85
8.57	1,2,3-TRIMETHOXYBENZENE	$C_9H_{12}O_3$	2.18
8.63	PHENOL, 2-METHOXY-4-(1-PROPENYL)-, (Z)-	$C_{10}H_{12}O_2$	2.44
9.05	4-ETHYLBIPHENYL	$C_{14}H_{14}$	2.53
9.30	4-METHYL-2,5-DIMETHOXYBENZALDEHYDE	$C_{10}H_{12}O_3$	1.74
10.08	PHENOL, 2,6-DIMETHOXY-4-(2-PROPENYL)-	$C_{11}H_{14}O_3$	3.12
10.43	DESASPIDINOL	$C_{11}H_{14}O_4$	1.73
19.06	1,4-BENZENEDICARBOXYLIC ACID, BIS(2-ETHYLHEXYL) ESTER	$C_{24}H_{38}O_4$	4.68

Table 1(b): GC-MS analysis of aqueous phase bio-oil obtained at optimized condition

RT (min)	Compound	Formula	Area%
	Aqueous Phase		
3.31	1,2,4,5-CYCLOHEXANETETROL, (1.ALPHA.,2.ALPHA.,4.ALPHA.,5.BETA.)-	$C_6H_{12}O_4$	3.24
3.85	CARBONIC ACID, 2,2,2-TRICHLOROETHYL CYCLOHEXYLMETHYL ESTER	$C_{10}H_{15}O_3Cl_3$	8.65
4.06	Z,Z-6,28-HEPTATRIACTONTADIEN-2-ONE	$C_{37}H_{70}O$	6.51
4.52	CYCLOHEXENE, 3,5-DIMETHYL-	C_8H_{14}	4.28
4.58	BUT-3-EN-1-YL 2-METHYLBUTANOATE	$C_9H_{16}O_2$	3.86
4.70	UNDECANOIC ACID, 11-MERCAPTO-	$C_{11}H_{22}O_2S$	4.03
5.15	PHOSPHONIC ACID, (P-HYDROXYPHENYL)-	$C_6H_7O_4P$	6.25
5.36	FURAN, TETRAHYDRO-2,5-DIMETHOXY-	$C_6H_{12}O_3$	2.75
5.56	2-ETHYL-5-PROPYLCYCLOPENTANONE	$C_{10}H_{18}O$	5.11
6.06	IMIDAZOLE, 2-AMINOCARBONYL-1-METHYL-	$C_5H_7ON_3$	7.14
6.64	1,3,5-CYCLOHEPTATRIENE, 1-METHOXY-	$C_8H_{10}O$	4.22
6.91	2-PROPENAMIDE, N-(4-AMINOBUTYL)-3-(3,4-DIHYDROXYPHENYL)-, (E)-	$C_{13}H_{18}O_3N_2$	11.20
7.04	BENZENE, (ETHENYLOXY)-	C_8H_8O	5.31
7.38	1,2-BENZENEDIOL, 3-METHOXY-	$C_7H_8O_3$	5.91
7.96	PHENOL, 2,6-DIMETHOXY-	$C_8H_{10}O_3$	9.14
8.56	PHENOL, 4-METHOXY-3-(METHOXYMETHYL)-	$C_9H_{12}O_3$	3.37
9.04	BENZENE, 1,2,3-TRIMETHOXY-5-METHYL-	$C_{10}H_{14}O_3$	2.14
9.10	2-PROPANONE, 1-(4-HYDROXY-3-METHOXYPHENYL)-	$C_{10}H_{12}O_3$	2.51
10.08	PHENOL, 2,6-DIMETHOXY-4-(2-PROPENYL)-	$C_{11}H_{14}O_3$	2.02
10.42	BENZENEMETHANOL, 2,5-DIMETHOXY-, ACETATE	$C_{11}H_{14}O_4$	2.34

APPENDIX II

Table1: Proximate and ultimate analyses of raw biomass and pre-treated samples (dry basis).

Pretreatment		Proximate analysis (wt%)			(MJ/kg)	Ultimate analysis (wt%)				
	Ro	AC	VM	FC	HHV	C	H	N	S	O
Raw	0.0	1.75±0.04	81.51±0.26	16.74±0.05	18.05±0.07	51.61±0.24	6.01±0.02	0.99±0.01	0.32±0.01	41.072±0.20
H_2O	0.4	1.40±0.02	84.21±0.27	14.39±0.04	18.22±0.06	48.97±0.24	5.99±0.02	0.82±0.01	0.30±0.01	42.52±0.21
	0.9	0.87±0.02	84.76±0.27	14.37±0.04	18.47±0.06	49.01±0.25	6.00±0.02	0.74±0.01	0.28±0.01	43.10±0.20
	2.1	0.75±0.02	85.01±0.26	14.25±0.04	18.67±0.06	49.07±0.25	5.99±0.02	0.75±0.01	0.29±0.01	43.16±0.20
	2.4	0.71±0.02	85.13±0.28	14.16±0.04	18.82±0.06	49.02±0.25	5.98±0.02	0.64±0.01	0.30±0.01	43.35±0.20
	2.7	0.63±0.02	85.21±0.28	14.17±0.03	19.17±0.07	49.12±0.24	5.98±0.02	0.61±0.01	0.29±0.01	43.38±0.21
H_2SO_4	Conc (w/w%)									
	0.5	0.78±0.02	88.28±0.27	10.94±0.03	18.62±0.05	50.34±0.25	5.76±0.02	0.79±0.01	0.23±0.01	42.10±0.21
	1.0	0.69±0.02	88.45±0.28	10.86±0.03	18.99±0.05	50.53±0.24	5.59±0.02	0.78±0.01	0.20±0.01	42.21±0.21
	1.5	0.53±0.02	88.76±0.29	10.71±0.03	19.64±0.06	50.63±0.25	5.45±0.03	0.71±0.01	0.21±0.01	42.47±0.20
	2.0	0.40±0.02	88.92±0.26	10.68±0.04	19.82±0.07	50.75±0.25	5.37±0.02	0.67±0.01	0.20±0.01	42.61±0.20
	2.5	0.34±0.02	89.09±0.29	10.57±0.03	19.98±0.06	50.81±0.25	5.31±0.03	0.59±0.01	0.19±0.01	42.76±0.20
NaOH	Conc (w/w%)									
	0.5	1.05±0.04	87.54±0.26	11.41±0.04	17.17±0.06	48.91±0.24	5.87±0.02	0.81±0.01	0.27±0.01	43.09±0.22
	1.0	1.08±0.03	87.16±0.26	11.77±0.04	17.09±0.06	48.84±0.24	5.83±0.02	0.69±0.01	0.19±0.01	43.38±0.21
	1.5	1.13±0.04	86.78±0.26	12.10±0.03	16.90±0.04	48.79±0.24	5.78±0.02	0.65±0.01	0.13±0.01	43.53±0.20
	2.0	1.20±0.04	86.23±0.27	12.57±0.04	16.77±0.06	48.74±0.25	5.72±0.02	0.59±0.01	0.10±0.01	43.65±0.21
	2.5	1.23±0.04	85.04±0.26	13.74±0.03	16.64±0.05	48.69±0.24	5.62±0.02	0.54±0.01	0.07±0.01	43.86±0.20

Table 2: Chemical compounds detected in bio-oil from raw and pretreated samples

RT(min)	Compound name	RNGS	WTNGS	ALTNGS	ACTNGS
			Peak area (%)		
2.26	Benzene	4.83	2.60	8.15	1.45
2.96	Propanoic acid	13.19	0.29	-	-
3.05	1,2-Ethanediol, monoacatate	-	-	4.18	2.53
3.52	3-Penten-2-one	-	0.04	-	-
3.76	Butanoic acid, 2-methylpropyl ester	0.84	-	-	-
4.16	Cyclobutanethiol	-	-	1.13	-
4.18	Formic acid, 2-propenyl ester	-	-	-	2.24
4.19	Aziridine, 1-methyl	1.10	-	-	-
4.20	1-Hydroxy-2-butanone	5.89	0.05	-	-
4.37	Tert-Butyl methylcarbonate	0.38	-	-	-
4.77	Cyclohexane	-	-	3.93	-
4.80	1,2-Cyclopentanediol, trans-	-	1.14	-	0.19
4.81	Acetic acid, 2-ethylbutyl ester	1.73	-	-	-
5.19	Propanedioic acid propyl-	-	-	-	0.61
5.28	1,2-Amino-4-methyl-1-pentanol	-	0.91	0.63	-
5.37	2-[2-methyl-2-aminoethyl]benzofuran	0.62	-	-	-
5.62	Cyclopentane	0.34	0.03	-	-
6.04	Furfural	6.58	25.06	7.70	13.24
6.16	Betazole	0.41	-	-	-
6.88	2-Furanmethanol	0.84	0.66	3.32	0.82
7.36	1,2-Propanediol, diacetate	-	-	-	0.54
8.54	3-Hepten-1-ol, acetate	-	-	1.44	1.04
8.67	Propanenitrile, 3-(methylamino)-	-	-	3.25	1.72
8.69	Ethanone, 1-(2-furanyl)	0.84	0.96	-	-
9.53	Carbamic acid, phenyl-, butyl ester	-	-	-	0.11
10.46	2-Furancarboxaldehyde, 5-methyl-	3.37	3.75	-	0.88
11.20	Phenol	9.29	7.33	19.19	15.38
12.04	1,3-Dimethyl-5-(adamantyl-1)benzene	0.13	-	0.87	-
12.68	1,2-Cyclopentanedione, 3-methyl-	3.26	2.84	3.97	1.94
13.59	Phenol, 3-methyl-	4.41	3.78	3.32	1.71
14.28	Benzyl alcohol	1.25	-	-	0.99
14.31	P-Cresol	3.91	3.49	-	-
14.56	Mequinol	0.26	0.27	-	0.46
16.53	Phenol, 2-ethyl	-	1.17	1.16	0.55
17.08	Phenol, 4-ethyl-	4.02	4.59	1.79	1.99

18.01	Catechol	3.63	13.07	11.75	20.56
18.46	1,4:3,6-Dianhydro-alpha-d-glucopyranose	-	-	-	1.72
18.48	Pentanal, 2,2-dimethyl-, hydrazone	0.33	0.31	2.59	-
18.87	Furan, 2,3-dihydro-4-(1-methylpropyl)-, (S)-	-	-	-	2.21
18.89	5-Hydroxymethylfurfural	-	4.25	-	-
19.12	3,4,5,7,8-Pentamethoxyflvone	-	-	1.48	-
19.77	1,2-Benzenediol, 4-methyl-	0.68	1.75	-	0.41
20.23	Phenylcyclopentyl sulfide	0.83	0.30	5.45	-
20.61	1,2-Benzenediol, 3-methyl-	-	2.83	2.31	1.16
20.88	d-Monnitol, 1,4-anhydro	-	0.76	-	0.49
22.13	N-Methyl-N-vinylthio-naphthalene-1-amine	-	-	7.26	1.01
22.14	Phenol, 2,6-dimethoxy-	3.15	1.98	-	-
22.62	Benzaldehyde, 2-hydroxy-	-	0.93	-	-
23.08	Benzenediol, 4-ethyl-	-	0.80	-	-
24.49	Benzonitrile, 2-chloro-6-nitro	0.20	-	-	-
24.59	4-Ethyl-3-oxabicyclo[4,4,0]decane	-	-	-	0.12
26.19	Levoglucosan	-	-	-	5.86
26.36	β-d-Glucopyranose 1 6-anhydro-	-	14.07	-	16.27

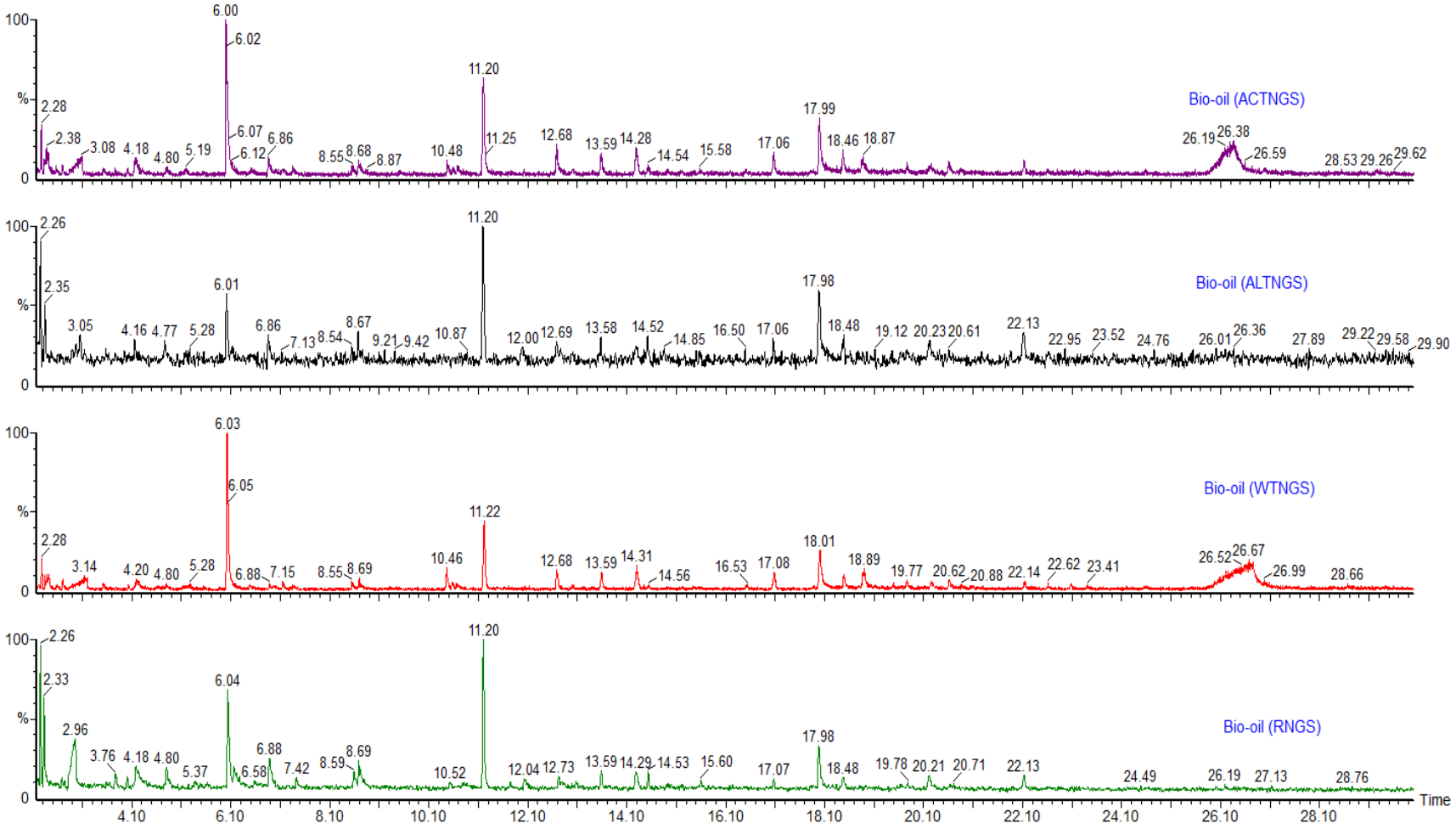

Figure GC-MS chromatogram of bio-oil samples from raw and pre-treated Napier grass

APPENDIX III

Table 1: Physicochemical properties of in-situ catalytic upgraded bio-oil organic phase

Catalyst	(wt%)	(g)	Biomass (g)	Bio-oil organic phase elemental analysis (%) C	H	N	S	O	DOD	HHV (MJ/kg)	PH
Raw	0.0	0.00	200.00	50.89	6.02	0.88	0.23	41.98	0.00	26.77	2.65
ZSM-5	0.5	1.00	200.00	58.92	6.42	0.85	0.44	33.37	20.51	27.11	2.99
	1.0	2.00	200.00	62.11	6.55	0.95	0.56	29.83	28.94	29.10	2.97
	2.0	4.00	200.00	64.40	6.76	0.53	0.53	27.78	33.83	30.07	2.88
	3.0	6.00	200.00	65.12	6.79	0.97	0.64	26.48	36.92	31.51	2.95
0.2HZSM-5	0.5	1.00	200.00	61.72	6.11	0.78	0.26	31.13	25.85	29.97	2.9
	1.0	2.00	200.00	63.01	6.23	0.81	0.34	29.61	29.47	33.18	2.70
	2.0	4.00	200.00	63.87	6.56	0.91	0.41	28.25	32.71	36.56	2.6
	3.0	6.00	200.00	66.09	6.22	0.87	0.39	26.43	37.04	37.34	2.6
0.3HZSM-5	0.5	1.00	200.00	61.95	6.21	0.81	0.28	30.75	26.75	28.88	2.60
	1.0	2.00	200.00	62.98	6.31	0.88	0.29	29.54	29.63	35.18	2.90
	2.0	4.00	200.00	64.51	6.33	0.96	0.24	27.96	33.40	35.89	3.00
	3.0	6.00	200.00	66.77	6.24	0.79	0.25	25.95	38.18	38.71	3.50

Table 2: Compounds detected in the upgraded organic phase oil over ZSM-5

	In-situ upgraded samples with ZSM-5		GC-MS peak area (%)		
RT (min)	Compound	Formula	1.0 wt%	3.0 wt%	2.0 wt%
3.02	2,5-CYCLOOCTADIEN-1-OL	C8H12O	5.48	0.00	0.00
3.02	1-HEXEN-3-YNE, 2-METHYL-	C7H10	0.00	0.00	0.00
3.02	2,3-DIMETHYL-CYCLOHEXA-1,3-DIENE	C8H12	0.00	0.00	0.00
3.02	1-TRIDECENE	C13H26	0.00	7.26	0.00
3.75	2-BUTYNE, 1,4-DICHLORO-	C4H4Cl2	3.05	0.00	1.62
3.79	BICYCLO[2.2.1]HEPT-5-ENE-2,2-DIMETHANOL	C9H14O2	0.00	3.72	0.00
3.86	TRICYCLO[3.2.1.0(2,4)]OCTANE, 3-METHYLENE-	C9H12	2.56	0.00	0.00
4.14	OCTADECANOIC ACID, PHENYL ESTER	C24H40O2	4.07	0.00	0.00
4.19	BICYCLO[2.2.2]OCT-5-EN-2-ONE, 7-SYN-HYDROXY-	C8H10O2	0.00	0.00	0.00
4.54	1,7,7-TRIMETHYLBICYCLO[2.2.1]HEPTAN-2-OL	C10H18O	4.19	0.00	0.00
4.57	5,6-DIBROMO-5-METHYL-HEX-1-ENE	C7H12Br2	0.00	0.00	0.00
4.57	1,1'-BICYCLOHEPTYL	C14H26	0.00	5.12	5.08
4.67	CYCLOBUTANECARBOXYLIC ACID, UNDEC-10-ENYL ESTER	C16H28O2	0.00	0.00	0.00
4.77	CYCLOPENTANE, 1,2-DIMETHYL-3-(1-METHYLETHYL)-	C10H20	0.00	4.59	3.77
4.84	3-UNDECENE, 6-METHYL-, (E)-	C12H24	8.82	0.00	0.00
5.17	TETRADECANE, 1-CHLORO-	C14H29Cl	3.04	0.00	0.00
5.33	2-HYDROXYMETHYL-2-METHYLCYCLOPENTANOL	C7H14O2	0.00	0.00	0.00
5.85	1,1-DIMETHYL-1-SILACYCLO-2,4-HEXADIENE	C7H12Si	1.88	0.00	0.00
5.92	BICYCLO[3.2.0]HEPT-2-ENE, 4-ETHOXY-, EXO-	C9H14O	0.00	0.00	0.00
6.00	4A-METHYL-1,2,4A,5,8,8A-HEXAHYDRO-NAPHTHALENE	C11H16	15.19	0.00	0.00

6.02	BENZENE, (OCTYLOXY)-	C14H22O	0.00	8.29	9.00
6.24	PIVALIC ACID, 2-TETRAHYDROFURYLMETHYL ESTER	C10H18O3	1.88	0.00	0.00
6.64	CYCLOHEXENE, 1,4-DIMETHYL-	C8H14	0.00	0.00	0.00
6.69	PHENOL, 4-BUTYL-	C10H14O	3.31	0.00	0.00
6.72	P-CRESOL	C7H8O	0.00	0.00	0.00
6.75	PHENOL, 2-METHYL-	C7H8O	3.06	3.25	0.00
6.93	PHENOL, 3-METHYL-	C7H8O	0.00	4.06	7.06
7.05	PHENOL, 2-METHOXY-	C7H8O2	4.21	0.00	0.00
7.08	1,3-HEPTADIENE, 2,3-DIMETHYL-	C9H16	0.00	7.23	12.41
7.10	3-HEPTYNE, 2,2-DIMETHYL-	C9H16	0.00	0.00	0.00
7.72	PHENOL, 2-ETHYL-	C8H10O	0.00	8.86	0.00
7.74	PHENOL, 3-ETHYL-	C8H10O	4.35	0.00	1.66
7.91	1-TRIMETHYLSILYLPENT-1-EN-4-YNE	C8H14Si	3.86	0.00	0.00
8.16	BENZOFURAN, 2,3-DIHYDRO-	C8H8O	0.00	0.00	0.00
8.18	1,2-BENZENEDIMETHANOL	C8H10O2	5.14	13.39	24.38
8.70	PHENOL, 4-ETHYL-2-METHOXY-	C9H12O2	5.99	0.00	0.00
8.97	CYCLOHEXENE, 2-ETHENYL-1,3,3-TRIMETHYL-	C11H18	0.00	4.69	0.00
8.99	2-METHOXY-4-VINYLPHENOL	C9H10O2	0.00	0.00	9.09
9.20	PHENOL, 2,6-DIMETHOXY-	C8H10O3	4.31	9.13	0.75
9.90	2,4-DIMETHOXYBENZYL ALCOHOL	C9H12O3	0.00	0.00	0.00
9.90	1,2,4-TRIMETHOXYBENZENE	C9H12O3	0.00	1.64	5.03
9.93	ETHANONE, 1-(2,3,4-TRIHYDROXYPHENYL)-	C8H8O4	2.04	0.00	0.00
10.44	5-TERT-BUTYLPYROGALLOL	C10H14O3	2.85	0.00	0.00
10.44	ETHYL BENZENE	C14H14	0.00	15.69	0.00
10.46	BENZENE, 1,2,3-TRIMETHOXY-5-METHYL-	C10H14O3	0.00	0.00	4.07
10.48	BENZENE, 1,1'-ETHYLIDENEBIS-	C14H14	0.00	0.00	8.40

10.52	BENZENE, [BIS(METHYLTHIO)METHYL]-	C9H12S2	0.00	0.00	2.77
10.54	PHENOL, 4-ETHYL-2-METHOXY-	C9H12O2	0.00	0.00	1.47
10.88	CYCLOOCTASILOXANE, HEXADECAMETHYL-	C16H48O8Si8	2.95	0.00	0.00
10.97	HEPTASILOXANE, 1,1,3,3,5,5,7,7,9,9,11,11,13,13-TETRADECAMETHYL-	C14H44O6Si7	0.75	0.00	0.00
10.98	BRALLOBARBITAL	C10H11O3N2Br	0.00	0.69	0.00
11.61	1,2-DIMETHOXY-4-(1-METHOXYETHENYL)BENZENE	C11H14O3	0.00	0.00	3.45
11.90	HEPTASILOXANE, 1,1,3,3,5,5,7,7,9,9,11,11,13,13-TETRADECAMETHYL-	C14H44O6Si7	3.41	0.00	0.00
12.81	OCTASILOXANE, 1,1,3,3,5,5,7,7,9,9,11,11,13,13,15,15-HEXADECAMETHYL-	C16H50O7Si8	2.12	0.00	0.00
12.91	SILANE, TRIMETHYL[5-METHYL-2-(1-METHYLETHYL)PHENOXY]-	C13H22OSi	0.00	0.00	0.00
13.75	TRISILOXANE, 1,1,1,5,5,5-HEXAMETHYL-3,3-BIS[(TRIMETHYLSILYL)OXY]-	C12H36O4Si5	1.13	0.00	0.00
15.39	TRISILOXANE, 1,1,1,5,5,5-HEXAMETHYL-3,3-BIS[(TRIMETHYLSILYL)OXY]-	C12H36O4Si5	0.00	2.40	0.00
17.39	2-BROMO-2-CYANO-N,N-DIMETHYLACETAMIDE	C5H7ON2Br	0.00	0.00	0.00
17.52	CYCLOHEXANECARBOXYLIC ACID, 2-METHYLBUTYL ESTER	C12H22O2	0.37	0.00	0.00

Table 3: Compounds detected in the upgraded organic phase oil over 0.2HZSM-5

	In-situ Upgraded samples 0.2HZSM-5		GC-MS peak area (%)		
RT	Compound	formula	1.0 wt%	3.0 wt%	2.0 wt%
3.02	Z,Z-6,25-TETRATRIACTONTADIEN-2-ONE	C34H64O	0.00	5.75	0.00
3.02	3-CHLOROPROPIONIC ACID, OCTADECYL ESTER	C21H41O2Cl	0.00	0.00	4.60
3.02	4-TRIDECENE, (Z)-	C13H26	4.77	0.00	0.00
3.64	PENTANOIC ACID, 2-PROPENYL ESTER	C8H14O2	4.13	5.45	0.00
3.92	1-PENTANOL, 5-(PHENYLMETHOXY)-	C12H18O2	0.00	0.00	3.72
3.92	BENZENE, (PHENOXYMETHYL)-	C13H12O	5.99	0.00	0.00
4.70	1-PENTENE, 2,4-DIMETHYL-	C7H14	0.00	0.00	2.16
4.90	ETHYLBENZENE	C8H10	0.00	1.47	0.00
4.99	P-XYLENE	C8H10	2.96	0.00	2.60
5.24	P-XYLENE	C8H10	0.00	1.97	0.00
5.48	2,3,4-HEXATRIENE, 2,5-DIMETHYL-	C8H12	0.00	0.00	1.82
6.00	BENZENE, 1,2,3-TRIMETHYL-	C9H12	4.11	0.00	0.00
6.05	N-VINYLIMIDAZOLE	C5H6N2	9.56	1.05	11.08
6.26	BENZENE, 1,2,4-TRIMETHYL-	C9H12	1.23	1.14	0.00
6.66	1-METHOXY-1,3-CYCLOHEXADIENE	C7H10O	0.00	0.00	1.20
6.77	BENZENE, 2-METHYL-	C7H8O	7.19	9.57	7.24
6.95	P-CRESOL	C7H8O	7.38	8.94	7.60
7.31	PHENOL, 2,6-DIMETHYL-	C8H10O	0.00	2.70	2.13
7.36	PHENOL, 2-ETHYL-5-METHYL-	C9H12O	0.00	2.21	3.38
7.51	PHENOL, 3-ETHYL-	C8H10O	2.19	3.27	2.74
7.63	PHENOL, 2,5-DIMETHYL-	C8H10O	5.86	8.17	5.97
7.77	PHENOL, 2-ETHYL-	C8H10O	17.37	16.46	17.05

8.03	PHENOL, 3-ETHYL-5-METHYL-	C9H12O	0.00	4.36	3.85
8.04	PHENOL, 2-ETHYL-6-METHYL-	C9H12O	3.25	0.00	0.00
8.28	PHENOL, 3-(1-METHYLETHYL)-	C9H12O	3.81	4.79	4.18
8.38	PHENOL, 3-ETHYL-5-METHYL-	C9H12O	7.45	10.51	7.20
8.94	ETHYLTETRAMETHYLCYCLOPENTADIENE	C12H18	3.33	4.60	3.67
9.31	1,3-CYCLOHEXADIENE, 1,3,5,5,6,6-HEXAMETHYL-	C12H20	3.84	4.46	3.13
9.55	TETRADECANE, 1-BROMO-	C14H29Br	0.00	0.00	2.31
9.55	1-ETHYL-1(1-CYCLOBUTYLIDENETHYL)CYCLOBUTANE	C12H20	2.68	3.12	0.00
9.96	3,7-BENZOFURANDIOL, 2,3-DIHYDRO-2,2-DIMETHYL-	C10H12O3	2.90	0.00	0.00
10.25	NONADECANE, 1-BROMO-	C19H39Br	0.00	0.00	2.38

Table 4: Compounds detected in the upgraded organic phase oil over 0.3HZSM-5

RT	In-situ Upgraded samples with 0.3HZSM-5		GC-MS peak area (%)		
	Compound	Formula	2.0wt%	1.0wt%	3.0wt%
3.02	1-HEXEN-3-ONE	C6H10O	4.31	0.00	0.00
3.02	1-HEXADECANOL, 2-METHYL-	C17H36O	0.00	3.33	0.00
3.02	CYCLODODECANOL, 1-ETHENYL-	C14H26O	0.00	0.00	4.04
3.63	ISOBUTYL NONYL CARBONATE	C14H28O3	0.00	4.40	0.00
3.63	PENTANOIC ACID, 2-PROPENYL ESTER	C8H14O2	0.00	0.00	5.84
3.64	BENZENE, 1-ETHOXY-4,4-DIMETHYL-	C9H18O	3.09	0.00	0.00
3.91	TOLUENE	C7H8	0.00	0.00	4.87
3.92	PHENOL, 2-(PHENYLMETHOXY)-	C13H12O2	4.64	0.00	0.00

3.92	PHENOL, 5-(PHENYLMETHOXY)-	C12H18O2	0.00	3.83	0.00
4.11	CYCLOHEXANOL, 1-ETHENYL-	C8H14O	0.00	0.00	2.84
4.80	BENZENE, 1-ETHOXY-4,4-DIMETHYL-	C9H18O	0.00	0.00	2.32
4.98	P-XYLENE	C8H10	2.06	4.02	3.46
5.22	BICYCLO[2.1.1]HEXAN-2-OL, 2-ETHENYL-	C8H12O	0.21	0.00	0.00
5.24	ETHYLBENZENE	C8H10	0.00	1.56	2.25
5.47	2,3,4-HEXATRIENE, 2,5-DIMETHYL-	C8H12	1.10	0.00	0.00
5.99	BENZENE, 1,2,4-TRIMETHYL-	C9H12	0.00	0.00	12.77
6.03	N-VINYLIMIDAZOLE	C5H6N2	10.69	0.00	6.03
6.04	BENZENE, (OCTYLOXY)-	C14H22O	0.00	9.21	0.00
6.25	BENZENE, 1,2,3-TRIMETHYL-	C9H12	0.00	0.00	1.37
6.65	CYCLOHEXAN-1-ETHANOL, 1-HYDROXYMETHYL-	C9H18O2	1.06	0.00	0.00
6.76	PHENOL, 2-METHYL-	C7H8O	6.45	6.86	5.63
6.95	P-CRESOL	C7H8O	7.55	7.07	5.93
7.15	BENZENE, 2-BUTENYL-	C10H12	0.00	1.17	0.00
7.30	PHENOL, 2,6-DIMETHYL-	C8H10O	1.47	1.87	0.00
7.36	PHENOL, 3-(1-METHYLETHYL)-	C9H12O	2.37	0.00	0.00
7.36	PHENOL, 2-ETHYL-5-METHYL-	C9H12O	0.00	2.07	0.00
7.50	PHENOL, 2-ETHYL-	C8H10O	2.44	2.37	0.00
7.62	PHENOL, 2,5-DIMETHYL-	C8H10O	5.22	5.59	4.69
7.76	PHENOL, 3-ETHYL-	C8H10O	17.68	14.02	13.54
8.02	PHENOL, 2-ETHYL-4-METHYL-	C9H12O	0.00	2.69	3.42
8.03	PHENOL, 2-ETHYL-6-METHYL-	C9H12O	2.39	0.00	0.00
8.27	PHENOL, 3-(1-METHYLETHYL)-	C9H12O	3.55	3.01	3.31
8.36	PHENOL, 3-ETHYL-5-METHYL-	C9H12O	6.69	6.86	5.06
8.53	BENZENEMETHANOL, 4-ETHYL-	C9H12O	2.32	0.00	0.00

8.53	PHENOL, 2-PROPYL-	C9H12O	0.00	2.15	0.00
8.86	PHENOL, 2,4,6-TRIMETHYL-	C9H12O	0.00	1.25	0.00
8.71	PHENOL, 2-ETHYL-4,5-DIMETHYL-	C10H14O	0.00	1.29	0.00
8.81	THYMOL	C10H14O	0.00	0.91	0.00
8.92	ETHYLTETRAMETHYLCYCLOPENTADIENE	C11H18	2.75	0.00	0.00
8.94	2,5-DIETHYLPHENOL	C10H14O	0.00	2.99	3.45
9.02	1H-INDENE, 2,3-DIHYDRO-4,5,7-TRIMETHYL-	C12H16	0.00	2.22	0.00
9.02	BENZENE, 1-(1-METHYLETHENYL)-2-(1-METHYLETHYL)-	C12H16	2.50	0.00	0.00
9.29	1,3-CYCLOHEXADIENE, 1,3,5,5,6,6-HEXAMETHYL-	C12H20	2.35	2.81	2.52
9.53	1-ETHYL-1(1-CYCLOBUTYLIDENETHYL)CYCLOBUTANE	C12H20	0.00	3.53	0.00
9.54	BENZENE, 1-METHOXY-4-(1-METHYLPROPYL)-	C11H16O	0.00	0.00	1.98
9.54	TRIDECANE, 1-BROMO-	C13H27Br	2.61	0.00	0.00
9.84	BENZENE, 2-(2-BUTENYL)-1,3,5-TRIMETHYL-	C13H18	1.75	0.00	0.00
9.95	HEPTADECANE, 1-BROMO-	C17H35Br	2.75	0.00	0.00
10.24	TRIDECANE, 1-BROMO-	C13H27Br	0.00	2.05	0.00
10.25	DODECANE, 1,12-DIBROMO-	C12H24Br2	0.00	0.00	2.49
11.53	OCTADECANE, 1-CHLORO-	C18H37Cl	0.00	0.87	2.18

APPENDIX IV

Table 1a: Effect of catalyst on Ex-situ deoxygenation of bio-oil

RT (min)	0.0 wt% catalyst , 60min reaction time, 400 °C compound	Area	%
5.462	1 3 5-Cycloheptatriene	567235904	2.364356
5.709	Phenol, 3-methyl-	741467136	3.090587
5.878	Phenol, 2-methyl-	634931392	2.646524
6.009	3-Heptyne, 2,2-dimethyl-	680837760	2.837872
6.171	Phenol, 2,6-dimethyl-	629944128	2.625737
6.221	3-Ethylphenol, methyl ether	703064128	2.930516
6.461	Phenol, 2,3-dimethyl-	1000523072	4.170386
6.591	Phenol, 2,3-dimethyl-	1073259776	4.473567
6.764	1,4-Benzenediol, 2,6-dimethyl-	562396928	2.344186
6.803	Phenol, 3,4-dimethyl-	686714048	2.862365
7.117	Phenol, 3,4,5-trimethyl-	9211428928	38.39513
7.413	2,3-Dimethoxytoluene	558092352	2.326244
7.66	2,4-Dimethoxytoluene	1346200960	5.611242
7.879	Phenol, 3-methoxy-2,4,5-trimethyl-	555905216	2.317127
7.921	1,2-Diethoxy-4-ethylbenzene	576405952	2.402578
7.956	Phenol, 3-methoxy-2,4,5-trimethyl-	649915904	2.708983
8.125	1,4-Benzenediol, 2,5-dimethyl-	567876736	2.367027
8.503	2(3H)-Naphthalenone, 4,4a,5,6,7,8-hexahydro-1-methoxy-	1043502848	4.349534
11.11	Hexadecanoic acid, methyl ester	1302580400	5.429423
12.094	Heptadecanoic acid, 16-methyl-, methyl ester	898856576	3.746619

Table 1b

RT (min)	ZSM-5 2% catalyst , 60min reaction time, 400 °C compound	Area	%
5.109	exo-2-Bromonorbornane	622474688	5.302348
5.494	Cycloheptatriene	454118336	3.868259
5.737	Bicyclobutylidene	706634624	6.019237
5.899	Cyclopentadiene	643728960	5.483395
6.04	2-Cyclopenten-1-one, 3,4,4-trimethyl-	546940096	4.658931
6.245	3-Ethylphenol, methyl ether	543831808	4.632454
6.386	Phenol, 2,6-dimethyl-	455874720	3.88322
6.485	Phenol, 2,3-dimethyl-	934025408	7.956191
6.608	dimethylnaphthalene	1134398720	9.663006
6.827	Phenol, 2,4-dimethyl-	517151872	4.40519
7.052	Phenol, 2,3,6-trimethyl-	628047808	5.349821
7.14	Phenol, 3-ethyl-5-methyl-	732453056	6.239163
7.292	2-Isopropylidene-3-methylhexa-3,5-dienal	498614304	4.247284
7.641	2,5-Diethylphenol	428567104	3.650609
7.676	Benzocycloheptatriene	430512032	3.667177
7.715	1H-Inden-1-one, 2,3-dihydro-3,3-dimethyl-	444419904	3.785646
7.98	Benzene, 1-ethoxy-4-ethyl-	417343072	3.555001
8.153	1,4-Benzenediol, 2,5-dimethyl-	524311584	4.466177
8.527	1,4-Benzenediol, 2,3,5-trimethyl-	621819324	5.296765
11.133	Hexadecanoic acid, methyl ester	454337440	3.870125

Table 1c

RT (min)	2% 0.2HZSM-5 catalyst , 60min, 400oC compound	Area	%
5.13	Phenol	571300416	4.237708
5.757	Bicyclobutylidene	806943168	5.985625
5.923	Phenol, 2-methyl-	763654656	5.664525
6.06	2-Cyclopenten-1-one, 3,4,4-trimethyl-	499590656	3.70579
6.216	Phenol, 2,6-dimethyl-	579524288	4.29871
6.261	Phenol, 3-ethyl-5-methyl-	475447296	3.526703
6.498	Phenol, 2,6-dimethyl-	1170902272	8.685347
6.628	5-á,8-á-Epoxy-3,5,8,8a-tetrahydro-1H-2-benzopyran	1005719936	7.460082
7.072	Phenol, 2,3,5-trimethyl-	540273920	4.007565
7.157	Cyclopropane, 1-bromo-2,2,3,3-tetramethyl-1-prop-1-ynyl-	1021077440	7.573998
7.566	Phenol, 2,3,5,6-tetramethyl-	652362240	4.838997
7.654	Phenol, 2-ethyl-4,5-dimethyl-	493963264	3.664048
7.693	2 6-dimethylbenzene	531029984	3.938996
8.003	2-Ethyl-5-n-propylphenol	566085824	4.199028
8.169	2 5-dimethylbenzene	546408640	4.05307
8.543	Methyl 5,7-hexadecadiynoate	1092841856	8.106322
8.98	2,3,5-trimethyl-Benzene	634850432	4.7091
10.397	dimethylnaphthalene	527207904	3.910645
10.68	Cyclohept[f]indene, 1,2,3,5,6,7,8,9-octahydro-	510383840	3.78585
11.145	Hexadecanoic acid, methyl ester	491784640	3.647888

Table 1d

RT (min)	2% 0.3HZSM-5 catalyst , 60min, 400 °C compound	Area	%
5.116	Phenol	360489408	1.788387
5.744	Phenol, 2-methyl-	5570792996	27.63669
5.916	p-Cresol	407235424	2.020294
6.043	2-Cyclopenten-1-one, 3,4,4-trimethyl-	405915264	2.013744
6.206	Phenol, 2,5-dimethyl-	417869536	2.073049
6.251	Phenol, 2-ethyl-6-methyl-	420344576	2.085328
6.502	Phenol, 2,6-dimethyl-	862104512	4.276898
6.618	Ethylbenzene	687802112	3.412184
7.059	Phenol, 2,3,6-trimethyl-	439339136	2.17956
7.147	Phenol, 3,4,5-trimethyl-	744555968	3.69374
7.556	Phenol, 2,3,5,6-tetramethyl-	391962176	1.944523
8.533	Methyl 4,6-tetradecadiynoate	901260992	4.471153
8.97	1,4-diethylBenzene	4392656332	21.79195
10.67	Trimethylnaphthalene	335475936	1.664295
11.139	Hexadecanoic acid, methyl ester	470332768	2.333319
11.499	Heptadecane, 9-hexyl-	339604640	1.684778
11.802	Oxirane-2-carboxylic acid, 3-(3,4,5-trimethoxyphenyl)-, methyl ester	455414752	2.259311
11.985	Octadecane, 3-ethyl-5-(2-ethylbutyl)-	454223488	2.253401
12.126	Methyl stearate	390752992	1.938524
19.368	Heptasiloxane, hexadecamethyl-	1709106560	8.478872

Table 2 a: Effect of Reaction temperature with 0.3HZSM-5 catalyst

RT (min)	2% 0.3HZSM-5 catalyst , 60min, 375°C compound	Area	%
3.184	1,3,5-Cycloheptatriene	46876564	1.953458
5.05	Phenol	148018208	6.168272
5.565	Cyclopentene, 3,4-dimethyl-	4451169	0.185491
5.671	Phenol, 2-methyl-	82812848	3.451009
5.844	p-Cresol	130806800	5.451032
5.971	Phenol, 2-methoxy-	101348088	4.223417
6.327	Phenol, 3-ethyl-	435249000	18.13786
6.43	Phenol, 2,4-dimethyl-	96408264	4.017562
6.549	Phenol, 2,3-dimethyl-	435136032	18.13316
6.772	Creosol	81561544	3.398864
6.998	Phenol, 3-(1-methylethyl)-	55759880	2.323647
7.082	Phenol, 2-ethyl-6-methyl-	83815152	3.492777
7.227	Phenol, 3-propyl-	45744360	1.906277
7.375	Benzene, 1,4-dimethoxy-2-methyl-	124670144	5.195302
7.587	Phenol, 3,5-diethyl-	45511288	1.896564
7.661	1H-Inden-1-one, 2,3-dihydro-3,3-dimethyl-	109788328	4.575142
7.869	Phenol, 2,6-dimethoxy-	62864296	2.619705
7.982	benzene, 2-methyl-4-propyl-	52383824	2.182959
8.476	Phenol, 4-methoxy-3-(methoxymethyl)-	46169104	1.923977
10.67	Trimethylnaphthalene	142656332	5.94483
11.093	Hexadecanoic acid, methyl ester	67639368	2.818694

Table 2 b

RT (min)	2% 0.3HZSM-5 catalyst , 60min, 425 °C compound	Area	%
3.187	heptane	62001100	4.670934
5.434	Cyclopentane	44228392	3.332004
5.681	Phenol, 3-methyl-	70646544	5.32225
6.143	benzene	133761896	10.07713
6.189	Phenol, 2-ethyl-5-methyl-	89672696	6.75561
6.44	Xylene	115188096	8.677846
6.563	Phenol, 4-ethyl-	97193992	7.322237
6.884	Phenol, 2,3,5-trimethyl-	91815232	6.917021
7.093	benzene 1-ethyl-4-methyl-	21313795	1.605703
7.142	Benzene	31346252	2.361511
7.505	Phenol, 2,3,5,6-tetramethyl-	158842800	11.96663
7.671	Benzene, 1-(1-methylethenyl)-3-(1-methylethyl)-	5508908	0.415021
7.946	Phenol, 4-(1,1-dimethylethyl)-2-methyl-	74825264	5.63706
7.999	Phenol, 2,3,5,6-tetramethyl-	79850640	6.015653
8.387	Benzene, 2-(2-butenyl)-1,3,5-trimethyl-	71667176	5.399141
10.768	Naphthalene trimethyl-	68184928	5.136801
11.381	5,7,9(11)-Androstatriene, 3-hydroxy-17-oxo-	7096983	0.534661
11.78	Morphinan-4,5-diol-6-one, 1-bromo-	18358456	1.383058
11.918	2,4,6-Cycloheptatrien-1-one, 3,5-bis-trimethylsilyl-	25423972	1.915348
12.101	Octadecanoic acid, (2-phenyl-1,3-dioxolan-4-yl)methyl ester, cis-	60454000	4.554381

Table 3a: Effect of 0.3HZSM-5 catalyst loading

RT (min)	1% 0.3HZSM-5 , 60min reaction time, 400oC compound	Area	%
5.109	exo-2-Bromonorbornane	22474688	0.425602
5.494	Cycloheptatriene	54118336	1.024835
5.737	Bicyclobutylidene	6634624	0.125639
5.899	Cyclopentadiene	6437289	0.121902
6.04	2-Cyclopenten-1-one, 3,4,4-trimethyl-	54694009	1.035736
6.245	3-Ethylphenol, methyl ether	454337440	8.603755
6.386	Phenol, 2,6-dimethyl-	455874720	8.632867
6.485	Phenol, 2,3-dimethyl-	934025408	17.68757
6.608	Bicyclo[2.2.2]octane, 1-bromo-4-methyl-	11343987	0.21482
6.827	Phenol, 2,4-dimethyl-	517151872	9.793268
7.052	Phenol, 2,3,6-trimethyl-	628047808	11.8933
7.14	Phenol, 3-methoxy-5-ethyl-	332453000	6.295638
7.292	2-Isopropylidene-3-methylhexa-3,5-dienal	49861430	0.944222
7.641	Trimethylnaphthalene	42856710	0.811574
7.676	Benzocycloheptatriene	30512032	0.577804
7.715	1H-Inden-1-one, 2,3-dihydro-3,3-dimethyl-	44441990	0.841595
7.98	Benzene, 1-ethoxy-4-ethyl-	417340000	7.903137
8.153	Benzene, 2,5-dimethyl-	52431158	0.992885
8.527	Benzene, 2,3,5-trimethyl-	621819324	11.77535
11.133	9-Octadecenoic acid (Z)-, tetradecyl ester	543831808	10.2985

Table 3b

RT (min)	3% 0.3HZSM-5 , 60min reaction time, 400oC compound	Area	%
5.071	Phenol	111847936	1.962608
5.455	Cycloheptatriene	100000122	1.754713
5.579	Bicyclo[2.2.2]octane	111449110	1.955609
5.698	Phenol, 3-methyl-	421271744	7.3921
5.864	Phenol, 2-methyl-	377078368	6.616634
5.998	Cyclopentane, trimethyl-	183132222	3.213441
6.157	Phenol, 2,6-dimethyl-	223723168	3.925694
6.203	Phenol, 3-ethyl-5-methyl-	344763392	6.0496
6.446	Phenol, 2,4-dimethyl-	528185984	9.268136
6.573	Benzene, 1-ethyl-2,3-dimethyl-	714646144	12.53997
6.792	Benzene, dimethyl-	229477120	4.02666
7.014	Phenol, 2,3,6-trimethyl-	300846688	5.278989
7.102	Phenol, 3-ethyl-5-methyl-	502529440	8.817938
7.25	Phenol, 3-ethyl-5-methyl-	21996388	0.385973
7.511	Phenol, 2-ethyl-4,5-dimethyl-	11011902	0.193227
7.603	methylnaphthalene	29364384	0.51526
7.641	Benzene, trimethyl-	247780096	4.347824
7.945	Phenol, 2,6-dimethyl-	137737968	2.416903
8.488	benzene 2-ethenyl-1 3 5-trimethyl	510852928	8.963991
11.097	Hexadecanoic acid, methyl ester	591250016	10.37473

Table 3c

RT (min)	4% 0.3HZSM-5 catalyst , 60min reaction time compound	Area	%
3.236	Toluene	36675040	2.188207
5.108	benzene	201750080	12.03737
5.738	methyl benzene	165285968	9.861746
5.904	Phenol, 3-methyl-	168954768	10.08064
6.204	Phenol, 2,6-dimethyl-	30914104	1.844482
6.249	Phenol, 2-ethyl-5-methyl-	48767460	2.909698
6.394	Phenol, 4-ethyl-	50119288	2.990355
6.492	Phenol, 2,5-dimethyl-	124143968	7.407019
6.619	ethyl benzene	282385152	16.84844
6.852	Phenol, 2-(1-methylethyl)-	52933568	3.158268
7.067	Phenol, 2-ethyl-5-methyl-	62333872	3.719135
7.151	Phenol, 3-ethyl-5-methyl-	114712752	6.844308
7.296	Phenol, 3-propyl-	51828568	3.092339
7.553	5-Isopropyl-2-methylphenyl 2-methylbutanoate	30614296	1.826594
7.655	Phenol, 2-methyl-5-(1-methylethyl)-	44436484	2.651292
8.004	1,10,25,26-Tetraaza-4,7-dioxatetracyclo[8.7.7.1(12,16).1(19,23)]hexacos-12,14,16(25),19,21,23(26)-hexaene	29096728	1.736049
8.216	Undecane, 2-methyl-	60673784	3.620086
12.036	Methyl stearate	46240612	2.758935
12.166	Hexadecanoic acid, 14-methyl-, methyl ester	41171472	2.456486
12.585	Octadecane, 3-ethyl-5-(2-ethylbutyl)-	32993464	1.968547

Table 4a: Effect of reaction time with 0.3HZSM-5 catalyst

RT (min)	2% 0.3HZSM-5 catalyst , 30min reaction time, 400 °C compound	Area	%
5.071	Phenol	312847936	4.72208
5.455	phenol methy-	220194176	3.323578
5.579	Bicyclo[2.2.2]octane	219449360	3.312336
5.698	methoxybenzene	421271744	6.358613
5.864	Benzene methyl-	377078368	5.691564
5.998	2-Cyclopenten-1-one, 2,3,4-trimethyl-	273132992	4.122628
6.157	Phenol, 2,6-dimethyl-	223723168	3.376844
6.203	Phenol, 3-ethyl-5-methyl-	344763392	5.203807
6.446	Phenol, 2,4-dimethyl-	528185984	7.97236
6.573	Phenol, 2,3-dimethyl-	714646144	10.78676
6.792	Phenol, 2,5-dimethyl-	229477120	3.463693
7.014	Phenol, 2,3,6-trimethyl-	300846688	4.540935
7.102	Phenol, 3-ethyl-5-methyl-	502529440	7.585104
7.25	Phenol, 3-ethyl-5-methyl-	219963888	3.320102
7.511	2-ethyl-1-isopropyl-4-methylbenzene	220119024	3.322444
7.603	Benzene, 4-(2-butenyl)-1,2-dimethyl-, (E)-	229364384	3.461992
7.641	1,4-Benzenediol, 2,5-dimethyl-	247780096	3.739956
7.945	Phenol, 4-(methoxymethyl)-2,6-dimethyl-	237737968	3.588381
8.488	1,4-Benzenediol, 2,3,5-trimethyl-	510852928	7.710738
11.097	Hexadecanoic acid, methyl ester	291250016	4.396084

Table 4b

RT (min)	2% 0.3HZSM-5 catalyst , 90min reaction time, 400 °C compound	Area	%
3.236	Toluene	36675040	2.188207
5.108	benzene	201750080	12.03737
5.738	methyl benzene	165285968	9.861746
5.904	Phenol, 3-methyl-	168954768	10.08064
6.204	Phenol, 2-methyl-	30914104	1.844482
6.249	Phenol, 5-methyl-	48767460	2.909698
6.394	Phenol, 4-ethyl-	50119288	2.990355
6.492	Phenol, 2,5-dimethyl-	124143968	7.407019
6.619	ethyl benzene	282385152	16.84844
6.852	Phenol, 2-(1-methylethyl)-	52933568	3.158268
7.067	Phenol, 2-ethyl-	62333872	3.719135
7.151	Phenol, 3-ethyl-	114712752	6.844308
7.296	Phenol, 3-propyl-	51828568	3.092339
7.553	Pentene	30614296	1.826594
7.655	Phenol	44436484	2.651292
8.004	Cyclopentene	29096728	1.736049
8.216	Hexane	60673784	3.620086
12.036	phenyl 2-methyl butanoate	46240612	2.758935
12.166	Hexadecanoic acid, 14-methyl-, methyl ester	41171472	2.456486
12.585	5,6-Dimethyldecane	32993464	1.968547

Table 5 a: Re-usability of 0.3HZSM-5

	3rd cycle		
	4% 0.3HZSM-5 catalyst , 60min, 400oC		
RT (min)	compound	Area	%
3.19	Cyclobutene, 2-propenylidene-	60736656	4.012578
4.538	Anisole	68944424	4.554825
5.063	Phenol	43053236	2.844319
5.438	Benzene, 1-methoxy-3-methyl-	87430424	5.776106
5.685	p-Cresol	74775240	4.940039
5.854	Phenol, 3-methyl-	62076768	4.101112
6.147	Phenol, 2,6-dimethyl-	67732408	4.474753
6.189	Phenol, 2-ethyl-5-methyl-	111683952	7.37842
6.447	dimethylbhenzene	132390688	8.746414
6.563	Phenol, 4-ethyl-	154521824	10.20851
6.803	2,5-Diethylphenol	48990572	3.236571
6.891	Phenol, 2,3,6-trimethyl-	39572748	2.61438
7.008	Phenol, 2-ethyl-4-methyl-	53030656	3.503479
7.092	Phenol, 4-ethyl-2-methyl-	172863888	11.42028
7.399	Phenol, 2-methyl-5-(1-methylethyl)-	39653572	2.61972
7.505	Phenol, 2-ethyl-4,5-dimethyl-	74744384	4.938001
7.671	Benzene, 4-(2-butenyl)-1,2-dimethyl-, (E)-	57978624	3.830368
7.946	1,3-Cyclohexadiene, 1,2,3,4,5,6-hexamethyl-	69299160	4.578261
8.489	3-Hydroxycarbofuran	42591424	2.81381
11.115	Hexadecanoic acid, methyl ester	51586180	3.40805

Table 5b

	4th cycle		
RT (min)	4% 0.3HZSM-5 catalyst , 60min, 400oC compound	Area	%
3.184	1,3,5-Cycloheptatriene	46876564	2.499616
5.05	Phenol	148018208	7.892828
5.565	2-Cyclopenten-1-one, 3,4-dimethyl-	44511692	2.373513
5.671	Phenol, 2-methyl-	82812848	4.415859
5.844	p-Cresol	130806896	6.975063
5.971	Phenol, 2-methoxy-	111348088	5.937454
6.327	Phenol, 3-ethyl-	63524900	3.387361
6.43	Phenol, 2,4-dimethyl-	96408264	5.140812
6.549	Phenol, 2,3-dimethyl-	435136032	23.20291
6.772	Creosol	81561544	4.349135
6.998	Phenol, 3-(1-methylethyl)-	55759880	2.973304
7.082	Phenol, 2-ethyl-6-methyl-	83815152	4.469305
7.227	Phenol, 3-propyl-	45744360	2.439243
7.375	Benzene, 1,4-dimethoxy-2-methyl-	124670144	6.647831
7.587	Phenol, 3,5-diethyl-	45511288	2.426815
7.661	1H-Inden-1-one, 2,3-dihydro-3,3-dimethyl-	49788328	2.654881
7.869	Phenol, 2,6-dimethoxy-	62864296	3.352135
7.982	Phenol, 2-methoxy-4-propyl-	52383824	2.793281
8.476	Phenol, 4-methoxy-3-(methoxymethyl)-	46169104	2.461892
11.093	Hexadecanoic acid, methyl ester	67639368	3.606758

Table 6 a: Composition of commercial fossil premium motor spirit and kerosene

	PMS		
RT (min)	compound	Area	%
3.08	Pentane, 2,3,3-trimethyl-	1768299392	4.28
3.17	Bicyclo[2.2.1]-2,5-heptadiene	5187063808	12.57
3.34	3-Trifluoroacetoxydodecane	1668718592	4.04
3.43	2-Undecyne	2148044544	5.20
4.03	2,Beta-dinitrostyrene	1958558080	4.75
4.10	1,3,7-Octatrien-5-yne	1230280448	2.98
4.15	1,5-Cyclooctanediol, diacetate	1539693056	3.73
4.34	4-(Aminomethyl)pyridine	2627020032	6.37
4.86	1-Hexen-4-yne, 3-ethylidene-2-methyl-	1421028864	3.44
4.95	7-Methylenecycloocta-1,3,5-triene	3593245184	8.71
5.00	Pyridine, 5-ethenyl-2-methyl-	1588348160	3.85
5.08	4-Bromo-7-methylenebicyclo[4.2.0]oct-2-ene	1653753344	4.01
5.20	Benzenepropanamine	2556382464	6.19
5.46	2,4-Bis(diazo)adamantane	1618031360	3.92
5.67	Benzene, 1-cyclopropyl-2-nitro-	1201821568	2.91
5.73	1,4-Cyclohexadiene, 3-ethenyl-1,2-dimethyl-	1652991232	4.01
5.95	1-Phenyl-1-butene	1409196800	3.41
6.43	Naphthalene, 1,4,5,8-tetrahydro-	1693162496	4.10
6.50	Cyclohexene, 3-methylene-4-(1,2-propadienyl)-	2934092544	7.11
6.81	1-(3,3-Dimethylbutyn-1-yl)-2,2-dimethylcyclopropene	1822737152	4.42

Table 6 b

RT (min)	**Fossil Kerosene** compound	Area	%
6.53	1,6-Pentalenedione, hexahydro-6a-(2-propynyl)-, cis-	11048182784	4.13
6.76	1-Methoxymethoxy-but-2-enyl)-benzene	11487042560	4.30
6.84	1H-Benzimidazole, 2-(difluoromethyl)	9558094848	3.58
6.92	Tricyclo[7.2.0.0(2,6)]undecan-5-ol, 2,6,10,10-tetramethyl-	9510418432	3.56
7.13	Indole-2-one, 2,3-dihydro-5-hydroxy-1,3-dimethyl-	14514954240	5.43
7.25	Benzonitrile, 4-(1-octynyl)-	8899064832	3.33
7.32	Morpholine, 4,4'-(2,4-hexadiynylene)di-	14906126336	5.58
7.60	1-Hydroxy-6-(4'-chlorobenzyl)-1,2,3,4,5,6-hexamethylcyclohexa-2,4-diene	15120615424	5.66
7.75	1,3,5-Trimethyl-2-(2-nitrovinyl)benzene	27539959808	10.30
7.90	1,3-Benzodioxole, 5-[1-[2-(2-butoxyethoxy)ethoxy]butyl]-	15437742080	5.78
8.01	Benzene, 1-(2-butenyl)-2,3-dimethyl-	12260535296	4.59
8.16	,4-Diaza-9-oxaspiro[5.5]undecane, 8-ethyl-8-methyl-	14755656704	5.52
8.23	cis-1-Chloro-9-octadecene	9413677056	3.52
8.29	Naphthalene, 1,4-dihydro-2,5,8-trimethyl-	9369500672	3.51
8.38	Naphthalene, 1-(1-methylethyl)-	11205061632	4.19
8.45	Pyrrolizin-1,7-dione-6-carboxylic acid, methyl(ester)	16833463296	6.30
8.56	2,4,6-Cycloheptatrien-1-one, 2-hydroxy-5-(3-methyl-2-butenyl)-4-(1-methylethenyl)-	18562246656	6.94
8.68	Naphthalene, 2,6-dimethyl-	11736007680	4.39
8.83	5,8,11,14-Eicosatetraynoic acid, methyl ester	15286890496	5.72
9.09	Naphthalene, 1-(1-methylethyl)-	9853754368	3.69

Table 6c: Composition of distillates collected

RT (min)	**3.0% 0.3HZSM-5 catalyst , 30min, 400 °C** compound	**Light fraction** Area	%
3.17	2,4-Hexadiene, 3-methyl-	163956352	4.82
3.22	2,2-Dimethoxybutane	178953536	5.26
3.31	1,6-Heptadien-3-yne	364337760	10.71
3.53	1,4-Hexadiene, 2,3-dimethyl-	254668096	7.49
3.66	Cyclopentene, 1,2,3-trimethyl-	217267952	6.39
3.90	1-Ethyl-5-methylcyclopentene	78010520	2.29
4.01	Cyclopentane, 2-ethylidene-1,1-dimethyl-	182547728	5.37
4.15	Benzene, 1,3-dimethyl-	204146560	6.00
4.23	p-Xylene	361955712	10.64
4.36	3-Octyne, 7-methyl-	72260856	2.12
4.44	Benzene, 1,3-dimethyl-	312030496	9.17
4.57	Cyclopropane, tetramethylpropylidene-	109600840	3.22
4.65	Anisole	168980624	4.97
4.76	2H-Pyran-2-one, 3,4,5,6-tetramethyl-	157589440	4.63
4.83	1,4-Hexadiene, 2,3,4,5-tetramethyl-	65255020	1.92
4.98	1,3,5-Cycloheptatriene, 7-ethyl-	72784848	2.14
5.03	Benzene, 1-ethyl-2-methyl-	124264120	3.65
5.06	Benzene, 1,2,3-trimethyl-	77539392	2.28
5.32	Benzene, 1-ethyl-4-methyl-	167535856	4.93
6.11	Undecane	67644544	1.99

Table 6d

RT (min)	3.0% 0.3HZSM-5 catalyst , 30min, 400oC Middle distillate compound	Middle distillate Area	%
3.89	1-Propene, 1-(2-propenyloxy)-, (Z)-	314615712	3.42
4.15	Benzene, 1,3-dimethyl-	252210496	2.74
4.36	2,4-Octadiyne	243287840	2.65
4.57	Formic acid, pyridin-2-ylmethyl ester	617339776	6.72
4.96	Benzene, 1-ethyl-2-methyl-	280054080	3.05
5.12	Benzene, 1-ethyl-4-methyl-	239447072	2.61
5.25	Benzene, 1,2,3-trimethyl-	417676736	4.55
5.35	1,3,5-Cycloheptatriene, 1-methoxy-	417114144	4.54
5.46	Bicyclo[3.2.0]hepta-2,6-diene, 5-methoxy-	742464832	8.08
5.71	Phenol, 3-methyl-	453288576	4.93
5.99	p-Cymene	273461312	2.98
6.03	Benzene, 1-methyl-4-(1-methylethenyl)-	438842944	4.78
6.17	Phenol, 2,3-dimethyl-	427399264	4.65
6.22	2-Ethylphenol, methyl ether	590721280	6.43
6.46	Phenol, 2,5-dimethyl-	496694528	5.41
6.81	1H-Indene, 1-ethyl-2,3-dihydro-1-methyl-	417209952	4.54
7.11	Phenol, 3,4,5-trimethyl-	390327776	4.25
7.51	5-Isopropyl-2-methylphenyl 2-methylbutanoate	314548928	3.42
23.25	Heptasiloxane, hexadecamethyl-	846029440	9.21
23.56	Benzoic acid, 2,4-bis[(trimethylsilyl)oxy]-, trimethylsilyl ester	1015349312	11.05

Table 6e

3% 0.3HZSM-5 catalyst, 30 min and 400 °C			
		Bottom product	
RT (min)	compound	Area	%
5.71	Phenol, 3-methyl-	387871232	5.66
5.87	Phenol, 2-methyl-	311928064	4.55
6.45	Phenol, 2,5-dimethyl-	608163392	8.88
6.58	Phenol, 4-ethyl-	530658912	7.75
7.02	Phenol, 2-(1-methylethyl)-	289489280	4.23
7.10	Phenol, 3-ethyl-5-methyl-	555533184	8.11
7.52	Phenol, 2-methyl-5-(1-methylethyl)-, acetate	277610336	4.05
7.65	1,4-Benzenediol, 2,6-dimethyl-	264615488	3.86
7.95	1-Penten-3-one, 2-methyl-1-(2,2,6-trimethylcyclohexen-1-yl)-	244782608	3.57
8.12	1,4-Benzenediol, 2,6-dimethyl-	251047872	3.67
8.49	1,4-Benzenediol, 2,3,5-trimethyl-	740681728	10.82
8.94	1,4-Benzenediol, 2,3,5-trimethyl-	237865248	3.47
9.10	5,8-Dimethyl-1,2,3,4-tetrahydro-1-naphthol	230070112	3.36
10.25	1H-Indene-4-carboxylic acid, 2,3-dihydro-1,1-dimethyl-, methyl ester	236475152	3.45
10.35	1-Naphthol, 5,7-dimethyl-	307893088	4.50
10.63	1-Naphthol, 2,5,8-trimethyl-	271655072	3.97
11.10	Pentadecanoic acid, 14-methyl-, methyl ester	364606240	5.32
11.58	Hexadecanoic acid, 14-methyl-, methyl ester	251338048	3.67
12.08	Heptadecanoic acid, 9-methyl-, methyl ester	261929008	3.82
12.49	Octadecane, 3-ethyl-5-(2-ethylbutyl)-	224316640	3.28